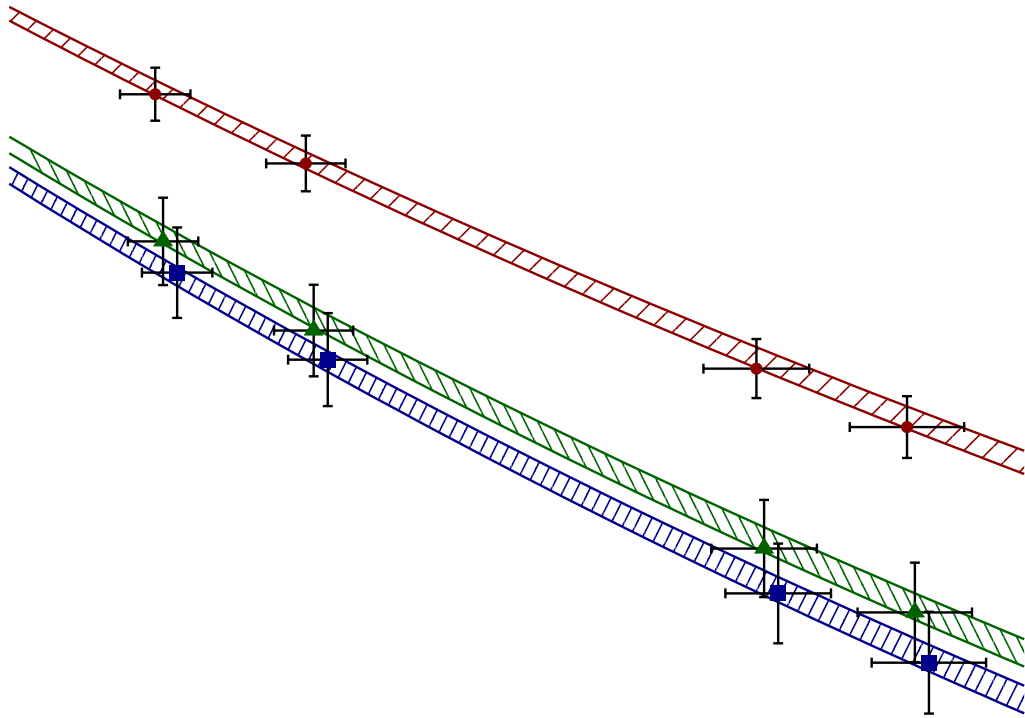


DOCTORAL THESIS

---

High precision applications of lattice gauge theories  
in the quest for new physics

---



Andrea Bussone

---

High precision applications of lattice gauge theories  
in the quest for new physics

---

CANDIDATE:                      Andrea Bussone  
SUPERVISOR:                    Michele Della Morte  
CO-SUPERVISOR:                Claudio Pica



UNIVERSITY OF  
SOUTHERN DENMARK

*Dissertation for the degree of Doctor of Philosophy*

**CP<sup>3</sup>-Origins**

Department of Mathematics and Computer Science

Submitted to the University of Southern Denmark

Corrected version:

Tuesday 3<sup>rd</sup> October, 2017

## Abstract

We present some aspects of high precision calculations in the context of Lattice Quantum Field Theory. This work is a collection of three studies done during my Ph.D. period.

First we present how to use the reweighting technique to compensate for the breaking of unitarity due to the use of different boundary conditions in the valence and sea sector. In particular when twisted boundary conditions are employed, with  $\theta$  twisting angle. In large volume we found that the breaking is negligible, while in rather small volumes an effect is present. The quark mass appears to change with  $\theta$  as a cutoff effect.

In the second part of the dissertation we present an optimization method for Hybrid Monte Carlo performances. The presented strategy is quite general and can be applied to Beyond Standard Model strongly interacting theories, for which the need for precision is becoming urgent nowadays. The work is based on the existence of a shadow Hamiltonian, an exactly conserved quantity along the Molecular Dynamics trajectory. The optimization method is economic since it only requires the forces to be measured, which are already used for the evolution from one configuration to the new one. We found predictions for the cost of the simulations with an accuracy of 10% and we could estimate the optimal parameters for the Omelyan integrator with mass-preconditioning and multi time-scale.

In the last part of the work we address the calculation of electromagnetic corrections to the hadronic contribution to the  $(g - 2)$  anomaly of the muon. A long standing discrepancy between theoretical calculations and experimental results is present. Each new Beyond Standard Model theory aims at solving the discrepancy with the introduction of New Physics. But before invoking New Physics we need to clear the sight from possible effects within the Standard Model. Firstly we discuss different implementations of QED on the lattice with periodic boundary conditions. Then we consider applications of that for the muon anomaly. In this exploratory study we carefully matched the masses of the charged pions in the theory with and without QED. In that way we are able to access directly the electromagnetic corrections to the anomaly with smaller statistical errors. We found a visible effect at the percent level although consistent with zero within two sigmas.

## Sammenfatning

Vi præsenterer nogle vigtige aspekter af højpræcisionsberegninger i forbindelse med lattice kvantefeltteori. Denne afhandling er en samling af tre studier udført i løbet af min Ph.d.-uddannelse.

Først præsenterer vi, hvordan man bruger reweighting-teknikken til at kompensere for unitæritetsbruddet forårsaget af brugen af forskellige randbetingelser i valens- og sea-sektoren. I særdeleshed når der anvendes twistede-randbet ingelse med twist-vinkel  $\theta$ . I store volumener fandt vi, at bruddet er ubetydeligt, mens der for små volumener findes en effekt. Kvarkmassen ser ud til at ændre sig med vinklen  $\theta$  som en såkaldt cut-of-effekt.

I anden del af afhandlingen præsenterer vi en optimeringsmetode til at forbedre ydelsen af Hybrid Monte Carlo-algoritmen. Den fremstillede strategi er generel og kan anvendes til stærkt vekselvirkende teorier udover standardmodellen for hvilke behovet for præcision er begyndt at blive nødvendigt. Strategien er baseret på eksistensen af en shadow Hamiltonian, en eksakt bevaret størrelse langs Molecular Dynamics-banen. Optimeringsmetoden er økonomisk, da den kun kræver, at kræfterne måles, og disse er allerede nødvendige for udviklingen fra en konfiguration til den næste. Vi fandt forudsigelser for omkostningerne ved simuleringerne med en nøjagtighed på 10 %, og vi kunne estimere de optimale parametre for Omelyan-integratoren med mass-preconditioning og multi time-scale.

Den sidste del af afhandlingen omhandler beregningen af de elektromagnetiske korrektioner til den hadroniske del af  $(g - 2)$ -anomalien for myonen. For denne observable størrelse eksisterer der en langvarig uoverensstemmelse mellem de teoretiske beregninger og de eksperimentelle resultater. Enhver ny teori udover standardmodellen stiler efter at løse denne uoverensstemmelse ved at introducere ny fysik, men før vi tyer til ny fysik, skal vi sikre os imod effekter genereret af standardmodellen selv. For det første diskuterer vi forskellige implementeringer af QED på gitteret med periodiske randbetingelser. Derefter betragter anvendelsen af disse for myon-anomalien. I dette eksplorative studie, matchede vi nøje masserne af de ladede pioner både i teorien med og uden QED. På denne måde har vi mulighed for direkte at få adgang til de elektromagnetiske korrektioner til anomalien med mindre statistiske usikkerheder. Vi fandt en synlig effekt på procentniveauet selvom resultatet er i overensstemmelse med nul inden for to standardafvigelse.

# Publications

This dissertation is based on the following published articles done at CP<sup>3</sup>-Origins during the three years of my Ph.D. studies:

- article A. Bussone, M. Della Morte, M. Hansen and C. Pica, “On reweighting for twisted boundary conditions,” *Comput. Phys. Commun.* (2017) doi:10.1016/j.cpc.2017.05.011 [arXiv:1609.00210 [hep-lat]]. ([Bussone \*et al.\*, 2017](#))
- conf. proc. A. Bussone, M. Della Morte, M. Hansen and C. Pica, “Reweighting twisted boundary conditions,” *PoS LATTICE 2015* (2016) 021 [arXiv:1509.04540 [hep-lat]]. ([Bussone \*et al.\*, 2016b](#))
- conf. proc. A. Bussone, M. Della Morte, V. Drach, M. Hansen, A. Hietanen, J. Rantaharju and C. Pica, “A simple method to optimize HMC performance,” *PoS LATTICE 2016* (2016) 260 [arXiv:1610.02860 [hep-lat]]. ([Bussone \*et al.\*, 2016a](#))
- conf. proc. A. Bussone, M. Della Morte and T. Janowski, “Electromagnetic corrections to the hadronic vacuum polarization of the photon within QED<sub>L</sub> and QED<sub>M</sub>,” [arXiv:17xx.xxxxx [hep-lat]]. *To appear in EPJ Web of Conferences.*

Other pieces of work were published during the same period. The following articles will be not discussed in the dissertation:

- article A. Bussone *et al.* [ETM Collaboration], “Mass of the b quark and B -meson decay constants from N<sub>f</sub>=2+1+1 twisted-mass lattice QCD,” *Phys. Rev. D* **93** (2016) no.11, 114505 doi:10.1103/PhysRevD.93.114505 [arXiv:1603.04306 [hep-lat]]. ([Bussone and others, 2016](#))

All publications can be acquired freely as on-line e-prints at arXiv.org.

Such a monstrous presumption to think that others could benefit from  
the squalid catalogue of your mistakes!

Fellini - 8<sup>1</sup>/<sub>2</sub>

# Acknowledgements

I would like to express my gratitude to Prof. Michele Della Morte and Prof. Claudio Pica. They guided and helped me in understanding how to do research during my time at CP<sup>3</sup>-Origins. I thank all the people that I met at CP<sup>3</sup>-Origins for sharing with me their passion and time.

I am indebted to Prof. Roberto Frezzotti and Dr. Petros Dimopoulos for their time spent giving me valuable advices.

I would like to thank my parents for the strength they constantly give me.

# Contents

<b>Abstract</b>	<b>iii</b>
<b>Sammenfatning</b>	<b>iv</b>
<b>Publications</b>	<b>v</b>
<b>Acknowledgements</b>	<b>vii</b>
<b>List of Figures</b>	<b>xii</b>
<b>List of Tables</b>	<b>xiv</b>
<b>Introduction</b>	<b>xv</b>
<b>1 Elements of non-Abelian lattice gauge theories</b>	<b>1</b>
1.1 QCD formal theory . . . . .	1
1.2 Symmetries of QCD-like theories . . . . .	3
1.2.1 $\mathbf{SU}(2)_L \otimes \mathbf{SU}(2)_R$ . . . . .	4
1.3 Renormalization . . . . .	6
1.3.1 Asymptotic freedom . . . . .	6
1.3.2 Hadron masses . . . . .	7
1.4 Lattice regularization . . . . .	7
1.4.1 Wilson plaquette gauge action . . . . .	8
1.4.2 Fermionic action . . . . .	8
1.5 Symanzik improvement programme . . . . .	10
1.5.1 $O(a)$ improved action . . . . .	11
1.6 Ward-Takahashi identities . . . . .	11
1.6.1 Formal theory . . . . .	12
1.6.2 Critical mass on the lattice . . . . .	12
1.7 Hybrid Monte Carlo simulations of gauge theories . . . . .	13
1.7.1 Markov chain . . . . .	14
1.7.2 How to build a Markov process . . . . .	14
1.7.3 Hybrid Monte Carlo simulation . . . . .	15
1.7.4 Dynamical fermions . . . . .	16
<b>2 Quantum electrodynamics on the lattice</b>	<b>18</b>
2.1 Global symmetries . . . . .	19
2.2 Infrared divergences . . . . .	20
2.3 Gauge symmetry: general considerations . . . . .	21



2.3.1	Gauge fixing	21
2.3.2	Gauge symmetry in finite volume	22
2.4	$\text{QED}_{\text{TL}}$ & $\text{QED}_{\text{L}}$	24
2.4.1	Fix of the residual gauge symmetry and zero mode	24
2.5	Generation of quenched QED configurations	25
2.5.1	Generation in Feynman gauge	25
2.6	Gauss law problem	26
2.7	Massive QED	27
2.7.1	Renormalizability: the need for Feynman gauge	28
2.7.2	Solution of the Gauss law problem	29
2.8	Wilson loops	30
2.8.1	Massless case	30
2.8.2	Massive case	30
<b>3</b>	<b>Reweighting twisted boundary conditions</b>	<b>33</b>
3.1	Twisted boundary conditions	34
3.2	Reweighting technique	35
3.3	Tree-level studies	36
3.4	Simulations and results	38
3.4.1	Small volumes	40
3.4.2	Large volumes	41
3.5	Quark mass dependence on the twisting angle	42
3.6	Conclusions	45
<b>4</b>	<b>Optimization of HMC performance</b>	<b>47</b>
4.1	Symplectic integrators: a toy model	48
4.1.1	Shadow hamiltonian	50
4.2	Mass preconditioning & multi time-scale	51
4.3	Benchmarks in small volumes	52
4.4	Cost of a simulation and its minimization	54
4.4.1	Acceptance & Matrix-Vector-Multiplication	55
4.4.2	Fits	56
4.4.3	Cost function	58
4.5	Comparison with simulations	58
4.6	Conclusions	59
<b>5</b>	<b>QED leading corrections to hadronic observables: the muon anomaly</b>	<b>61</b>
5.1	Introduction	63
5.2	Details on the computation of the vacuum polarization including QED corrections	65
5.2.1	Critical mass	65
5.2.2	Pseudoscalar spectrum	67
5.2.3	Finite volume and photon mass effects	69
5.2.4	Massless limit in $\text{QED}_{\text{M}}$	70
5.3	Vacuum polarization	71
5.3.1	Lattice regularization	73
5.3.2	Scalar vacuum polarization	74
5.3.3	Padé fits	75
5.4	Time moments	76
5.4.1	Infinite volume	76
5.4.2	Finite volume	77

5.5	Subtracted scalar HVP . . . . .	77
5.6	Conclusions . . . . .	78
<b>6</b>	<b>Conclusions and Outlooks</b>	<b>82</b>
	<b>Appendixes</b>	<b>84</b>
<b>A</b>	<b>Ward-Takahashi Identities</b>	<b>84</b>
A.1	WTIs proof . . . . .	84
A.2	Singlet One-point-split current . . . . .	86
A.2.1	Formal derivation . . . . .	86
A.2.2	Lattice derivation . . . . .	87
A.3	Bare PCAC relation on the lattice . . . . .	87
<b>B</b>	<b>Reweighting factors and reweighted observables</b>	<b>89</b>
B.1	Tree-level reweighting factors . . . . .	89
B.1.1	Dirac-Wilson operator and eigenvalues . . . . .	89
B.1.2	Reweighting factors: tree-level analytic evaluation . . . . .	90
B.2	Observables with TBCs . . . . .	91
B.2.1	Plaquette . . . . .	91
B.2.2	Valence twisting and pion dispersion relation . . . . .	92
<b>C</b>	<b>HMC simulations</b>	<b>95</b>
C.1	Acceptance in HMC simulations . . . . .	95
C.2	Multiple time-scale Omelyan shadow Hamiltonian . . . . .	96
C.3	Forces in HMC . . . . .	98
C.3.1	Mass preconditioning forces . . . . .	99
C.4	Number of configurations and parameters in the optimization study . . . . .	101
<b>D</b>	<b>Quantum electrodynamics on the lattice: supplementary material</b>	<b>103</b>
D.1	Fourier transform . . . . .	103
D.1.1	Reality condition . . . . .	103
D.2	Generation in Feynman gauge . . . . .	104
D.3	Extended Coulomb gauge . . . . .	105
D.3.1	Extended Coulomb via Feynman gauge . . . . .	105
D.3.2	Generation in the extended Coulomb gauge . . . . .	106
D.4	Zero mode fixing equation of motion . . . . .	108
D.5	Generation of quenched QED <sub>M</sub> configurations . . . . .	108
D.5.1	Feynman gauge . . . . .	109
D.5.2	Coulomb gauge . . . . .	109
D.6	Wilson loop in quenched approximation . . . . .	111
D.7	Coordinate space method . . . . .	112
D.7.1	Luscher-Weisz . . . . .	112
D.7.2	Borasoy-Krebs . . . . .	115
<b>E</b>	<b>Electromagnetic critical mass shift in lattice perturbation theory</b>	<b>116</b>
E.1	Feynman rules of the Wilson theory . . . . .	116
E.1.1	Photon propagator . . . . .	116
E.1.2	Fermion propagator . . . . .	116
E.1.3	Vertexes . . . . .	117

<b>Contents</b>	<b>xi</b>
<hr/>	
E.1.4 Clover term . . . . .	118
E.2 Electromagnetic fermion self-energy . . . . .	120
E.3 Tadpole improved lattice perturbation theory . . . . .	126
<b>F Explicit form of the HVP</b>	<b>128</b>
<b>Bibliography</b>	<b>131</b>

# List of Figures

2.1	<i>Wilson loop values in a volume <math>V = 32^4</math> and their comparison with the infinite volume predictions calculated through the Lüscher-Weisz algorithm. . . . .</i>	31
2.2	<i>Comparison of Wilson loop values from simulations and infinite volume predictions calculated through the Borasoy-Krebs algorithm. . . . .</i>	32
3.1	<i>Results for the reweighting factor mean and variance employing the exact formulae in the tree-level case. Each point corresponds to a cubic lattice of the form <math>L^4</math> with <math>N_f = 2</math>, <math>N_c = 2</math> and <math>m = 0.1</math>. . . . .</i>	37
3.2	<i>Comparison between the stochastic and exact estimates of the reweighting factor and its variance on the trivial gauge configuration for <math>\theta = 0.1</math>, <math>L = 8</math> using one and two levels of factorization in the numerical case. Both plotted against the number <math>N_\eta</math> of Gaussian vectors in each level. . . . .</i>	39
3.3	<i>Monte Carlo history of the reweighting factor relative to its mean for the <math>8^3 \times 16</math> ensemble and with <math>N_\eta=300</math>. . . . .</i>	39
3.4	<i>Monte Carlo average of the reweighting factor, averaged over the entire number of configurations vs <math>N_\eta</math>. The figures correspond to a volume <math>V = 8^3 \times 16</math>. . . . .</i>	40
3.5	<i>Monte Carlo history of the reweighted plaquette. The figures correspond to a volume <math>8^3 \times 16</math>. . . . .</i>	41
3.6	<i>Pion dispersion relation for <math>V = 8^3 \times 16</math>. Each point is obtained with a different (growing with <math>\theta</math>) number of independent steps in the determination of the reweighting factor and <math>N_\eta \gtrsim 600</math> in each step. . . . .</i>	42
3.7	<i>Pion dispersion relation for <math>V = 24^3 \times 32</math>. The reweighting factor at a given <math>\theta</math> is obtained by a telescopic product involving all the previous ones, each one estimated using <math>N_\eta \gtrsim 600</math>. . . . .</i>	42
3.8	<i>Pion effective masses for <math>\theta_s = \theta_v = \theta</math> on a <math>8^3 \times 32</math> lattice at <math>\beta = 2.2</math>, <math>m_0 = -0.72</math> (left panel) and comparison of the corresponding plateau masses (red) with the result from <math>\theta_s = 0</math> as a function of <math>\theta = \theta_v</math> (right panel). . . . .</i>	44
3.9	<i><math>m_{\text{PCAC}}</math> as a function of <math>m_0</math> computed for <math>m_0 = -0.72</math>, <math>-0.735</math> and <math>-0.75</math> at <math>\beta = 2.2</math> and <math>V = 8^3 \times 16</math>. The curves correspond to three different values of <math>\theta = \theta_v = \theta_s</math>. . . . .</i>	45
4.1	<i>Scaling behavior with <math>\delta\tau = 1/n</math> for <math>\Delta H</math> and <math>\Delta(\delta H)</math> in small volumes. <math>\Delta(\delta H)</math> is built from the knowledge of the forces at the beginning and the end of the trajectory. Lines are shown to guide the eye. . . . .</i>	53
4.2	<i>Benchmarks for the Poisson brackets measurements. Direct measurement (red crosses) corresponds to the measure of <math>\Delta H</math> during the trajectory. Force method (blue stars) employs the knowledge of the forces. From the left to the right panel the minimum of <math>\Delta H</math> is scaling as expected. . . . .</i>	54

4.3	Acceptance as a function of the preconditioning mass. Force method 1 and 2 (red segments and violet boxes) are employing the formulae in Eqs. 4.4.35, 4.4.34. $\Delta H$ method (green crosses) correspond to the measurement of $H$ (also used for the accept/reject step). Measurement (blue crosses) correspond to simple counting. . . . .	56
4.4	Variances of the forces as a function of the mass preconditioning parameter. For very small $\mu$ the HMC variance is dominant, outside this region the Gauge variance is the dominant one. In the intermediate $\mu$ region we have an hierarchy of forces that corresponds to the level assignments. For large $\mu$ we have an inverted hierarchy. The figure corresponds to $m_0 = -0.72$ . . . . .	57
4.5	#MVM in Hasenbusch and HMC levels as a function of $\mu$ for $m_0 = -0.72$ . . . . .	57
4.6	Ratio Cost/Cost <sub>min</sub> around the minimum $(n, m, \mu) \simeq (5, 3, 0.3)$ is displayed as curve level. Acceptance rate lines are drawn. Bare mass $m_0 = -0.72$ . . . . .	58
4.7	Cost at the minimum, comparison with simulation. Each point correspond to a different set of parameters $\mu, n, m$ . In black comparison with direct simulations is made. . . . .	59
5.1	Summary of the hadronic contributions to $a_\mu$ . The light contribution makes the 90% of the total, while the strange and the charm account for 8% and 2% respectively. Plots taken from the plenary talk given by H. Wittig at 2016 the Lattice Conference. . . . .	63
5.2	Leading order QED corrections to the HVP in the continuum theory. Squares corresponds to insertions of conserved current. All orders of QCD are understood when drawing the diagrams. Diagrams (a) and (b) are included in our calculation, while (c) and (d) are absent. . . . .	66
5.3	Comparison between the critical mass from lattice perturbation theory in Feynman gauge using the one-loop result Eq. E.48 (blue stars) and the tadpole resummation Eq. E.49 (green crosses). Orange triangles represents values from lattice simulations. The QCD critical mass is shown for comparison (red line). . . . .	67
5.4	Effective neutral pseudoscalar masses for different photon masses and comparison with QCD and $Q(C+E_L)D$ . . . . .	68
5.5	Effective pseudoscalar masses for $m_\gamma = 0.1$ and different charge content. . . . .	68
5.6	Neutral pseudoscalar masses versus PCAC mass for different charges. . . . .	69
5.7	Square average of neutral pseudoscalar masses versus bare PCAC masses for different photon masses. . . . .	69
5.8	Dispersion relation for the charged and neutral pions in the A3 ensemble. . . . .	71
5.9	Dispersion relation for charged and neutral pions for $m_\gamma = 0.1$ . The solid lines are the expectations from the continuum dispersion relation. . . . .	71
5.10	Schematic representation of the subtracted scalar Hadronic Vacuum Polarization. In the low $q^2$ region, "Model", we use for example Padé fit to estimate the HVP and we integrate the result. In the mid- $q^2$ region we numerically integrate directly the lattice data. In the large $q^2$ region we use perturbation theory. . . . .	73
5.11	HVP as a function of $r_0\hat{q}^2$ with and without the inclusion of QED. . . . .	80
5.12	Comparisons of the HVP on the matched ensembles. . . . .	81
B.1	Dirac-Wilson spectrum for different values of $\theta$ in $V = 4^4$ volume and mass $m_0 = 0.2$ . . . . .	90
B.2	Diagrammatic expression of the Eq. B.2.14. We show on the diagram the momentum flow. . . . .	93
B.3	Diagrammatic expression of the Eq. B.2.14 in the presence of the constant $U(1)$ interaction. The state correspond to a charged pion with momentum $\underline{B}$ . . . . .	93

# List of Tables

3.1	<i>Ensembles used and simulation parameters in the reweighting of TBCs.</i> . . . . .	38
4.1	<i>Parameters corresponding to the minimum cost of simulations and number of configurations produced.</i> . . . . .	59
5.1	<i>Different SM contributions to the theoretical value of <math>a_\mu</math>.</i> . . . . .	62
5.2	<i>Gauge configuration parameters and results in QCD, see Ref. (Capitani et al., 2015).</i> . . . . .	66
5.3	<i>Pseudoscalar masses in Coulomb gauge QED<sub>L</sub> (denoted with <math>m_\gamma = 0</math>) and QED<sub>M</sub>. The resulting pion masses go from 380 MeV to 640 MeV.</i> . . . . .	68
5.4	<i>QED<sub>L</sub> leading order finite volume corrections.</i> . . . . .	70
5.5	<i>QED<sub>M</sub> next-to-leading order finite volume corrections.</i> . . . . .	70
D.1	<i>Table showing the values of <math>-\frac{2}{q^2} \ln(w(I, I))</math> related to the Wilson loops in the infinite lattice in QED and massive QED (Feynman gauge), meant to save PhDs from struggling too much.</i> . . . . .	112

# Introduction

The current description of interactions among elementary particles, the Standard Model of particle physics, has passed all experimental tests, and it is a well established theory. Despite this, it has several shortcomings. It is not able to explain what is the nature of dark matter, the cosmological constant, why neutrinos oscillate and if general relativity can be unified with quantum mechanics, to name some of the main ones. New Physics signals, beyond the Standard Model, are therefore extensively searched by particle physicists (both experimentalists and theorists) to gain insights on the correct extension of it. That proceeds in two ways, through direct and indirect searches. The lattice approach can contribute to each of them. In this thesis we discuss some aspects of high precision calculations necessary to better understand the Standard Model and its contribution to physical observables.

*Indirect Search:* new particles can produce sizeable contributions to rare decays, which are suppressed in the Standard Model because, for example, of its flavor structure. For this reason a precise determination of the parameters controlling flavor mixing in the Standard Model is needed in the quest for New Physics. Such parameters can be extracted from the comparison of experimental data with theoretical predictions. The latter typically depend on hadronic matrix elements, which are inherently non-perturbative. Lattice QCD is the most powerful, first-principle, systematically-improvable approach to reliably compute those. Partially quenched twisted boundary conditions are used in lattice calculations for example to compute form factors. Twisted boundary conditions for fermion fields in spatial directions allow for the lattice momenta to be continuously varied. Usually the sea quarks still obey periodic boundary conditions. The break of unitarity, already at the perturbative level, can have an effect due to the finite volume. Such an effect can have impact when aiming at percent level precision in calculations of physical quantities. We devoted Chap. 3 to the discussion of such effects in a QCD-like theory. We used reweighting techniques to change the boundary conditions for the sea fermions and compensate for the unitarity violation.

Staying within the indirect search, one of the most outstanding achievements in experimental physics is the precision measurement of the muon anomalous magnetic moment  $(g - 2)_\mu$ . A  $3\sigma$  tension between theoretical calculations and experimental results is still present and a better theoretical understanding is needed. The main uncertainty in the theoretical prediction comes from the leading, and next to leading, hadronic vacuum polarization where the lattice can, and must, significantly improve since the new experiments will reduce the experimental uncertainty. In this context we have started to investigate electromagnetic corrections to the hadronic leading order vacuum polarization contribution to  $(g - 2)_\mu$  by using QCD configurations with  $N_f = 2$  dynamical quarks produced by the Coordinated Lattice Simulations (CLS) initiative. The accuracy of lattice estimates of some relevant hadronic quantities has reached the percent level and so electromagnetic corrections cannot be neglected any longer. In Chap. 5 we discuss preliminary results on the QED corrections to the hadronic contribution to the muon anomaly.

---

*Direct Search:* Another way of testing possible extensions of the Standard Model is through lattice investigations of Strongly Interacting gauge theories with different gauge groups, fermions in representations possibly different from the fundamental one, and scalars. Such theories may provide viable models for Dynamical Electro-Weak Symmetry Breaking. An example of that is the Technicolor theory. Since the field is relatively young on the lattice, existing results so far are at the qualitative level. However times are ripe now to develop methods and algorithms in order to introduce some of the improvements already exploited in the lattice QCD field. For this reason any progress to render simulations easier is welcome but sophisticated algorithms and integrators are quite hard to optimize. In this sense we have worked on the optimization for the mass preconditioning and multi time-scale integrator in Beyond Standard Model theories, for the case of the Omelyan integrator using the measurements of the driving forces and their variances during the molecular dynamics step, in order to estimate Hamiltonian violations. In this kind of theories the balance between forces can be very different from the one in QCD and the need for a general strategy is urgent. The above mentioned work is presented in Chap. 4 where a general strategy to optimize algorithms for a class of Beyond Standard Model theories on the lattice is presented.

This work is divided in the following way:

- In Chap. 1 we review the main concepts at the heart of Lattice Gauge Theories with focus on the relevant topics for our studies.
- In Chap. 2 we discuss how to implement QED on a finite volume with periodic boundary conditions, where the so called zero mode problem arises. The main focus there is on the so-called L regularization of the zero mode and the massive approach.
- In Chap. 3 we present the use of reweighting techniques to compensate for the breaking of unitarity caused by the use of different boundary conditions for valence and sea quarks.
- In Chap. 4 we give a recipe for the optimization of HMC performances in Beyond Standard Model theories making use of the existence of an exactly conserved quantity, the Shadow Hamiltonian.
- In Chap. 5 we present preliminary results on the electromagnetic corrections on the hadronic vacuum polarization relevant for the muon anomaly. There we suggest a new strategy to isolate such effects.
- Chap. 6 contains the conclusions with the main results given in this work and outlooks.





# Chapter 1

## Elements of non-Abelian lattice gauge theories

In this chapter we briefly review the relevant concepts for the simulations of *non-Abelian* quantum gauge theories on the lattice. We specialize to the known example of Quantum Chromodynamics (QCD). Lattice regularization is a first principle systematically-improvable tool to address non-perturbative physics. Lattice QCD has been successfully applied to calculations of many properties of hadrons. Most importantly for determinations of fundamental parameters of the Standard Model, such as quark masses, strong coupling constant, and calculations of form factors, needed for the Cabibbo-Kobayashi-Maskawa matrix elements. Furthermore the lattice gives good control of statistical as well as systematic errors, e.g. continuum, infinite volume and chiral extrapolations. This chapter does not intend to give a complete description of non-Abelian lattice gauge theories but more of a review on the main concepts covered by this work.

The chapter is organized as follows; in Section 1 we briefly review the fields content in QCD and the definition of a lattice. In section 2 we review the symmetries associated to a QCD-like theory and how they can be realized at the quantum level. There we concentrate on *chiral* symmetry, particularly relevant for Wilson fermions on the lattice. In Section 3 we sketch the renormalization procedure on a general ground and we review the concept of *asymptotic freedom* and *dimensional transmutation*. In Section 4 we present the lattice regularization and postulate the gauge and fermion action in the Wilson formulation. We also review the Nielsen-Ninomiya no-go theorem, which predicts the existence of *doublers*, cured with Wilson fermions. In Section 5 we show how to systematically reduce the discretization effects to  $O(a^2)$  for on-shell quantities. We specialize to the  $O(a)$  improvement of the action through the introduction of the so-called *clover* term. Section 6 contains a discussion on the the critical mass, i.e. the bare mass for which the Wilson fermions on the lattice become massless, and how it emerges from the explicit *hard* breaking of chiral symmetry. Section 7 contains a general discussion about the Hybrid Monte Carlo method relevant for the generation of gauge configurations on the lattice.

### 1.1 QCD formal theory

The theory of Quantum Chromodynamics (QCD) is the result of many ideas and experimental results, its aim is to explain the strong force between elementary constituents of matter: quarks and gluons. The particles that participate in the strong force are the *hadrons* and they are divided in two classes:

- *Baryons*, e.g. protons, neutrons, etc., that have spin 1/2, 3/2, ... (fermions),
- *Mesons*, e.g. pions, kaons, etc., that have integer spin 0, 1, ... (bosons).

The concept of quarks arose from the need to have a realization at the Lagrangian level of the  $\mathbf{SU}(N_f)$  flavor symmetry that is observed in the low mass spectrum of mesons and baryons ( $N_f$  being the number of fermion species).

The starting point for the quantization procedure through the Feynman path integral is the classical action, given as the integral over the space-time volume of the Lagrangian density

$$S(A, \psi, \bar{\psi}) = \int d^4x \mathcal{L}(A, \psi, \bar{\psi}). \quad (1.1.1)$$

In QCD the action is a functional of gluon ( $A$ ) and quark fields ( $\bar{\psi}, \psi$ ) and is invariant under  $\mathbf{SU}(N_c)$  gauge transformations, with  $N_c = 3$  number of colors in the QCD case. The QCD Lagrangian describes the interaction between spin 1/2 quarks with mass  $m$  and massless spin 1 gluons. It is given by

$$\mathcal{L}_{\text{QCD}} = -\frac{1}{4} F_{\mu\nu}^a F_{\mu\nu}^{a} + \sum_f^{N_f} \bar{\psi}_f (i\not{D} - m_f) \psi_f, \quad (1.1.2)$$

where natural units are used ( $\hbar = c = 1$ ) and  $F_{\mu\nu}^a$  is the field strength tensor

$$F_{\mu\nu}^a = \partial_\mu A_\nu^a - \partial_\nu A_\mu^a - gf^{abc} A_\mu^b A_\nu^c. \quad (1.1.3)$$

The indexes  $a, b$  and  $c$  run over the  $N_c^2 - 1$  color degrees of freedom,  $f^{abc}$  are the structure constants of the  $\mathbf{SU}(N_c)$  group,  $g$  is the coupling constant of the strong interaction,  $\not{D} = \gamma_\mu D^\mu$  is the covariant derivative  $D_\mu = \partial_\mu + igA_\mu$ , the  $\gamma$  matrices satisfy the anticommutation relation  $\{\gamma^\mu, \gamma^\nu\} = 2g^{\mu\nu}$ , where  $g^{\mu\nu}$  is the metric tensor of the Minkowski space-time. In principle nothing forbids to write a  $\theta$ -term in the action as

$$\theta \epsilon^{\mu\nu\sigma\rho} F_{\mu\nu}^a F_{\rho\sigma}^a, \quad (1.1.4)$$

that breaks parity and time-reversal symmetries, with  $\epsilon^{\mu\nu\sigma\rho}$  antisymmetric tensor and  $\theta$  real parameter. Here we assume those symmetries to be conserved, as there is no experimental evidence of such a violation in QCD.

The third term of the gluon field strength tensor in Eq. 1.1.3 gives rise to a three- and four-gluons vertexes in Eq. 1.1.2. That is a peculiarity of non-Abelian theories, in fact there is no analogous term in QED where the gauge group is Abelian.

The dimensions, in unit of mass, of the fields are:

- fermion spin 1/2 fields  $[\psi]=3/2$ ,
- boson spin 1 fields  $[A]=1$ .

QCD is formulated in Minkowski space and by employing a Wick transformation we *rotate* to the Euclidean space. The rotation can be done if the Osterwalder-Schrader reflection positivity condition is fulfilled (Osterwalder and Schrader, 1973, Osterwalder and Schrader, 1975). The Euclidean continuum space is then replaced by a discretized finite box (lattice)

$$\Lambda = \{x = (x_0, x_1, x_2, x_3) : x_\mu = an_\mu, n_\mu \in [0, L_\mu] \subset \mathbb{Z}\},$$

where  $a$  is the separation between points on the lattice (*lattice spacing*) and  $L_\mu$  is the lattice extent in direction  $\mu$ . Boundary conditions have to be chosen and usually periodic ones are employed to

retain translational invariance of the theory.

The quantization procedure is then carried out by means of the Feynman path integral. The partition function is defined as

$$\mathcal{Z} = \int \mathcal{D}[A, \psi, \bar{\psi}] e^{-S_{\text{QCD}}(A, \psi, \bar{\psi})}, \quad (1.1.5)$$

where  $\mathcal{D}[A, \psi, \bar{\psi}]$  is the path integral measure. The path integral defined in this way is ill-defined because of gauge ambiguities, we will introduce the gauge fixing procedure in Sect. 2.3.1. The expectation value of an operator  $\mathcal{O}$  is then given as

$$\langle \mathcal{O} \rangle = \frac{1}{\mathcal{Z}} \int \mathcal{D}[A, \psi, \bar{\psi}] \mathcal{O}(A, \psi, \bar{\psi}) e^{-S_{\text{QCD}}(A, \psi, \bar{\psi})}. \quad (1.1.6)$$

## 1.2 Symmetries of QCD-like theories

We consider a QCD-like formal theory in Euclidean space with a degenerate doublet of quarks<sup>1</sup>  $\Psi = (u, d)^t$ , i.e.  $m_u = m_d \equiv m$ . The Lagrangian for such a theory reads

$$\mathcal{L}[A, \Psi, \bar{\Psi}] = \mathcal{L}_{\text{YM}} + \mathcal{L}_{\text{F}} = \frac{1}{4} F_{\mu\nu}^a F_{\mu\nu}^a + \bar{\Psi}(x) (\not{D} + M) \Psi(x), \quad (1.2.7)$$

where  $M$  is the mass matrix in *flavor* space. The above Lagrangian exhibits the following symmetry groups:

- *Poincaré = Lorentz + space-time translations* group, which is the semi-direct product of the groups

$$\mathbf{T} \rtimes \mathbf{SO}(4).$$

- Local (gauge) group of *color*,  $N_c = 3$

$$\mathbf{SU}(N_c).$$

- When the masses vanish,  $m = 0$ , there is the additional global *chiral* symmetry

$$\mathbf{U}(2)_{\text{L}} \otimes \mathbf{U}(2)_{\text{R}} \sim \mathbf{U}(1)_{\text{V}} \otimes \mathbf{U}(1)_{\text{A}} \otimes \mathbf{SU}(2)_{\text{L}} \otimes \mathbf{SU}(2)_{\text{R}}.$$

Symmetries lead to conservation of *Noether currents*,  $\partial_\mu J_\mu = 0$ , in the classical theory. By integrating over space the temporal component of the current we obtain the conserved *charge Q* along a solution of the equation of motion.

$$Q \equiv \int_{\mathbb{R}^3} J_0 d^3x, \quad (1.2.8)$$

$$\int_{\mathbb{R}^3} \partial_\mu J_\mu d^3x = \int_{\mathbb{R}^3} \partial_0 J_0 d^3x + \int_{\mathbb{R}^3} \nabla \cdot \underline{J} d^3x = \frac{\partial}{\partial x_0} \int_{\mathbb{R}^3} J_0 d^3x = \frac{\partial Q}{\partial x_0} \equiv 0, \quad (1.2.9)$$

where we have used that fields are localized in space and they vanish “quick enough” at infinity<sup>2</sup>. The charge operator generates symmetry transformations when acting on the fields.

The symmetries of a quantum field theory can be realized in three different ways:

- à la Wigner (exact symmetry).
- à la Nambu-Goldstone (spontaneously broken symmetry).
- Anomalous (not realized symmetry).

<sup>1</sup>This choice correspond to the so-called *isospin symmetric limit*.

<sup>2</sup>On the lattice we can think to have chosen periodic boundary conditions

**Wigner** The vacuum of the theory  $|0\rangle$  is invariant under the correspondent transformation, namely

$$\hat{Q}|0\rangle = 0. \quad (1.2.10)$$

In this situation particles form symmetry *multiplets* and particles in the same multiplet have same mass.

**Nambu-Goldstone** The vacuum is not invariant under the transformation, i.e.

$$\hat{Q}|0\rangle \neq 0. \quad (1.2.11)$$

In that case particles do not form degenerate multiplets. Nonetheless *Goldstone theorem* (Goldstone, 1961) states: for each charge  $Q$  of the spontaneously broken symmetry exists a massless scalar particle, called *Goldstone boson*.

We remark that Wigner and Nambu-Goldstone realizations do not exclude each other. For example a symmetry group  $\mathbf{G}$  can be partially broken to a proper subgroup  $\mathbf{H} \subset \mathbf{G}$ . The symmetry in  $\mathbf{H}$  is then realized à la Wigner while the remnant, the coset  $\mathbf{G}/\mathbf{H}$ , is realized à la Nambu-Goldstone.

**Anomalous** A symmetry is *anomalous* if it is an exact symmetry at the level of the action but it is not preserved as a symmetry of the path integral. If the Action is invariant under the symmetry, the invariance can be “lost” from the integration measure or from the specification of boundary conditions. Even though the anomaly raises from a particular choice of the regularization it is independent of that. If a global symmetry is anomalous then it contributes finitely to a physical process, as the  $\mathbf{U}_A(1)$  in QCD.

### 1.2.1 $\mathbf{SU}(2)_L \otimes \mathbf{SU}(2)_R$

We start from the *vector* and *axial* transformations

$$\mathbf{SU}(2)_V : \Psi \rightarrow e^{-i\omega_f \sigma_f / 2} \Psi \simeq \left(1 - i\omega_f \frac{\sigma_f}{2}\right) \Psi, \quad \bar{\Psi} \rightarrow \bar{\Psi} e^{i\omega_f \sigma_f / 2} \simeq \bar{\Psi} \left(1 + i\omega_f \frac{\sigma_f}{2}\right), \quad (1.2.12)$$

$$\mathbf{SU}(2)_A : \Psi \rightarrow e^{i\omega_f \sigma_f \gamma_5 / 2} \Psi \simeq \left(1 + i\omega_f \frac{\sigma_f}{2} \gamma_5\right) \Psi, \quad \bar{\Psi} \rightarrow \bar{\Psi} e^{i\omega_f \sigma_f \gamma_5 / 2} \simeq \bar{\Psi} \left(1 + i\omega_f \frac{\sigma_f}{2} \gamma_5\right), \quad (1.2.13)$$

where the  $\sigma_f$  are the Pauli matrices in flavor space. The associated conserved currents are

$$J_\mu^{Vf} \equiv V_\mu^f = \frac{1}{2} \bar{\Psi} \sigma_f \gamma_\mu \Psi, \quad J_\mu^{Af} \equiv A_\mu^f = \frac{1}{2} \bar{\Psi} \sigma_f \gamma_\mu \gamma_5 \Psi. \quad (1.2.14)$$

From the above currents we can define the charges  $\hat{Q}_V^f$  and  $\hat{Q}_A^f$ , and by considering them as operators we find that they obey to the so-called *charge algebra*

$$\left[\hat{Q}_V^f, \hat{Q}_V^g\right] = i\epsilon^{fgh} \hat{Q}_V^h, \quad \left[\hat{Q}_A^f, \hat{Q}_V^g\right] = i\epsilon^{fgh} \hat{Q}_A^h, \quad \left[\hat{Q}_A^f, \hat{Q}_A^g\right] = i\epsilon^{fgh} \hat{Q}_V^h. \quad (1.2.15)$$

The Pauli matrices are the generators of the transformations and they belong to the *Lie algebra* of  $\mathbf{SU}(2)$  that we denote as<sup>3</sup>  $\mathfrak{su}(2)$ . Even though the  $\mathbf{SU}(2)_A$  is not closed, as clear from the charge

<sup>3</sup>The  $\mathfrak{su}(2)$  algebra contains *hermitian* and *traceless*  $2 \times 2$  matrices.

algebra relations, we can factorize the vector and axial algebras by considering the two groups  $\mathbf{SU}(2)_L$  and  $\mathbf{SU}(2)_R$ .

In order to write the *left* and *right* transformations we define the correspondent *projectors*

$$P_{L/R} = \frac{1 \mp \gamma_5}{2}, \quad (1.2.16)$$

from which we write down the projected spinors

$$\Psi_{L/R} = \frac{1 \mp \gamma_5}{2} \Psi, \quad \bar{\Psi}_{L/R} = \bar{\Psi} \frac{1 \pm \gamma_5}{2}. \quad (1.2.17)$$

The transformations in the new basis are

$$\mathbf{SU}(2)_L : \quad \Psi_L \rightarrow e^{i\omega_{Lf}\sigma_f} \Psi_L \simeq (1 + i\omega_{Lf}\sigma_f) \Psi_L, \quad \bar{\Psi}_L \rightarrow \bar{\Psi}_L e^{-i\omega_{Lf}\sigma_f} \simeq \bar{\Psi}_L (1 - i\omega_{Lf}\sigma_f), \quad (1.2.18)$$

$$\mathbf{SU}(2)_R : \quad \Psi_R \rightarrow e^{i\omega_{Rf}\sigma_f} \Psi_R \simeq (1 + i\omega_{Rf}\sigma_f) \Psi_R, \quad \bar{\Psi}_R \rightarrow \bar{\Psi}_R e^{-i\omega_{Rf}\sigma_f} \simeq \bar{\Psi}_R (1 - i\omega_{Rf}\sigma_f). \quad (1.2.19)$$

In this form the two Lie algebras are closed, i.e. they are factorized and written as  $\mathfrak{su}(2)_L \otimes \mathfrak{su}(2)_R$ . If we put  $\omega_L = \omega_R$  we obtain again the vector case, indeed the latter is a *sub-algebra*

$$\mathfrak{su}(2)_V \subset \mathfrak{su}(2)_L \otimes \mathfrak{su}(2)_R.$$

When the quark masses do not vanish,  $m \neq 0$ , some of the aforementioned symmetries are broken. The group  $\mathbf{SU}(2)_L \otimes \mathbf{SU}(2)_R$  suffers from two kind of symmetry breaking:

1. *explicit*, but *soft*<sup>4</sup>, when  $m \neq 0$ ,
2. *spontaneous*, à la Nambu-Goldstone.

**Explicit symmetry breaking** This kind of breaking is due to different and not vanishing quark masses (in QCD only).

When the breaking is due to an operator with dimension smaller than 4 the UV divergences are the same of the theory without its presence. The parameter, in front of the operator, is then multiplicatively renormalizable (Weinberg, 1973).

**Spontaneous symmetry breaking** The group is spontaneously broken to the vector subgroup

$$\mathbf{SU}(2)_L \otimes \mathbf{SU}(2)_R \rightarrow \mathbf{SU}(2)_V$$

which remain an exact symmetry since we are working in the isospin symmetric limit.

The  $\mathbf{SU}(2)_V$  symmetry is realized à la Wigner while  $\mathbf{SU}(2)_A$  à la Nambu-Goldstone. This means that the QCD vacuum has to satisfy

$$\hat{Q}_V^f |0\rangle = 0, \quad \hat{Q}_A^f |0\rangle \neq 0. \quad (1.2.20)$$

The  $N_f^2 - 1$  Goldstone bosons are the pions (in  $N_f = 2$ ), which have zero mass for vanishing quark masses  $m = 0$ .

---

<sup>4</sup>In this context means that the introduced divergences are only logarithmic.

## 1.3 Renormalization

The Lagrangian in Eq. 1.1.2 is the starting point for the quantization of the theory and is called *bare* Lagrangian. The procedure of quantization leads to interpret fields as operators that act on the Hilbert space of the physical states. For a given physical process, during the evolution from the initial to the final state, intermediate off-shell particles also play a rôle. These virtual degrees of freedom lead to UV divergences in the perturbative expansion of the Green's functions in the quantum theory. The perturbative expansion is carried out through a loop expansion that is a formal expansion in powers of  $\hbar$  of the functional generator of the theory.

The strategy to give meaning to a quantum field theory is divided in two steps:

1. Regularization. The regularization modifies the behavior in the high energy region by introducing, for example, an energy cutoff<sup>5</sup>  $\Lambda$ . The regularized theory always leads to finite results.
2. Renormalization. One calculates, in the regularized theory, physical quantities in number equal to the number of free parameters that enter in the bare Lagrangian. Holding fixed these calculated quantities one performs the limit  $\Lambda \rightarrow \infty$ , that generates in the couplings a dependence upon  $\Lambda$ .

If at the end of the procedure all the observables stay finite as  $\Lambda \rightarrow \infty$  then the theory is renormalizable. One can prove this is the case in  $d = 4$  space-time dimensions if the Lagrangian density contains only operators<sup>6</sup> with dimension  $d_O \leq 4$ .

The choice of the renormalization conditions (e.g. the Green's functions on which they are imposed and their precise values) and of the renormalization point  $\mu$  (i.e. the momentum scale at which the conditions are imposed) is conventional. Such choices characterize what is called *renormalization scheme*. There are important remarks, which we should have in mind when we build a renormalizable field theory:

- In a given renormalization scheme, renormalized Green's functions (and derived quantities) are independent of the UV-regularization. This leads to the concept of *universality* in Quantum Field Theory.
- Physical observables are independent of the renormalization scheme.
- Renormalized parameters as well as renormalization conditions can be chosen conventionally (e.g. mass independent schemes). Conventional renormalized parameters can always be eliminated in favor of (an equal *finite* number of) physical quantities. A theory predicts only relationships among physical quantities.

### 1.3.1 Asymptotic freedom

The running of the coupling constant is governed by the QCD beta function, at one-loop in perturbation it is found to be

$$\mu \frac{\partial g}{\partial \mu} = \beta(g) = -\frac{g^3}{16\pi^2} \left( \frac{11N_c - 2N_f}{3} \right) + \mathcal{O}(g^5) \equiv -\frac{b}{2}g^3, \quad (1.3.21)$$

<sup>5</sup>In the case of a lattice this is done by lattice spacing  $a \propto 1/\Lambda$ .

<sup>6</sup>We can also add operators with  $d_O > 4$  scaled by inverse powers of the UV cutoff ( $1/\Lambda^{d_O-4}$ ) as long as we do not include the associated parameters in the set of free parameters to be kept fixed in the renormalization step.

where  $N_c = 3$  and  $N_f \leq 6$  (“active” flavors). Upon increasing the energy scale  $\mu$ , the strong charge decreases and in the limit of high energy scale it vanishes. This is the reason why QCD is an asymptotically free theory, for  $b > 0$ .

By solving the one-loop beta function in Eq. 1.3.21 we can investigate the behavior of the strong coupling constant. When  $g^2(\mu_1)$  and  $g^2(\mu_2)$  are both in the perturbative region, we obtain

$$g^2(\mu_2) = \frac{g^2(\mu_1)}{1 + bg^2(\mu_1) \ln \mu_2/\mu_1}. \quad (1.3.22)$$

From the above equation we see that by fixing  $g(\mu_1)$  to be in the perturbative region then for  $\mu_2 > \mu_1$  the coupling is decreasing and still in that region.

Usually in the literature the  $\Lambda_{\text{QCD}}$  parameter is defined, i.e. an integration constant of the Renormalization Group Equations. At one-loop it is given by

$$g^2(\mu) = \frac{1}{b \ln \frac{\mu}{\Lambda_{\text{QCD}}}}. \quad (1.3.23)$$

From the knowledge of the value  $g^2$  at the scale  $\mu$  one obtains at which scale the perturbation theory ceases to be valid. For  $\mu \simeq \Lambda_{\text{QCD}}$  the coupling becomes large. In that region hadrons are the real physical degrees of freedom. A state can propagate freely if and only if it is colorless, according to the *confinement hypothesis*, i.e. in asymptotically free theories only singlet states under gauge force can be asymptotic states.

### 1.3.2 Hadron masses

Let be  $M_H$  the mass of a given hadron that is a composite state of quarks and gluons in QCD with massless quarks. For dimensional reasons the renormalized mass at the renormalization point will be

$$M_H = \mu f_H(g(\mu)), \quad (1.3.24)$$

where  $f_H$  is a typical dimensionless function of the given hadron. The hadron mass cannot depend on the choice of the renormalization point, meaning that

$$\frac{dM_H}{d\mu} = 0 = f_H(g) + \beta(g) \frac{\partial f_H}{\partial g}. \quad (1.3.25)$$

By using the one-loop beta function in Eq. 1.3.21 we find the solution

$$M_H = c_H \mu \exp\left(-\frac{1}{bg^2}\right), \quad (1.3.26)$$

where  $c_H$  is an integration constant. If we substitute  $\Lambda_{\text{QCD}}$  from Eq. 1.3.23 we may rewrite the solution as

$$M_H = c_H \Lambda_{\text{QCD}}. \quad (1.3.27)$$

The above equation shows the non-perturbative feature of the hadron masses. All the hadronic masses can be expressed in terms of the same fundamental scale  $\Lambda_{\text{QCD}}$ .

## 1.4 Lattice regularization

The Euclidean lattice quantum field theory, postulated by Wilson (Wilson, 1974), represents an invariant regularization of the theory described by the Lagrangian in Eq. 1.2.7, where the rôle of the cut-off is played by the inverse of the lattice spacing  $a$ .



The gauge fields on the lattice are introduced as elements of the gauge group  $U_\mu(x) \in \mathbf{SU}(N_c)$ . They are related to the algebra through the exponentiation

$$U_\mu(x) = \exp \left[ ia A_\mu^a(x + a\hat{\mu}) T^a \right], \quad (1.4.28)$$

with  $T^a$  the  $N_c^2 - 1$  generators. They live on the links that connect the site  $x$  to  $x + a\hat{\mu}$  and for this reason they are usually called *links*. Fermions are described by Grassmann variables, i.e. anticommuting fields, and they live on the sites of the lattice and carry Dirac and color indexes. The way to deal with fermions is to introduce *pseudofermions*, i.e. boson variables with the wrong statistics, in the generation of configurations, as we will see in Sect. 1.7. In addition, for fermionic observables, Wick contractions are employed, meaning that we calculate the exact fermionic contribution on each gauge field background.

Any form of the action on the lattice is allowed as long as it reproduces the correct formal theory Eq. 1.2.7 in the naive continuum limit, i.e.  $a \rightarrow 0$ , it is gauge invariant and a Lorentz scalar. In this sense a lattice action is not unique. In the lattice community a variety of gauge actions have been employed: Wilson plaquette (Wilson, 1974), Luscher-Weisz (Luscher and Weisz, 1985), Iwasaki glue (Iwasaki, 1985), etc; and fermion actions: Wilson (Wilson, 1974), staggered (Kogut and Susskind, 1975), twisted mass (Frezzotti *et al.*, 2000), domain wall (Kaplan, 1992), overlap, etc. We present here the Wilson plaquette gauge action and Wilson fermions, relevant for the rest of the work.

### 1.4.1 Wilson plaquette gauge action

The Wilson plaquette action is given by

$$S_G = \beta \sum_{\mu < \nu} \left( 1 - \frac{1}{N_c} \Re \text{Tr} P_{\mu\nu} \right), \quad (1.4.29)$$

where  $\beta = 2N_c/g_0^2$ , and  $P_{\mu\nu}$  the plaquette in the  $(\mu, \nu)$  plane,

$$P_{\mu\nu} = U_\mu(x) U_\nu(x + a\hat{\mu}) U_\mu^\dagger(x + a\hat{\nu}) U_\nu^\dagger(x). \quad (1.4.30)$$

The action is gauge invariant and reproduces the formal Yang-Mills (YM) action up to  $O(a^2)$  discretization errors.

### 1.4.2 Fermionic action

We write the action for a fermion as

$$S_F = \sum_{x, y \in \Lambda} \bar{\psi}(x) D(x, y) \psi(y).$$

In many Beyond Standard Model (BSM) strongly interacting theories the representation for the fermions is varied. For the sake of simplicity we consider throughout this introductory chapter the fermion to transform under the fundamental representation of the gauge group.

#### Naïve fermions

The naïve fermion action is given by the discretized version of the formal one by replacing the derivative with the central discretized derivative,

$$S_{\text{NF}} = a^4 \sum_{x \in \Lambda} \sum_{\mu} \bar{\psi}(x) \left[ \gamma_\mu \bar{\nabla}_\mu + m_0 \right] \psi(x). \quad (1.4.31)$$

Where we have defined the  $\nabla^\pm$  forward and backward derivatives, and  $\bar{\nabla}$  the symmetric derivative

$$\begin{aligned}\nabla_\mu^+ \psi(x) &= \frac{1}{a} [U_\mu(x)\psi(x + a\hat{\mu}) - \psi(x)], \\ \nabla_\mu^- \psi(x) &= \frac{1}{a} [\psi(x) - U_\mu^\dagger(x - a\hat{\mu})\psi(x - a\hat{\mu})], \\ \bar{\nabla}_\mu \psi(x) &\equiv \frac{\nabla_\mu^+ + \nabla_\mu^-}{2} = \frac{1}{2a} [U_\mu(x)\psi(x + a\hat{\mu}) - U_\mu^\dagger(x - a\hat{\mu})\psi(x - a\hat{\mu})].\end{aligned}\quad (1.4.32)$$

The propagator at tree-level, i.e.  $U_\mu = \mathbf{1}$ , is found by transforming in Fourier space and considering the inverse of the bilinear operator in the action in Eq. 1.4.31,

$$\tilde{D}^{-1}(p) = \frac{m - \frac{i}{a}\gamma^\mu \sin(ap_\mu)}{m^2 + \sum_\mu \left[ \frac{\sin(ap_\mu)}{a} \right]^2}.\quad (1.4.33)$$

The poles of the propagator correspond to on-shell particles that satisfies the correct energy dispersion relation. In the case of naïve fermions we obtain  $2^4 = 16$  fermions instead of one, that means there are 15 unphysical fermions. This is the well known *doublers* problem.

#### Nielsen-Ninomiya no-go theorem

A very nice review on the exact chiral symmetry on the lattice is given in Ref. (Luscher, 1998). The Nielsen-Ninomiya no-go theorem states that the following properties cannot hold at the same time:

1. Ultra-locality<sup>7</sup>. The Dirac operator in momentum space  $\tilde{D}(p)$  is analytic and periodic function of the momenta  $p_\mu$  with period  $2\pi/a$ .
2. Correct continuum behavior. For momenta far below the cutoff  $p_\mu \ll \pi/a$  the Dirac operator is  $\tilde{D}(p) = i\gamma_\mu p_\mu + O(ap^2)$ .
3. No doublers.  $\tilde{D}(p)$  is invertible  $\forall p_\mu \neq 0$  in the first Brillouin zone.
4. Exact chirality.  $\{D, \gamma_5\} = 0$  in the limit of vanishing mass.

#### Wilson fermions

In order to avoid doublers we introduce the Wilson term,  $-\frac{ar}{2}\bar{\psi}\nabla_\mu^-\nabla_\mu^+\psi$  an irrelevant operator<sup>8</sup>. Such an operator breaks in a *hard* way the symmetry  $\mathbf{SU}(2)_L \otimes \mathbf{SU}(2)_R$ . Chiral symmetry is restored in the continuum and massless limit, but on the lattice the limit  $m_0 \rightarrow 0$  does no longer correspond to the chiral limit. See Sect. 1.6.2 for further details.

The Wilson fermionic Lagrangian on the lattice is written as

$$\mathcal{L}_F = \bar{\psi}(x) \left[ \gamma_\mu \bar{\nabla}_\mu - \frac{ar}{2} \nabla_\mu^- \nabla_\mu^+ + m_0 \right] \psi(x),\quad (1.4.34)$$

<sup>7</sup>The interaction range is spread over a finite number of points on the lattice.

<sup>8</sup>Operators of dimension  $d > 4$  multiplied by a power  $d-4$  of the lattice spacing  $a^{d-4}$ . These are called irrelevant in the sense they do not destroy the renormalizability of the theory.

with  $r$  the Wilson parameter, usually set to one, and we have introduced the Laplacian

$$\begin{aligned}\nabla_\mu^- \nabla_\mu^+ \psi(x) &= \frac{1}{a^2} [U_\mu(x)\psi(x+a\hat{\mu}) - U_\mu^\dagger(x-a\hat{\mu})U_\mu(x)\psi(x) - \psi(x) + U_\mu^\dagger(x-a\hat{\mu})\psi(x-a\hat{\mu})] \\ &= \frac{1}{a^2} [U_\mu(x)\psi(x+a\hat{\mu}) + U_\mu^\dagger(x-a\hat{\mu})\psi(x-a\hat{\mu}) - 2\psi(x)].\end{aligned}\quad (1.4.35)$$

The Lagrangian on the lattice reads

$$\begin{aligned}\mathcal{L}_F &= \bar{\psi}(x) \left( m_0 + \frac{4r}{a} \right) \psi(x) + \\ &\quad + \frac{1}{2a} \sum_\mu [\bar{\psi}(x)U_\mu(x)(\gamma_\mu - r)\psi(x+a\hat{\mu}) - \bar{\psi}(x)U_\mu^\dagger(x-a\hat{\mu})(\gamma_\mu + r)\psi(x-a\hat{\mu})]\end{aligned}\quad (1.4.36)$$

$$\begin{aligned}&= \bar{\psi}(x) \left( m_0 + \frac{4r}{a} \right) \psi(x) \\ &\quad + \frac{1}{2a} \sum_\mu [\bar{\psi}(x)U_\mu(x)(\gamma_\mu - r)\psi(x+a\hat{\mu}) - \bar{\psi}(x+a\hat{\mu})U_\mu^\dagger(x)(\gamma_\mu + r)\psi(x)],\end{aligned}\quad (1.4.37)$$

in the last step we have shifted the space-time of the second term since when we consider the action, that is a sum over the whole space-time, a shift does not affect the result.

The Wilson term gives an additional mass proportional to  $2r/a$  to all the doublers. Hence in the continuum limit they get infinite mass and they decouple from the theory. It should be mentioned that the Wilson fermion action reproduces the formal fermionic one up to  $O(a)$  effects. The Osterwalder-Schrader reflection positivity condition was proven to hold for Wilson fermions at finite lattice spacing ([Luscher, 1977](#)).

## 1.5 Symanzik improvement programme

As we saw in the previous section discretization errors are typically of  $O(a^2)$  for the gauge action and of  $O(a)$  for the fermionic part. The Symanzik improvement programme ([Symanzik, 1983a](#), [Symanzik, 1983b](#)) gives a systematical reduction of the discretization effects. The central idea is to add irrelevant terms that eliminate the unwanted effects. To do so we write an effective action (and operators) that describes the behavior of the lattice theory at finite lattice spacing toward the continuum limit. Let us assume that the lattice action  $S$  generates  $O(a)$  discretization errors and it depends on the field  $\phi$  and a coupling  $g_0$ . The effective action can be written as

$$S_{\text{eff}} = S_0 + a \int d^4x \mathcal{L}_1(x) + O(a^2),\quad (1.5.38)$$

where  $S_0$  is the formal-continuum action we would like to reproduce as  $a \rightarrow 0$ , and  $\mathcal{L}_1$  is given by linear combination of operators of dimension 5 that have the same symmetry of the lattice action  $S$ . Similarly we write for the field

$$\phi_{\text{eff}}(x) = \phi_0(x) + a\phi_1(x) + O(a^2),\quad (1.5.39)$$

where  $\phi_0$  is the continuum counterpart and  $\phi_1$  is a  $d+1$  dimensional operator, if  $d = [\phi_0]$ , with same quantum numbers as  $\phi$ .

The strategy is to look at expectation values of composite effective operators and expand it in  $a$

through the formulae given above,

$$\begin{aligned} \langle \phi_{\text{eff}}(x_1) \phi_{\text{eff}}(x_2) \dots \phi_{\text{eff}}(x_n) \rangle &= \langle \phi_0(x_1) \phi_0(x_2) \dots \phi_0(x_n) \rangle - a \int d^4z \langle \phi_0(x_1) \phi_0(x_2) \dots \phi_0(x_n) \mathcal{L}_1(z) \rangle \\ &\quad + a \sum_{k=1}^n \langle \phi_0(x_1) \phi_0(x_2) \dots \phi_1(x_k) \dots \phi_0(x_n) \rangle + O(a^2), \end{aligned} \quad (1.5.40)$$

where the expectation values on the r.h.s. are taken in the formal theory with action  $S_0$ . Then we modify the lattice action  $S$  and the field  $\phi$  by higher dimensional operators such that they cancel the  $O(a)$  terms in the equation. Contact terms can arise from the integration over the space-time, i.e. when  $z = x_k$  for some  $k$ , and a prescription should be given to treat them. They can be included in a redefinition of the field  $\phi_1$  and we do not worry about them in the following.

### 1.5.1 $O(a)$ improved action

Here we briefly review the improvement for the Wilson fermion action. The final result has  $O(a^2)$  cutoff effects. The Lagrangian  $\mathcal{L}_1$  can be written as linear combination of the following fields

$$\mathcal{O}_1 = \bar{\psi} i \sigma_{\mu\nu} F_{\mu\nu} \psi, \quad (1.5.41)$$

$$\mathcal{O}_2 = \bar{\psi} D_\mu D_\mu \psi + \bar{\psi} \overleftarrow{D}_\mu \overleftarrow{D}_\mu \psi, \quad (1.5.42)$$

$$\mathcal{O}_3 = m \text{Tr} [F_{\mu\nu} F_{\mu\nu}], \quad (1.5.43)$$

$$\mathcal{O}_4 = m \left( \bar{\psi} \gamma_\mu D_\mu \psi - \bar{\psi} \overleftarrow{D}_\mu \gamma_\mu \psi \right), \quad (1.5.44)$$

$$\mathcal{O}_5 = m^2 \bar{\psi} \psi. \quad (1.5.45)$$

We can eliminate redundant terms if we restrict ourself to improvement of *on-shell quantities*, for which the equations of motion can be used. After this step we are left with the operators in Eqs. 1.5.41, 1.5.43 and 1.5.45. Another reduction can be made by noticing that the operators  $\mathcal{O}_3$  and  $\mathcal{O}_5$  are already present in the original Lagrangian. Hence their insertion amount in a rescaling of the bare coupling  $g_0$  and mass  $m_0$ . Finally for the improved action we obtain (Sheikholeslami and Wohlert, 1985)

$$S_{\text{IMP}} = S_{\text{F}} + a^5 \sum_{x \in \Lambda} c_{\text{SW}} \bar{\psi}(x) \frac{i}{4} r \sigma_{\mu\nu} \widehat{F}_{\mu\nu}(x) \psi(x), \quad (1.5.46)$$

where  $\sigma_{\mu\nu} = \frac{1}{2} [\gamma_\mu, \gamma_\nu]$  and  $\widehat{F}_{\mu\nu} = \frac{1}{8i} [Q_{\mu\nu}(x) - Q_{\nu\mu}(x)]$ , with the definition

$$\begin{aligned} Q_{\mu\nu}(x) &= U_\mu(x) U_\nu(x + a\hat{\mu}) U_\mu^\dagger(x + a\hat{\nu}) U_\nu^\dagger(x) + U_\nu(x) U_\mu^\dagger(x - a\hat{\mu} + a\hat{\nu}) U_\nu^\dagger(x - a\hat{\mu}) U_\mu(x - a\hat{\mu}) \\ &\quad + U_\mu^\dagger(x - a\hat{\mu}) U_\nu^\dagger(x - a\hat{\mu} - a\hat{\nu}) U_\mu(x - a\hat{\mu} - a\hat{\nu}) U_\nu(x - a\hat{\nu}) \\ &\quad + U_\nu^\dagger(x - a\hat{\nu}) U_\mu(x - a\hat{\nu}) U_\nu(x + a\hat{\mu} - a\hat{\nu}) U_\mu^\dagger(x). \end{aligned} \quad (1.5.47)$$

## 1.6 Ward-Takahashi identities

The Ward-Takahashi identities (WTIs) are obtained by imposing that expectation values are invariant under transformations of fermionic variables that are symmetries. For simplicity, in the following we omit the Yang-Mills part of the action. The Ward-Takahashi identities are the true content of a symmetry, as the Noether theorem is in the classical theory. At the quantum level, thanks to these identities, we have an infinite set of relations among quantities. The concepts presented here will be used in Chap. 3, where we investigate the change of the critical mass in small volumes due to twisted boundary conditions.

### 1.6.1 Formal theory

In this section we derive the naïve WTI for the  $\mathbf{SU}(2)_V$  and  $\mathbf{SU}(2)_A$  transformations. For a formal derivation of the WTI structure see App. A, in the following we use a local operator  $\mathcal{O}(y)$  for the sake of simplicity. We read the fermionic action from Eq. 1.2.7, and we assume that the mass matrix is proportional to the identity in flavor space  $M = m\mathbf{1}$ .

#### $\mathbf{SU}(2)_V$

The infinitesimal transformations are written in Eq. 1.2.12. The associated WTI is

$$\partial_\mu^x \langle V_\mu^f(x) \mathcal{O}(y) \rangle = \delta^4(x-y) \langle \delta \mathcal{O}(y) \rangle, \quad (1.6.48)$$

where  $V_\mu^f$  is given in Eq. 1.2.14.

#### $\mathbf{SU}(2)_A$

The infinitesimal transformations are given in Eq. 1.2.13. The associated WTI is

$$\begin{aligned} \partial_\mu^x \langle A_\mu^f(x) \mathcal{O}(y) \rangle &= 2m \langle P^f(x) \mathcal{O}(y) \rangle + \delta^4(x-y) \langle \delta \mathcal{O}(y) \rangle \\ &\stackrel{m=0}{=} \delta^4(x-y) \langle \delta \mathcal{O}(y) \rangle, \end{aligned} \quad (1.6.49)$$

where  $A_\mu^f$  is given in Eq. 1.2.14 and

$$P^f \equiv \bar{\Psi} \frac{\sigma_f}{2} \gamma_5 \Psi. \quad (1.6.50)$$

We see that the axial current  $A_\mu^f$  is not conserved if  $m \neq 0$ , since there is an explicit symmetry breaking. The above equation in the case of  $m \neq 0$  is called *partially conserved axial current* (PCAC) *relation* and the mass term defined in this way is called  $m_{\text{PCAC}}$ .

By assuming the fields in  $\mathcal{O}$  to be localized outside a region  $R$ , in which the parameter  $\omega_f(x)$  lives, the variation of the operator vanishes  $\delta \mathcal{O} = 0$  and we obtain

$$\partial_\mu^x \langle A_\mu^f(x) \mathcal{O}(y) \rangle = 2m \langle P^f(x) \mathcal{O}(y) \rangle. \quad (1.6.51)$$

### 1.6.2 Critical mass on the lattice

For the derivation of the vector and axial current on the lattice with Wilson fermions see App. A. The vector current on the lattice satisfies the naïve WTI, up to cutoff effects, but for the axial case the relation is not straightforward (Bochicchio *et al.*, 1985). A very nice review on broken symmetries is given in Ref. (Testa, 1998). The main issue there is that the variation under axial transformations of the Wilson term,  $\chi_A^f$ , cannot be recast as a total derivative. That means we are left with an *unwanted piece*. We report here the bare PCAC relation on the lattice

$$\partial_\mu^- \langle A_\mu^f(x) \mathcal{O}(y) \rangle = 2m_0 \langle P^f(x) \mathcal{O}(y) \rangle + \langle \chi_A^f(x) \mathcal{O}(y) \rangle. \quad (1.6.52)$$

We know that in the formal classical limit  $\chi_A^f$  has to vanish, its general form is an operator of dimension 5 times the lattice spacing  $\chi_A^f = a\mathcal{O}_5$ , and the said operator may contain power divergences that compensate the factor  $a$ .

Hence the task is to build a finite operator out of  $\mathcal{O}_5$  by renormalization procedure. We know from renormalization that composite operators mix under renormalization with operators of the same

and lower dimension. There are no operators of dimension 5 entering in the mixing (Curci, 1986), which would appear with logarithmically divergent coefficients, hence we can write

$$\overline{\mathcal{O}}_5 = Z_5 \left[ \mathcal{O}_5 + \frac{2\overline{m}}{a} P^f + \frac{Z_A - 1}{a} \partial_\mu^- A_\mu^f \right]. \quad (1.6.53)$$

The coefficients  $\overline{m}$  and  $Z_A$  do not run with the scale, and  $Z_5$  is a logarithmically divergent coefficient. By substituting back in the bare PCAC relation the above equation we obtain

$$\partial_\mu^- \langle \hat{A}_\mu^f(x) \mathcal{O}(y) \rangle = 2(m_0 - \overline{m}) \langle P^f(x) \mathcal{O}(y) \rangle + \langle \overline{\chi}_A^f(x) \mathcal{O}(y) \rangle, \quad (1.6.54)$$

where  $\hat{A}_\mu^f \equiv Z_A A_\mu^f$  and  $\overline{\chi}_A^f \equiv a \overline{\mathcal{O}}_5 / Z_5$ .

Now we enforce the condition  $\langle \overline{\chi}_A^f(x) \mathcal{O}(y) \rangle \rightarrow 0$  as  $a \rightarrow 0$ . By choosing  $\mathcal{O}(y) = P_R^g(y)$  and renormalizing the fundamental fields we obtain

$$\partial_\mu^- \langle A_{\mu R}^f(x) P_R^g(y) \rangle = 2m_{\text{AWI}} \langle P^f(x) P_R^g(y) \rangle, \quad (1.6.55)$$

where  $m_{\text{AWI}} = m_0 - \overline{m}$ . It should be stressed that the  $\overline{m}$  is itself a function of  $m_0$  and the other parameters of the theory, i.e.  $\overline{m} = \overline{m}(m_0, g_0) = f(g_0, am_0)/a$ .

The unrenormalized PCAC mass is

$$m_{\text{PCAC}} \equiv \frac{m_{\text{AWI}}}{Z_A} = \frac{\partial_\mu^- \langle A^f(x) P^g(y) \rangle}{2 \langle P^f(x) P^g(y) \rangle} = \frac{Z_P}{Z_A} m_{\text{PCAC},R}. \quad (1.6.56)$$

The renormalization constants and the renormalized mass do not depend on the kinematical parameters such as the time  $x_0$  we insert the current. Changing the kinematical parameters accounts for probing the PCAC relation in a different way. If we consider two different kinematical configurations at the same  $(g_0, am_0)$  point in the bare space and we measure the associated unrenormalized current masses then the difference will be of order  $a$ . This is exactly what we studied in Chap. 3 testing different kinematical configurations by injecting momentum through twisted boundary conditions.

## 1.7 Hybrid Monte Carlo simulations of gauge theories

The Hybrid Monte Carlo is the most widely used algorithm to generate lattice QCD configurations including dynamical fermions, see Ref. (Kennedy, 2006) for a review on the topic. In this section we present the HMC method for simulations of gauge theories on the lattice. The following discussion is a standard-textbook one, nice reviews are found in Refs. (Duane *et al.*, 1987, Gattringer and Lang, 2010, Lippert, 1997, Luscher, 2010).

Suppose we want to compute the expectation value of an operator  $\Omega[U]$ , with  $U_\mu$  links on the lattice governed by the action  $S_G[U]$ , in QFT this is given by

$$\langle \Omega \rangle = \frac{1}{\mathcal{Z}} \int \mathcal{D}[U] e^{-S_G[U]} \Omega[U]. \quad (1.7.57)$$

In the Monte Carlo method one samples the distribution  $P_S$  given by

$$P_S = \frac{e^{-S_G[U]}}{\mathcal{Z}}, \quad \text{and evaluates } \overline{\Omega} = \frac{1}{N_{\text{cnfs}}} \sum_{j=1}^{N_{\text{cnfs}}} \Omega[U_j], \quad (1.7.58)$$

on a sequence  $\{U_j\}$  of configurations. By taking  $N_{\text{cnfs}} \gg 1$  we have, thanks to the central limit theorem,

$$\bar{\Omega} = \langle \Omega \rangle + \mathcal{O}\left(\frac{1}{\sqrt{N_{\text{cnfs}}}}\right). \quad (1.7.59)$$

The way to generate such a sequence of configurations is to build a *Markov process*. The concepts illustrated in this Section will be used as building blocks for the study in Chap. 4 where we optimize the performance of the HMC algorithm in presence of multilevel integrators and mass-preconditioning for the fermionic forces.

### 1.7.1 Markov chain

For the sake of simplicity let us consider a generic field  $\phi$  with associated action  $S(\phi)$ . A Markov process is a stochastic procedure that generates new configuration  $\phi'$  starting from a previous  $\phi$  with a probability  $P_M(\phi \rightarrow \phi')$ , called *transition probability*.

The transition probability has to satisfy the following properties:

- Aperiodicity,  $P_M(\phi \rightarrow \phi') > 0 \forall \phi$ , i.e. the process does not get trapped in cycles.
- $P_M(\phi \rightarrow \phi') \geq 0 \forall \phi, \phi'$ , and  $\sum_{\phi'} P_M(\phi \rightarrow \phi') = 1 \forall \phi$ . It guarantees that  $P_M$  is a probability distribution in  $\phi'$  for each  $\phi$  and the corresponding Markov chain is ergodic<sup>9</sup>.

Since a Markov process does not have sinks or sources in the probability space, we need to satisfy the *balance equation*

$$\sum_{\phi} P_S(\phi) P_M(\phi \rightarrow \phi') = \sum_{\phi'} P_S(\phi') P_M(\phi' \rightarrow \phi), \quad (1.7.60)$$

i.e. the total probability to end up in a configuration  $\phi'$  has to be the same to the total probability to hop out of a configuration  $\phi'$ . On the r.h.s.  $P_S(\phi')$  can be factorized out of the sum, which then is equal to one, and the above equation becomes

$$\sum_{\phi} P_S(\phi) P_M(\phi \rightarrow \phi') = P_S(\phi'). \quad (1.7.61)$$

The balance equation states that  $P_S(\phi')$  is a fixed point of the Markov process, i.e. the equilibrium distribution is preserved by the update process.

Any Markov chain converges to a unique fixed point distribution  $P_S(\phi)$  provided that satisfies the *detailed balance condition*

$$P_S(\phi) P_M(\phi \rightarrow \phi') = P_S(\phi') P_M(\phi' \rightarrow \phi). \quad (1.7.62)$$

### 1.7.2 How to build a Markov process

Here we describe how to build a Markov process, to this end we divide the strategy in two parts:

1. Suggest a new configuration  $\phi'$  with probability  $P_C(\phi \rightarrow \phi')$ .
2. Accept the suggestion with probability  $P_A(\phi \rightarrow \phi')$ , and if rejected stay with the old configuration  $\phi$ .

---

<sup>9</sup>Any point of the configuration space is reached.

A choice for  $P_A$  that satisfies the detailed balance for any choice of  $P_C$  is the Metropolis accept/reject algorithm,

$$P_A(\phi \rightarrow \phi') = \min \left( 1, \frac{P_S(\phi')P_C(\phi' \rightarrow \phi)}{P_S(\phi)P_C(\phi \rightarrow \phi')} \right). \quad (1.7.63)$$

An ideal choice for  $P_C(\phi \rightarrow \phi')$  should give large acceptance rate which does not depend too strongly on the size of the system we want to simulate and should minimize the autocorrelation between successive configurations. The standard choice for  $P_C$  is given by the Hybrid Molecular Dynamics algorithm.

### 1.7.3 Hybrid Monte Carlo simulation

The HMC algorithm is a Markov process and it consists of

- Molecular dynamics (MD) trajectories,
- Metropolis test.

We introduce a fictitious time  $\tau$ , *Markov time*, and a set of conjugate momenta<sup>10</sup>  $\pi(\tau)$ , for each dynamical degree of freedom, with Gaussian distribution. The Hamiltonian of the system is then given by, in matrix/vector notation,

$$H(\pi, \phi) = \frac{1}{2}\pi^2 + S(\phi) = T(\pi) + S(\phi), \quad (1.7.64)$$

where  $\pi^2 = \sum_{x \in \Lambda} \pi^2(x)$ . The HMC forms a Markov chain with fixed point  $e^{-H(\pi, \phi)}$ , which is the desired distribution,

$$\langle \Omega \rangle = \langle \Omega \rangle_H = \frac{1}{Z_H} \int \mathcal{D}[\pi, \phi] e^{-H(\pi, \phi)} \Omega[\phi], \quad (1.7.65)$$

since  $\Omega$  does not depend on the momenta the functional integration in  $\pi$  is canceled out by the partition function. The procedure consists in

1. Select initial random momenta  $\pi$  from a Gaussian distribution  $P_G(\pi)$  of zero mean and unit variance,
2. Evolve the system in the  $(\phi, \pi)$  space according to the Hamilton equations

$$\frac{d\pi}{d\tau} = -\frac{\partial S}{\partial \phi}, \quad \frac{d\phi}{d\tau} = \pi. \quad (1.7.66)$$

$\Delta H$  is the violation in the energy conservation caused by the integrator at the end of the trajectory, and the probability is denoted as  $P_H[(\phi, \pi) \rightarrow (\phi', \pi')]$ .

3. Accept/reject the suggested configuration with probability  $P_A[(\phi, \pi) \rightarrow (\phi', \pi')] = \min(1, e^{-\Delta H})$ .

The transition probability for the  $\phi$  field is given by

$$P_M(\phi' \rightarrow \phi) = \int \mathcal{D}[\pi, \pi'] P_G(\pi) P_H[(\phi, \pi) \rightarrow (\phi', \pi')] P_A[(\phi, \pi) \rightarrow (\phi', \pi')], \quad (1.7.67)$$

that has to satisfy the detailed balance condition.

<sup>10</sup>In  $SU(N_c)$  gauge theories the conjugate momenta are  $\pi_\mu(x) = i\pi_\mu^a T^a$ , with  $T^a$  generators.



**Detailed balance condition** To satisfy the detailed balance condition we need

- Area preserving of the integration measure  $\mathcal{D}[\phi, \pi]$ ,
- Reversibility of the trajectory.

The dynamic has to be reversible, hence

$$P_H[(\phi, \pi) \rightarrow (\phi', \pi')] = P_H[(\phi', -\pi') \rightarrow (\phi, -\pi)]. \quad (1.7.68)$$

First we write the identity

$$\begin{aligned} P_G(\pi)P_S(\phi)P_A[(\phi, \pi) \rightarrow (\phi', \pi')] &= e^{-H(\phi, \pi)} \min(1, e^{-\Delta H}) \\ &= \min(e^{-H(\phi, \pi)}, e^{-H(\phi', \pi')}) = e^{-H(\phi', \pi')} \min(1, e^{\Delta H}), \end{aligned} \quad (1.7.69)$$

and we notice that  $H(\phi, \pi) = H(\phi, -\pi)$  from which we infer

$$P_S(\phi)P_G(\pi) \propto P_H(\phi, \pi) = e^{-H(\phi, \pi)} = e^{-H(\phi, -\pi)} = P_H(\phi, -\pi) \propto P_S(\phi)P_G(-\pi). \quad (1.7.70)$$

Combining the two equations we found earlier integrating over  $\mathcal{D}[\pi, \pi']$  recalling that  $\mathcal{D}[\pi, \pi'] = \mathcal{D}[-\pi, -\pi']$ , we obtain

$$\begin{aligned} P_S(\phi)P_M(\phi \rightarrow \phi') &= P_S(\phi) \int \mathcal{D}[\pi, \pi'] P_G(\pi) P_H[(\phi, \pi) \rightarrow (\phi', \pi')] P_A[(\phi, \pi) \rightarrow (\phi', \pi')] \\ &= P_S(\phi') \int \mathcal{D}[\pi, \pi'] P_G(-\pi) P_H[(\phi', -\pi') \rightarrow (\phi, -\pi)] P_A[(\phi', -\pi') \rightarrow (\phi, -\pi)] \\ &= P_S(\phi') P_M(\phi' \rightarrow \phi), \end{aligned} \quad (1.7.71)$$

that is the detailed balance condition.

#### 1.7.4 Dynamical fermions

We would like to include in our simulations fermions  $\psi$  governed by the action  $S_F = \bar{\psi} M[\phi] \psi$ , with  $M(\phi)$  a generic local operator. To do so we replace the Grassmann fields  $\bar{\psi}, \psi$  with bosonic fields  $\chi^*, \chi$ . The simulated theory is obtained by integrating out the fermion fields and dynamical fermion loops are included through a stochastic representation of the fermionic determinant. Hence the distribution to consider is

$$\begin{aligned} P_S &\propto \int \mathcal{D}[\bar{\psi}, \psi] \exp(-S(\phi) - \bar{\psi} M(\phi) \psi) \propto e^{-S(\phi)} \det M(\phi) \\ &\propto \int \mathcal{D}[\chi^*, \chi] \exp\{-S(\phi) - \chi^* M^{-1} \chi\}. \end{aligned} \quad (1.7.72)$$

In the relevant case of the  $\gamma_5$ -version of the Dirac-Wilson operator<sup>11</sup>  $M(\phi) = \gamma_5 D_W(U)$ , to ensure the convergence of the bosonic Gaussian integral we double the number of simulated fermions,  $\det M \rightarrow (\det M)^2$ , and the probability becomes

$$\begin{aligned} P_S &\propto e^{-S(\phi)} (\det M(\phi))^2 \propto e^{-S(\phi)} \det(M(\phi) M^\dagger(\phi)) \\ &\propto \int \mathcal{D}[\chi^*, \chi] \exp\{-S(\phi) - \chi^* (M^\dagger M)^{-1} \chi\}. \end{aligned} \quad (1.7.73)$$

<sup>11</sup>Notice it is hermitian, but it can have negative eigenvalues.

The Hamilton equations for the  $\phi$  fields in this framework become

$$\begin{aligned} \frac{d\pi}{d\tau} &= -\frac{\partial S}{\partial \phi} - \chi^* \frac{\partial(M^\dagger M)^{-1}}{\partial \phi} \chi \\ &= -\frac{\partial S}{\partial \phi} + \chi^* (M^\dagger M)^{-1} \left[ M^\dagger \frac{\partial M}{\partial \phi} + \frac{\partial M^\dagger}{\partial \phi} M \right] (M^\dagger M)^{-1} \chi \equiv F_\phi + F_{\text{Ferm}}, \end{aligned} \quad (1.7.74)$$

$$\frac{d\phi}{d\tau} = \pi. \quad (1.7.75)$$

It is easy to see that a number of conjugate gradient inversions,  $\eta = (M^\dagger M)^{-1} \chi$ , are required in order to compute the HMC part of the force,  $F_{\text{Ferm}}$ . The fields  $\chi$  and  $\chi^*$  are held fixed during the molecular dynamics steps and updated in between.

It should be mentioned that the sample of the distribution in Eq. 1.7.72 can be performed if the measure of the path integral is real and positive, only in this way we can interpret it as a probability distribution. That interpretation breaks down, for example, if the term in Eq. 1.1.4 with  $\theta \neq 0$  is included in the action.



## Chapter 2

# Quantum electrodynamics on the lattice

The main goal of lattice QCD is to calculate in a non-perturbative manner observables needed in phenomenological applications. Most of the relevant hadronic quantities are computed in the so called isosymmetric limit, i.e. neglecting the up and down quark mass difference and the QED interactions. Nowadays, for some observables, the accuracy of lattice estimates has reached the percent level and the above mentioned effects cannot be neglected any longer, a recent review on that is found in Ref. ([Tantalo, 2014](#)) .

The inclusion of the quark mass difference is quite straightforward from the theoretical point of view and it requires only additional computational effort, e.g. reweighting technique ([Finkenrath et al., 2012](#)) or direct simulations. Since the inclusion of QED on a lattice presents some subtleties that are ultimately related to the long-range nature of electromagnetic interactions, we have reserved to them this introductory chapter.

In QED simulations the so-called *zero mode problem* is present, which appears by looking at unphysical contributions to a given process or amplitude. The different contributions are divergent and this is well understood in the view of the *Bloch-Nordsieck theorem*, which states that physical quantities in QED are IR divergent free ([Bloch and Nordsieck, 1937](#)). Furthermore in a periodic lattice Gauss's law forbids charged states to propagate ([Hayakawa and Uno, 2008](#)).

The most popular way to deal with this problem is to subtract the zero mode and remove it from the dynamics. This is done in several ways:

- QED<sub>TL</sub>, the zero mode is set to zero on each configuration.
- QED<sub>L</sub>, the spatial zero modes are set to zero, on each time-slice on each configuration.
- QED<sub>C</sub>, the zero mode is absent due to a special choice of boundary conditions.
- QED<sub>M</sub>, a photon mass term is introduced, i.e. the zero mode is generated with a Gaussian distribution with zero mean value.

It is well understood that QED<sub>TL</sub> does not possess reflection positivity, and consequently a positive definite Hamiltonian, while QED<sub>L</sub> does have it. In Ref. ([Borsanyi and others, 2015](#)) finite volume effects were computed only for masses in QED<sub>TL</sub> and QED<sub>L</sub>, a similar work was done for QED<sub>C</sub> ([Lucini et al., 2016](#)). In QED<sub>M</sub> the spatial zero modes are regularized, as in perturbation theory, with a Gaussian weight. Here we are forced to produce configurations with different photon masses, since eventually we will extrapolate the results to vanishing mass ([Endres et al., 2016](#)).

The implementation of QED has been studied since long time with pioneering work in (Duncan *et al.*, 1996) in the framework of quenched QED+QCD (qQ(C+E<sub>TL</sub>)D).

All the studies, until now, are mostly focused on the hadron spectrum. In the last years the field was very active and recent studies have been performed qQED+dynamical QCD (qQED+QCD) (Blum *et al.*, 2010, Basak and others, 2014). The best result, at the present, in the fully dynamical Q(C+E<sub>L</sub>)D simulations has been achieved by the BMW collaboration (Borsanyi and others, 2015) where the proton-neutron mass splitting with about  $5\sigma$  statistical significance is given. In Ref. (Endres *et al.*, 2016) a first hadron spectrum determination in qQED<sub>M</sub>+QCD was presented. It should be mentioned that another quenched QED strategy is given in (de Divitiis *et al.*, 2013) in which the path integral and corresponding observables are expanded to order  $\alpha_{\text{em}}$ . There the QED corrections are extracted directly from the observables as  $O(1)$  effects rather than  $O(\alpha_{\text{em}})$  ones.

The introduction of a photon mass is particularly interesting since it changes the finite volume effects from power-like to exponential-like, avoiding the infinite volume extrapolation but introducing an extrapolation in the photon mass. The C\* approach is also an elegant solution to the zero mode problem and it comes at the cost of flavor violations. No further discussions are given here since we did not explore that approach in our projects.

The chapter is organized as follows; in Section 1 we briefly discuss the global symmetries in the framework of Q(C+E)D, in Section 2 we present the problem of IR divergences on the lattice QED in non-compact formulation. Section 3 is devoted to general considerations on the gauge symmetry, as gauge fixing and completeness in finite volume. The fixing of eventual residual symmetries and zero modes is discussed in Section 4. Section 5 contains the recipe for the generation of quenched QED configurations in Feynman gauge. In Section 6 we illustrate the impossibility of building charged states in a finite volume with periodic boundary conditions and how this is avoided in QED<sub>TL</sub> and QED<sub>L</sub>. In Section 7 we present the other solution to the Gauss law problem, the *massive IR regularization* on the lattice for QED. Section 8 contains the comparison of Wilson loops in QED<sub>TL</sub>, QED<sub>L</sub> and QED<sub>M</sub> with the corresponding predictions in the infinite volume.

## 2.1 Global symmetries

The electromagnetic formal theory with fermions in Euclidean space is given by the following Lagrangian

$$\mathcal{L}[A_\mu, \Psi, \bar{\Psi}] = \mathcal{L}_{\text{QED}} + \mathcal{L}_{\text{F}} = \frac{1}{4} F_{\mu\nu} F_{\mu\nu} + \bar{\Psi}(x) (eQ\not{D} + M) \Psi(x), \quad (2.1.1)$$

where  $F_{\mu\nu} = \partial_\mu A_\nu - \partial_\nu A_\mu$  is the field-strength tensor for the gauge degrees of freedom,  $\Psi$  is a fermionic flavor multiplet,  $M$  is the mass and  $Q$  the charge matrices.  $A_\mu$  is a real vector field with dimension [1]. A  $\theta$ -term is not forbidden, that is parity and time reversal violating term

$$\theta \epsilon^{\mu\nu\rho\sigma} F_{\mu\nu} F_{\rho\sigma} = \theta F_{\mu\nu} \tilde{F}_{\mu\nu}, \quad (2.1.2)$$

with  $\theta$  real parameter and  $\epsilon^{\mu\nu\rho\sigma}$  antisymmetric tensor, but QED conserves those symmetries. The  $\theta$ -term is related to *instantonic contributions* and it is known that in an Abelian  $\mathbf{U}(1)$  theory it does not have any physical effect, in contrast to non-Abelian theories, hence we can safely neglect it.

The following discussion can be found in Ref. (Blum *et al.*, 2007). We know that QCD exhibits chiral symmetry, as we saw in Sect. 1.2, given by the following group, in presence of three fermion species,  $N_f = 3$

$$\mathbf{G}_{\text{QCD}}(N_f = 3) = \mathbf{SU}(N_f)_L \otimes \mathbf{SU}(N_f)_R \otimes \mathbf{U}(1)_V, \quad (2.1.3)$$

where we have omitted the  $\mathbf{U}(1)_A$  since it is *anomalous*.

In Q(C+E)D we find that some global symmetries, present in QCD, are explicitly broken by the electromagnetic interactions. Notice we are considering two electromagnetic charges to be the same. The explicit breaking can be seen through the Ward-Takahashi identity for the flavor non-singlet axial current  $A_\mu^f = \bar{\Psi}\gamma_\mu\gamma_5 T^f\Psi$ , with  $T^f$  one of the generators of  $\mathbf{SU}(N_f)$  (see Eq. 1.6.51 for the case  $N_f = 2$  in QCD),

$$\partial_\mu A_\mu^f = ieA_\mu\bar{\Psi}[T^f, Q]\gamma_\mu\gamma_5\Psi - \frac{\alpha}{2\pi}\text{Tr}[Q^2 T^f]F_{\mu\nu}\tilde{F}_{\mu\nu}. \quad (2.1.4)$$

For  $N_f = 3$  we have  $N_f^2 - 1 = 8$  generators and the first term in the above equation vanishes when  $f = 3, 6, 7, 8$  while the second does it for  $f = 1, 2, 4, 5, 6, 7$  and a combination of  $f = 3$  and  $8$ , which is

$$\frac{1}{2}T'^3 = \frac{\sqrt{3}}{2}T^8 - \frac{1}{2}T^3. \quad (2.1.5)$$

Thus the inclusion of QED effects leads to the symmetry group

$$\mathbf{G}_{\text{QCD+QED}}(N_f = 3) = \mathbf{SU}'(2)_L \otimes \mathbf{SU}'(2)_R \otimes \mathbf{U}(1)_V \quad (2.1.6)$$

where the prime are subgroups  $\mathbf{SU}'(2) \subset \mathbf{SU}(3)$  generated by  $T^6, T^7, T'^3$ . Then the QCD dynamics break spontaneously the group to

$$\mathbf{H}_{\text{QCD+QED}}(N_f = 3) = \mathbf{SU}'(2)_V \otimes \mathbf{U}(1)_V. \quad (2.1.7)$$

## Landau Pole

In QED the known *Landau pole* is present. The one-loop  $\beta$ -function in QED is given by

$$\mu \frac{\partial e}{\partial \mu} = \frac{e^3}{12\pi^2}, \quad (2.1.8)$$

and by solving the differential equation we find

$$e^2(\mu) = \frac{e^2(\mu_0)}{1 - \frac{e^2(\mu_0)}{6\pi^2} \ln \frac{\mu}{\mu_0}}. \quad (2.1.9)$$

It is clear that there is a singularity at  $\mu = \mu_0 \exp\left[\frac{6\pi^2}{e^2(\mu_0)}\right]$ , the so-called Landau pole.

By plugging in physical number we find that the pole is beyond the Planck scale, and practically unreachable in present lattices.

## 2.2 Infrared divergences

On the lattice we introduce the electromagnetic field in a dynamical way by employing the *non-compact* formulation. QED with compact formulation suffers from a phase transition around  $\beta \approx 1.2$  as first seen in Ref. (Creutz *et al.*, 1979). For large unphysical electromagnetic coupling a transition from the Coulomb phase to a confining phase is present<sup>1</sup>. In the following we will deal only with fields in the non-compact formulation to avoid the above mentioned unphysical

<sup>1</sup>The phase transition is due to the introduction of lattice artifacts, like photon self-interaction.

phase transition. Gauge invariance on the lattice still requires the coupling between fermions and compact variables but we have the freedom to choose the non-compact formulation for the pure QED part of the action. But in this framework we are forced to fix the gauge, in order to make finite the path integral.

One of the main difference with QCD is that the physical states can have energy arbitrary close to zero because the theory does not have a mass gap. For this reason finite volume effects are expected to be important<sup>2</sup>, since the interaction is long-ranged. Furthermore QED can lead to an IR divergent theory (Portelli, 2013), if one considers different contributions (diagrams) to a physical quantity. To elucidate this point we look at a one photon loop contribution to a correlation function in the formal theory

$$I = \int \frac{d^4k}{(2\pi)^4} \frac{f(k, p_1, p_2, \dots, p_n)}{k^4}, \quad (2.2.10)$$

where  $k$  is the momentum flowing in the loop,  $p_1, p_2, \dots, p_n$  are the external momenta, and we assume that  $f(k, p_1, p_2, \dots, p_n) \underset{k \rightarrow 0}{\propto} k^{-\epsilon}$ . In the situation where  $\epsilon > 0$  the integrand is divergent in the limit  $k \rightarrow 0$ , and it is an IR divergence if the singularity is not integrable. However it should be noted that the IR divergences do not affect physical results when we consider all the possible contributing diagrams. This statement is the essence of the Bloch-Nordsieck theorem (Bloch and Nordsieck, 1937) and the more general *Kinoshita-Lee-Nauenberg theorem* (Kinoshita, 1962, Lee and Nauenberg, 1964).

On the lattice the integral becomes a discrete sum over momenta, which depend on the volume and the type of boundary conditions. By choosing periodic boundary conditions in the gauge sector the allowed momenta are  $p_\mu = \frac{2\pi}{L_\mu} k_\mu$ , where  $L_\mu$  is the lattice extent in direction  $\mu$  and  $k_\mu \in \left(-\frac{L_\mu}{2}, \frac{L_\mu}{2}\right] \subset \mathbb{Z}$ . The vanishing momentum  $p^2 = 0$  is part of the reciprocal lattice and the discretized version of the integral is hence *ill-defined*. Thus we need an IR regularization of the theory on the lattice if we are interested in potentially IR divergent contributions.

## 2.3 Gauge symmetry: general considerations

In the following we will show how to generate QED configurations in the quenched approximation<sup>3</sup>. The crucial point is the gauge fixing procedure and the removal of zero mode (the latter prescription makes the theory IR “divergent free” in the sense explained in the previous Section).

### 2.3.1 Gauge fixing

In the non-compact formalism we are forced to fix the gauge in order to make the path integral well defined. The ill-definiteness arises from the fact that we cannot invert the gauge operator and calculate the photon propagator. This is a direct consequence of gauge invariance: there exist gauge equivalent transformations that do not affect the physics, called *orbits*.

In the Faddeev-Popov approach (Faddeev and Popov, 1967) one considers a constraint in the path integral in a way that each orbit is intersected only once<sup>4</sup>, then the path integral can be

<sup>2</sup>QCD finite volume effects go as  $e^{-m_\pi L}$ .

<sup>3</sup>Sea and valence quarks are treated in a different way, i.e. sea quarks are not charged while valence ones are.

<sup>4</sup>In other words we want a representative configuration for each orbit and the other elements in the orbit are related to it by a smooth gauge transformation. No Gribov ambiguities are present.

re-written as

$$\begin{aligned} \int \mathcal{D}[A_\mu] e^{-S(A)} &\propto \int \mathcal{D}[A_\mu] \det \left( \frac{\partial G}{\partial \Omega} \right) \Big|_{G=0} \delta(G(A)) e^{-S(A)} \\ &\propto \int \mathcal{D}[A_\mu] \det \left( \frac{\partial G}{\partial \Omega} \right) \Big|_{G=0} \exp \left( -S(A) - \frac{1}{2\alpha} \int d^4x G(A)^2 \right) \end{aligned} \quad (2.3.11)$$

where  $G$  is the gauge condition to impose, i.e.  $G(A) = 0$ , and  $\alpha$  is a free parameter used to approximate the Dirac delta. The derivative of the gauge condition with respect to  $\Omega$  has to be interpreted as the functional derivative of the gauge transformed field, i.e.  $G(A^\Omega)$ , with respect to a gauge transformation, given by the function  $\Omega$ . The determinant is called *Faddeev-Popov determinant* and can be expressed as a Gaussian integral by introducing fictitious fermionic variable called *ghosts*. The ghost term contributes to the overall normalization and it does not couple with the gauge fields, i.e. QED is ghosts free.

### 2.3.2 Gauge symmetry in finite volume

When we introduce fermions in our system we should care about the zero mode of the photon field, and removing it leads to an IR “divergent free” theory on the lattice. The following discussion is based on Ref. (Blum *et al.*, 2007). In the rest of the work we do not explicitly say when the lattice spacing  $a$  is set to 1. It is easy to restore the proper powers of lattice spacing in the expressions using dimensional analysis. We introduce only one fermion  $\psi$ , with charge one, and we couple it to the photon through the term in the Lagrangian

$$\mathcal{L}_F[A_\mu, \bar{\psi}, \psi] = \frac{1}{2} \sum_\mu \bar{\psi}(x) \gamma_\mu (\nabla_\mu^+ + \nabla_\mu^-) \psi(x), \quad (2.3.12)$$

where the variables  $A_\mu$  are placed in the mid-point of the link  $x, x + \hat{\mu}$  and the forward and backward derivatives are

$$\begin{aligned} \nabla_\mu^+ \psi(x) &= U_\mu(x) \psi(x + \hat{\mu}) - \psi(x) = e^{ieqA_\mu(x + \hat{\mu}/2)} \psi(x + \hat{\mu}) - \psi(x), \\ \nabla_\mu^- \psi(x) &= \psi(x) - U_\mu^\dagger(x - \hat{\mu}) \psi(x - \hat{\mu}) = \psi(x) - e^{-ieqA_\mu(x - \hat{\mu}/2)} \psi(x - \hat{\mu}). \end{aligned} \quad (2.3.13)$$

The Lagrangian is invariant under a gauge transformation  $\Lambda$ , which we recall to act on the fields as

$$\begin{aligned} A'_\mu(x + \hat{\mu}/2) &= A_\mu(x + \hat{\mu}/2) + \partial_\mu^+ \Lambda(x), \\ \psi'(x) &= e^{i\Lambda(x)} \psi(x), \\ \bar{\psi}'(x) &= \bar{\psi}(x) e^{-i\Lambda(x)}. \end{aligned} \quad (2.3.14)$$

By imposing periodic boundary condition on  $A'_\mu$  and  $\psi'$  we discover that the function  $\Lambda$  does not have to respect periodic boundary condition but instead a weaker condition:

$$\Lambda(x + L_\mu \hat{\mu}) = \Lambda(x) + 2\pi r_\mu, \quad (2.3.15)$$

where the  $r_\mu \in \mathbb{Z}$ , are *quantized* as a consequence of the periodicity of the fermions<sup>5</sup>. A general form for a gauge transformation that respect the above condition is

$$\Lambda(x) = \Lambda^{(0)}(x) + 2\pi \sum_{\mu=0}^3 r_\mu \frac{x_\mu}{L_\mu}, \quad (2.3.16)$$

<sup>5</sup>This makes clear how the allowed gauge transformations depend on the fermionic boundary conditions. One may modify the latter to get rid of unwanted terms (Lucini *et al.*, 2016).



where  $\Lambda^{(0)}(x)$  satisfies periodic boundary conditions.

By Fourier transforming the gauge transformed gauge field we learn how it is expressed in momentum space

$$\tilde{A}'_{\mu}(p) = \tilde{A}_{\mu}(p) + \sqrt{V} \frac{2\pi r_{\mu}}{L_{\mu}} \delta(p) + i\hat{p}_{\mu} \tilde{\Lambda}^{(0)}(p), \quad (2.3.17)$$

where we have defined  $\hat{p}_{\mu} = \frac{2}{a} \sin(ap_{\mu}/2)$ . We would like to eliminate all the  $\mathbf{U}(1)$  redundancies. For this reason we need to gauge fix through a condition and we shall use the Coulomb gauge. The matter is to determine whether the Coulomb gauge is sufficient to do it, or in other words we need to establish if it is a *complete gauge fixing*.

**Intermezzo: Non-completeness of Coulomb gauge** We want to find a particular gauge transformation that transforms the fields satisfying the Coulomb condition into another one satisfying the same condition. For the sake of simplicity let us assume to be in a finite box with vanishing lattice spacing.

We are searching for a function  $\phi$  that does the job. We split  $\phi$  according to the relation Eq. 2.3.16 and the gauge transformation on the gauge field becomes

$$A'_{\mu}(x) = A_{\mu}(x) + \frac{2\pi r_{\mu}}{L_{\mu}} + \partial_{\mu} \phi^{(0)}(x). \quad (2.3.18)$$

By imposing the Coulomb condition on both fields before and after the transformation we find an equation for  $\phi^{(0)}$ ,

$$\sum_j \partial_j A'_j(x) = 0 = \sum_j \cancel{\partial_j A_j(x)} + \sum_j \partial_j \partial_j \phi^{(0)}(x) = \nabla^2 \phi^{(0)}(x). \quad (2.3.19)$$

Since the differential equation does not give informations about the time behavior we can write the solution in the following way

$$\phi^{(0)}(t, \underline{x}) = T(t) \hat{\phi}^{(0)}(\underline{x}), \quad \text{with } T(t) \neq 0, \quad (2.3.20)$$

and the differential equation is restated as

$$\nabla^2 \hat{\phi}^{(0)}(\underline{x}) = \left( \frac{\partial^2}{\partial x^2} + \frac{\partial^2}{\partial y^2} + \frac{\partial^2}{\partial z^2} \right) \hat{\phi}^{(0)}(\underline{x}) = 0. \quad (2.3.21)$$

In rectangular coordinates the equation is separable and the solution is written in terms of the three ordinary differential equation by assuming (Jackson, 1998)

$$\hat{\phi}^{(0)}(x, y, z) = X(x)Y(y)Z(z). \quad (2.3.22)$$

Substituting back in Eq. 2.3.21 and dividing the result by  $\hat{\phi}^{(0)}(x, y, z)$  we obtain

$$\frac{1}{X(x)} \frac{\partial^2 X}{\partial x^2} + \frac{1}{Y(y)} \frac{\partial^2 Y}{\partial y^2} + \frac{1}{Z(z)} \frac{\partial^2 Z}{\partial z^2} = 0. \quad (2.3.23)$$

The solution of such an equation is given by

$$\begin{cases} \frac{1}{X(x)} \frac{\partial^2 X}{\partial x^2} = -\alpha^2, \\ \frac{1}{Y(y)} \frac{\partial^2 Y}{\partial y^2} = -\beta^2, \\ \frac{1}{Z(z)} \frac{\partial^2 Z}{\partial z^2} = \gamma^2. \end{cases} \longrightarrow \begin{cases} X(x) = A \cos(\alpha x) + B \sin(\alpha x), \\ Y(y) = C \cos(\beta y) + D \sin(\beta y), \\ Z(z) = E \cosh(\gamma z) + F \sinh(\gamma z). \end{cases} \quad (2.3.24)$$

where we have the relation  $\alpha^2 + \beta^2 = \gamma^2$ .

The solution  $\phi^{(0)}$  is just a product of the ones we found and the unknown function  $T(t)$  (but periodic in  $t$ ). In order to determine the constants we impose the boundary conditions on  $X, Y, Z$  which follow from the periodic boundary conditions for  $\phi^{(0)}$ .

At this stage it is clear that if we try to impose periodic boundary conditions on  $Z$  the only solution is  $Z = \text{const}$  ( $\gamma = 0$  implies  $\alpha, \beta = 0$ ) which makes  $\widehat{\phi}^{(0)} = \text{const}$ .

We conclude that there is no gauge transformation left in the spatial direction satisfying Eq. 2.3.21, apart for the constant. We still have the redundancy  $T(t)$ , which means that the Coulomb gauge is not complete in a finite volume.

## 2.4 QED<sub>TL</sub> & QED<sub>L</sub>

In this section we present the two IR regularization know in the literature as QED<sub>TL</sub> and QED<sub>L</sub>. Both are inspired by the gauge fixing procedure.

### 2.4.1 Fix of the residual gauge symmetry and zero mode

In the previous section we have shown how the redundancies related to  $\widetilde{\Lambda}(p_0, \underline{p} \neq \underline{0})$  are eliminated by the Coulomb gauge fixing. Based on the previous Section, we need to fix the residual symmetry generated by:

- $\widetilde{\Lambda}(p_0 \neq 0, \underline{0})$ , spatially uniform gauge transformations, i.e.  $\phi^{(0)}(x) = T(t) \times \text{const}$ ,
- $r_\mu$ , space-time uniform gauge transformations, i.e.  $\phi(x) = \text{const}$ .

#### $\widetilde{\Lambda}(p_0 \neq 0, \underline{0})$ redundancy

We can see from Eq. 2.3.17 that  $\Lambda(p_0 \neq 0, \underline{0})$  is acting on  $\widetilde{A}_0$ , while does not change the spatial components  $\widetilde{A}_i$ . The transformation of the temporal one is

$$\widetilde{A}'_0(p_0 \neq 0, \underline{0}) = \widetilde{A}_0(p_0 \neq 0, \underline{0}) + i\hat{p}_0 \widetilde{\Lambda}^{(0)}(p_0 \neq 0, \underline{0}). \quad (2.4.25)$$

Then we can always gauge transform  $\widetilde{A}_0$  to zero and in this way fix the the redundancy

$$\widetilde{A}'_0(p_0 \neq 0, \underline{0}) = 0 \implies \widetilde{\Lambda}^{(0)}(p_0 \neq 0, \underline{0}) = i \frac{1}{\hat{p}_0} \widetilde{A}_0(p_0 \neq 0, \underline{0}). \quad (2.4.26)$$

The Coulomb gauge condition with the supplement of the Eq. 2.4.26 is usually referred to as *extended Coulomb gauge*.

#### $r_\mu$ redundancy

Eq. 2.3.17 for space-time uniform gauge transformations becomes

$$\widetilde{A}'_\mu(0) = \widetilde{A}_\mu(0) + \sqrt{V} \frac{2\pi r_\mu}{L_\mu} \quad (2.4.27)$$

Here we cannot always gauge transform to zero, since the  $r_\mu$  are integers, but we can in principle “partially” eliminate  $\widetilde{A}_\mu$ , which means to transform it in the interval

$$0 \leq \widetilde{A}'_\mu(0) < \frac{2\pi\sqrt{V}}{L_\mu}, \quad (2.4.28)$$

by choosing a suitable  $r_\mu$ . In this way we have eliminated all the redundancies in the Coulomb gauge in finite volume<sup>6</sup>.

### Zero modes

We already saw that the zero modes  $\tilde{A}_\mu(0), \tilde{A}_0(p_0 \neq 0, \underline{0})$  enter in the dynamics only through the coupling of the photon to matter fields.

A *quenching* of the zero mode, used in the literature, can be the following

$$\text{QED}_{\text{TL}} : \tilde{A}_\mu(0) = 0. \quad (2.4.29)$$

That clearly violates the “quantization condition” on the  $r_\mu$ , see Eq. 2.3.15, i.e. they must be integers. This is equivalent to violate the periodic boundary conditions on the fermion field, hence it is a quantifiable finite volume effect. Another way to quench those modes is to add the following constraints

$$\text{QED}_{\text{L}} : \begin{cases} \tilde{A}_\mu(0) = 0 \\ \tilde{A}_j(p_0 \neq 0, \underline{0}) = 0 \end{cases}. \quad (2.4.30)$$

This choice is used in simulation with dynamical fermion and the error consists, again, in a quantifiable finite volume effect (Borsanyi and others, 2015).

## 2.5 Generation of quenched QED configurations

In this section we summarize how to generate QED configurations in Feynman gauge. For the generation in Coulomb gauge see App. D.3.

### 2.5.1 Generation in Feynman gauge

The Feynman gauge is given by fixing  $\alpha = 1$  in the Faddeev-Popov approach in Eq. 2.3.11 and using the Lorenz gauge condition as constraint, i.e.

$$G(A) = \partial_\mu A_\mu. \quad (2.5.31)$$

As we noticed earlier the ghosts are factorized and they do not modify the form of the action, so the Lagrangian becomes

$$\mathcal{L}_{\text{QED}}[A_\mu] = \frac{1}{4} \sum_{\mu, \nu} (\partial_\mu A_\nu - \partial_\nu A_\mu)^2 + \frac{1}{2} \left( \sum_\mu \partial_\mu A_\mu \right)^2. \quad (2.5.32)$$

By recalling that on the lattice the integration by parts reads

$$\sum_{x \in \Lambda} g(x) \partial_\mu^+ f(x) = - \sum_{x \in \Lambda} f(x) \partial_\mu^- g(x), \quad (2.5.33)$$

---

<sup>6</sup>This prescription is also known as QED<sub>SF</sub> and it was argued in Ref. (Patella, 2017) that this theory unlikely possesses a transfer matrix.

the total action can be rewritten as

$$\begin{aligned}
S &= \frac{1}{4} \sum_{x \in \Lambda} \left\{ \sum_{\mu, \nu} [\partial_\mu^+ A_\nu - \partial_\nu^+ A_\mu]^2 + \frac{1}{2} [\sum_\mu \partial_\mu^+ A_\mu]^2 \right\} \\
&= \frac{2}{4} \sum_{x \in \Lambda} \sum_{\mu, \nu} \left\{ \partial_\mu^+ A_\nu \partial_\mu^+ A_\nu - \partial_\mu^+ A_\nu \partial_\nu^+ A_\mu + \partial_\nu^+ A_\nu \partial_\mu^+ A_\mu \right\} \\
&= \frac{1}{2} \sum_{x \in \Lambda} \sum_{\mu, \nu} \left\{ -A_\nu \partial_\mu^- \partial_\mu^+ A_\nu + \cancel{A_\nu \partial_\mu^- \partial_\nu^+ A_\mu} - \cancel{A_\nu \partial_\nu^- \partial_\mu^+ A_\mu} \right\} \\
&= -\frac{1}{2} \sum_{x \in \Lambda} \sum_{\mu, \nu} A_\nu(x + \hat{\nu}/2) \partial_\mu^- \partial_\mu^+ A_\nu(x + \hat{\nu}/2).
\end{aligned} \tag{2.5.34}$$

By Fourier transform the fields, Eq. D.1.3, we find that the gauge operator is diagonal in momentum space, for the computations see the App. D.2, and the action is

$$S = \sum_{p \in \tilde{\Lambda}} \frac{\hat{p}^2}{2} \sum_\nu |\tilde{A}_\nu(p)|^2, \tag{2.5.35}$$

where  $\hat{p}^2 = \sum_\mu \hat{p}_\mu^2$ .

The generation of the electromagnetic field in Feynman gauge amount in generate the Fourier components according to a Gaussian distribution and then transform back to obtain the field in coordinate space.

## 2.6 Gauss law problem

In this section we present the Gauss (and Ampère) law problem in finite volume and how it is solved by fixing the zero mode (Hayakawa and Uno, 2008, Davoudi and Savage, 2014). The problem consists in the impossibility to build states with non-vanishing charge.

The Gauss law is given by

$$\sum_j \partial_j E_j(x) = \rho(x), \tag{2.6.36}$$

where  $\underline{E}$  is the electric field and  $\rho$  the charge density distribution in space. In a finite volume with periodic boundary conditions on the fields the charge is always vanishing, indeed

$$Q = \int_{V_3} d^3x \rho(x) = \int_{V_3} d^3x \sum_j \partial_j E_j(x) = \int_{\partial V_3} d\Sigma \underline{E}(x) \cdot \hat{n} = 0, \tag{2.6.37}$$

where  $Q$  is the charge,  $V_3$  the spatial volume,  $\partial V_3$  its boundary,  $\Sigma$  the surface element and  $\hat{n}$  its normal. The above result can be understood as follow: the lines of the field that are going outside of the volume are the same coming inside after a complete revolution over the torus, because of the periodic boundary conditions. This simple argument shows how a single charge is forbidden in a finite volume.

By fixing the zero mode to be constant<sup>7</sup> one can show that we allow for non-vanishing charges in the finite volume. The constraint  $\int d^4x A_\mu = c_\mu$ , with  $c_\mu$  constant (in configuration space),

<sup>7</sup>Zero is not strictly necessary.

leads to the *non-local* Lagrangian, see the App. D.4 for details, with  $j_\mu$  external current

$$\mathcal{L}[A_\mu, j_\mu] = \frac{1}{4} \sum_{\mu, \nu} F_{\mu\nu}^2 + \sum_{\mu} (j_\mu - \frac{c_\mu}{\alpha}) A_\mu + \frac{1}{2\alpha} \sum_{\mu} A_\mu \int d^4y A_\mu(y), \quad (2.6.38)$$

which violates reflection positivity because the last term connects fields at arbitrary positive and negative times, as noted in Ref. (Borsanyi and others, 2015).

The Euler-Lagrange equation of motion are, Eq. D.4.40

$$\sum_{\nu} \partial_{\nu} F_{\nu\mu}(x) = j_{\mu}(x) + b_{\mu}, \quad (2.6.39)$$

with  $b_\mu$  given by Eq. D.4.39,

$$b_{\mu} = \frac{1}{\alpha} \left( \int d^4y A_{\mu}(y) - c_{\mu} \right). \quad (2.6.40)$$

Effectively, by constraining the zero mode to a constant, we introduced a uniform time independent background current in the system. By integrating in the spatial volume the time component to obtain the charge we find

$$\int_{V_3} d^3x \sum_{\mu} \partial_{\mu} F_{\mu 0}(x) = \int_{V_3} d^3x \sum_j \partial_j E_j(x) \equiv 0 = \int_{V_3} d^3x j_0(x) + \int_{V_3} d^3x b_0 = Q + b_0 V_3, \quad (2.6.41)$$

which implies  $b_0 = -Q/V_3$ . Intuitively we are spreading an opposite charge over the volume, in this way we solve locally the problem of a charge in a finite volume but not globally, because the total net charge is still vanishing. Analogous arguments hold for the Ampere law.

Furthermore one can recover the imposed constraint by looking at  $b_0$

$$b_0 = \frac{1}{\alpha} \left( \int d^4x A_0(x) - c_0 \right) = -Q/V_3 \implies \int d^4x A_0(x) = -\alpha Q/V_3 + c_0 \xrightarrow{\alpha \rightarrow 0} c_0. \quad (2.6.42)$$

## 2.7 Massive QED

As we saw in the previous sections one way to correct the Gauss law, and therefore allow for a net charge on a finite volume, is to fix the zero mode to be constant, e.g.  $\tilde{A}_\mu(p=0) = 0$ , but the resulting Lagrangian violates reflection positivity. The other solution, QED<sub>L</sub>, possesses reflection positivity but the constraint is still non-local and many properties of local quantum field theory are not automatically guaranteed<sup>8</sup>.

The most economical and straightforward choice that retains locality is the massive approach on the lattice, first presented in Ref. (Endres *et al.*, 2016). As in perturbation theory one can add a mass term for the photon, which act as an IR regulator, and at the end take the limit of vanishing photon mass,  $m_\gamma \rightarrow 0$ . We know that under some condition, which will be clarified in the following, the theory is still renormalizable.

In the following we will investigate massive QED with different gauge fixing terms.

<sup>8</sup>For example: renormalizability, volume-independence of renormalization constants, Symanzik improvement programme, etc.

### 2.7.1 Renormalizability: the need for Feynman gauge

The first issue we encounter with massive QED is the renormalizability, nice discussions on the subject are found in Refs. (Zinn-Justin, 2002, Ruegg and Ruiz-Altaba, 2004). We start with the Proca action

$$S_{\text{Proca}} = \int d^4x \left[ \frac{1}{4} F_{\mu\nu}^2 + \frac{1}{2} m_\gamma^2 A_\mu^2 \right]. \quad (2.7.43)$$

The propagator in Fourier space is

$$\Delta_{\mu\nu}(k) = \frac{\delta_{\mu\nu} + k_\mu k_\nu / m_\gamma^2}{k^2 + m_\gamma^2} \xrightarrow{k \rightarrow \infty} \frac{1}{m_\gamma^2}, \quad (2.7.44)$$

that in the infinite momentum limit goes to a constant, hence the resulting theory seems to be non-renormalizable by power-counting (Reisz, 1988). We can overcome the non-renormalizability by adding a *free massive scalar* field  $\chi$  to the action

$$S_{\text{Stueck}} = \int d^4x \left[ \frac{1}{4} F_{\mu\nu}^2 + \frac{1}{2} m_\gamma^2 A_\mu^2 - \frac{1}{2} (\partial_\mu \chi)^2 + m_\chi^2 \chi^2 \right] = S_{\text{Proca}} + \int d^4x \left[ -\frac{1}{2} (\partial_\mu \chi)^2 + m_\chi^2 \chi^2 \right]. \quad (2.7.45)$$

Now by operating the following change of variables

$$A_\mu = A'_\mu + \frac{1}{m_\gamma} \partial_\mu \chi, \quad (2.7.46)$$

which has the look of a gauge transformation, the field-strength is left invariant, while the mass term changes as

$$\frac{1}{2} m_\gamma^2 A_\mu^2 = \frac{1}{2} m_\gamma^2 (A'_\mu)^2 + m_\gamma A'_\mu \partial_\mu \chi + \frac{1}{2} (\partial_\mu \chi)^2. \quad (2.7.47)$$

The resulting action is given by

$$S = \int d^4x \left[ \frac{1}{4} (F'_{\mu\nu})^2 + \frac{1}{2} m_\gamma^2 (A'_\mu)^2 + m_\gamma A'_\mu \partial_\mu \chi - \frac{1}{2} m_\chi^2 \chi^2 \right], \quad (2.7.48)$$

and the integration over  $\chi$ , done by completing the square, leads to

$$\begin{aligned} S &= \int d^4x \left[ \frac{1}{4} (F'_{\mu\nu})^2 + \frac{1}{2} m_\gamma^2 (A'_\mu)^2 + \frac{m_\gamma^2}{2m_\chi^2} (\partial_\mu A'_\mu)^2 \right] \\ &\equiv \int d^4x \left[ \frac{1}{4} (F'_{\mu\nu})^2 + \frac{1}{2} m_\gamma^2 (A'_\mu)^2 + \frac{1}{2\xi} (\partial_\mu A'_\mu)^2 \right], \end{aligned} \quad (2.7.49)$$

that is the Proca action with the addition of a Lorenz gauge fixing term with parameter  $\xi \equiv m_\gamma^2/m_\chi^2$ . The propagator in momentum space now looks

$$\Delta_{\mu\nu}(k) = \frac{\delta_{\mu\nu}}{k^2 + m_\gamma^2} + \frac{(\xi - 1)k_\mu k_\nu}{(k^2 + m_\gamma^2)(k^2 + \xi m_\gamma^2)} \xrightarrow{k \rightarrow \infty} 0, \quad (2.7.50)$$

which as the correct UV behavior, and the theory is renormalizable by power counting.

### 2.7.2 Solution of the Gauss law problem

We want to investigate the possibility of having a charge in a box in the case of massive QED in the Feynman gauge ( $\xi = 1$ ), see Eq. 2.7.49.

The action in the presence of a coupling with an external current  $j_\mu$  is

$$\int d^4x \left[ \frac{1}{4} (F'_{\mu\nu})^2 + \frac{1}{2} m_\gamma^2 (A'_\mu)^2 + \frac{1}{2} (\partial_\mu A'_\mu)^2 + j_\mu A'_\mu \right] \quad (2.7.51)$$

and the Euler-Lagrange equation of motion is given by

$$\sum_\nu \partial_\nu F'_{\nu\mu}(x) = j_\mu(x) + (m_\gamma^2 - \square) A'_\mu. \quad (2.7.52)$$

By integrating in the spatial volume the time component, to find the charge, we have

$$\text{l.h.s.} : \int_{V_3} d^3x \sum_\nu \partial_\nu F'_{\nu 0}(x) = \int_{V_3} d^3x \sum_j \partial_j E'_j(x) \equiv 0 \quad (2.7.53)$$

that is still vanishing due to periodic boundary condition imposed on the fields, while the r.h.s. of Eq. 2.7.52 becomes

$$\text{r.h.s.} : \int_{V_3} d^3x j_0(x) + \int_{V_3} d^3x (m_\gamma^2 - \square) A'_0 = Q + \int_{V_3} d^3x (m_\gamma^2 - \square) A'_0. \quad (2.7.54)$$

By combining the results we get that the condition on the charge is

$$Q = \int_{V_3} d^3x (\square - m_\gamma^2) A'_0, \quad (2.7.55)$$

from which we conclude that the charge is not restricted to be zero, in contrast to massless QED in a finite box (with the same periodic boundary conditions).

**Coulomb gauge and mass term** We can ask ourself what happens if we use a different gauge condition on top of the addition of the mass term. The Lagrangian in the case of Coulomb gauge fixing is given by

$$\mathcal{L} = \frac{1}{4} (F_{\mu\nu})^2 + \frac{1}{2} m_\gamma^2 A_\mu^2 + \frac{1}{2} \sigma (\partial_i A_i)^2, \quad (2.7.56)$$

where  $\sigma$  is a dimensionless parameter and it ensures that in the massless limit the fields satisfies the Coulomb gauge condition.

By following Ref. (Mück, 2013) we find that the propagator for the above Lagrangian is given by

$$\Delta_{\mu\nu}(k) \propto \frac{1}{k^2 + m_\gamma^2} \left[ \delta_{\mu\nu} + \frac{(k^2 + m_\gamma^2 + \sigma |\underline{k}|^2) k_\mu k_\nu + 2\sigma |\underline{k}|^2 k_i (\delta_{i\mu} k_\nu + \delta_{i\nu} k_\mu) + \sigma m_\gamma^2 \delta_{i\mu} \delta_{j\nu} k_i k_j}{m_\gamma^2 (k^2 + m_\gamma^2 + \sigma |\underline{k}|^2) + \sigma |\underline{k}|^2} \right], \quad (2.7.57)$$

which has a smooth massless limit but in the infinite momentum limit goes to a constant, hence the theory is not renormalizable by power counting. It should be noted that the second term, which is responsible for the non renormalizability of the theory, becomes a pure gauge term, in the

massless limit, when the photon is coupled to a conserved current, i.e.  $\partial_\mu J_\mu = 0 \leftrightarrow k_\mu \tilde{J}_\mu = 0$ , and it does not play any role<sup>9</sup>.

The problem of the charge it is also solved in this particular setting and the conclusion made for the previous section can be applied also here. Although one has to remember to take first the infinite volume limit, such that the zero mode problem is resolved, then the massless limit, such that we recover a renormalizable theory (at least by perturbation theory power counting) and finally the continuum limit, which strictly speaking does not exist because of the Landau pole. That because there is no mechanism similar to the Stueckelberg one at the moment for the massive QED with Coulomb gauge condition.

## 2.8 Wilson loops

We tested the code written for the generation of quenched QED configurations by calculating the exact value of the Wilson loops in an infinite lattice, see appendix D.6. The expectation value of a square Wilson loop in the plane  $(\mu, \nu)$  is given by

$$w_{\mu\nu}(I, I) = \exp(-2e^2 Q^2 [C_\mu(I, 0) - C_\nu(I, I\hat{\nu})]), \quad (2.8.58)$$

where  $C_\mu(I, x)$  is the sum of propagators in the  $\mu$  direction, which is one side of the Wilson loop,

$$C_\mu(I, x) = a^2 ID(x) + a^2 \sum_{\tau=1}^{I-1} (I - \tau) D(x + a\tau\hat{\mu}), \quad (2.8.59)$$

and  $D$  is the massless/massive scalar propagator in coordinate space on the lattice. The propagator is calculated in the infinite volume through the Lüscher-Weisz algorithm (Lüscher and Weisz, 1995), see App. D.7 for the algorithm details, while the Borasoy-Krebs algorithm in Ref. (Borasoy and Krebs, 2005) is employed for the massive propagator. For Lorentz invariance  $w_{\mu\nu}(I, I)$  takes always the same value for each choice  $\mu, \nu$ , so we write directly  $w(I, I)$ .

### 2.8.1 Massless case

In Fig. 2.1 we show the comparison between the generation in Feynman and (extended) Coulomb gauge with the infinite lattice predictions (calculated in App. D.6). The quantity plotted is the log of the average of the Wilson loop over 100 configurations in a  $32^4$  volume, with  $eQ = 1$ . The errors are calculated with the standard deviations since the configurations are not correlated at all.

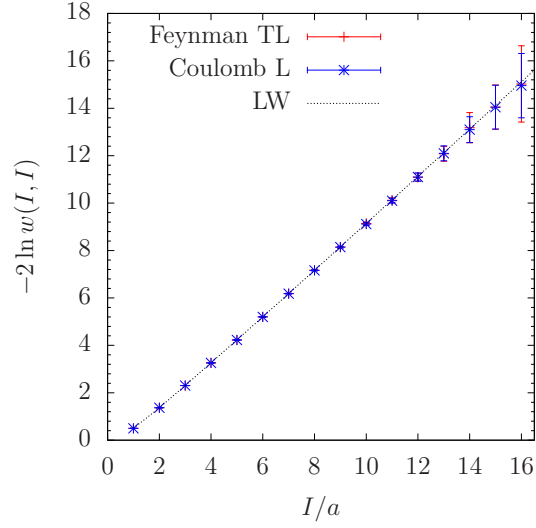
### 2.8.2 Massive case

In Fig. 2.2 we show the comparison between the generation in Feynman and Coulomb gauge,  $eQ = 1$ , with the infinite lattice predictions, calculated as explained above. The quantity plotted is the log of the average of the Wilson loop over 100 configurations in a  $32^4$  volume, with  $eQ = 1$ . The errors are calculated through the standard deviations.

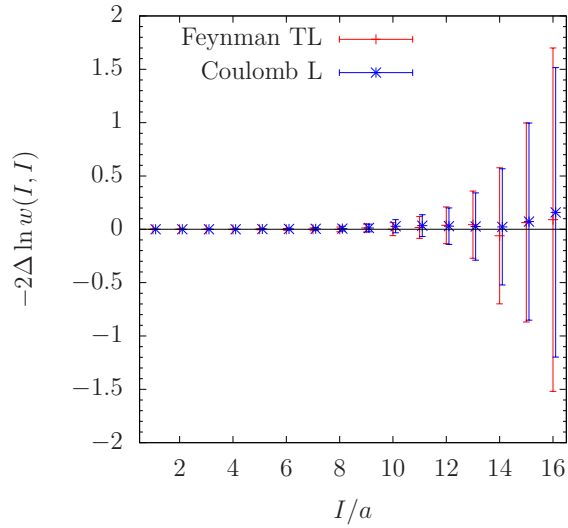
---

<sup>9</sup>On the lattice we may encounter a noise cancellations problem, since the term has to disappear on average.



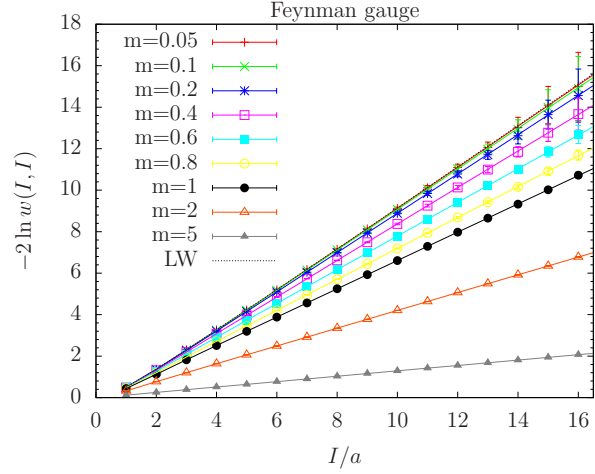


(a) Comparison between the Wilson loop values in Feynman (red segments) and extended Coulomb gauge (blue stars) and the infinite lattice predictions (LW) (dashed line).

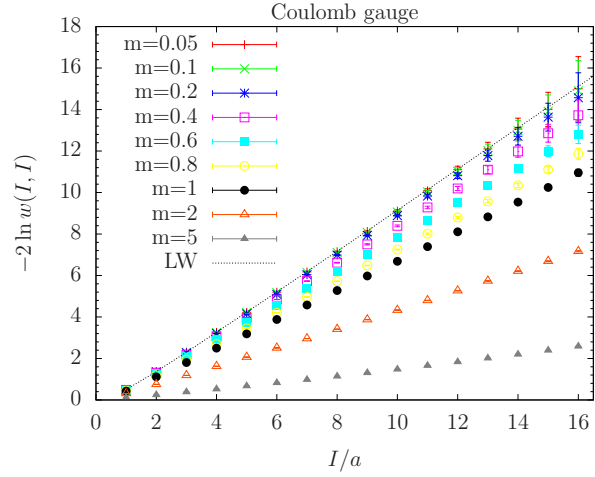


(b) Difference between the Wilson loop values calculated in Feynman and extended Coulomb gauge and the infinite lattice predictions.

Figure 2.1: Wilson loop values in a volume  $V = 32^4$  and their comparison with the infinite volume predictions calculated through the Lüscher-Weisz algorithm.



(a) Massive Feynman gauge. Comparison with the massless result (dashed line) using the Luscher-Weisz algorithm and massive one (solid line) using the Borasoy-Krebs algorithm.



(b) Massive Coulomb gauge. Comparison with the massless result (dashed line) Luscher-Weisz.

Figure 2.2: Comparison of Wilson loop values from simulations and infinite volume predictions calculated through the Borasoy-Krebs algorithm.



## Chapter 3

# Reweighting twisted boundary conditions

Simulations of Euclidean quantum field theories are necessarily performed in a finite space-time volume, hence imposition of boundary conditions on the fields has to be made. Although different choices for boundary conditions have the same correct infinite volume limit, its approach depends on the choice. Recent examples, in lattice QED, of different finite volume effects can be found in (Lucini *et al.*, 2016) (C\* boundary conditions) and in (Borsanyi and others, 2015) (periodic boundary conditions along with exclusion of zero modes). Algorithmic efficiency and sampling properties of the simulations are also affected by the boundary conditions. Examples of that can be found in (Luscher and Schaefer, 2011) for the use of open boundary conditions in lattice QCD to bypass the freezing of topology ((Mages *et al.*, 2017) for the same with C\* boundary conditions), and in (Della Morte and Giusti, 2011) for the use of generalized boundary conditions in order to exponentially improve the signal-to-noise ratio in glueball correlation functions computed in the pure gauge theory.

Usually in lattice QCD (anti)-periodic boundary conditions in (time)-space are imposed on the fermionic fields. That leads to a quantization of the spatial momenta in units of  $2\pi/L_\mu$ . In a two body hadron decay the energies of the resulting particles cannot assume physical values unless their masses are consistent with the momentum quantization rule. In addition, for several phenomenological applications a fine resolution of small momenta is needed, examples include form factors (as  $K \rightarrow \pi \ell \nu$  transition), charge radius of the pion, and the hadronic vacuum polarization of the photon (relevant for  $g - 2$  anomaly). This still represents a severe limitation, in order to have the lowest non-zero momentum around 100 MeV we need lattices of about 12 fm. Since we also want to keep discretization effects under control lattice spacings  $a$  around 0.1 fm and below are necessary, then simulations are still expensive in computer time.

Twisted boundary conditions (TBCs) were first introduced in (de Divitiis *et al.*, 2004, Bedaque, 2004) and they serve as a solution to the problem of quantized momenta on the lattice in QCD. TBCs correspond to periodic ones up to a phase, the twisting angle  $\theta$ , for fermion fields in spatial directions only and they allow the lattice momenta to be continuously varied. TBCs represent a standard tool in the lattice community. They were used in the computation of quantities above mentioned (see (Flynn *et al.*, 2007, Brandt *et al.*, 2013, Della Morte *et al.*, 2012) for a selection of them) and also for RI-MOM scheme (Arthur and Boyle, 2011) and matching between Heavy Quark Effective Theory and QCD (Della Morte *et al.*, 2014).

In all the simulations so far the twisting is only applied in the valence sector while the sea fermions obey periodic boundary conditions. This kind of set-up is usually referred to as *partial*

*twisting*. That introduces a unitarity breaking as a boundary effect, which has to disappear in the infinite volume limit. In (Sachrajda and Villadoro, 2005) this was explicitly checked by means of Chiral Perturbation Theory for meson masses, decay constants and semileptonic form factors. This also suggests that reweighting techniques might be used to change the boundary conditions for the sea fermions and compensate for the unitarity violation.

In the following we will see that resulting reweighting factors are ratios of fermionic determinants that go to one in the infinite volume limit. In that regime is also difficult to give a reliable estimate of the reweighting factors, since they are extensive quantities. Unitarity violations, if present, are expected in rather small volumes where the reweighting factors can be reliably calculated.

The chapter is organized as follows; in Section 1 we review twisted boundary conditions, in Section 2 we recall the reweighting method and specialize it to the twisted boundary conditions case, in Section 3 we introduce the multi-step method based on tree-level exact studies on reweighting factors and their variances. Simulation parameters and Monte-Carlo results in small and large volumes are presented in Section 4. Section 5 contains pion and quark mass dependence on the twisting angle. Section 6 contains our conclusions. The chapter reflects the work presented in Refs. (Bussone *et al.*, 2017, Bussone *et al.*, 2016b).

### 3.1 Twisted boundary conditions

Generic boundary conditions for fermion fields in lattice QCD on a torus are discussed in (Sachrajda and Villadoro, 2005). There it is pointed out that fields do not need to be single valued on the torus, while the action does. Hence periodicity conditions on the fermions can be of the form

$$\Psi(x + L_\mu \hat{\mu}) = V_\mu \Psi(x), \quad \mu = 1, 2, 3, \quad (3.1.1)$$

where  $\Psi$  is a flavor multiplet and  $V_\mu$  represents a unitary transformation associated to a symmetry of the action. Similarly, for the  $\bar{\Psi}$  one requires

$$\bar{\Psi}(x + L_\mu \hat{\mu}) = \bar{\Psi}(x) V_\mu^\dagger, \quad \mu = 1, 2, 3. \quad (3.1.2)$$

If we consider generic values of the diagonal quark mass matrix, one concludes that  $V_\mu$  also has to be diagonal in flavor space, i.e.

$$\psi(x + L_\mu \hat{\mu}) = e^{i\theta_\mu} \psi(x), \quad (3.1.3)$$

where the twisting angles  $\theta_\mu$  have been introduced for each flavor ( $\psi$  is a component of the  $\Psi$  flavor multiplet) and

$$\theta_\mu = (0, \underline{\theta}), \quad \text{where } \theta_j \in [0, 2\pi) \text{ are fixed.} \quad (3.1.4)$$

By Fourier transforming the equation Eq. 3.1.3 we obtain

$$\int d^4k e^{ik \cdot (x + L_\mu \hat{\mu})} \tilde{\psi}(k) = e^{i\theta_\mu} \int d^4k e^{ik \cdot x} \tilde{\psi}(k). \quad (3.1.5)$$

Since the fermionic field is an arbitrary function of  $k$ , in order to satisfy the above equality the exponentials have to be identical

$$\exp \left[ i \left( k_\mu - \frac{\theta_\mu}{L_\mu} \right) L_\mu \right] = 1 \implies \begin{cases} k_0 = \frac{2\pi}{L} z_0 \\ k_j = \frac{2\pi}{L} z_j + \frac{\theta_j}{L}, \quad \text{when } j = 1, 2, 3 \end{cases}, \quad (3.1.6)$$

where the  $z$ 's are integer numbers,  $z_\mu \in (-L_\mu/2, L_\mu/2] \subset \mathbb{Z}$ . Eq. 3.1.6 shows the equivalence between TBCs and momenta shift. Note that in the infinite volume limit the  $\theta$ -term disappear,

for fixed  $\theta$ , in Eq. 3.1.6. On the contrary, when the gap between momenta is not negligible, thanks to  $\theta$  we have direct access to values of momenta that are not allowed with PBCs.

An equivalent way to impose TBCs is due to (Bedaque, 2004). We can fix the fermionic fields to be periodic and introduce a *constant*  $\mathbf{U}(1)$  interaction with constant background magnetic potential  $\underline{A} = \underline{\theta}/L$ , vanishing electric, magnetic fields and vanishing electric potential. This interaction can be implemented by transforming the standard  $\mathbf{SU}(N_c)$  gauge links  $U_\mu(x)$  in the following way

$$\mathcal{U}_\mu(x) = \exp \left[ i \frac{\theta_\mu}{L_\mu} \right] U_\mu(x) = \begin{cases} U_0(x) \\ \exp \left[ i \frac{\theta_j}{L_j} \right] U_j(x), & \text{when } j = 1, 2, 3, \end{cases} \quad (3.1.7)$$

note that the exponential factor is independent of  $x$ . The fermions  $\psi$  are kept with PBCs and in order to see the equivalence between the two formulations it is enough to observe that the phase can be re-absorbed by re-writing the  $\psi$  fields in terms of

$$\chi(x) = e^{i \underline{\theta} \cdot \underline{x}/L} \psi(x), \quad (3.1.8)$$

and to notice that the  $\chi$  are indeed periodic up to a phase, as for Eq. 3.1.3.

In practice,  $\mathbf{SU}(N_c)$  gauge configurations are typically produced for one specific choice of  $\theta$ , and the angle is then varied only when computing the quark propagators, which is cheaper in terms of CPU-time with respect to the generation of configurations. As a consequence, the quark propagators in the sea and valence sectors differ, which causes a breaking of unitarity already at the perturbative level.

## 3.2 Reweighting technique

In the following we use the un-improved Wilson action in Eq. 1.4.37, with the links  $U_\mu(x)$  replaced by the  $\mathcal{U}_\mu(x)$  as in Eq. 3.1.7, and Wilson plaquette action in Eq. 1.4.29 for the gauge links. The link redefinition does not change the plaquette (see Eq. B.2.12), and therefore the pure gauge term in the action. The covariant derivatives and the Wilson term are, on the contrary, modified. For this purpose we denote the Dirac operator with gauge link  $U_\mu$  and  $\theta$ -angle as  $D[U, \theta]$ . Once the fermionic degrees of freedom are integrated out on each  $\mathbf{SU}(N_c)$  gauge background, the  $\theta$ -dependence from the sea sector is completely absorbed in the fermionic determinant.

Let us imagine we want to compute the value of some observables for one choice of bare parameters  $B = \{\beta', m'_1, m'_2, \dots, m'_{n_f}, \theta'_\mu, \dots\}$  using the configurations produced at a slightly different set of parameters  $A = \{\beta, m_1, m_2, \dots, m_{n_f}, \theta_\mu, \dots\}$ . To do so we need to compute on each configuration of the  $A$ -ensemble the reweighting factor  $W_{AB} = P_B/P_A$ , which is the ratio of the two probability distributions and it is an extensive quantity,  $P_A[U] = e^{-S_G[\beta, U]} \prod_{i=1}^{N_f} \det(D[U, \theta] + m_i)$  ( $N_f$  being the number of fermion species). The expectation values on the  $B$ -ensemble can then be expressed as

$$\langle \mathcal{O} \rangle_B = \frac{\langle \tilde{\mathcal{O}} W_{AB} \rangle_A}{\langle W_{AB} \rangle_A}, \quad (3.2.9)$$

with  $\tilde{\mathcal{O}}$  being the observable defined after Wick contractions, and  $\langle \dots \rangle_A$  indicates that expectation values have to be taken on the  $A$ -ensemble. By specializing ourself to the case where only the fermionic  $\theta$ -angles are changed from one bare set to the other, we obtain the following expression of the reweighting factor

$$W_\theta = \det(D_W[U, \theta] D_W^{-1}[U, 0]) = \det(D_W[\mathcal{U}, 0] D_W^{-1}[U, 0]), \quad (3.2.10)$$

where we have also chosen  $D$  to be  $D_W$ , i.e., the massive Dirac-Wilson operator. Following (Finkenrath *et al.*, 2013) we see that ratios of determinants as those above can be estimated stochastically. For a normal matrix  $M$ , whose spectrum is  $\lambda(M)$ , the following representation of the determinant holds

$$\frac{1}{\det M} = \int \mathcal{D}[\eta] \exp(-\eta^\dagger M \eta) < \infty \iff \Re \lambda(M) > 0. \quad (3.2.11)$$

The positivity condition ensures the absolute convergence of the integral and the integral can be evaluated stochastically. We can generate an ensemble of complex random vectors, say  $\{\eta_k, k = 1, 2, \dots, N_\eta\}$  according to a probability distribution  $p(\eta)$ . The distribution  $p(\eta)$  of the vectors  $\eta$  is usually taken to be Gaussian,  $p(\eta) = \exp(-\eta^\dagger \eta)$ , and in that case, the determinant (or its inverse) can be written as

$$\frac{1}{\det M} = \left\langle \frac{e^{-\eta^\dagger M \eta}}{p(\eta)} \right\rangle_{p(\eta)} = \frac{1}{N_\eta} \sum_{k=0}^{N_\eta} e^{-\eta_k^\dagger (M-1) \eta_k} + \mathcal{O}\left(\frac{1}{\sqrt{N_\eta}}\right). \quad (3.2.12)$$

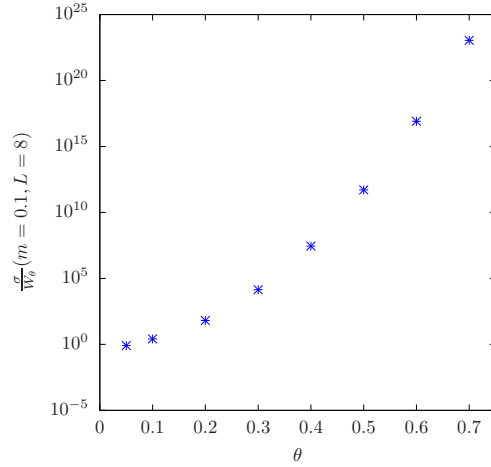
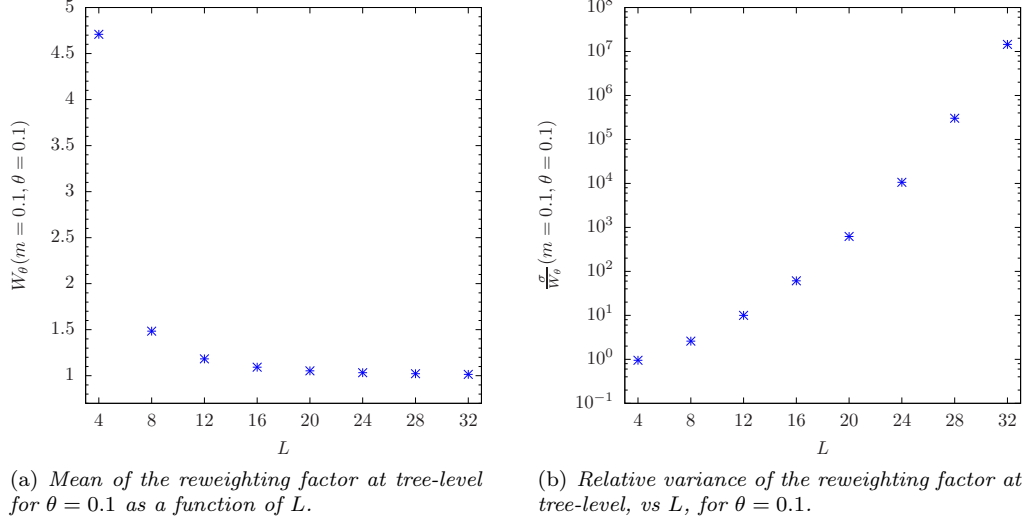
It is straightforward to generalize the positivity condition above in order to ensure the convergence of the stochastic estimates of all Gaussian moments. In the case of an hermitian matrix one obtains

$$\begin{aligned} \left\langle \frac{e^{-2\eta^\dagger M \eta}}{p(\eta)^2} \right\rangle_{p(\eta)} &= \int \mathcal{D}[\eta] \exp[-\eta^\dagger (2M - \mathbf{1}) \eta] < \infty \iff \lambda(M) > \frac{1}{2}, \\ &\vdots \\ \left\langle \frac{e^{-N\eta^\dagger M \eta}}{p(\eta)^N} \right\rangle_{p(\eta)} &= \int \mathcal{D}[\eta] \exp[-\eta^\dagger [NM - (N-1)\mathbf{1}] \eta] < \infty \iff \lambda(M) > \frac{N-1}{N} \xrightarrow{N \rightarrow \infty} 1. \end{aligned} \quad (3.2.13)$$

All eigenvalues should therefore be larger than unity. In particular, in the numerical studies presented here we will always consider the square of the hermitian version of the Dirac-Wilson operator,  $Q = \gamma_5 D_W$ , which is to say we consider the case of two degenerate flavors.

### 3.3 Tree-level studies

In the App. B.1 we give results for the spectrum of the free Dirac-Wilson operator. This provides some insights on the large volume asymptotic scaling of the reweighting factors and their variances. Given the finite-volume nature of twisting, a rather obvious expectation is that the reweighting factors approach the value 1 at fixed  $\theta$  and in large volumes. That is confirmed at tree-level, as shown in Fig. 3.1(a). On the other hand, the reweighting factor remains an extensive quantity, and the corresponding variance grows in the same limit, which is therefore very difficult to be reached numerically. It is clear from Fig. 3.1(b) that the noise to signal ratio grows at least exponentially as the volume is increased at fixed  $\theta$ . The same exponential growth is observed as  $\theta$  is made larger at fixed  $L$  (see Fig. 3.1(c)). A factorization of the observable has been proven to be effective in this case in various instances (Della Morte and Giusti, 2011, Luscher and Weisz, 2001) and in analogy to what has been done in (Finkenrath *et al.*, 2013) for the case of mass reweighting, we will pursue a similar approach here. A natural choice is to split the determinants ratio in the following telescopic



(c) Relative variance of the reweighting factor at tree-level, vs  $\theta$ , for  $L = 8$ .

Figure 3.1: Results for the reweighting factor mean and variance employing the exact formulae in the tree-level case. Each point corresponds to a cubic lattice of the form  $L^4$  with  $N_f = 2$ ,  $N_c = 2$  and  $m = 0.1$ .

way

$$A = D_W(\theta)D_W^{-1}(0) = \prod_{\ell=0}^{N-1} A_\ell, \quad \text{with } A_\ell = D_W(\theta_{\ell+1})D_W^{-1}(\theta_\ell) \simeq \mathbf{1} + O(\delta\theta),$$

$$\theta_\ell = \delta\theta \cdot \ell \quad \text{and} \quad \delta\theta = \frac{\theta}{N}, \quad (3.3.14)$$

where  $A_\ell$  are now matrices deviating from the identity by small amounts of  $O(\delta\theta)$ . This also reduce the relative fluctuation of the reweighting factor, as can be seen in Fig. 3.1(b). The inverse



determinant and its error  $\varepsilon_{|A^{-1}|}$  are then reconstructed in terms of the  $N$  corresponding estimators  $1/\det A_\ell$  and  $\varepsilon_{|A_\ell^{-1}|}$ , one for each factor  $A_\ell$  in the equation above, as

$$\frac{1}{\det A} = \prod_{\ell=0}^{N-1} \frac{1}{\det A_\ell} = \prod_{\ell=0}^{N-1} \left\langle \frac{\exp(-\eta^{(\ell),\dagger} A_\ell \eta^{(\ell)})}{p(\eta^{(\ell)})} \right\rangle_{p(\eta^{(\ell)})}, \quad (3.3.15)$$

and

$$\varepsilon_{|A^{-1}|}^2 = \sum_{\ell=0}^{N-1} \left[ \varepsilon_{|A_\ell^{-1}|}^2 \prod_{k \neq \ell} \det(A_k)^{-2} \right]. \quad (3.3.16)$$

Based on the tree-level results we have presented, the expression on the r.h.s. of the equation above is given by a sum of  $N$  terms, each one depending exponentially on  $\delta\theta$  (for values of  $\delta\theta$  such that the variance in Fig. 3.1(c) is approximately growing exponentially with the twisting angle) and therefore, at fixed  $\delta\theta$ , the squared error of the telescopic product is expected to grow linearly with  $\theta$ . That is to be compared to the exponential growth of the error one would obtain by attempting to compute the ratio of determinants for large shifts in  $\theta$  in one single step.

### 3.4 Simulations and results

For the numerical computations, we have used gauge configurations produced for the **SU**(2) gauge theory with two fermions in the fundamental representation. Dynamical configurations have been generated using un-improved Wilson fermions and the Wilson plaquette gauge action. This model is a QCD-like theory, featuring chiral symmetry breaking and confinement. The outcome of the present study should hence remain qualitatively unchanged for the case of lattice QCD. Indeed, at tree-level the reweighting factors scale with a power of  $N_c$ , see Eq. B.1.4.

In Table 3.1 we collect details about the ensembles used in this work, for completeness, the value  $m_c$  of the bare mass parameter yielding massless fermions is estimated to be  $-0.77(2)$  at  $\beta = 2.2$  (Lewis *et al.*, 2012, Hietanen *et al.*, 2014, Arthur *et al.*, 2016). We have considered both

$V$	$\beta$	$m_0$	$N_{\text{cnf}}$	traj. sep.
$8^3 \times 16$	2.2	-0.6	980	10
$24^3 \times 32$	2.2	-0.65	374	20
$24^3 \times 32$	2.2	-0.72	360	10

Table 3.1: *Ensembles used and simulation parameters in the reweighting of TBCs.*

small and large volumes, which we will discuss separately.

At fixed value of  $\theta$  the effect of twisting and therefore of reweighting is at its largest in small volumes, based on the tree-level studies. This is the region where the stochastic methods should provide reliable estimates. We restricted ourselves to the case of reweighting to spatially isotropic<sup>1</sup>  $\theta$  angles and adopted the hermitian  $\gamma_5$ -version of the Dirac-Wilson operator with two flavors, since that automatically fulfills the applicability condition<sup>2</sup> in Eq. 3.2.11.

In order to get an insight on the number  $N_\eta$  of Gaussian vectors necessary to obtain a reliable estimate of the reweighting factor, we computed it on the trivial ( $U_\mu(x) = \mathbf{1}$ ) gauge configuration and compared it to the analytical tree-level prediction. The results are shown in Fig. 3.2. There,

<sup>1</sup>Notice that for non-isotropic  $\theta$  parity is explicitly broken.

<sup>2</sup>Notice that  $Q[U, 0]$  and  $Q[\mathcal{U}, 0]$  commute.

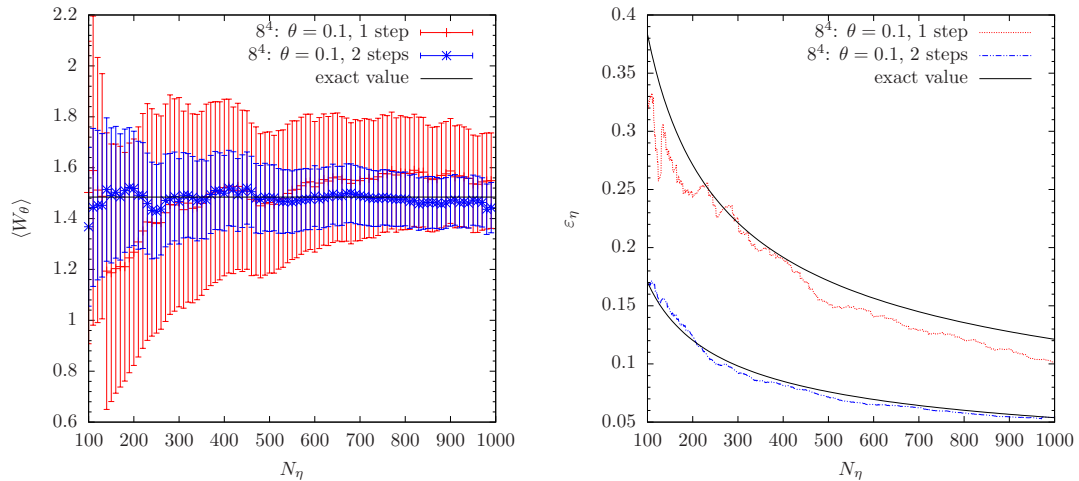


Figure 3.2: Comparison between the stochastic and exact estimates of the reweighting factor and its variance on the trivial gauge configuration for  $\theta = 0.1$ ,  $L = 8$  using one and two levels of factorization in the numerical case. Both plotted against the number  $N_\eta$  of Gaussian vectors in each level.

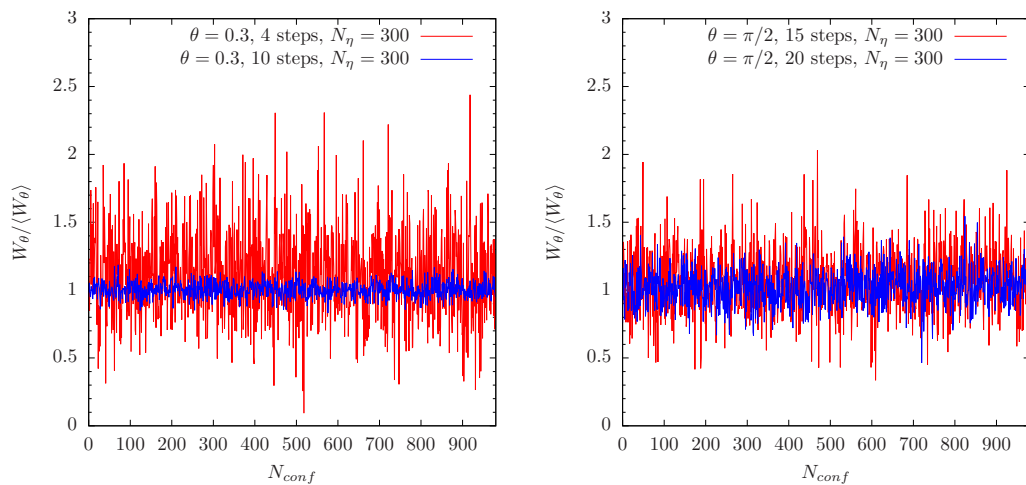


Figure 3.3: Monte Carlo history of the reweighting factor relative to its mean for the  $8^3 \times 16$  ensemble and with  $N_\eta = 300$ .

by looking at the statistical error, one sees that about 300 Gaussian vectors are necessary for  $\epsilon_\eta$  to reach the correct scaling with  $N_\eta$ .

Turning now to actual Monte Carlo data, in particular from the  $8^3 \times 16$  ensemble, we found that under a similar condition ( $N_\eta \gtrsim 300$ ) the reweighting factor on each configuration deviates by more than a factor 10 in magnitude from its gauge average in a few cases only (see Fig. 3.3). This prevents the averages to be dominated by large fluctuations (“spikes”), which would cause large

statistical errors, and sets a lower limit on  $N_\eta$ . In Figs. 3.4(a) and 3.4(b) we show the mean of the reweighting factor, with each point resulting from an average over  $10^3$  configurations, as a function of  $N_\eta$ . A good scaling of the error is visible, according to  $N_\eta^{-1/2}$ , up to  $N_\eta \approx 500$ . At that point the statistical noise saturates the gauge noise, and therefore the error on the gauge average does not decrease any further by increasing  $N_\eta$ . This sets an upper limit to about 600 for the number of Gaussian vectors to be used in the stochastic evaluation of the determinants ratio. In addition, it implies that for  $N_\eta \gtrsim 600$  one can safely consider the gauge noise only in the error analysis. In the following, we do that by a standard (single-elimination) jackknife plus binning procedure.

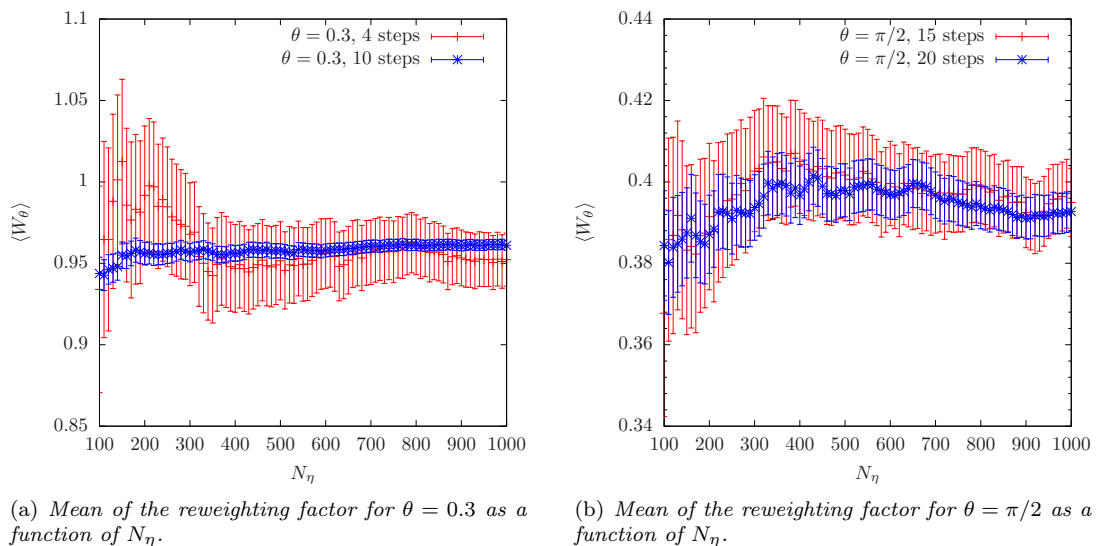


Figure 3.4: Monte Carlo average of the reweighting factor, averaged over the entire number of configurations vs  $N_\eta$ . The figures correspond to a volume  $V = 8^3 \times 16$ .

### 3.4.1 Small volumes

In the small volume regime the effect of partial twisting and the associated breaking of unitarity may be large, and we want to compensate for it by reweighting the observable at hand. In order to isolate the contribution due to the determinants ratio, we looked first at the plaquette, for which the entire dependence on  $\theta$  comes from the quarks in the sea only, see App. B.2. Here and in the following we neglect autocorrelations since measurements are separated by 10 to 20 molecular dynamics units. In any case, a binning procedure, using bins of length up to 10, provides entirely consistent results.

In Fig. 3.5(a) we show the results after reweighting only one flavor, i.e., by taking the square root of the stochastic evaluation of the determinants ratio estimated for the  $Q^2[U, \theta]$  operators (Aoki and others, 2012, Finkenrath *et al.*, 2012). Notice that here and in the following, whenever the root-trick above is used, we consider rather heavy quarks and pions ( $am_\pi \geq 0.45$ ) and we therefore do not expect ambiguities in the sign of the one-flavor determinant. Effects are visible within statistical errors for large values of  $\theta$  only. Those are more pronounced when both flavors are reweighted, as depicted in Fig. 3.5(b). In addition, in this case, the reweighted results can be

checked by a direct HMC simulation<sup>3</sup> at  $\theta \neq 0$ . Notice that we are discussing pernil shifts, which we access by using very large statistics ( $\approx 10^4$  configurations). We interpret this slight tension as signalling the limit of validity of the reweighting method for the application discussed here. In the following, we therefore restrict the values of the twisting angle to the interval  $[0, \pi/2]$ .

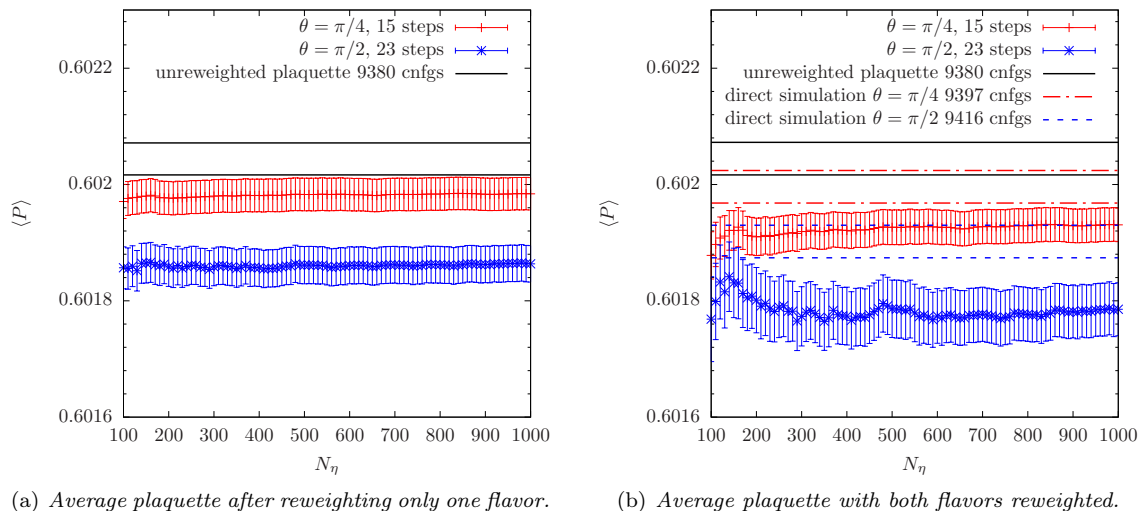


Figure 3.5: Monte Carlo history of the reweighted plaquette. The figures correspond to a volume  $8^3 \times 16$ .

The other quantity we have analyzed is the pion dispersion relation. After twisting only one flavor in the valence, the lowest energy state coupled to a spatially summed interpolating field is expected to become a “quenched” pion with momentum  $\vec{p} = \pm\vec{\theta}/L$ , see App. B.2. In order to remove this quenching effect we have reweighted the relevant correlators for the twisting of one flavor in the sea and we have extracted the effective energies from their time-symmetrized versions. In Fig. 3.6 we display the results for the dispersion relation and we compare them to the un-reweighted, partially twisted, data (i.e., with twisting in the valence only), to the continuum prediction  $(aE)^2 = (am_\pi)^2 + 3(a\theta)^2/L^2$  (we use  $\vec{\theta} = \theta(1, 1, 1)$ ) and to the lattice free boson theory prediction  $\cosh(aE) = 3 + \cosh(am_\pi) + 3\cos(a\theta/L)$ . Over the entire range of  $\theta$  values explored there is no significant effect within errors. Let us remark that, following (Boyle *et al.*, 2008), all two-point functions have been computed using  $Z_2 \times Z_2$  single time-slice stochastic sources.

### 3.4.2 Large volumes

As suggested by the tree-level studies, in large volumes, the accuracy in the determination of the reweighting factors and the overall effect of twisting are very much reduced, compared to the previous case. We have looked at the pion dispersion relation for two different values of  $m_\pi$  as we expect to detect possibly sizeable effects for rather light quarks. However, at the volume considered ( $V = 24^3 \times 32$ ), it appears as one can safely neglect any breaking of unitarity. The results are shown in Fig. 3.7. Indeed, reweighting does not seem to yield any significant effect within the half a percent statistical errors.

<sup>3</sup>For the one-flavor case one would have to consider the RHMC algorithm.

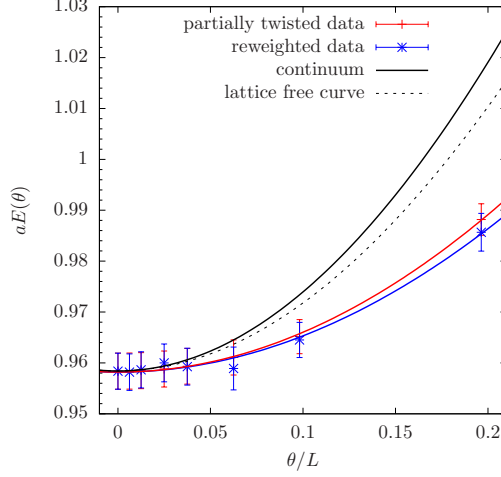


Figure 3.6: *Pion dispersion relation for  $V = 8^3 \times 16$ . Each point is obtained with a different (growing with  $\theta$ ) number of independent steps in the determination of the reweighting factor and  $N_\eta \gtrsim 600$  in each step.*

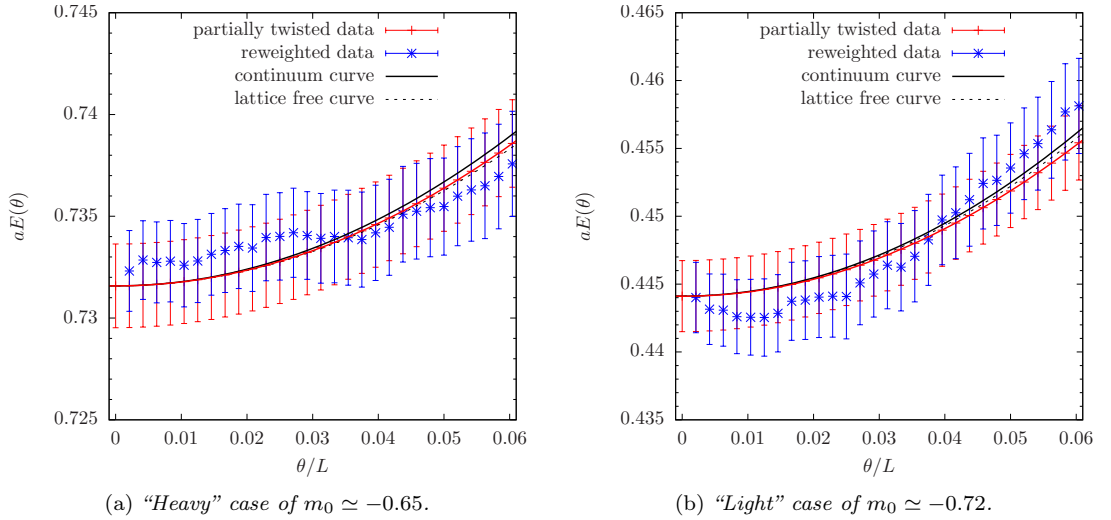


Figure 3.7: *Pion dispersion relation for  $V = 24^3 \times 32$ . The reweighting factor at a given  $\theta$  is obtained by a telescopic product involving all the previous ones, each one estimated using  $N_\eta \gtrsim 600$ .*

### 3.5 Quark mass dependence on the twisting angle

As mentioned above, non-periodic boundary conditions ( $\theta \neq 0$ ) for fermionic fields are equivalent to introducing a constant  $\mathbf{U}(1)$  interaction, through an external field  $B_\mu(x) = B_\mu$  coupled to periodic fermions. That amounts to replacing the links  $U_\mu$  with the links  $\mathcal{U}_\mu$  given by

$$\mathcal{U}_\mu(x) = e^{iaB_\mu} U_\mu(x), \quad (3.5.17)$$

where  $B_\mu = \theta_\mu/L_\mu$ . In this case the PCAC relation remains unaffected since the new links  $U_\mu(x)$ , being proportional to the identity in flavor, still commute with the Pauli matrices<sup>4</sup>. That implies that the vector transformations are still exact symmetries at finite lattice spacing with Wilson fermions, and that the PCAC relation remains formally the same. Cutoff effects on the other hand depend on the choice of boundary conditions, that has actually been exploited in order to compute improvement coefficients (see, for example, Refs. (Luscher *et al.*, 1997, Durr and Della Morte, 2004)), within the Symanzik improvement programme for Wilson fermions in QCD. In some instances, even after improvement, the quark mass defined through the PCAC relation in rather small volumes, turned out to have a quite pronounced residual (i.e.,  $O(a^2)$ ) dependence on the boundary conditions (Sommer *et al.*, 2004). That is expected to be even larger here, with unimproved Wilson fermions. For completeness, the bare PCAC quark mass  $m_{\text{PCAC}}$  can be defined through the spatially integrated axial Ward identity as:

$$m_{\text{PCAC}} = \frac{\partial_0 \langle A_0(x_0) O(0) \rangle}{2 \langle P(x_0) O(0) \rangle}, \quad (3.5.18)$$

with  $A_\mu$  the axial current,  $P$  the pseudoscalar density (both spatially summed over the  $x_0^{\text{th}}$  time-slice) and  $O$  an interpolating field, which in our case will be simply given by the pseudoscalar density localized at the origin.

---

**Intermezzo: PCAC with TBCs** In the PCAC relation we want the variation of the Wilson term to vanish in the naïve continuum limit,  $a \rightarrow 0$  (see Sect. 1.6.2). Now we have another dimension [1] field to take into account with respect to case with no constant  $U(1)$  interaction. This means that we can write additional operators that mix with  $\mathcal{O}_5$ . In particular we find, following App. A.3 in the case of degenerate flavors,

$$\bar{\mathcal{O}}_5 = Z_5 \left[ \mathcal{O}_5 + \frac{2\bar{m}}{a} P^f + \frac{Z_A - 1}{a} \partial_\mu A_\mu^f + 2 (\bar{B}_\mu)^2 P^f + \tilde{B}_\mu \partial_\mu^- P^f \right], \quad (3.5.19)$$

where  $f$  is a flavor index. By substituting back the above expression in Eq. 1.6.52 we obtain

$$\partial_\mu^- \langle \hat{A}_\mu^f(x) \mathcal{O}(y) \rangle = 2 (m_0 - \bar{m} - a \bar{B}_\mu \bar{B}_\mu) \langle P^f(x) \mathcal{O}(y) \rangle - a \tilde{B}_\mu \partial_\mu^- \langle P^f(x) \mathcal{O}(y) \rangle + \langle \bar{\chi}_A^f(x) \mathcal{O}(y) \rangle. \quad (3.5.20)$$

One of the two extra term, compared to Eq. 1.6.54, is vanishing when we consider the integrated WTI. In particular by projecting to zero momentum we find that the following integral is vanishing ( $B_0 = 0$ )

$$a \tilde{B}_j \int d^3x \partial_j^- \langle P^f(x) \mathcal{O}(y) \rangle = 0, \quad (3.5.21)$$

because we have chosen PBCs for our fields.

In this case  $m_{\text{AWI}}$  in Eq. 1.6.55 is given by

$$m_{\text{AWI}} = m_0 - \bar{m} - a \bar{B}_j^2 = m_0 - f(g_0, am_0, a^2 B_j^2)/a, \quad (3.5.22)$$

hence the zero quark mass is attained when the bare mass is equal to the critical value

$$m_c = f(g_0, am_c, a^2 B_j^2)/a, \quad (3.5.23)$$

---

<sup>4</sup>We are working with two degenerate massive flavors, i.e. the isosymmetric limit.

which is a function of  $g_0$  and  $B_j^2 = \theta_j^2/L^2$  bare parameters. We should note that the function  $f$  depends quadratically on  $B_j$  due to Lorentz invariance.

For the present discussion, it is useful to introduce  $\theta_v$  as the spatially isotropic twisting angle used for all fermions in the valence and  $\theta_s$  as the corresponding one for all fermions in the sea. We produced small volume configurations for different values of  $\theta_s$  and on those we measured quark and pion masses while changing  $\theta_v$ . That can actually be used to get an idea of what the effect of reweighting should be, and we will see that the observations above are confirmed. In particular, at fixed  $\theta_v$ , results depend at most at the percent level only on  $\theta_s$ .

In Fig. 3.8 we show the pion effective masses computed on about 4000 independent configurations generated for lattices of size  $8^3 \times 32$  at  $\beta = 2.2$  and  $m_0 = -0.72$ . All the results in the left panel refer to unitary points, i.e.  $\theta_s = \theta_v$ . Naively one would expect the results to lie on top of each other as they all correspond to zero-momentum pions at the same bare parameters. We ascribe the difference to the dependence of the critical bare mass  $m_c$  on both  $\theta_s$  and  $\theta_v$ , as explained above. Since  $m_c$  is obtained from the PCAC operator identity the dependence on the twisting angles is a boundary, therefore finite volume, cutoff effect. This explains why the continuum dispersion relation is rather poorly reproduced in small volumes and for large values of the twisting angle, as shown in Fig. 3.6. Upon twisting, not only the pions get boosted, but also at least one of the quark masses decreases, such that the two effects partly compensate. In the right panel of Fig. 3.8 the final estimates of the masses are shown as a function of  $\theta = \theta_v$ . The square points are the unitary ones, corresponding to the plateaux in the left panel, whereas the triangle ones are obtained by using configurations produced at  $\theta_s = 0$  on which two-point functions are computed for different values of  $\theta_v = \theta$ . It is clear that by reweighting the sea twisting angle to the valence one at most a percent effect could have been produced here in the case  $\theta_s = 0$ ,  $\theta_v = \pi/2$ .

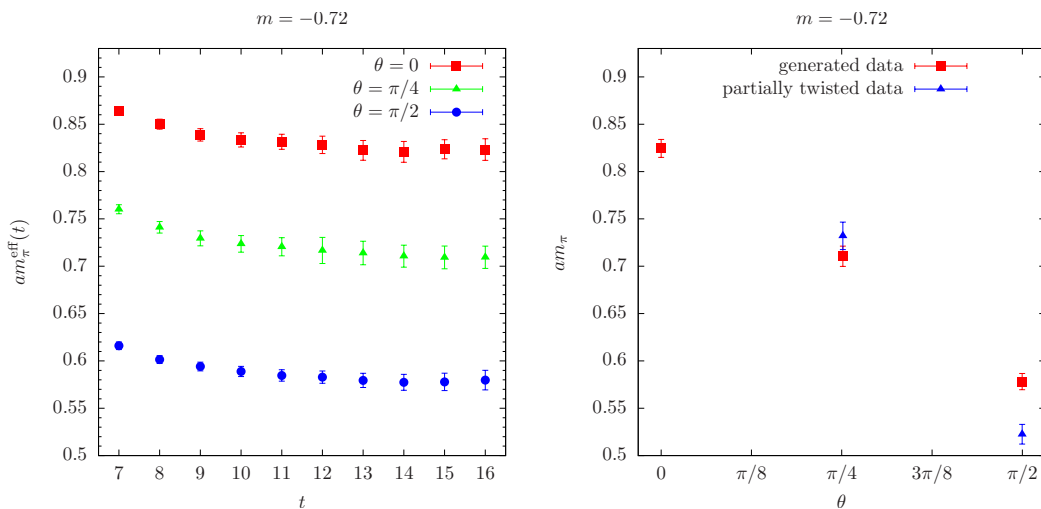


Figure 3.8: Pion effective masses for  $\theta_s = \theta_v = \theta$  on a  $8^3 \times 32$  lattice at  $\beta = 2.2$ ,  $m_0 = -0.72$  (left panel) and comparison of the corresponding plateau masses (red) with the result from  $\theta_s = 0$  as a function of  $\theta = \theta_v$  (right panel).

The bare PCAC quark mass, in the un-improved theory, can be related to the bare parameter

$m_0$  as

$$m_{\text{PCAC}}(\beta, \theta) = Z(\beta, \theta) (m_0 - m_c(\beta, \theta)) , \quad (3.5.24)$$

where  $Z$  is a normalization factor and  $m_c$  is the value of the bare mass parameter defining the massless limit. As a consequence of the breaking of chiral symmetry with Wilson fermions  $m_c$  is different from zero, as opposite to the case of Ginsparg-Wilson or staggered fermions, where at least some axial transformations are preserved and that is enough to rule out an additive renormalization of the bare mass. We are here restricting the attention to the case  $\theta_s = \theta_v = \theta$  and we are working at fixed  $\beta$ . By looking at  $m_{\text{PCAC}}$  as a function of  $m_0$ , for  $m_0$  slightly larger than  $m_c$ , one obtains a family of linear curves parameterized by  $\theta$ . The slope of the curves is given by  $Z$ , while the value of  $m_0$  where the curves intercept the horizontal axis corresponds to  $m_c$ . That is exactly what is shown in Fig. 3.9 for  $m_0 = -0.72, -0.735$  and  $-0.75$  (with  $\beta$  fixed to 2.2 and  $V = 8^3 \times 32$ ). Whereas the dependence of  $Z$  on  $\theta$  is not significant,  $m_c$ , as anticipated, changes substantially with the twisting angle. At  $\theta = \pi/2$  and for  $m_0 = -0.75$  the PCAC mass is roughly one half of the value at  $\theta = 0$ . We find that corresponding ratio for pion masses is within 1.5 and 1.7, which, given the small volumes we have considered, is quite consistent with the scaling in a chirally broken theory.

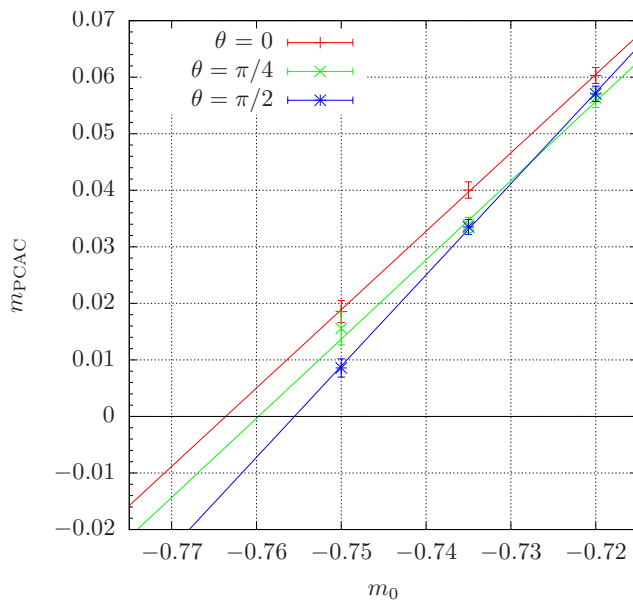


Figure 3.9:  $m_{\text{PCAC}}$  as a function of  $m_0$  computed for  $m_0 = -0.72, -0.735$  and  $-0.75$  at  $\beta = 2.2$  and  $V = 8^3 \times 16$ . The curves correspond to three different values of  $\theta = \theta_v = \theta_s$ .

Finally, let us remark that similar shifts in the quark mass have been discussed for the case of constant external magnetic fields (Brandt *et al.*, 2016). We emphasize that here we are showing that such effects are present also in the case of vanishing magnetic field and constant (vector) potential.

## 3.6 Conclusions

We explored in detail an application of reweighting techniques to the case of modifications in the spatial periodicity of fermions. We have thoroughly studied the approach at tree-level and we have



provided constraints for the convergence of the stochastic estimates of all the Gaussian moments of the reweighting factors. We have also established the large volume scaling of the average and the variance at tree-level.

At the numerical level, we have performed a complete and detailed study of purely gluonic as well as fermionic quantities in both large and small volumes. We considered the plaquette and the pion dispersion relation, the latter in the two regimes. In both cases we found the effects of reweighting to be at the sub-percent level for values of  $\theta$  up to  $\pi/2$ . In our implementation, for the large volumes considered, we found that the reweighting method, with  $N_\eta \approx 600$  is a factor 4-5 cheaper compared to generating new configurations for different values of the twisting angle, assuming that about 20 molecular dynamics units are needed to decorrelate subsequent configurations. We performed this comparison in units of matrix-vector multiplications.

Perhaps the most important observation, which, as far as we know, has so far not been investigated in a dedicated way in the literature, is on the dependence of the critical mass for Wilson fermions on the periodicity phases in the boundary conditions. Although a cutoff effect, it could be rather large in a theory with  $O(a)$  discretization effects. Since the result is that the hadron masses, and not only their momentum, change as  $\theta$  changes, the corresponding dispersion relations may look very different at finite and coarse lattice spacings compared to the continuum predictions.



## Chapter 4

# Optimization of HMC performance

Gauge theories formulated on Euclidean lattices can be treated as statistical system and are amenable to numerical simulations. When matter fields (scalars or fermions) are dynamically present, the gauge-field configurations are typically generated using Molecular Dynamics (MD) algorithms, which come with different variations of the Hybrid Monte Carlo (HMC) (Duane *et al.*, 1987). Such algorithms depend on a large number of parameters, whose optimal choices depend on the model and the regime (e.g. concerning masses and volumes) considered. The generation of configurations in large volumes at light quark masses is still very demanding. For larger volumes the simulations become obviously more expensive. For lighter quarks the condition number of the Dirac operator increases, hence the number of iterations needed by the solver (to invert the operator) increases.

The case of QCD has been extensively studied because of its obvious phenomenological relevance. Roughly speaking HMC algorithms can be classified according to the factorization of the quark determinant adopted (typically either mass-preconditioning (Hasenbusch, 2001), or even/odd preconditioning (DeGrand and Rossi, 1990), or domain-decomposition (Luscher, 2005), or rational factorization (Clark and Kennedy, 2007)) and the symplectic integrator(s) used, the simplest being the leapfrog integrator, and the most popular being the second order minimum norm integrator or Omelyan integrator (Omelyan *et al.*, 2003, Takaishi and de Forcrand, 2006). The factorization of the determinant translates into a splitting of fermionic forces in the Molecular Dynamics, and depending on the hierarchy of such forces various nested integrators can be used, where each force is integrated along a trajectory with a different time-step (Sexton and Weingarten, 1992, Urbach *et al.*, 2006). No complete studies are present for Beyond Standard Model (BSM) strongly interacting models, where the hierarchy of the forces can be completely different from the QCD case.

In dynamical simulations the Molecular Dynamics step is the most time consuming part, hence it is of paramount importance to speed it up as much as possible. For symplectic integrators a shadow Hamiltonian exists, that is conserved, and can be used to optimize the parameters of a simulation. In Ref. (Kennedy and Clark, 2007) the shadow Hamiltonian was introduced to make simulations with dynamical fermions cheaper by means of symplectic integrators that conserve in a better way the energy without decreasing the integration step-size too much. The idea in the present work is to minimize the fluctuations of the Hamiltonian deviations from the shadow Hamiltonian along the trajectory. The strategy we will follow is general and it is also suitable for BSM models.

In the following we restrict the attention to the case of one particular integrator, Omelyan (with  $\alpha = 1/6$ ), because it is a rather common choice, requires less computations and existing data (as long as the norm of the forces have been stored) can be readily used for the tuning. We employ

a three-time scale integrator with mass-preconditioning and we show that once the forces and their variances are measured, assuming they only depend on the mass-preconditioning parameter  $\mu$  (and bare mass parameter  $m_0 - m_c$ ), we are able to find the optimal integrator parameters. Thanks to choice of  $\alpha = 1/6$  in the integrator, the implementation of the Poisson brackets is not needed since their rôle is played by the forces. It should be noted that the tuning of the integrator parameters also depends on the choice of the inverter, the precision of the force and the Hamiltonian measurement. The strategy we present is applicable also for a different set of the aforementioned choices. Our minimization method gives predictions accurate at the 10% level, which we consider quite satisfactory. For completeness we consider an  $\mathbf{SU}(2)$  gauge group with a doublet of un-improved Wilson fermions in the fundamental representation and Wilson plaquette gauge action, further details on the simulations set-up can be found in App. C.4.

The chapter is organized as follow; in Section 1 we review symplectic integrators and the existence of a shadow Hamiltonian associated to them for the case of position and momentum variables in  $\mathbb{R}^2$ . In Section 2 we give our set-up for the integrator, preconditioning and multi-scale integration and we show the explicit form of the shadow Hamiltonian and how it depends on the forces. In Section 3 we test the goodness of our measurement of Poisson brackets and we show that the shadow Hamiltonian is indeed conserved along the trajectory. In Section 4 we relate the acceptance rate in simulations to the variance of the shadow Hamiltonian and ultimately to the force variances; the cost of a simulation is also defined. There we also present the functional form of the fits employed in  $\mu$  (and the bare mass  $m_0$ ). Section 5 contains the comparison of the cost of actual simulation with the one found through our minimization method. Section 6 contains our conclusions. The work presented in this chapter is presented in (Bussone *et al.*, 2016a).

## 4.1 Symplectic integrators: a toy model

To each symplectic integrator corresponds a constant of motion related to the original Hamiltonian of the system we want to simulate. The constant of motion is referred to as *shadow* Hamiltonian. See Ref. (Yoshida, 1992) for a review. Let us examine the case of the 1D harmonic oscillator. The Hamiltonian of such a system is

$$H = \frac{p^2}{2} + \frac{q^2}{2}, \quad (4.1.1)$$

and the exact solution is given by the following map

$$\begin{pmatrix} p' \\ q' \end{pmatrix} = \begin{pmatrix} \cos \tau & -\sin \tau \\ \sin \tau & \cos \tau \end{pmatrix} \begin{pmatrix} p(0) \\ q(0) \end{pmatrix}, \quad (4.1.2)$$

where  $(q(0), p(0))$  is the initial condition and  $(q', p')$  is the  $\tau$ -time evolved point in the phase space  $(q, p)$ . Without loss of generality let us assume  $\tau > 1$ .

### Euler

The easiest way to solve the differential equation numerically is to employ the Euler method. In that case the map is given by

$$\begin{pmatrix} p' \\ q' \end{pmatrix} = \begin{pmatrix} 1 & -\tau \\ \tau & 1 \end{pmatrix} \begin{pmatrix} p(0) \\ q(0) \end{pmatrix}. \quad (4.1.3)$$

The map is not symplectic and the time evolved Hamiltonian is found to be

$$H(\tau) = H(0) + \frac{\tau^2}{2} [p^2(\tau) + q^2(\tau)] \neq H(0). \quad (4.1.4)$$

The above equation tells us that at each integration time step the energy of the system is increasing and eventually diverges from  $H$ , i.e. the error is *unbounded*.

### Symplectic Euler

One can make the Euler map in Eq. 4.1.3 symplectic by modifying it as

$$\begin{pmatrix} p' \\ q' \end{pmatrix} = \begin{pmatrix} 1 - \tau^2 & -\tau \\ \tau & 1 \end{pmatrix} \begin{pmatrix} p(0) \\ q(0) \end{pmatrix}. \quad (4.1.5)$$

The associated Hamiltonian at the time  $\tau$  is given by

$$H(\tau) = H(0) + \frac{\tau^2}{2} [3p^2(0) + q^2(0)] \neq H(0), \quad (4.1.6)$$

and is not conserved along the trajectory. Nonetheless we do have a constant of motion  $H'$  given by

$$H' = \frac{1}{2}(p^2 + q^2) + \frac{\tau}{2}pq = H + \frac{\tau}{2}pq. \quad (4.1.7)$$

The parameter  $\tau$  is fixed from the beginning in the integration, and we can see from direct inspection that indeed  $H'(p(t = \tau), q(t = \tau); \tau) = H'(p(t = 0), q(t = 0); \tau)$ . The error in the Hamiltonian is now bounded and cannot grow. Thus if we start from a point  $(p(0), q(0)) = (0, 1)$  after few iterations the time evolved point will be on the ellipse<sup>1</sup> given by  $p^2 + q^2 + \tau pq = 1$  and therefore the error is of order  $\tau$ .

One can prove that the symplectic map in Eq. 4.1.5 describes the exact  $\tau$ -time evolution of a Hamiltonian system, with  $\tilde{H}$  that has the expression in power of  $\tau$

$$\begin{aligned} \tilde{H} &= H + \tau H_1 + \tau^2 H_2 + \tau^3 H_3 + \dots, \\ H_1 &= \frac{1}{2} H_p H_q = \frac{1}{2} pq, \\ H_2 &= \frac{1}{12} (H_{pp} H_q^2 + H_{qq} H_p^2) = \frac{1}{12} (p^2 + q^2) = \frac{1}{6} H, \\ H_3 &= \frac{1}{12} H_{pp} H_{qq} H_q H_p = \frac{1}{12} pq = \frac{1}{6} H_1, \\ &\vdots \end{aligned} \quad (4.1.8)$$

and it is exactly conserved during the trajectory. Through a “brute force” calculation to the 17-th order in  $\tau$ , using MATHEMATICA along with Ref. (Weyrauch and Scholz, 2009), we found that the shadow Hamiltonian is given by

$$\begin{aligned} \tilde{H} &= \frac{1}{2} (p^2 + q^2 + \tau pq) \left[ 1 + \frac{\tau^2}{6} + \frac{\tau^4}{30} + \frac{\tau^6}{140} + \frac{\tau^8}{630} + \frac{\tau^{10}}{2772} + \frac{\tau^{12}}{12012} + \frac{\tau^{14}}{51480} + \frac{\tau^{16}}{218790} \right] \\ &\equiv \frac{1}{2} (p^2 + q^2 + \tau pq) P(\tau) = H' P(\tau). \end{aligned} \quad (4.1.9)$$

There is a clear factorization of a polynomial in  $\tau$ ,  $P(\tau)$ , and since  $\tilde{H}$  is conserved then also  $H'$  is conserved.

<sup>1</sup>The exact solution is parametrized by a circle  $p^2 + q^2 = 1$  in the phase space.

### 4.1.1 Shadow hamiltonian

The Hamilton equations in compact form are given by

$$\frac{dz}{dt} = \{z, H(z)\} \equiv D_H z. \quad (4.1.10)$$

where we introduced  $z \in \mathbb{R}^{2n} = \{(p, q)\}$ , and the Poisson brackets are given by

$$\{\star, H\} = \frac{\partial \star}{\partial q} \frac{\partial H}{\partial p} - \frac{\partial \star}{\partial p} \frac{\partial H}{\partial q}. \quad (4.1.11)$$

The formal solution of the differential equation takes the form  $z(\tau) = e^{\tau D_H} z(0)$ . By choosing a separable Hamiltonian,  $H(q, p) = T(p) + V(q)$ , we have the operator identification  $D_H = D_T + D_V$  and the solution can be formally written through the evolution operator as follows

$$z(\tau) = e^{\tau(D_T + D_V)} z(0). \quad (4.1.12)$$

More explicitly

$$\begin{aligned} \text{momenta evolution } e^{\tau D_V} : f(z(0)) = f(p, q) &\rightarrow f(z(\tau)) = f(p - \tau V_q, q), \\ \text{positions evolution } e^{\tau D_T} : f(z(0)) = f(p, q) &\rightarrow f(z(\tau)) = f(p, q + \tau T_p), \end{aligned} \quad (4.1.13)$$

where  $f$  is an arbitrary function of  $z$ .

Let us specialize to the Omelyan integrator (Omelyan *et al.*, 2003). The evolution operator in this case is

$$\exp[\alpha \tau D_V] \exp\left[\frac{\tau}{2} D_T\right] \exp[\tau(1 - 2\alpha) D_V] \exp\left[\frac{\tau}{2} D_T\right] \exp[\alpha \tau D_V], \quad (4.1.14)$$

with  $\alpha$  free parameter. By using the Baker-Campbell-Hausdorff (BCH) formula we obtain that the shadow Hamiltonian  $\tilde{H}$  is related to the one we want to simulate,  $H$ , as follows

$$\tilde{H} = H + \tau^2 \left\{ \frac{6\alpha^2 - 6\alpha + 1}{12} D_V [D_V(T)] + \frac{1 - 6\alpha}{24} D_T [D_V(T)] \right\} + O(\tau^4). \quad (4.1.15)$$

By putting  $\alpha = 1/6$  the second term in curly brackets vanishes. The remainder is proportional to  $D_V [D_V(T)]$ . In the case of  $V = V(q)$  and  $T = p^2/2$  this operator is related to the force,

$$\begin{aligned} D_V(T) &= \{T, V\} = \cancel{V_p T_q} - V_q T_p = -p V_q, \\ D_V [D_V(T)] &= \{-p V_q, V\} = \{V, p V_q\} = V_q (p V_q)_p - \cancel{V_p (p V_q)_q} = V_q (V_q + p V_{qp}) = V_q^2 \equiv F^2. \end{aligned} \quad (4.1.16)$$

The shadow Hamiltonian in the case of Omelyan integrator with  $\alpha = 1/6$  is given by

$$\tilde{H} = H + \frac{(\tau F)^2}{72} + O(\tau^4). \quad (4.1.17)$$

### Time reversible integrators

Let us assume we have a time reversible integrator given by

$$E(\tau) = \exp(\tau A) \exp(\tau B), \quad (4.1.18)$$

if we expand it according to BCH formula we get

$$E(\tau) = \exp(\tau\gamma_1 + \tau^2\gamma_2 + \tau^3\gamma_3 + \dots). \quad (4.1.19)$$

By imposing the time reversibility condition  $E(\tau)E(-\tau) = \mathbf{1}$  we get, at the second order in  $\tau$

$$E(\tau)E(-\tau) = \exp(\tau\gamma_1 + \tau^2\gamma_2) \exp(-\tau\gamma_1 + \tau^2\gamma_2) = \exp(2\tau^2\gamma_2 + O(\tau^3)) = \mathbf{1}, \quad (4.1.20)$$

which tells us that  $\gamma_2 = 0$ . By iterating the same steps at the order  $\tau^4, \tau^6, \dots$  we obtain  $\gamma_4 = \gamma_6 = \dots = 0$ , (Yoshida, 1990).

## 4.2 Mass preconditioning & multi time-scale

We turn now to real HMC simulations of QFT. A way to reduce the fluctuations of the force is to employ the *mass preconditioning* of the quark determinant (Hasenbusch and Jansen, 2003). The definitions for the massive and hermitian Dirac operators are the following

$$D_m = D + m_0, \quad Q = \gamma_5 D_m. \quad (4.2.21)$$

The Dirac matrix is modified as follows

$$\begin{aligned} D_m &= D_{\text{HMC}} \times D_{\text{Hase}}, & D_{\text{HMC}} &= D_m + \mu, & D_{\text{Hase}} &= (D_m + \mu)^{-1} D_m, \\ Q^2 &= Q_{\text{HMC}}^2 \times Q_{\text{Hase}}^2, & Q_{\text{HMC}}^2 &\equiv (D_m^\dagger + \mu)(D_m + \mu), & Q_{\text{Hase}}^2 &\equiv Q(D_m^\dagger + \mu)^{-1}(D_m + \mu)^{-1}Q, \end{aligned} \quad (4.2.22)$$

where we introduced a new mass term  $\mu$ , the *Hasenbusch mass*. The probability distribution in Eq. 1.7.73 depends on the determinant of the Dirac operator that now becomes the product of two determinants

$$\begin{aligned} \det D_m &= \det D_{\text{HMC}} \times \det D_{\text{Hase}}, \\ \det Q^2 &= \det Q_{\text{HMC}}^2 \times \det Q_{\text{Hase}}^2. \end{aligned} \quad (4.2.23)$$

In particular, employing the  $\gamma_5$  version of the Dirac-Wilson operator, the distribution with which the configurations are generated is given by

$$P_S \propto \int \mathcal{D}[\phi_1, \phi_1^\dagger, \phi_2, \phi_2^\dagger] \exp\left(-S_G[U] - \phi_1^\dagger (Q_{\text{Hase}}^2)^{-1} \phi_1 - \phi_2^\dagger (Q_{\text{HMC}}^2)^{-1} \phi_2\right), \quad (4.2.24)$$

where we introduced a set of pseudo-fermions for each determinant. In our simulation we will have three (*driving*) forces: Gauge, HMC, Hasenbusch. The preconditioned HMC operator should be a reasonable approximation of the massive Dirac operator, cheaper in time to invert, and its determinant should be positive. The *condition number* of the HMC and the Hasenbusch operator are reduced compared to the original one,  $Q^2$ . This is best understood in the twisted mass-preconditioning as explained in Ref. (Urbach *et al.*, 2006). Suppose that the  $\lambda_{\text{max}}$  and  $\lambda_{\text{min}}$  are respectively the maximal and minimal eigenvalues of  $Q^2$ . Then its condition number is given by  $\lambda_{\text{max}}/\lambda_{\text{min}}$ . The condition number of  $D_m D_m^\dagger + \mu^2$  is about  $\lambda_{\text{max}}/\mu^2$  and the one of  $(D_m D_m^\dagger + \mu^2)/Q^2$  around  $\mu^2/\lambda_{\text{min}}$ . Now by taking  $\mu^2 \approx \sqrt{\lambda_{\text{max}}/\lambda_{\text{min}}}$  the Hasenbusch and the HMC term will be better conditioned with respect to  $Q^2$ .

A further acceleration can be achieved by considering *multiple time-step integrators* (Urbach *et al.*, 2006). It consists of taking different integration step sizes for different forces. Multiple time-step also helps to maintain under control large driving forces. As pointed out in Ref. (Joo *et*

*al.*, 2000) large driving forces lead to *instabilities* in HMC simulations. To avoid them the time step must be small if the driving force are large. Multiple time-step integrators are a valuable tool if the forces differ by orders of magnitude in absolute value.

We employ a three time-scale integrator and assume that in the outermost level there is the evolution for  $S_1$  with time step  $\delta\tau = \tau/n$ , in the middle the integrator for  $S_2$  with  $m$  steps and the innermost is for  $S_3$  with  $k$  steps.

The shadow Hamiltonian associated to the Omelyan integrator with three time-scales and mass preconditioning is a quite lengthy expression (see App. C.3) but once we set the parameter  $\alpha = 1/6$  it is given by

$$\tilde{H} = H + \frac{\delta\tau^2}{72} \left[ [\hat{S}_1, [\hat{S}_1, \hat{T}]] + \frac{1}{4m^2} [\hat{S}_2, [\hat{S}_2, \hat{T}]] + \frac{1}{16m^2k^2} [\hat{S}_3, [\hat{S}_3, \hat{T}]] \right] + O(\delta\tau^4). \quad (4.2.25)$$

We use the conventions adopted in (Kennedy *et al.*, 2013, Kennedy and Clark, 2007) and the above formula becomes

$$\tilde{H} = H + \frac{\delta\tau^2}{72} \left[ \mathbf{e}_i(S_1) \mathbf{e}^i(S_1) + \frac{\mathbf{e}_i(S_2) \mathbf{e}^i(S_2)}{4m^2} + \frac{\mathbf{e}_i(S_3) \mathbf{e}^i(S_3)}{16m^2k^2} \right] + O(\delta\tau^4), \quad (4.2.26)$$

where  $\mathbf{e}_i$  is the  $\mathbf{SU}(N_c)$  derivative and  $i$  a collective index for space-time, direction and number of generators.  $\mathbf{e}_i(S)\mathbf{e}^i(S)$  gives the force associated to the action  $S$  summed over all space-time point, directions, color and eventually spin, as expected, since the Hamiltonian is an extensive quantity. The shadow Hamiltonian reduces to

$$\begin{aligned} \tilde{H} &= H + \frac{\delta\tau^2}{72} \sum_{x,\mu,a} \left[ T_{R,1} (F_1^{a\mu}(x))^2 + T_{R,2} \frac{(F_2^{a\mu}(x))^2}{4m^2} + T_{R,3} \frac{(F_3^{a\mu}(x))^2}{16m^2k^2} \right] + O(\delta\tau^4) \\ &\equiv H + \frac{\delta\tau^2}{72} \left( |\mathcal{F}_1|^2 + \frac{|\mathcal{F}_2|^2}{4m^2} + \frac{|\mathcal{F}_3|^2}{16m^2k^2} \right) + O(\delta\tau^4) \equiv H + \delta H + O(\delta\tau^4), \end{aligned} \quad (4.2.27)$$

that is a function only of the forces used during the simulations.

For the derivation of the various forces see the results in App. C.3. We immediately see that the shadow Hamiltonian is related to the different parts of the force weighted by the corresponding normalization for the generators  $T_R$  in the given representation  $R$ . Note that the gauge is always in the fundamental  $T_R = T_f = 1/2$ , while the fermionic parts may be in different representation. Already at this point one can see what drove our assignments for the different levels. We want to suppress the contribution of the *largest* force (the gauge one) and hence that will go in the innermost level, followed by the HMC force and the Hasenbusch one at the outermost level.

In the following we specialize to the case of the Omelyan integrator with  $\alpha = 1/6$ . We consider an  $\mathbf{SU}(2)$  gauge group with a doublet of un-improved Wilson fermions in the fundamental representation and Wilson plaquette gauge action. For completeness the value  $m_c$  of the bare mass parameter yielding massless fermions is estimated to be  $-0.77(2)$  at  $\beta = 2.2$  (Lewis *et al.*, 2012, Hietanen *et al.*, 2014, Arthur *et al.*, 2016).

### 4.3 Benchmarks in small volumes

In order to test the measurements of the Poisson brackets we check the scaling with  $\delta\tau$  of  $|\Delta H| \propto \delta\tau^2$ , since the Omelyan integrator is a *second order integrator*. Furthermore we test the scaling of  $|\Delta(\delta H) + \Delta H| \propto \delta\tau^4$ , indeed, since  $\tilde{H}$  is conserved along the trajectory, the following relation holds

$$\Delta\tilde{H} = 0 = \Delta H + \Delta(\delta H) + O(\delta\tau^4) \implies \Delta H = -\Delta(\delta H) + O(\delta\tau^4). \quad (4.3.28)$$



The difference at the end of the trajectory is given by

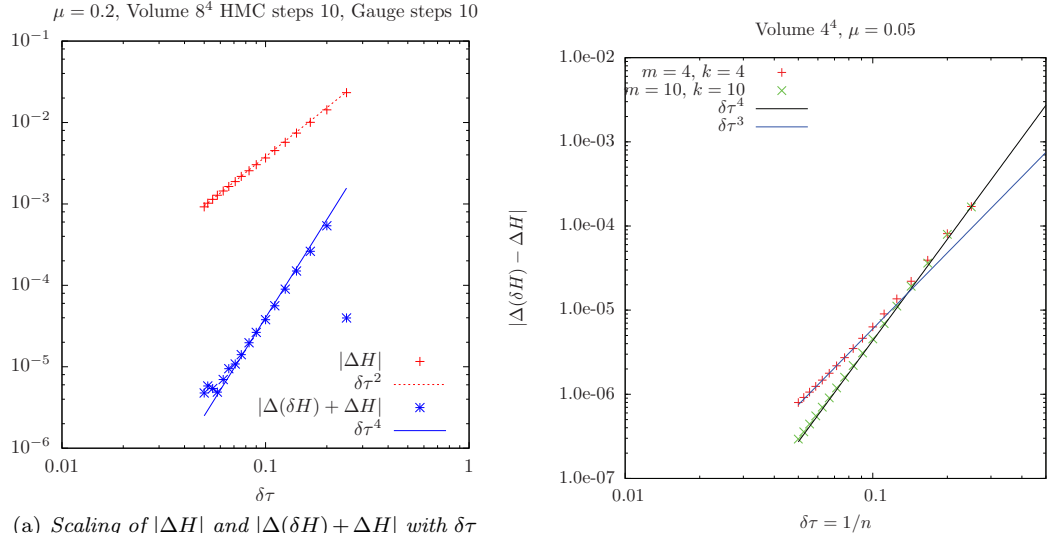
$$\Delta(\delta H) = \frac{\delta\tau^2}{72} \left( |\mathcal{F}_{1,f}|^2 - |\mathcal{F}_{1,i}|^2 + \frac{|\mathcal{F}_{2,f}|^2 - |\mathcal{F}_{2,i}|^2}{4m^2} + \frac{|\mathcal{F}_{3,f}|^2 - |\mathcal{F}_{3,i}|^2}{16m^2k^2} \right), \quad (4.3.29)$$

where the forces are evaluated at the beginning  $i$  and the end  $f$  of the trajectory.

For the tests we have run one trajectory from a thermalized configuration with the following set-up for the levels in the integration,  $\tau_f = 1$ ,

- level 1: Hasenbusch,  $n = 4, 5, \dots, 20$ ,
- level 2: HMC,  $m = 10$ ,
- level 3: Gauge,  $k = 10$ .

The results in small volumes are shown in Fig. 4.1. In Fig. 4.1(b) we see in the small  $\delta\tau$  region the emergence of a contribution of order  $\delta\tau^3$ . This comes from the ambiguity in the measurement of



(a) Scaling of  $|\Delta H|$  and  $|\Delta(\delta H) + \Delta H|$  with  $\delta\tau$  in  $V = 8^4$  at fixed inner levels steps  $m = 10$  and  $k = 10$ .

(b) Scaling of  $|\Delta(\delta H) + \Delta H|$  with  $\delta\tau$  in  $V = 4^4$  for two different choices of the inner level steps.

Figure 4.1: Scaling behavior with  $\delta\tau = 1/n$  for  $\Delta H$  and  $\Delta(\delta H)$  in small volumes.  $\Delta(\delta H)$  is built from the knowledge of the forces at the beginning and the end of the trajectory. Lines are shown to guide the eye.

$\mathcal{F}_2$ , that is the time in which we measure it in the sub-level steps. In other words different forces are measured at different times. In formulae we can write

$$|\mathcal{F}_2|^2 = |\mathcal{F}_2^{m \rightarrow \infty}|^2 + \mathcal{O}\left(\frac{\delta\tau}{m}\right), \quad (4.3.30)$$

where  $\delta\tau/m$  gives a correction to  $\delta H$  of order  $1/m^3$ . This term induces a contribution of order  $\delta\tau^3$  in  $|\Delta(\delta H) + \Delta H|$  that can be suppressed by choosing a large number of steps  $m$ . The same

phenomenon may appear for  $\mathcal{F}_3$  but the extra term will be suppressed by a power  $mk$  and gives a correction to  $\delta H$  of order  $1/m^3k^3$ , which is completely negligible for  $k = 10$ .

Another useful test is to measure directly  $\Delta H$  along the trajectory and compare it with the one built from the knowledge of the forces, Eq. 4.3.28. The results for  $16^4$  volume are shown in Fig. 4.2. It is worth to notice that the minimum of  $\Delta H$  scales as predicted by increasing  $n$ . When the minimum (or a maximum) is attained, then  $\Delta H$  cannot decrease (increase) any further due to the existence of the shadow Hamiltonian, and it is well understood in terms of the various underlying force contributions.

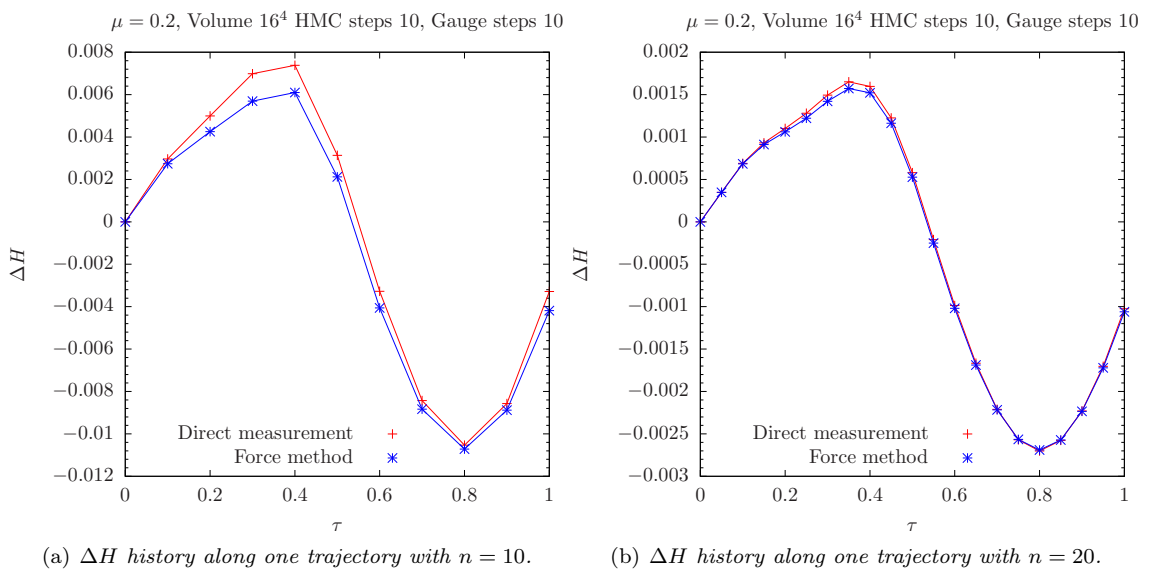


Figure 4.2: *Benchmarks for the Poisson brackets measurements. Direct measurement (red crosses) corresponds to the measure of  $\Delta H$  during the trajectory. Force method (blue stars) employs the knowledge of the forces. From the left to the right panel the minimum of  $\Delta H$  is scaling as expected.*

## 4.4 Cost of a simulation and its minimization

Although the cost of a simulation is not unique we define it as

$$\text{Cost} = \frac{\#\text{MVM}}{P_{\text{acc}}}. \quad (4.4.31)$$

The number of Matrix-Vector-Multiplications ( $\#\text{MVM}$ ) is a machine independent quantity<sup>2</sup>. Furthermore we neglect the autocorrelation since that conceivably has a mild dependence on  $\mu$  and therefore should be mostly contribute as an overall factor to the cost.

<sup>2</sup>The gauge part contributes for a maximum of about 5% of the cost, hence is negligible. We also took into account the gauge part as a check and it does not affect the results of this work.

#### 4.4.1 Acceptance & Matrix-Vector-Multiplication

We link the acceptance  $P_{\text{acc}}$  to  $\Delta H$  through the Creutz formula, see App. C.1,

$$P_{\text{acc}}(\Delta H) = \text{erfc} \left( \sqrt{\text{Var}(\Delta H)/8} \right), \quad (4.4.32)$$

and the connection between the variances of  $\Delta H$  and  $\delta H$  is given by (Clark *et al.*, 2008, Clark *et al.*, 2011)

$$\text{Var}(\Delta H) \simeq 2\text{Var}(\delta H). \quad (4.4.33)$$

In the following our goal is to optimize the choice of parameters  $\mu, n, m, k$ , (for different bare masses  $m_0$ ), while keeping the choice of the integrator, the solver and the number of Hasenbusch splittings fixed. We can also fix the bare masses, but a stabilization in terms of  $\chi$ -square of the fits is seen once we fit also in  $m_0$ . But we should mention that it is not strictly necessary.

Let us illustrate how to get to the above relation Eq. 4.4.33. We trade  $\Delta H$  for  $\Delta(\delta H)$  through Eq. 4.3.28. By using Eq. 4.3.29 we can compute the variance (and neglecting all the covariances),

$$\begin{aligned} \text{Var}[\Delta(\delta H)] \equiv \frac{\delta\tau^4}{(72)^2} & \left[ \text{Var}(|\mathcal{F}_{1,f}|^2) + \text{Var}(|\mathcal{F}_{1,i}|^2) + \frac{\text{Var}(|\mathcal{F}_{2,f}|^2) + \text{Var}(|\mathcal{F}_{2,i}|^2)}{(4m^2)^2} \right. \\ & \left. + \frac{\text{Var}(|\mathcal{F}_{3,f}|^2) + \text{Var}(|\mathcal{F}_{3,i}|^2)}{(16m^2k^2)^2} \right]. \end{aligned} \quad (4.4.34)$$

Under the further assumption that the final and initial forces are extracted from the same distribution,  $\exp(-H)$  (Clark *et al.*, 2010), and they are independent for long enough trajectories, we obtain

$$\text{Var}[\Delta(\delta H)] \simeq \frac{2\delta\tau^4}{(72)^2} \left[ \text{Var}(|\mathcal{F}_1|^2) + \frac{\text{Var}(|\mathcal{F}_2|^2)}{(4m^2)^2} + \frac{\text{Var}(|\mathcal{F}_3|^2)}{(16m^2k^2)^2} \right] = 2\text{Var}(\delta H). \quad (4.4.35)$$

We have tested Eq. 4.4.33 by calculating in two different ways the acceptance. We refer to the acceptance calculated with the formula in Eq. 4.4.35 ( $\text{Var}(\delta H)$ ) as “Force method 1”, while “Force method 2” is used for the acceptance calculated with Eq. 4.4.34 ( $\text{Var}[\Delta(\delta H)]$ ). “Force method 1” is the one going to be used in the rest of the work. There the acceptance rate is calculated from the variance of  $\delta H$ . For each trajectory we calculate the average of  $\delta H$  over each of the uppermost level step. The result is then used to build the variance over the trajectories, where the average forces over the sub-levels are used. In “Force method 2” the acceptance is calculated from the variance of  $\Delta(\delta H)$ . To do that we calculate the difference of  $\delta H$  at the beginning and the end of each trajectory and we extract the variance over the trajectories. In Fig. 4.3 we compare the two methods described above to extract the acceptance of a simulation in a small  $V = 4^4$  volume. The simulations are carried out starting from a thermalized configuration and running  $10^3$  trajectories. There the two methods are compared with the direct measurement and the acceptance built directly from  $\Delta H$ . Both methods seem to reasonably reproduce the data.

The total average number of MVM is given in terms of the averages at each level by

$$\#\text{MVM} = (2n + 1)\#\text{MVM}_1(\mu) + 2n(2m + 1)\#\text{MVM}_2(\mu). \quad (4.4.36)$$

The analysis is done with standard statistical error propagation since each simulation, for different choices of  $n, m, k, \mu$  and  $m_0$ , is independent.

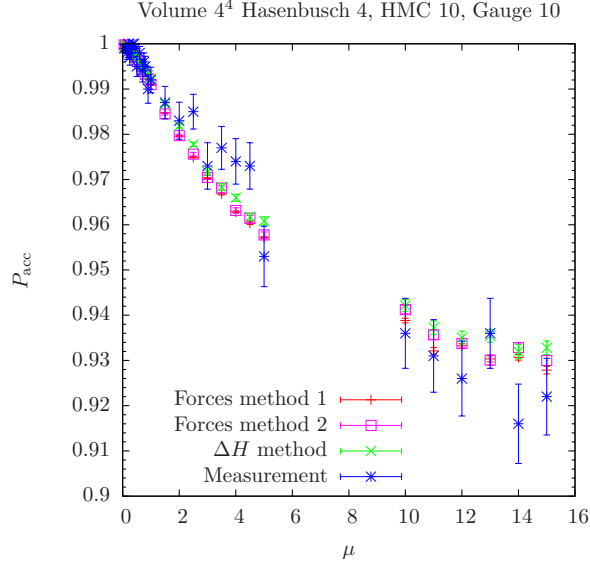


Figure 4.3: Acceptance as a function of the preconditioning mass. Force method 1 and 2 (red segments and violet boxes) are employing the formulae in Eqs. 4.4.35, 4.4.34.  $\Delta H$  method (green crosses) correspond to the measurement of  $H$  (also used for the accept/reject step). Measurement (blue crosses) correspond to simple counting.

#### 4.4.2 Fits

The idea is to assume that  $\text{Var}(\delta H)$  and  $\#\text{MVM}$  depend explicitly upon  $n, m$  and  $k$  as in Eqs. 4.4.35, 4.4.36 and the dependence on  $\mu$  (and  $m_0$ ) of  $\text{Var}(|\mathcal{F}_i|^2)$  is the only quantity to be modeled, along with  $\#\text{MVM}_i$ .

In Figs. 4.4, 4.5 we show the result of the fits in  $\mu$  and  $m_0 - m_c$  for large volume  $V = 34^4$  and  $m_0 = -0.72$ . In Fig. 4.4 we show the variances for the different forces and their resulting fits. We can identify two different regions: a *strong* dependence region for small  $\mu$  and a *weak* dependence region for large  $\mu$ . In the weak dependence region we have an *inverted hierarchy* with respect to what was our choice. In Fig. 4.5 we show the number of MVMs per step and sub-step and their fits.

The fits were performed in  $m_0$  and  $\mu$  using the following curves

$$\begin{aligned}
 \text{Var}(\mathcal{F}_{\text{Hase}}) &= \frac{a\mu^2}{(m_0 - m_c)^2} + \left[ b + \frac{c\mu^2}{(m_0 - m_c)^2} + d\mu^4 \right] \exp(-e\mu^2) \\
 \text{Var}(\mathcal{F}_{\text{HMC}}) &= a + b\mu^2 + \frac{c}{\mu} + \frac{d(m_0 - m_c)^2}{\mu} + e\mu^4, \\
 \text{Var}(\mathcal{F}_{\text{Gauge}}) &= a + \frac{b}{(m_0 - m_c)^2}, \\
 \#\text{MVM}_{\text{Hase}} &= \left( a + \frac{b}{m_0 - m_c} \right) + c \ln \mu, \\
 \#\text{MVM}_{\text{HMC}} &= a + \frac{b}{\mu} + \left( c + \frac{d}{m_0 - m_c} \right) \frac{1}{\mu^2}.
 \end{aligned} \tag{4.4.37}$$

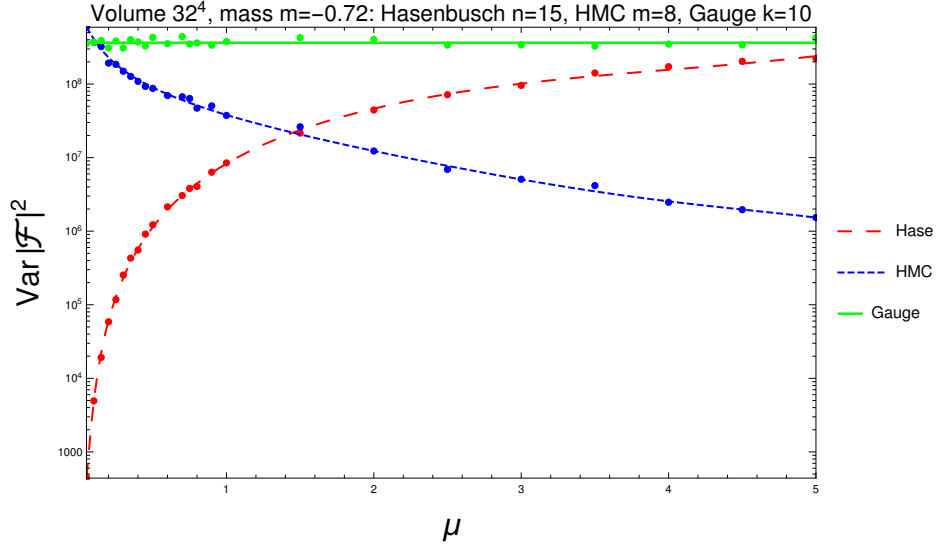


Figure 4.4: *Variances of the forces as a function of the mass preconditioning parameter. For very small  $\mu$  the HMC variance is dominant, outside this region the Gauge variance is the dominant one. In the intermediate  $\mu$  region we have an hierarchy of forces that corresponds to the level assignments. For large  $\mu$  we have an inverted hierarchy. The figure corresponds to  $m_0 = -0.72$ .*

Only terms that reduced significantly the  $\chi^2$  were included in the fitting curves.

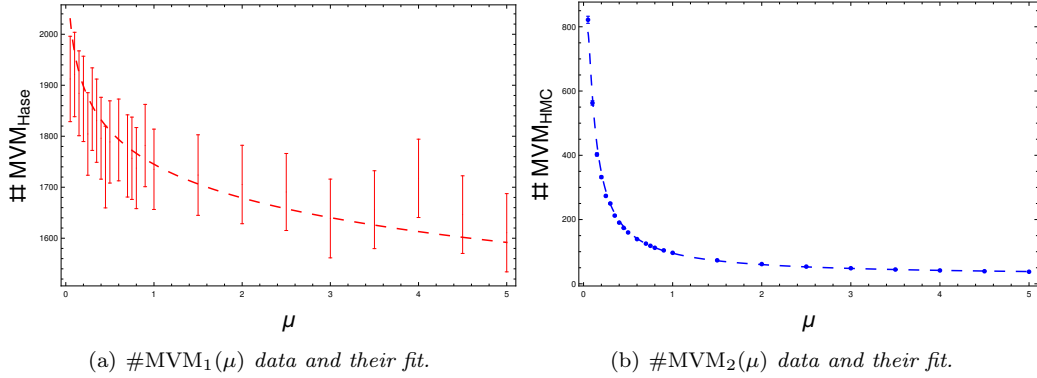
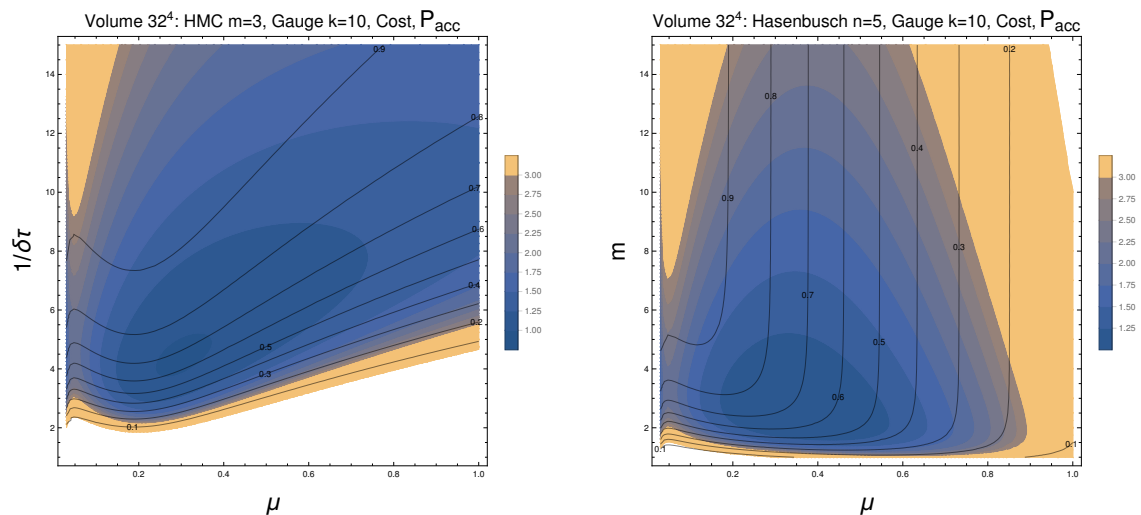


Figure 4.5: *#MVM in Hasenbusch and HMC levels as a function of  $\mu$  for  $m_0 = -0.72$ .*

### 4.4.3 Cost function

We can now build the cost as a function of  $n, m, k, \mu$  and  $m_0$ . For simplicity we fix  $k = 10$ , and in order to find the minimum in the other parameters we require<sup>3</sup>  $P_{\text{acc}} \gtrsim 70\%$ . The minimization is carried out at fixed bare mass, in the following we specialize to  $m_0 = -0.72$  since the results for other bare masses are qualitatively the same. With this set-up we found the minimum,  $\text{Cost}_{\text{min}}$ , to be at  $(n, m, \mu) \approx (5, 3, 0.3)$ . In Fig. 4.6 we show the cost, normalized to the minimum, and the acceptance in the plane  $(\mu, n)$  and  $(\mu, m)$ . In Fig. 4.6(a) we fix  $m = 3$  and it can be seen that the minimum is close to the boundary  $P_{\text{acc}} \sim 70\%$ . By taking the cost of a simulation to be  $1 < \text{Cost}/\text{Cost}_{\text{min}} < 1.25$  the window in parameter space is quite broad  $0.2 \lesssim \mu \lesssim 0.7$  and  $3 \lesssim n \lesssim 8$ . Same conclusions can be drawn for the Fig. 4.6(b).



(a)  $\text{Cost}/\text{Cost}_{\text{min}}$  with  $m = 3$  as function of  $\mu$  and  $n$ .

(b)  $\text{Cost}/\text{Cost}_{\text{min}}$  with  $n = 5$  as function of  $\mu$  and  $n$ .

Figure 4.6: Ratio  $\text{Cost}/\text{Cost}_{\text{min}}$  around the minimum  $(n, m, \mu) \simeq (5, 3, 0.3)$  is displayed as curve level. Acceptance rate lines are drawn. Bare mass  $m_0 = -0.72$ .

## 4.5 Comparison with simulations

We have run simulations around the minima found with the above methodology for each bare mass  $m_0$ , Tab. 4.1. The results for the cost from simulations and predictions are shown in Fig. 4.7 for the different  $m_0 - m_c$ . Each prediction point represents the minimum cost with different bare mass  $m_0$ , mass-preconditioning  $\mu$ , number of steps in the uppermost level  $n$  and middle level  $m$  ( $k$  is fixed to 10). The result in Fig. 4.7 represent the central result of this work. It tests the validity of the assumptions made so far and it nicely predicts the value of the cost within factors 3 to 4.

<sup>3</sup>This requirement is needed for the Creutz formula to hold true.

$m_0$	$\mu$	$n$	$m$	$N_{\text{cnf}}$
-0.72	0.29	5	3	463
-0.735	0.22	5	3	403
-0.75	0.18	5	4	167

Table 4.1: Parameters corresponding to the minimum cost of simulations and number of configurations produced.

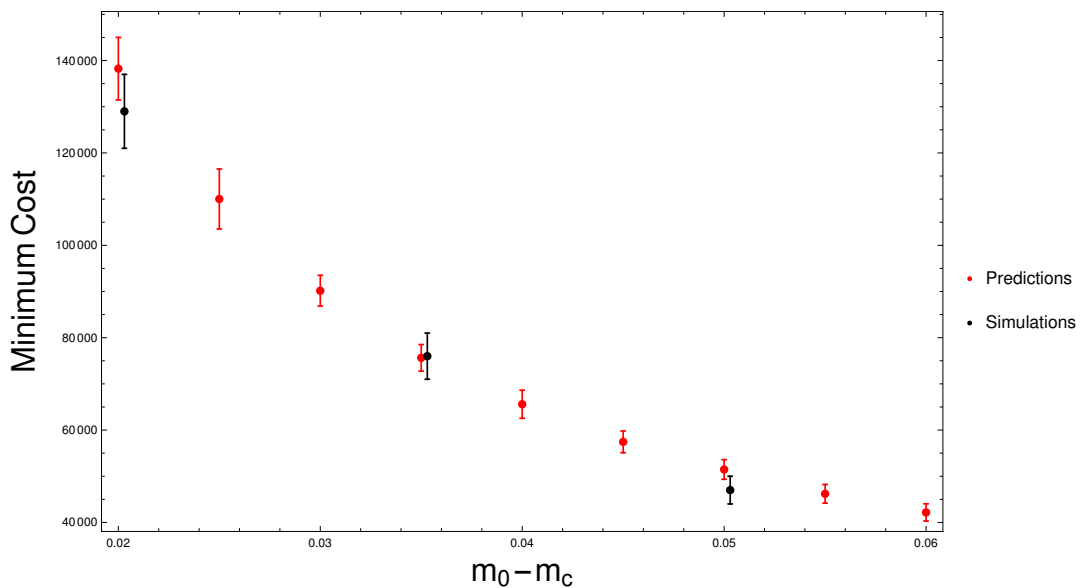


Figure 4.7: Cost at the minimum, comparison with simulation. Each point correspond to a different set of parameters  $\mu, n, m$ . In black comparison with direct simulations is made.

## 4.6 Conclusions

We presented a strategy to optimize the parameters of the Omelyan integrator with  $\alpha = 1/6$ , Hasenbusch mass preconditioning and three time-scales. We have studied the scaling behavior of  $\Delta H$  in  $\delta\tau$  and the goodness of the Poisson brackets measurements through the driving forces in a HMC simulation. We have also generalized the shadow hamiltonian in the presence of multiple-time scales splitting.

We have shown that once the variances of the forces are measured, at fixed bare mass, as a function of the mass-preconditioning parameter the optimal set-up for the integrator can be found. Our method relies on the existence of a shadow Hamiltonian.

We found that the minimum of the cost is quite broad as a function of the mass-preconditioning mass and the number of steps in a level. Nonetheless we are able to give reliable estimates of the cost in agreement with actual simulations. An important observation is that we do not need to modify extensively preexisting codes, since practically all of them have to measure the forces during a trajectory.

The schematic recipe followed by this work is the following:

- Start with a *reasonable* choice for the simulation of  $(n, m, k)$  at fixed  $m_0$ .
- Measure the forces in each level, which we already computed for the evolution, and calculate  $|\mathcal{F}_i|^2 = \sum_{x, \mu, a} T_{R,i} (F_i^{a\mu}(x))^2$  and its variance  $\text{Var}(|\mathcal{F}_i|^2)$ .
- Measure the number of MVMs in each level.
- By fitting the dependence in  $\mu$  we are able to predict the cost dependence on  $(n, m, k, \mu)$  (and  $m_0$ ) with accuracy within 10%.

Generalizing it to a larger number of Hasenbusch levels on different quark determinant splitting (Luscher, 2005, Cè *et al.*, 2017) is rather straightforward, especially as long as covariances can be neglected. The results are encouraging and we plan to consider different strongly interacting BSM models.





## Chapter 5

# QED leading corrections to hadronic observables: the muon anomaly

The  $(g - 2)_\mu$  is one of the most precise measurement in particle physics and it serves as a test of the Standard Model (SM). The anomalous magnetic moment of a lepton  $\ell$  mediates helicity flip transitions, which implies that quantum corrections are proportional to  $\delta a_\ell \propto m_\ell^2/M^2$ , with  $M$  being the mass of a heavy particle inside or outside the SM. This tells us that the anomalous magnetic moment can be used for indirect search of New Physics (NP) beyond the SM. The sensitivity to new particles grows quadratically with the mass of the lepton of interest. The muon is then a good candidate for the search of NP, since the  $\tau$  is ruled out because of its short lifetime. Notice that the above argument can be also used to see that there is an enhanced sensitivity to the hadronic contributions that are notoriously difficult to extract.

The persistent 3-4  $\sigma$  tension between the experimental value and theoretical calculation has generated a lot of interests in the past years. In Tab. 5.1 we give the results for the experimental measure of  $a_\mu$  as well as the different theoretical contributions in the SM according to Ref. (Amsler and others, 2008). The QED value is calculated with a 5-loop computation, the EW with a 2-loop computation, the HVP at LO and NLO is calculated through the measurement of the cross section of  $e^+e^-$  into hadrons,  $\sigma(e^+e^- \rightarrow \text{Hadrons})$ , and the HLbL (light by light scattering) through large  $N_c$  arguments. At this order the contributions to the anomalous magnetic moment of the muon can be separated as

$$a_\mu^{\text{SM}} = a_\mu^{\text{QED}} + a_\mu^{\text{EW}} + a_\mu^{\text{HAD}}.$$

For a review on the topic see Ref. (Jegerlehner and Nyffeler, 2009). We can clearly see that the dominant contribution to the anomalous magnetic moment is due to QED and at the level we are today in the experiment we need to include all the possible contributions from the Standard Model.

Recently  $Z'$  models were introduced to explain the violations of lepton flavor universality because of tensions in the measurements of  $R_K = \mathcal{B}(B \rightarrow K\mu^+\mu^-)/\mathcal{B}(B \rightarrow Ke^+e^-)$  and  $R_{K^*}$  compared to the SM expectations. In Ref. (Di Chiara *et al.*, 2017) the authors argue that a vectorial coupling to the  $Z'$  could also alleviate the discrepancy between the  $g - 2$  measurement and the SM prediction. Every extension beyond the SM has to deal with the  $(g - 2)_\mu$  anomaly to survive, hence its crucial importance.

The lattice regularization can give a non-perturbative answer to the determination of the hadronic vacuum polarization contribution to the muon magnetic anomaly, that is the one dominating the error and represents the second most important contribution. Especially in view of the

Contribution	$a_\mu \times 10^{10}$	$\delta a_\mu \times 10^{10}$
$a_\mu^{\text{QED}}$ (5-loop)	11658471.895	0.008
$a_\mu^{\text{EW}}$ (2-loop)	15.36	0.1
$a_{\mu,\text{LO}}^{\text{HAD}}$	692	4
$a_{\mu,\text{NLO}}^{\text{HAD}}$	-9.84	0.06
$a_{\mu,\text{NLO}}^{\text{HLbL}}$	10.5	2.6
$a_\mu^{\text{SM}}$	11659180	5
$a_\mu^{\text{Exp}}$	11659209	6
$\Delta a_\mu$	29	8

Table 5.1: *Different SM contributions to the theoretical value of  $a_\mu$ .*

new planned experiments E989 at FNAL and E34 at J-PARC that will improve the determination of  $a_\mu$  by a factor four on the experimental side.

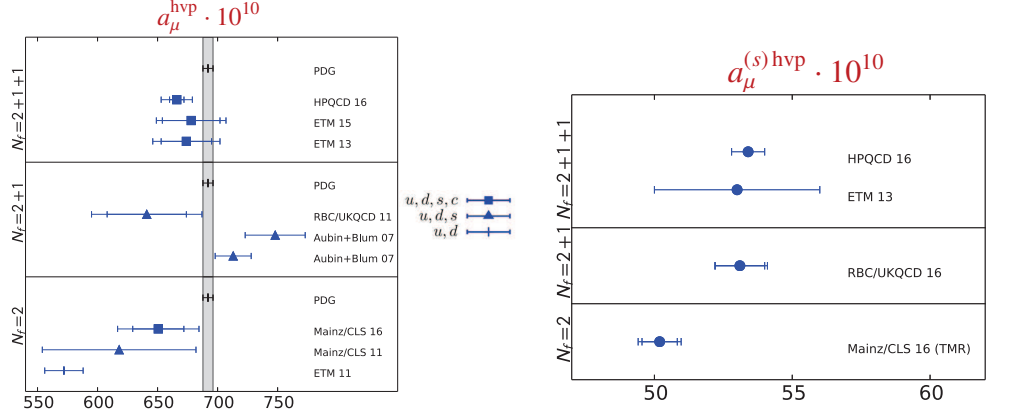
In the last decade the lattice community has made a huge effort to determine the hadronic contribution to  $(g-2)_\mu$ . A first attempt was made in (Blum, 2003) and a complete quenched study with Wilson fermions was made in (Gockeler *et al.*, 2004).

A study with two degenerate Wilson fermions in QCD can be found in (Della Morte *et al.*, 2017), there a variety of techniques are employed as Padé fits (Aubin *et al.*, 2012), time-momentum representation (Bernecker and Meyer, 2011) and time-moments (Chakraborty *et al.*, 2016). See Ref. (Blum and others, 2016) for an analogous use of those techniques for the calculation of the leading strange quark-connected contribution to  $(g-2)_\mu$ . In Fig. 5.1 we give a summary on the status of  $a_\mu^{\text{HAD}}$  with lattice calculations. For a review on the subject see Ref. (Blum *et al.*, 2012).

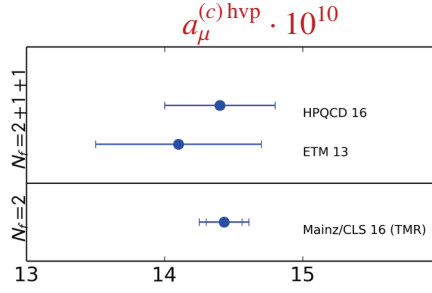
Recently the inclusion of QED has been considered for the HVP (Boyle *et al.*, 2016). Taking into account QED effects is important if the lattice estimate has to be competitive with the  $e^+e^-$  cross section method, since the latter already include all the contributions from different sectors of the SM. Furthermore in (Carloni Calame *et al.*, 2015) an alternative method to measure the hadronic contribution using experimental data employing a space-like kinematics is proposed, which allows for a direct comparison with lattice estimates.

Here we present an application of the concepts introduced in Chap. 2. We present preliminary results on the Hadronic Vacuum Polarization (HVP) of the photon, required to compute the leading correction to the anomalous magnetic moment of the muon.

The chapter is organized as follows; in Section 1 we review the muon anomaly in Minkowski space in QFT. Section 2 is devoted to the details on the chosen lattice set-up to extract electromagnetic corrections to the vacuum polarization. There we discuss the electromagnetic shift in the critical mass, and present preliminary results on the pseudoscalar meson masses. We also correct the masses for finite volume and photon mass effects. In Section 3 we present the Vacuum Polarization and its form in lattice regularization with Wilson fermions. A variety of techniques are presented, as Padé fits and time moments (Section 4). Section 5 collects the central results of the work and we give preliminary estimates on the electromagnetic corrections to the muon anomaly. Section 6 contains our conclusion.



(a) Light  $u-d$  contribution to the hadronic  $a_\mu$ . (b) Strange  $s$  contribution to the hadronic  $a_\mu$ .



(c) Charm  $c$  contribution to the hadronic  $a_\mu$ .

Figure 5.1: Summary of the hadronic contributions to  $a_\mu$ . The light contribution makes the 90% of the total, while the strange and the charm account for 8% and 2% respectively. Plots taken from the plenary talk given by H. Wittig at 2016 the Lattice Conference.

## 5.1 Introduction

At the classical level an orbiting particle with electromagnetic charge  $e$  and mass  $m$  has a dipole magnetic moment given by  $\underline{\mu}_L = \frac{e}{2m} \underline{L}$ , where  $\underline{L} = m \underline{r} \times \underline{v}$  is the orbital angular momentum, and through that interacts with an external magnetic field in such a way that it is energetically favorable for the particle to align its magnetic dipole with it, i.e.

$$H = -\underline{\mu} \cdot \underline{B}. \quad (5.1.1)$$

For a particle  $\ell$  with spin  $\underline{S}$  and electromagnetic charge  $Q$ , in units of  $e$ , the magnetic moment is given by

$$\underline{\mu}_\ell = g_\ell \frac{Qe}{2m} \underline{S}, \quad (5.1.2)$$

At classical level the Dirac value is exactly  $g_\ell = 2$ .

When considering loop corrections the gyro-magnetic ratio gets quantum contributions. We define

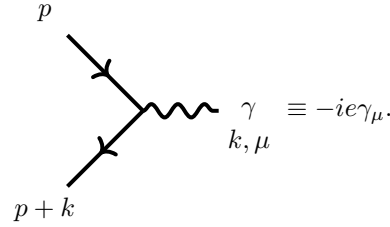
the deviation from its classical value as the *anomalous magnetic moment*

$$a_\ell = \frac{g_\ell - 2}{2}. \quad (5.1.3)$$

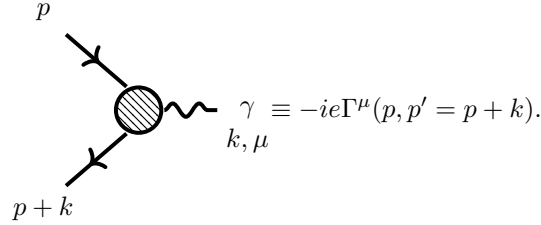
The first calculation of the leading contribution to the anomalous magnetic moment was done by (Schwinger, 1948) and the effect of the quantum fluctuation due to virtual lepton-photon interaction (vertex) was found to be

$$a_\ell^{\text{QED}} = \frac{\alpha}{2\pi}, \quad \text{where } \ell = e, \mu, \tau.$$

We start the discussion in Minkowski space. At tree-level the lepton-photon vertex is given by following expression



After quantization the vertex receives corrections and can be written as



The form of  $\Gamma^\mu(p, p')$  can be constrained by means of Lorentz invariance and current conservation, i.e.  $k_\mu \Gamma^\mu = 0$ , yielding to

$$\Gamma_\mu(p, p') = A\gamma_\mu + B(p_\mu + p'_\mu), \quad (5.1.4)$$

where  $A$  and  $B$  are real coefficients. With the use of the Gordon identity

$$\bar{u}(p')\gamma_\mu u(p) = \bar{u}(p')\frac{1}{2m} [(p_\mu + p'_\mu) + i[\gamma_\mu, \gamma_\nu](p^\nu - p'^\nu)] u(p), \quad (5.1.5)$$

we arrive to

$$\Gamma_\mu(p, p') = \gamma_\mu F_1(k^2) + i[\gamma_\mu, \gamma_\nu] \frac{k^\nu}{2m} F_2(k^2), \quad (5.1.6)$$

with  $F_1$  and  $F_2$  form factors.

The vertex renormalization in QED gives

$$-ie\Gamma_\mu(p, p' = p) = -ie\gamma_\mu, \quad (5.1.7)$$

from which we infer that  $F_1(k^2 = 0) = 1$ , i.e. the charge of the lepton in units of  $e$ , to *all orders* in perturbation theory.

By considering a non-relativistic electron scattered by a static potential one can show that the gyromagnetic ratio is given by

$$g_\ell = 2 + 2F_2(k^2 = 0), \quad (5.1.8)$$

and at leading order in QED  $F_2(0) = 0$ . This means that the gyromagnetic ratio becomes

$$g_\ell = 2 + O(\alpha) \rightarrow a_\ell = \frac{g_\ell - 2}{2} = O(\alpha). \quad (5.1.9)$$

## 5.2 Details on the computation of the vacuum polarization including QED corrections

We turn to the actual calculation of the HVP on the lattice. We work in the electroquenched approximation and use dynamical QCD configurations generated by the CLS initiative with two degenerate flavors of non-perturbatively  $O(a)$  improved Wilson fermions (Fritzsch *et al.*, 2012). We consider QED<sub>L</sub> and QED<sub>M</sub> to deal with the finite-volume zero modes, see Chap. 2. We fix the gauge to the Coulomb one in QED<sub>L</sub>. While in the massive case we fix it to Feynman.

In Fig. 5.2 we report the relevant diagrams for the leading order QED corrections to the HVP (only “continuum” diagrams are shown). Notice that those diagrams are at the same order in  $\alpha$  as the HLbL, that is not included. A computation including QED contribution must be performed to see whether those effects increase or decrease the discrepancy between the theoretical and the experimental muon anomaly. In this exploratory study we neglect quark-disconnected diagrams, which are flavor-symmetry and Zweig suppressed, and all diagrams involving charged sea quarks (electroquenched approx.). We would like to compare the HVP with and without electromagnetic effects. The two HVPs will be different functions of the renormalized parameters, and to have a meaningful comparison we need to consider them at the same renormalized parameters values. One way to go could be to rescale the bare values for the change in the quark mass, the strong coupling (reflected in the change of the lattice spacing) and the electromagnetic coupling, when considering the electromagnetic corrections to the HVP. We expect all those changes to be at the percent level. For this reason we neglect the change in the lattice spacing and the change in the electromagnetic coupling. A percent change in the mass for quite light quark masses will cause a large change in the pion masses, since we are working with Wilson fermions<sup>1</sup> (see Sect. 5.2.1). We take into account this effect by matching the charged (or neutral) pion masses in Q(C+E)D with the pion mass in QCD as we will see in Sect. 5.2.2.

In addition we make sure that the volumes and photon masses used in QED<sub>M</sub> are such that the correct dispersion relation is reproduced by the energy levels extracted from the charged pions two-point functions.

It should be noted that the leading electromagnetic order corrections to the HVP can be extracted also in the perturbative way as in the spirit of (de Divitiis *et al.*, 2013).

### 5.2.1 Critical mass

We start by first calculating the effect of the QED inclusion on the critical mass. This will serve as a cross-check of our implementations of QED<sub>L</sub> and QED<sub>M</sub>. We add to preexistent QCD

<sup>1</sup>There is a multiplicative plus additive renormalization in the mass.

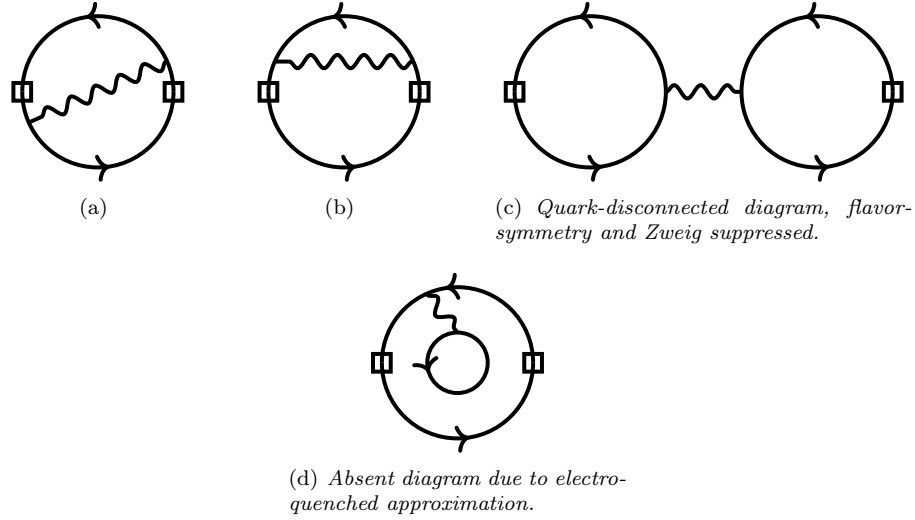


Figure 5.2: Leading order QED corrections to the HVP in the continuum theory. Squares corresponds to insertions of conserved current. All orders of QCD are understood when drawing the diagrams. Diagrams (a) and (b) are included in our calculation, while (c) and (d) are absent.

configurations the quenched QED configurations by forming a  $U(3)$  gauge theory with un-improved fermions.

By using lattice perturbation theory one can estimate the QED effect on the quark mass. We take here the results given in the App. E for the QED case. We calculate the expected shift in the A ensembles with parameters given in Tab. 5.2. In particular by using the approximations given in

Run	$L/a$	$\beta$	$c_{sw}$	$\kappa$	$\kappa_c$	$am_\pi$	$m_\pi L$	$a[\text{fm}]$	$m_\pi[\text{MeV}]$
A3	32	5.20	2.01715	0.13580	0.1360546	0.1893(6)	6.0	0.079(3)(2)	473
A4	32	5.20	2.01715	0.13590	0.1360546	0.1459(6)	4.7	0.079(3)(2)	364
A5	32	5.20	2.01715	0.13594	0.1360546	0.1265(8)	4.0	0.079(3)(2)	316

Table 5.2: Gauge configuration parameters and results in QCD, see Ref. (Capitani et al., 2015).

the App. E we arrive to the critical mass calculated in the two different approximations: Eq. E.48, where 1-loop QED diagrams are taken only, and Eq. E.49, where the QED tadpole is resummed to all orders.

In order to do the comparison with the simulations we need to find an operative definition of the critical mass  $m_c$  after the inclusion of QED. We consider the unphysical theory with two quarks degenerate in mass and charge  $\Psi = (u, d)$ . We use the PCAC mass to find the critical mass, since  $m_{\text{PCAC}} = Z(\beta, e^2) (m_0 - m_c(\beta, e^2))$ . The PCAC quark mass can be defined through the spatially integrated axial Ward identity, as in Eq. 3.5.18,

$$m_{\text{PCAC}} = \frac{\partial_0 \langle A_0^-(\underline{p} = \underline{0}, x_0) P^+(0) \rangle}{\langle P^-(\underline{p} = \underline{0}, x_0) P^+(0) \rangle}, \quad (5.2.10)$$

where we have the following definitions,

$$\begin{aligned}
 P^-(x) &= \bar{\Psi}(x)\gamma_5\frac{1}{2}(\tau^1 + i\tau^2)\Psi(x) = \bar{u}(x)\gamma_5d(x), \\
 P^+(x) &= \bar{\Psi}(x)\gamma_5\frac{1}{2}(\tau^1 - i\tau^2)\Psi(x) = \bar{d}(x)\gamma_5u(x), \\
 A_0^-(x) &= \bar{\Psi}(x)\gamma_0\gamma_5\frac{1}{2}(\tau^1 + i\tau^2)\Psi(x) = \bar{u}(x)\gamma_0\gamma_5d(x).
 \end{aligned}
 \tag{5.2.11}$$

By using Eq. 5.2.10 we extract the PCAC mass for each value of  $m_\gamma$ . At fixed photon mass we then perform an extrapolation, guided by chiral perturbation theory, to find the critical mass. In Fig. 5.3 we show a preliminary result for the critical mass in QCD+qQED<sub>M</sub> simulation, or Q(C+E<sub>M</sub>)D in the following. The picture emerging is quite clear, once we include QED the quarks become more massive, and the results are compatible with the finite-volume lattice perturbation theory predictions.

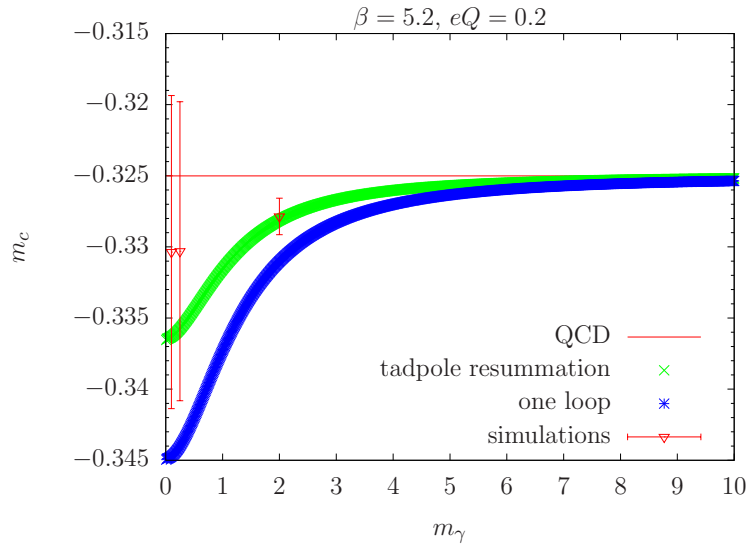


Figure 5.3: Comparison between the critical mass from lattice perturbation theory in Feynman gauge using the one-loop result Eq. E.48 (blue stars) and the tadpole resummation Eq. E.49 (green crosses). Orange triangles represents values from lattice simulations. The QCD critical mass is shown for comparison (red line).

### 5.2.2 Pseudoscalar spectrum

Here we give preliminary results on the masses in the pseudoscalar sector. The masses are calculated by cosh effective mass and fitted to a constant in the plateau region. We used one point source per configuration. The error is given by using a jackknife procedure. We implemented the QED<sub>L</sub> and QED<sub>M</sub> at the physical value of the electric charge  $e \simeq 0.3$ ,  $Q_u = 2/3$  and  $Q_d = -1/3$ . The results are found in Tab. 5.3. In Fig. 5.4 we show the typical effect of the massive QED inclusion and its comparison with QED<sub>L</sub>. For such small photon masses the result is quite stable and the comparison is made with the QCD result. It is clear from the plot that the pseudoscalar masses become larger, as expected since the quark masses increase. In Fig. 5.5 we show the change with



Run	$am_\gamma$	$m_\gamma L$	$am_{\pi^0,0.2}$	$am_{\pi^0,0.1}$	$am_{\pi^-} - am_{\pi^+}$	$N_{\text{cnf}}$
A3	0	x	.2549(9)	.2071(9)	.2330(9)	312
A3	0.1	3.2	.2556(7)	.2074(8)	.2337(8)	330
A3	0.25	8.0	.2553(7)	.2072(8)	.2331(8)	330
A4	0	x	.2240(8)	.1691(9)	.1994(9)	400
A4	0.1	3.2	.2252(9)	.1699(9)	.2005(9)	380
A4	0.25	8.0	.2246(8)	.1700(10)	.1998(9)	380
A5	0	x	.2105(7)	.1526(9)	.1849(8)	501
A5	0.1	3.2	.2114(7)	.1528(9)	.1856(8)	481
A5	0.25	8.0	.2111(7)	.1531(9)	.1852(8)	481

Table 5.3: Pseudoscalar masses in Coulomb gauge  $QED_L$  (denoted with  $m_\gamma = 0$ ) and  $QED_M$ . The resulting pion masses go from 380 MeV to 640 MeV.

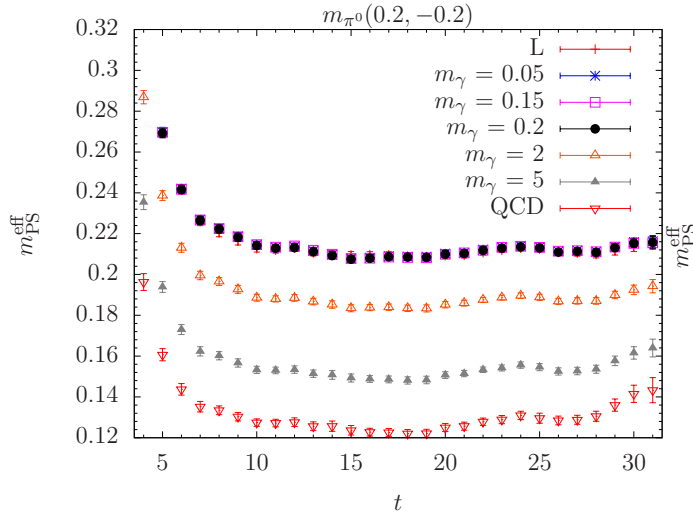


Figure 5.4: Effective neutral pseudoscalar masses for different photon masses and comparison with QCD and  $Q(C+E_L)D$ .

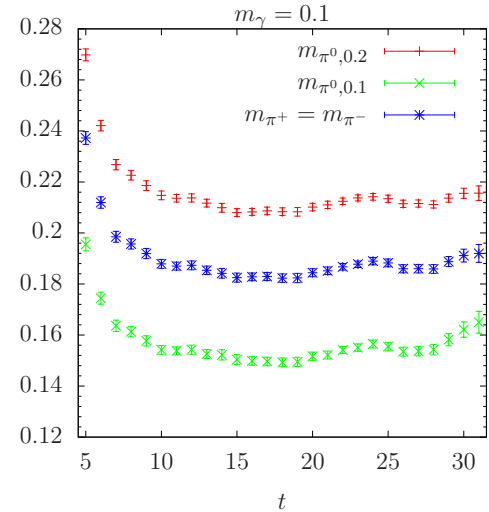


Figure 5.5: Effective pseudoscalar masses for  $m_\gamma = 0.1$  and different charge content.

the charge content. For such chiral masses in QCD we know that the square of the pseudoscalar mass is linear as a function of the bare PCAC mass. We found the same linearity after the inclusion of the massive QED field (for QED case see (Duncan *et al.*, 1996)). In Fig. 5.6 we show the neutral pseudoscalar mass as a function of the PCAC mass for  $m_\gamma = 0.1$ . Another example of that is given in Fig. 5.7, where we plot the average square masses of the  $u\bar{u}$  and  $d\bar{d}$  states, i.e.  $\overline{m_{\text{PS}}^2} = \frac{1}{2}(m_{\text{PS}}^2(eQ = 0.2) + m_{\text{PS}}^2(eQ = -0.1))$ , versus the sum of the two different PCAC masses, as suggested in (Duncan *et al.*, 1996)<sup>2</sup>. This means, upon identifying  $eQ_1 = 0.2$  and

<sup>2</sup>There it is pointed out that the linear average would introduce non analytic terms in the quark masses, while the square averaging respect the chiral symmetry expected from the full theory.

$eQ_2 = -0.1$ , that we expect the following dependence:

$$\overline{m^2}_{\text{PS}} = A(eQ_1, eQ_2) + m_{\text{PCAC}}(eQ_1)B(eQ_1, eQ_2) + m_{\text{PCAC}}(eQ_2)B(eQ_2, eQ_1). \quad (5.2.12)$$

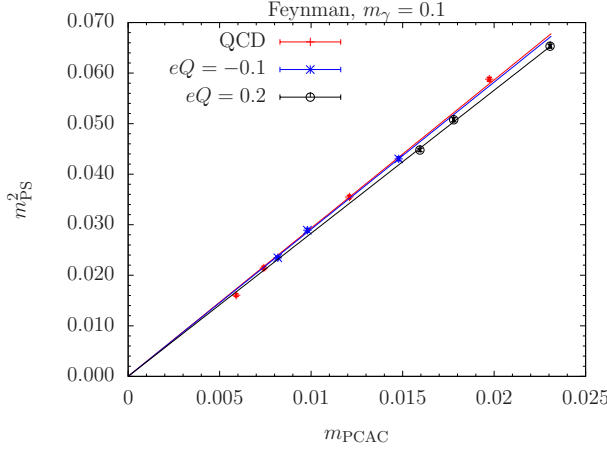


Figure 5.6: Neutral pseudoscalar masses versus PCAC mass for different charges.

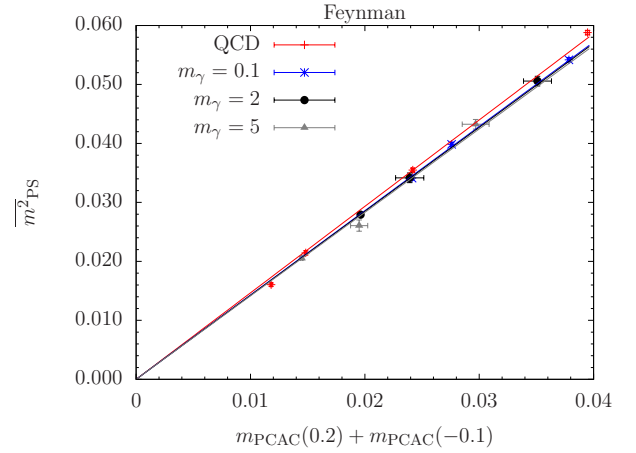


Figure 5.7: Square average of neutral pseudoscalar masses versus bare PCAC masses for different photon masses.

### 5.2.3 Finite volume and photon mass effects

We can take into account for finite volume and photon mass effects and correct the lattice results. The relevant formulae are given in Ref. (Borsanyi and others, 2015) for QED<sub>L</sub>, and Ref. (Endres et al., 2016) for QED<sub>M</sub>. We report them here for completeness and remind the reader that we are using lattice units.

Since the preliminary results concern only one volume, in QED<sub>L</sub>, we do not perform the fit but instead we give an estimate based on the lattice results

$$\delta_V m_{\pi^\pm}^{2,\text{LO}} = m_{\pi^\pm}^2(L, T \rightarrow \infty) - m_{\pi^\pm}^2(L, T) \simeq \frac{Q^2 \alpha \kappa m_{\pi^\pm}(L, T)}{L}, \quad (5.2.13)$$

with  $\kappa = 2.837297(1)$ . Results are given in Tab. 5.4 and we can conclude that finite volume effects are completely negligible.

In QED<sub>M</sub> we use the analytic formulae for the extracted masses at each volume

$$\begin{aligned} \delta_V m_{\pi^\pm}^{\text{LO}} &= 2\pi Q^2 \alpha m_\gamma \left[ \mathcal{I}_1(m_\gamma L) - \frac{1}{(m_\gamma L)^3} \right], \\ \delta_V m_{\pi^\pm}^{\text{NLO}} &= \pi Q^2 \alpha \frac{m_\gamma^2}{m_{\pi^\pm}} \left[ 2\mathcal{I}_{1/2}(m_\gamma L) + \mathcal{I}_{3/2}(m_\gamma L) \right], \end{aligned} \quad (5.2.14)$$

where  $\mathcal{I}_n(z)$  is defined as

$$\mathcal{I}_n(z) = \frac{1}{2^{n+1/2} \pi^{3/2} \Gamma(n)} \sum_{\nu \neq 0} \frac{K_{3/2-n}(z|\underline{\nu}|)}{(z|\underline{\nu}|)^{3/2-n}}, \quad (5.2.15)$$

Run	$m_{\pi^\pm}^2$	$\delta_V m_{\pi^\pm}^{2,\text{LO}}$
A3	0.0537(4)	0.00015(1)
A4	.0398(4)	0.00013(1)
A5	.0342(3)	0.00012(1)

 Table 5.4:  $QED_L$  leading order finite volume corrections.

with  $\underline{\nu} \in \mathbb{Z}^3$  and  $K_n$  modified Bessel function of the second kind. At leading order we obtain the following corrections

$$\begin{aligned}\delta_V m_{\pi^\pm}^{\text{LO}}(m_\gamma = 0.1) &= -.000097(1), \\ \delta_V m_{\pi^\pm}^{\text{LO}}(m_\gamma = 0.25) &= -.000023(1),\end{aligned}\tag{5.2.16}$$

that are negligible at this stage. For completeness next-to-leading order results are given in Tab. 5.5. After we have corrected for the finite volume effects we need to remove the photon mass ones. Here

Run	$m_\gamma$	$m_{\pi^\pm}$	$\delta_V m_{\pi^\pm}^{\text{NLO}}$
A3	0.1	.2337(8)	.000022(1)
A3	0.25	.2331(8)	$3.7(1) \times 10^{-7}$
A4	0.1	.2005(9)	.000026(1)
A4	0.25	.1998(9)	$4.3(1) \times 10^{-7}$
A5	0.1	.1856(8)	.000028(1)
A5	0.25	.1852(8)	$4.7(1) \times 10^{-7}$

 Table 5.5:  $QED_M$  next-to-leading order finite volume corrections.

we should consider the fit at next-to-leading order but since we have only two masses we use the formula at leading order, given by

$$\delta m_{\pi^\pm}^{\text{LO}} = m_{\pi^\pm}(m_\gamma \rightarrow \infty) - m_{\pi^\pm}(m_\gamma) = -\frac{\alpha}{2} Q^2 m_\gamma.\tag{5.2.17}$$

The results are the following

$$\begin{aligned}\delta m_{\pi^\pm}^{\text{LO}}(m_\gamma = 0.1) &= .00036(1), \\ \delta m_{\pi^\pm}^{\text{LO}}(m_\gamma = 0.25) &= .00091(1),\end{aligned}\tag{5.2.18}$$

we can conclude that photon mass effects are also negligible.

#### 5.2.4 Massless limit in $QED_M$

It was pointed out in Ref. (Patella, 2017) that in the limit of small photon mass the effective energy has a linear  $t$  behavior and furthermore is constant as we change the momentum  $\underline{p}$ . Here we look

at the behavior of the effective energy in the regime of small photon mass. The result is found by mimicking the calculations given in (Patella, 2017) and we report here the result for completeness

$$E_{\text{eff}}(t, \underline{p}) \stackrel{m_\gamma \rightarrow 0}{\simeq} \frac{(Q_u - Q_d)^2 e^2}{m_\gamma^2 V} t - \frac{d}{dt} \ln \langle \mathcal{O}(t, \underline{0}) \overline{\mathcal{O}}(0) \delta_{Q^T, 0} \rangle_{\text{TL}},$$

where  $\mathcal{O} = \pi^+$  is the pion interpolating field, the charge is  $Q_u - Q_d = 1$ ,  $Q^T = Q_u + Q_d$  and  $\langle \dots \rangle_{\text{TL}}$  is the expectation value taken in the QED<sub>TL</sub> formulation. In the regime in which the above formula is valid the effective mass is independent from the momentum, plus a linear term in  $t$  must be subtracted by hand before extracting the effective energy. The linear term was recognized and studied in the non-relativistic approach in (Endres *et al.*, 2016) and explicitly subtracted. Notice that in our case  $m_\gamma^2 V$  is around three orders of magnitude bigger than the one in (Endres *et al.*, 2016), that explains why we do not see the linear behavior in  $t$ , Fig. 5.5.

In Fig. 5.8 we show the dispersion relation and we observe that it follows the continuum-like curve. In Fig. 5.9 we see that after the inclusion of the massive QED field the charged pion effective energy in the A5 ensemble matches the one in A3 with QCD only, this observation will be useful later.

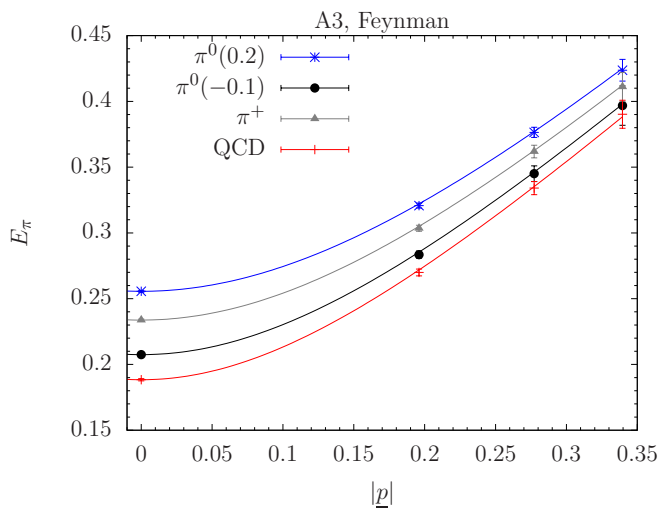


Figure 5.8: Dispersion relation for the charged and neutral pions in the A3 ensemble.

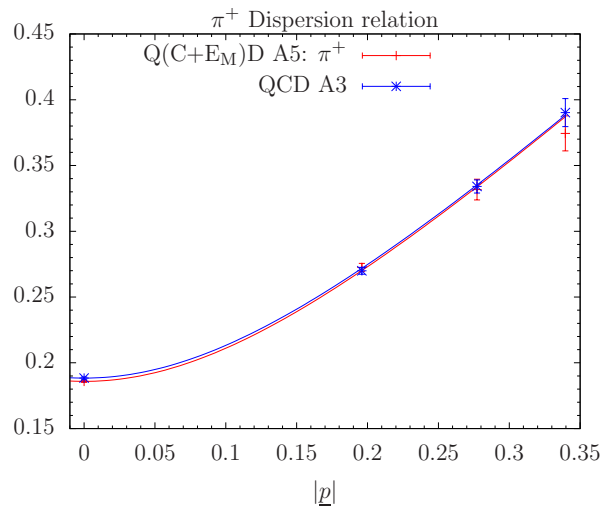


Figure 5.9: Dispersion relation for charged and neutral pions for  $m_\gamma = 0.1$ . The solid lines are the expectations from the continuum dispersion relation.

### 5.3 Vacuum polarization

The quark electromagnetic current is defined as

$$J_\mu(x) = \sum_f^{N_f} Q_f J_\mu^f(x) = \sum_f^{N_f} Q_f \bar{\psi}_f(x) \gamma_\mu \psi_f(x), \quad (5.3.19)$$

where  $f$  denotes the flavor index and  $Q_f$  the associated charge ( $e = 1$ ), see App. A.2.1 for a derivation of the one-point-split current in the formal theory. In the case of  $N_f = 2$  with  $\Psi = (u, d)$ ,  $Q_u = 2/3$  and  $Q_d = -1/3$ , the electromagnetic current is a mixture of  $\mathbf{1}$  and  $\sigma^3$  matrices in flavor space

$$J_\mu(x) = \bar{\Psi}(x)\gamma_\mu \left[ \frac{Q_u}{2} (\mathbf{1} + \sigma^3) + \frac{Q_d}{2} (\mathbf{1} - \sigma^3) \right] \Psi(x). \quad (5.3.20)$$

The Euclidean HVP tensor is defined as

$$\Pi_{\mu\nu}^{ff'}(q) = \int d^4x e^{iq \cdot x} \langle J_\mu^f(x) J_\nu^{f'}(0) \rangle, \quad (5.3.21)$$

and can be decomposed thanks to Lorentz invariance and current conservation as follows

$$\Pi_{\mu\nu}^{ff'}(q) = (\delta_{\mu\nu}q^2 - q_\mu q_\nu) \Pi^{ff'}(q^2), \quad (5.3.22)$$

leading to the scalar VP  $\Pi^{ff'}(q^2)$ , where the flavors  $f$  and  $f'$  need not to be the same. The total vacuum polarization is then a sum over the possible flavors

$$\Pi(q^2) = \sum_{f,f'} Q_f Q_{f'} \Pi^{ff'}(q^2). \quad (5.3.23)$$

The leading order contribution to the anomalous magnetic moment of the muon ( $a_\mu^{\text{HLO}}$ ) for space-like momenta is related to the scalar VP as follows

$$a_{\mu,\text{LO}}^{\text{HAD}} = \left( \frac{\alpha}{\pi} \right)^2 \int_0^\infty dq^2 f(q^2) \hat{\Pi}(q^2), \quad (5.3.24)$$

where  $\hat{\Pi}$  is the renormalized scalar VP and we have defined the following quantities

$$\begin{aligned} \hat{\Pi}(q^2) &\equiv 4\pi^2 [\Pi(q^2) - \Pi(0)], \\ Z &\equiv \frac{\sqrt{q^4 + 4m_\mu^2 q^2} - q^2}{2m_\mu^2 q^2}, \\ f(q^2) &\equiv \frac{m_\mu^2 q^2 Z^3 (1 - q^2 Z)}{1 + m_\mu^2 q^2 Z^2}. \end{aligned} \quad (5.3.25)$$

The integrand function  $f(q^2) \hat{\Pi}(q^2)$  is peaked around values of  $q^2 \sim (\sqrt{5} - 2) m_\mu^2$ , but the lowest momentum on the lattice is quite far from this value for typical lattice sizes<sup>3</sup>. We divide the  $\hat{\Pi}(q^2)$  in three regions to reduce its model dependence (Golterman *et al.*, 2014). For small  $q^2$  we should rely on a parametrization of  $\hat{\Pi}(q^2)$ , which is then convoluted with  $f(q^2)$  to find  $a_\mu$ . The extraction of  $\Pi(0)$  is quite difficult since the statistical accuracy deteriorates as  $q \rightarrow 0$ . In the mid- $q^2$  region one integrates directly the lattice data multiplied by  $f(q^2)$ . The muon anomaly  $a_\mu$  in the large  $q^2$  region is computed using perturbation theory (a 3-loop computation is available in Ref. (Chetyrkin *et al.*, 1996)). The situation is schematically shown in Fig. 5.10.

<sup>3</sup>That is the reason why TBCs are used in this kind of calculations, see Chap. 3

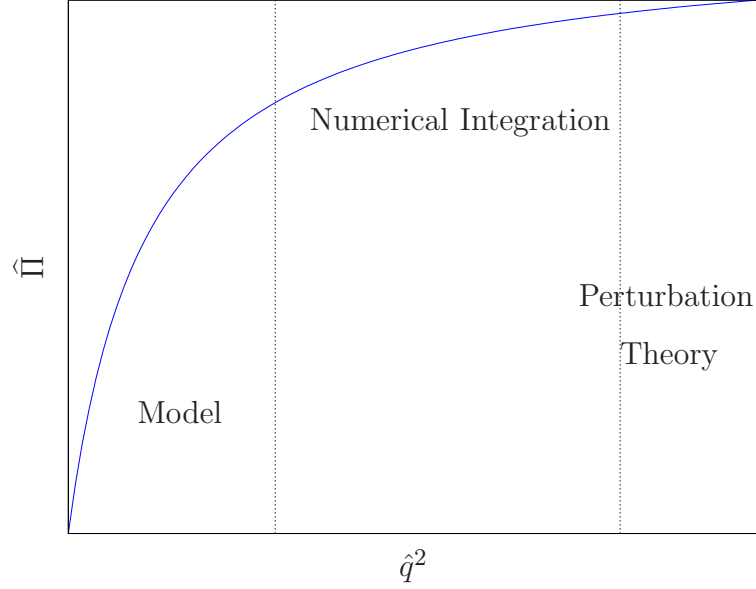


Figure 5.10: *Schematic representation of the subtracted scalar Hadronic Vacuum Polarization. In the low  $q^2$  region, “Model”, we use for example Padé fit to estimate the HVP and we integrate the result. In the mid- $q^2$  region we numerically integrate directly the lattice data. In the large  $q^2$  region we use perturbation theory.*

### 5.3.1 Lattice regularization

We build the electromagnetic current in Q(C+E)D as the Noether current of the infinitesimal  $\mathbf{U}(1)$  vector transformation

$$\begin{aligned}\delta_V \psi_f(x) &= i\alpha(x) Q_f \psi_f(x), \\ \delta_V \bar{\psi}_f(x) &= -i\alpha(x) \bar{\psi}_f(x) Q_f.\end{aligned}\tag{5.3.26}$$

On the lattice we implement the one-point-split current, which is the conserved current of the  $\mathbf{U}_V(1)$ <sup>4</sup>, and given as

$$V_\mu^f(x) = \frac{1}{2} [\bar{\psi}_f(x) U_\mu(x) (\gamma_\mu - r) \psi_f(x + \hat{\mu}) + \bar{\psi}_f(x + \hat{\mu}) U_\mu^\dagger(x) (\gamma_\mu + r) \psi_f(x)],\tag{5.3.27}$$

in the case of Wilson fermions<sup>5</sup> with  $r$  parameter of the Wilson term, see App. A.2.2 for the derivation of the current. The VP tensor is found to be

$$\Pi_{\mu\nu}(x) = \left\langle \left( \sum_f^{N_f} Q_f V_\mu^f(x) \right) \left( \sum_{f'}^{N_f} Q_{f'} V_\nu^{f'}(0) \right) \right\rangle\tag{5.3.28}$$

<sup>4</sup>For  $N_f = 2$  Eq. 2.1.7 modifies as  $\mathbf{H}_{\mathbf{Q}(C+E)D}(N_f = 2) = \mathbf{U}'(1)_V \otimes \mathbf{U}(1)_V$ , where  $\mathbf{U}'(1)_V$  is the subgroup of  $\mathbf{SU}(2)_V$  generated by  $\sigma^3$ .

<sup>5</sup>For both the improved and un-improved theory.

and by Fourier transforming the above expression we get

$$\Pi_{\mu\nu}(\hat{q}) = \sum_{n \in \Lambda} e^{iq \cdot (x + \hat{\mu}/2 + \hat{\nu}/2)} \Pi_{\mu\nu}(n), \quad (5.3.29)$$

where we recall  $q_\mu \in \tilde{\Lambda}$  and  $\hat{q}_\mu = 2 \sin(q_\mu/2)$ .

When considering the diagonal term,  $\mu = \nu$ , we need to take into account contact terms that modify the expression we have given in the formal theory<sup>6</sup>. The contact term is given by

$$\begin{aligned} J_\mu^{f,\text{ct}}(x) &= \frac{1}{2} [\bar{\psi}_f(x) U_\mu(x) (r - \gamma_\mu) \psi_f(x + \hat{\mu}) + \bar{\psi}_f(x + \hat{\mu}) U_\mu^\dagger(x) (\gamma_\mu + r) \psi_f(x)], \\ \Pi_{\mu\nu}^{f,\text{ct}}(\hat{q}) &= -\delta_{\mu\nu} \langle J_\mu^{f,\text{ct}}(0) \rangle. \end{aligned} \quad (5.3.30)$$

The HVP is now given by Eqs. 5.3.30, 5.3.29, namely

$$\Pi_{\mu\nu}^{ff'}(\hat{q}) = \left[ \sum_{x \in \Lambda} e^{iq \cdot (x + \hat{\mu}/2 + \hat{\nu}/2)} \langle V_\mu^f(x) V_\nu^{f'}(0) \rangle \right] - \delta_{\mu\nu} \delta_{ff'} \langle J_\mu^{f,\text{ct}}(0) \rangle, \quad (5.3.31)$$

which fulfills the WTI

$$\hat{q}_\mu \Pi_{\mu\nu}^{ff'} = 0 = \hat{q}_\nu \Pi_{\mu\nu}^{ff'}. \quad (5.3.32)$$

For the explicit form of the HVP after Wick contractions see App. F.

We relate the HVP to the scalar VP by using the continuum relation

$$\Pi_{\mu\nu}^{ff'}(\hat{q}) = (\delta_{\mu\nu} \hat{q}^2 - \hat{q}_\mu \hat{q}_\nu) \Pi^{ff'}(\hat{q}^2) + \mathcal{O}(\hat{q}^4). \quad (5.3.33)$$

The term  $\mathcal{O}(\hat{q}^4)$  denotes all the higher order terms invariant under hypercubic transformations. Those vanish in the continuum limit and in an anisotropic finite volume, e.g.  $L \neq T$ , the hypercubic invariance is further broken.

The scalar VP has order  $a$  effects since the conserved vector current is not improved. One way to improve the current would be to consider the following modification

$$V_\mu^{\text{impr}}(\hat{q}) = V_\mu(\hat{q}) + c \sin(q_\nu/2) \sum_n e^{iq \cdot x} T_{\mu\nu}(x), \quad (5.3.34)$$

where  $T_{\mu\nu}(x) = \bar{\psi}(x) \sigma_{\mu\nu} \psi(x)$  and  $c$  is a constant to be fitted to remove the order  $a$  effects for on-shell improvement of the matrix elements of the current  $V$ . See Ref. (Gockeler *et al.*, 2004) for Wilson fermions in the qQCD case.

### 5.3.2 Scalar vacuum polarization

In order to extract the scalar VP we have to analyze the relation Eq. 5.3.33.

**Off diagonal components** For  $\mu \neq \nu$  the equation becomes

$$\Pi_{\mu\nu}^{ff'}(\hat{q}) = -\hat{q}_\mu \hat{q}_\nu \Pi^{ff'}(\hat{q}^2), \quad (5.3.35)$$

<sup>6</sup>Contact terms arise from the overlapping of composite operators.

and by summing over all the possible  $N$  permutations of the indexes with  $\mu \neq \nu$  and the same  $\hat{q}^2$  we obtain

$$\Pi^{ff'}(\hat{q}^2) = -\frac{1}{\hat{q}_\mu \hat{q}_\nu} \Pi_{\mu\nu}^{ff'}(\hat{q}) \implies \sum_{\mu \neq \nu} \Pi^{ff'}(\hat{q}^2) = N \Pi^{ff'}(\hat{q}^2) = -\sum_{\mu \neq \nu} \frac{1}{\hat{q}_\mu \hat{q}_\nu} \Pi_{\mu\nu}^{ff'}(\hat{q}), \quad (5.3.36)$$

from which we extract the scalar VP,

$$\Pi^{ff'}(\hat{q}^2) = -\frac{1}{N} \sum_{\mu \neq \nu} \frac{\Pi_{\mu\nu}^{ff'}(\hat{q})}{\hat{q}_\mu \hat{q}_\nu}. \quad (5.3.37)$$

**Diagonal components** For the diagonal component  $\mu = \nu$  the Eq. 5.3.33 becomes

$$\Pi_{\mu\mu}^{ff'}(\hat{q}) = (\hat{q}^2 - \hat{q}_\mu^2) \Pi^{ff'}(\hat{q}^2), \quad (5.3.38)$$

and again by summing over  $\mu$  we find the equation for the extraction of the scalar vacuum polarization

$$\sum_{\mu} \Pi_{\mu\mu}^{ff'}(\hat{q}) = \sum_{\mu} (\hat{q}^2 - \hat{q}_\mu^2) \Pi^{ff'}(\hat{q}^2) = (4\hat{q}^2 - \underbrace{\sum_{\mu} \hat{q}_\mu^2}_{\hat{q}^2}) \Pi^{ff'}(\hat{q}^2) = 3\hat{q}^2 \Pi^{ff'}(\hat{q}^2), \quad (5.3.39)$$

that is given by

$$\Pi^{ff'}(\hat{q}^2) = \frac{1}{3\hat{q}^2} \sum_{\mu} \Pi_{\mu\mu}^{ff'}(\hat{q}). \quad (5.3.40)$$

### Tensor zero mode subtraction

In this work we use a modified version of the HVP tensor, in particular we subtract the zero mode contribution (ZMS) from it

$$\Pi_{\mu\nu}^{\text{ZMS}}(\hat{q}) = \sum_{n \in \Lambda} e^{iq \cdot (n + \hat{\mu}/2 + \hat{\nu}/2)} \Pi_{\mu\nu}(n) - \sum_{n \in \Lambda} \Pi_{\mu\nu}(n) = \Pi_{\mu\nu}(\hat{q}) - \Pi_{\mu\nu}(\hat{q} = 0). \quad (5.3.41)$$

It has been shown in (Bernecker and Meyer, 2011) that in the infinite volume limit, thanks to Lorentz symmetry, the zero mode contribution vanishes whereas in the finite volume it is not constrained and can differ from zero. By using the ZMS version improvements in the signal-to-noise in the low  $\hat{q}^2$  region can be seen, see for example Ref. (Blum and others, 2016).

#### 5.3.3 Padé fits

Since the integrand in Eq. 5.3.24 is strongly peaked around the muon mass we need a good description of the scalar VP in low  $\hat{q}^2$  region. Furthermore what enters in the integral for the muon anomaly is the subtracted VP, meaning that we need to extrapolate the value  $\Pi(\hat{q}^2 = 0)$ . To do so we need to parametrize the VP as a function of  $\hat{q}^2$ .

It is known that the Taylor expansion of the VP does not converge and yields to very poor fits in terms of  $\chi^2$ . The Padé expansion effectively increases the radius of convergence of the sum. We can recast the Padé fits in the following form

$$R_{mn}(\hat{q}^2) = \Pi(0) + \hat{q}^2 \left( \delta_{mn} c + \sum_{i=0}^{m-1} \frac{a_i}{b_i + \hat{q}^2} \right),$$

where  $n = m, m + 1$  and  $\Pi(0)$ ,  $a_i$ 's and  $b_i$ 's are the parameters to be fitted.



## 5.4 Time moments

Another way to extract the scalar VP at zero momentum involves time moments. Those give derivatives of the scalar VP with respect to  $\hat{q}^2$  at zero (Chakraborty *et al.*, 2016). We start from Eq. 5.3.33 and we consider only the diagonal spatial components  $\mu = \nu = j$

$$\Pi_{jj}^{ff'}(\hat{q}) = (\hat{q}^2 - \hat{q}_j) \Pi^{ff'}(\hat{q}^2). \quad (5.4.42)$$

If we restrict to momenta of the kind  $\hat{q} = (\hat{q}_0, \mathbf{0})$  and we sum over  $j$  we obtain

$$\sum_j \Pi_{jj}^{ff'}(\hat{q}_0) = 3\hat{q}_0^2 \Pi^{ff'}(\hat{q}_0^2).$$

The scalar VP is then given by

$$\hat{q}_0^2 \Pi^{ff'}(\hat{q}_0^2) = \frac{1}{3} \sum_j \Pi_{jj}^{ff'}(\hat{q}_0) = \frac{1}{3} \sum_j \left\{ \left[ \sum_{x_0, \underline{x} \in \Lambda} e^{iq_0 x_0} \langle V_j^f(n) V_j^{f'}(0) \rangle \right] - \delta_{ff'} \langle J_j^{f, \text{ct}}(0) \rangle \right\} \quad (5.4.43)$$

### 5.4.1 Infinite volume

In order to obtain the time moments relations we consider derivatives with respect to  $q_0$  evaluated at zero<sup>7</sup>,

$$\begin{aligned} \left. \frac{\partial^{2k}}{\partial q_0^{2k}} \left( q_0^2 \Pi^{ff'}(q_0^2) \right) \right|_{q_0=0} &= \frac{1}{3} \sum_{j, x_0, \underline{x}} \langle V_j^f(x) V_j^{f'}(0) \rangle \left( \frac{\partial^{2k}}{\partial q_0^{2k}} e^{iq_0 x_0} \right) \Big|_{q_0=0} \\ &= \frac{1}{3} \sum_{j, x_0, \underline{x}} \langle V_j^f(x) V_j^{f'}(0) \rangle (i)^{2k} x_0^{2k} e^{iq_0 x_0} \Big|_{q_0=0} \\ &= \frac{1}{3} \sum_{j, x_0, \underline{x}} (-)^k x_0^{2k} \langle V_j^f(x) V_j^{f'}(0) \rangle \equiv G_{2k}^{ff'}. \end{aligned} \quad (5.4.44)$$

We have an infinite tower of relations from which we can build the Taylor expansion of the scalar VP

$$\Pi^{ff'}(q_0^2) = \sum_{k=1}^{\infty} G_{2k}^{ff'} \frac{q_0^{2k-2}}{(2k)!} = \frac{1}{3} \sum_{j, x_0, \underline{x}} \langle V_j^f(x) V_j^{f'}(0) \rangle \sum_{k=0}^{\infty} (-)^k x_0^{2k} \frac{q_0^{2k-2}}{(2k)!}. \quad (5.4.45)$$

Notice that for  $k = 1$  in the above formula we obtain

$$\Pi^{ff'}(q_0^2 = 0) = \frac{1}{2} \frac{\partial^2}{\partial q_0^2} \left( q_0^2 \Pi^{ff'}(q_0^2) \right) \Big|_{q_0=0} = -\frac{1}{6} \sum_j \sum_{x_0, \underline{x}} x_0^2 \langle V_j^f(x) V_j^{f'}(0) \rangle, \quad (5.4.46)$$

for any parametrization of  $\Pi(q_0^2)$ , used to estimate  $\Pi(0)$  for the subtracted scalar VP.

<sup>7</sup>The contact term does not contribute since it is a constant.

### 5.4.2 Finite volume

On the lattice we are forced to work with finite volumes, meaning that momenta are quantized and derivatives have to be replaced by finite differences.

We use the symmetric derivative definition because the error is proportional to  $h^2$ , with  $h$  being the separation between adjacent momenta

$$\begin{aligned}
\frac{\Delta f(q_0)}{\Delta q_0} &= \frac{1}{2} \left( \frac{T}{2\pi} \right) \left[ f \left( q_0 + \frac{2\pi}{T} \right) - f \left( q_0 - \frac{2\pi}{T} \right) \right], \\
\frac{\Delta^2 f(q_0)}{\Delta q_0^2} &= \frac{1}{2^2} \left( \frac{T}{2\pi} \right)^2 \left[ f \left( q_0 + \frac{4\pi}{T} \right) - 2f(q_0) + f \left( q_0 - \frac{4\pi}{T} \right) \right], \\
&\vdots \\
\frac{\Delta^{2n} f(q_0)}{\Delta q_0^{2n}} &= \frac{1}{2^{2n}} \left( \frac{T}{2\pi} \right)^{2n} \sum_{k=0}^n (-)^k \binom{n}{k} f \left[ q_0 + (n-2k) \frac{2\pi}{T} \right].
\end{aligned} \tag{5.4.47}$$

By applying the above formulae to the expression of the scalar VP in Eq. 5.4.43 we have to evaluate the finite difference of the exponential

$$\begin{aligned}
\left. \frac{\Delta e^{iq_0 x_0}}{\Delta q_0} \right|_{q_0=0} &= \frac{1}{2} \left( \frac{T}{2\pi} \right) e^{iq_0 x_0} \left[ e^{i2\pi x_0/T} - e^{-i2\pi x_0/T} \right] \Big|_{q_0=0} \\
&= \frac{T}{2\pi} e^{iq_0 x_0} i \sin \left( \frac{2\pi}{T} x_0 \right) \Big|_{q_0=0} = \frac{T}{2\pi} i \sin \left( \frac{2\pi}{T} x_0 \right), \\
\left. \frac{\Delta^2 e^{iq_0 x_0}}{\Delta q_0^2} \right|_{q_0=0} &= \left( \frac{T}{2\pi} \right)^2 i^2 \sin^2 \left( \frac{2\pi}{T} x_0 \right), \\
&\vdots \\
\left. \frac{\Delta^{2n} e^{iq_0 x_0}}{\Delta q_0^{2n}} \right|_{q_0=0} &= \left( \frac{T}{2\pi} \right)^{2n} (-)^n \sin^{2n} \left( \frac{2\pi}{T} x_0 \right).
\end{aligned} \tag{5.4.48}$$

By combining all the results the master formula for the time moments is given by

$$\left. \frac{\Delta^{2k}}{\Delta q_0^{2k}} \hat{q}_0^2 \Pi^{ff'}(\hat{q}_0^2) \right|_{q_0=0} = \frac{1}{3} \sum_{j, x_0, \underline{x}} \left( \frac{T}{2\pi} \right)^{2k} (-)^k \sin^{2k} \left( \frac{2\pi}{T} x_0 \right) \langle V_j^f(x) V_j^{f'}(0) \rangle. \tag{5.4.49}$$

Now we can give a specific Padé approximation of  $\Pi^{ff'}(\hat{q}_0^2)$ , put it in the l.h.s. of the above formula and determine the parameters by equating the results with the r.h.s. of Eq. 5.4.49. Given a representation of the scalar VP with  $N$  parameters we need the same number of equations (given by the master formula). Then we solve the highly non-linear system in order to extract the relevant parameters. By increasing the number of parameters we are forced to increase the number of derivatives to take into account and therefore the number of momenta to consider, see Eq. 5.4.47. This affects the estimate of an extremely local, in Fourier space, quantity as  $\Pi^{ff'}(\hat{q}^2 = 0)$ .

## 5.5 Subtracted scalar HVP

In this section we collect the main results for the subtracted scalar HVP. In Fig. 5.11(a) we show the results in the case of QCD, while in Fig. 5.11(b) the unsubtracted HVP with inclusion of massive

and massless QED. Notice that  $\widehat{\Pi}$  versus  $r_0^2 \hat{q}^2$  is a renormalized plot. The value of the Sommer parameter  $r_0/a$  is calculated starting from gluonic observables that do not get electromagnetic contributions in qQED. We therefore use the values of  $r_0/a$  computed in QCD, those can be found in Ref. (Fritzsch *et al.*, 2012).

The shape of the scalar VP is qualitatively the same with or without QED. In Fig. 5.12(a) we show the effect of QED inclusion and the comparison is made thanks to the matching condition presented in Sect. 5.2. The usefulness of the matching condition is twofold; on one side it allows for a comparison between different ensembles, on the other side we know that the HVP is strongly dependent on the pion masses (Della Morte *et al.*, 2012), hence we need to match the pion masses if we want to extract the EM effects.

It can be seen in Fig. 5.12(c) how the QED effect is consistent with a constant within errors. More precisely the effect is about 7% and compatible with zero within two/three combined sigmas. That suggests to look directly at the difference of the subtracted scalar HVPs, Fig. 5.12(b). A naïve way to proceed is to model the HVPs once in QCD and once in Q(C+E)D and calculate  $a_\mu$  in the two theories. The difference encodes the QED corrections once the results have been extrapolated to the same pion masses. This introduces large systematics due to the two fits and washes out the QED effects. Instead we follow a different approach where we first match the pion masses and then we model the difference for the HVPs directly. Notice this represents a one less-fit procedure dependent approach. After a good description of the difference of the HVPs is found we convolute that with the  $f(\hat{q}^2)$  and get the result for  $a_\mu^{\text{HAD,QED}}$ .

For a preliminary estimate of the electromagnetic effects we model the difference with Padé fits  $R_{10}$  and  $R_{11}$  and a mixed fit, namely linear rising in  $\hat{q}^2$  and then constant. By integrating the different fits numerically we find

$$\begin{aligned} a_\mu^{\text{HAD,QED}}(R_{10}) &= (60 \pm 28) \times 10^{-10}, \\ a_\mu^{\text{HAD,QED}}(R_{11}) &= (50 \pm 24) \times 10^{-10}, \\ a_\mu^{\text{HAD,QED}}(\text{mixed}) &= (35 \pm 14) \times 10^{-10}. \end{aligned} \tag{5.5.50}$$

We see that at this level the systematics, as expected, still dominate the error. One crucial thing to notice is that the electromagnetic effects go in the direction of reduce the tension between the theoretical and experimental value. We checked that the conclusions do not change when considering QED<sub>L</sub> as we can see from Fig. 5.11(b). It appears that all the issues related to the QED<sub>L</sub> formulation (Patella, 2017) are under control or do not have effect on the quantities we have analyzed so far.

## 5.6 Conclusions

We presented preliminary results for the electromagnetic effects on several observables. We discussed the change in the critical mass due to the inclusion of electromagnetic interactions and compared with perturbation theory calculations. We found the linearity of the square pseudoscalar mass in the PCAC mass. We gave results for the light pseudoscalar spectrum and we found completely negligible finite volume and photon mass effect. We made sure that in QED<sub>M</sub> we extracted the right energy values, and that the massive approach does not reduce to a “very complicated way” to use QED<sub>TL</sub>. For the HVP we presented a strategy to give an estimate on the electromagnetic corrections, which schematically consists in:

- matching the (charged) pion masses in different ensembles, with and without QED,
- looking directly at the difference of the subtracted HVPs in the Q(C+E)D and QCD matched ensembles.

---

In this way we were able to see a clear signal for the HVP that at the end reflected in an estimate for the muon anomaly. Perhaps the most important result is that the electromagnetic corrections in the muon anomaly clearly ameliorate the tension between theory and experiment.

The results are very encouraging and we plan to consider the inclusion of twisted boundary conditions, in order to stabilize the fits in  $\hat{q}^2$ , as well as analyze different ensembles available in the CLS initiative, in order to study the cutoff dependence, but mostly the pion mass dependence of the EM effects.

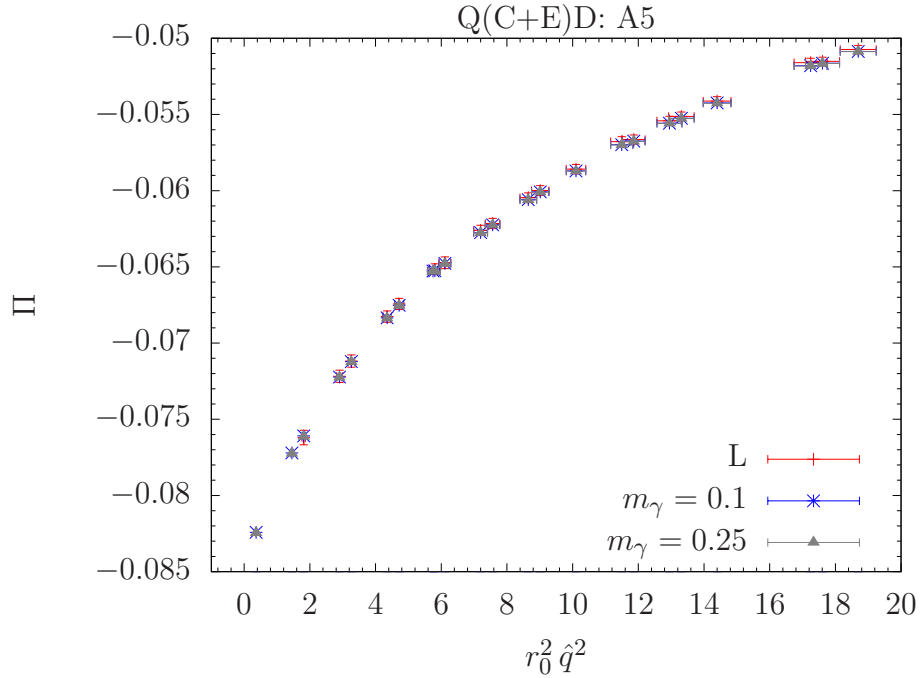
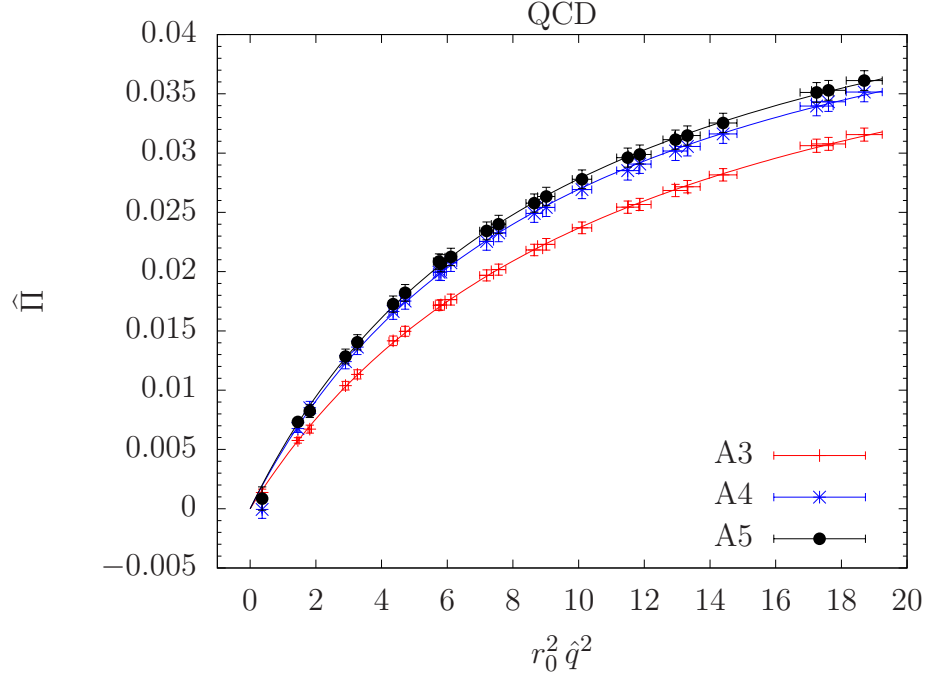
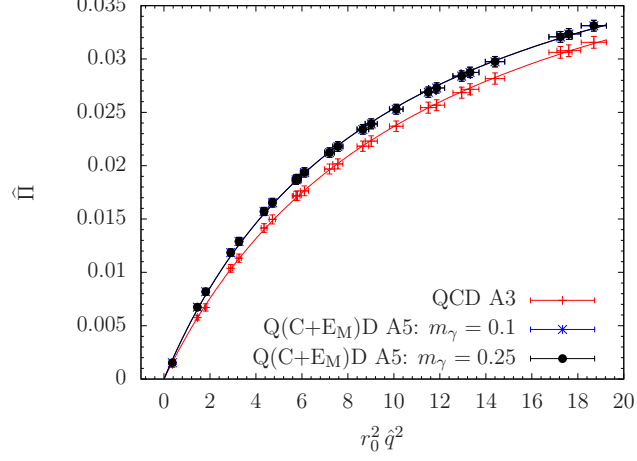
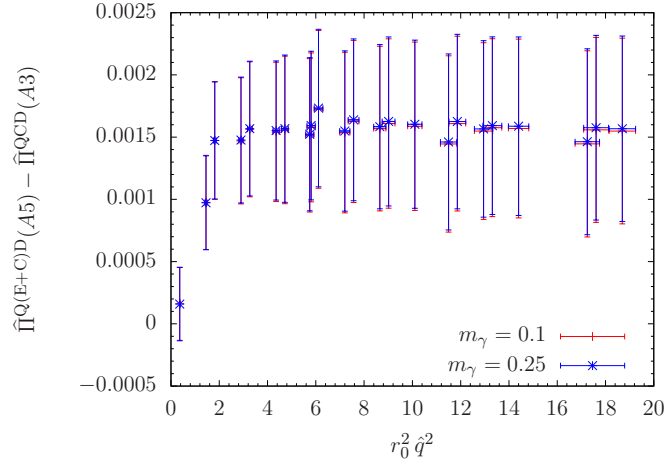


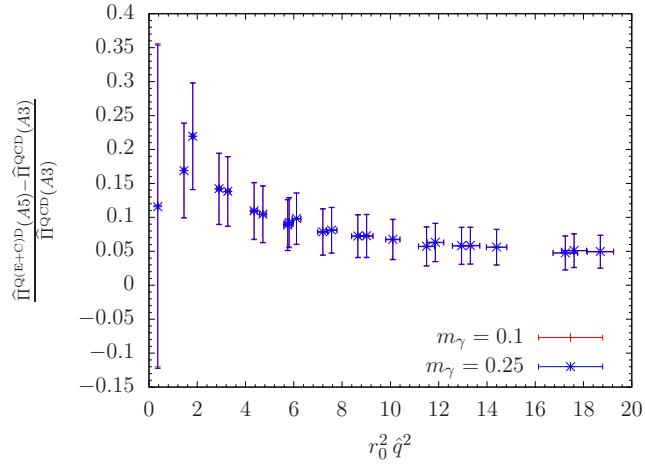
Figure 5.11: HVP as a function of  $r_0 \hat{q}^2$  with and without the inclusion of QED.



(a) Comparison of the scalar VP with and without QED.



(b) Difference of the HVP with and without QED.



(c) Relative difference of the QCD and Q(C+E)D HVP.

Figure 5.12: Comparisons of the HVP on the matched ensembles.



## Chapter 6

# Conclusions and Outlooks

The goal of the different projects presented in this thesis was to accurately assess some residual systematic effects in high-precision non-perturbative applications of Lattice Gauge Theories.

We studied the viability of reweighting techniques for twisted boundary conditions in the spatial directions for fermionic fields. There we suggested to compensate for the breaking of unitarity due to the choice of different boundary conditions in the valence and sea sector. This project started in order to estimate the above mentioned violations in the computation of renormalization factors for the minimal walking Technicolor theory, using the RI-MOM scheme and partially twisted boundary conditions. We performed a complete study of the reweighting approach from tree-level to actual Monte Carlo simulations. We studied gluonic and fermionic observables in large and small volumes and we saw that the effect of the reweighting is at the sub-percent level. In small volumes we found a quite pronounced sensitivity of the critical mass for un-improved Wilson fermions to changes in the twisting angle. That is clearly a cutoff and finite volume effect that could be rather large for large twisting angles.

In the second part of the thesis we presented an optimization of the HMC algorithm. No optimization study exists for BSM theories on the lattice. The lattice BSM field is relatively young and the time for more precise result has come. We proposed a new strategy to find optimal parameters in the case of the Omelyan integrator and Hasenbusch mass-preconditioning. The entire method is based on the existence of an exactly conserved quantity, the Shadow Hamiltonian. Its implementation is straightforward and we only needed to calculate the driving forces used during the Molecular Dynamics step. We implemented our strategy in the case of multi-time scales and mass-preconditioning, and we found the general form of the Shadow Hamiltonian in that case. Once the forces during the trajectory were measured we were able to give predictions on the cost and acceptance of a simulation within 10% accuracy. Before that a rule of thumb was used to find optimal parameters. The method can be also implemented on-line during the generation of configurations. That is quite an appealing possibility, were the algorithm correct itself changing the optimized parameters for the trajectories during thermalization.

Since the twisted boundary conditions represent an IR regularization as a mass term, during the time of the optimization project I also developed a twisted-boundary-preconditioning. Unfortunately, as we saw in the reweighting study, the pion mass becomes smaller by increasing the twisting angle. This means that there is an even worse conditioning number for the Dirac-Wilson operator, hence no speed-up was achieved. Furthermore larger forces were found, compared to the mass-preconditioning study, and the algorithm ran earlier into instabilities.



In the last part of the thesis we presented a new way to isolate electromagnetic effects for the hadronic contribution to  $(g - 2)_\mu$ . We added quenched QED configurations to preexistent QCD ones. We considered two different regularizations of the finite volume zero mode. We were able to see a clear effect, even for physical quark charges and electromagnetic coupling. The crucial question to be answered in the future is whether the effect we have seen is going to be larger for smaller pion masses or not. Within the limitations of the computation (single lattice spacing, pion mass around 400 MeV), we saw an effect of the same size as the discrepancy (in  $a_\mu$ ) between theory and experiments. That is intriguing and it is clearly a motivation for continuing and improving this study. In order to reduce the systematics, the first thing to do is to analyze more volumes, pion masses and different lattice spacings, already available from the CLS initiative. Other improvements can be achieved by considering the addition of a clover term for the electromagnetic part of the action, as well as improving the vector current, in order to have better control on the continuum extrapolation. Another crucial effect to include in the hadronic muon anomaly in the future is the quark mass splitting. This effect can go in the opposite direction of the EM effects. An example of that is visible in the proton-neutron mass splitting. The reweighting technique can be employed to include those effects and the experience acquired in the reweighting of twisted boundary conditions can be useful.

During the work on the muon anomaly we started to explore the possibility of using different gauge conditions in order to eliminate the zero mode problem. So far in the literature no one has considered the use of temporal gauge. On a lattice with periodic boundary conditions it is not possible to fix the temporal gauge in all the sites. We need to fix two different gauges, for example temporal in all the sites excluding one and Coulomb gauge on the remaining. Furthermore we would like to have a massive approach since it gives exponentially suppressed finite volume effects. That possibility is even less clear since no siml-Stueckelberg mechanism is developed in this case. The temporal gauge may be particularly useful there as it would presumably remove time-dependent corrections to the effective masses, which are due to the zero mode in  $A_0$ . This is definitely a new possibility worth to explore.



# Appendix A

## Ward-Takahashi Identities

A multilocal operator is given by

$$\mathcal{O}(x_1, x_2, \dots, x_n) \equiv \mathcal{O}_1(x_1)\mathcal{O}_2(x_2)\dots\mathcal{O}_n(x_n) = \prod_{k=1}^n \mathcal{O}_k(x_k), \quad (\text{A.1})$$

and its expectation value is formally given by the functional integral

$$\langle \mathcal{O}(x_1, x_2, \dots, x_n) \rangle = \frac{1}{\mathcal{Z}} \int \mathcal{D}[A_\mu, \psi, \bar{\psi}] e^{-S_{\text{YM}}(A_\mu) - S_{\text{F}}(A, \psi, \bar{\psi})} \mathcal{O}(x_1, x_2, \dots, x_n), \quad (\text{A.2})$$

where  $S_{\text{YM}}$  is the pure gauge Yang-Mills action and  $S_{\text{F}}$  stands for the fermionic action coupled to gauge fields, see eq. 1.2.7 for the corresponding Lagrangians in QCD-like theories.

As we know the functional integral is ill-defined and we need a regularization.

### A.1 WTIs proof

The Ward-Takahashi identity (WTI) are found by requiring the invariance of the expectation value under symmetry transformations of fermionic variables. For the sake of simplicity we will omit in the following the pure gauge action in the functional integral and in the partition function.

In order to derive the WTI we consider a generic case where  $\mathbf{G}$  is the *global* symmetry group under investigation. The spinors transform linearly with respect the representation  $\mathcal{G}(g)$  of the group, with  $g \in \mathbf{G}$ , i.e.

$$\psi'_\alpha = \mathcal{G}_{\alpha\beta}(g)\psi_\beta. \quad (\text{A.3})$$

We consider the infinitesimal transformation as

$$\delta\psi_\alpha = i\omega^a t_{\alpha\beta}^a \psi_\beta, \quad (\text{A.4})$$

with  $t^a$  hermitian and antisymmetric generators of the algebra corresponding to the symmetry group.

By hypothesis the action is invariant under the symmetry transformation and we suppose that

also the functional measure is<sup>1</sup>

$$\begin{aligned} \mathcal{S}(\bar{\psi}', \psi') &= \mathcal{S}(\bar{\psi}, \psi), \\ \mathcal{D}[\bar{\psi}', \psi'] &= \mathcal{D}[\bar{\psi}, \psi]. \end{aligned} \quad (\text{A.5})$$

The  $k$ -th operator  $\mathcal{O}_k(x_k)$ , in the multilocal, transforms as follows

$$\delta(\mathcal{O}_k(x_k))_\alpha = i\omega^a(\mathcal{R}_k^a)_{\alpha\beta}(\mathcal{O}_k(x_k))_\beta \quad (\text{A.6})$$

where  $\mathcal{R}_k^a$  is the representation under which the operator transforms, that can be different from the one of the fundamental fields.

From these definitions it follows that the multilocal operator transforms as

$$\delta(\mathcal{O}(x_1, x_2, \dots, x_n))_\alpha = \sum_{k=1}^n \mathcal{O}_1(x_1) \dots \delta(\mathcal{O}_k(x_k))_\alpha \dots \mathcal{O}_n(x_n). \quad (\text{A.7})$$

We make the transformation local, i.e.  $\omega^a \equiv \omega^a(x)$  smooth functions, and in the following we omit the matrix indexes  $\alpha, \beta$ . The action will now change as follows

$$\mathcal{S}_F(\psi', \bar{\psi}') = \mathcal{S}_F(\psi, \bar{\psi}) - i \int d^4x (\partial_\mu \omega^a(x)) J_\mu^a(x) \stackrel{\text{by P.}}{=} \mathcal{S}_F(\psi, \bar{\psi}) + i \int d^4x (\partial_\mu J_\mu^a(x)) \omega^a(x), \quad (\text{A.8})$$

where we assumed that  $\omega$  is a smooth function that vanishes outside some bounded region  $R$ , and  $J_\mu^a$  the current associated to the transformation. The operator will change as

$$\mathcal{O}'(x_1, x_2, \dots, x_n) = \mathcal{O}(x_1, x_2, \dots, x_n) + i \sum_{k=1}^n \omega^a(x_k) \mathcal{O}_1(x_1) \mathcal{O}_2(x_2) \dots \mathcal{R}_k^a \mathcal{O}_k(x_k) \dots \mathcal{O}_n(x_n). \quad (\text{A.9})$$

The expectation value cannot change under the symmetry transformation, hence

$$\langle \mathcal{O}'(x_1, \dots, x_n) \rangle = \langle \mathcal{O}(x_1, \dots, x_n) \rangle. \quad (\text{A.10})$$

The transformed expectation value has the form

$$\begin{aligned} \langle \mathcal{O}'(x_1, x_2, \dots, x_n) \rangle &= \frac{1}{\mathcal{Z}'} \int \mathcal{D}[\bar{\psi}', \psi'] e^{-\mathcal{S}_F(\psi', \bar{\psi}')} \mathcal{O}'(x_1, x_2, \dots, x_n) \\ &\simeq \frac{1}{\mathcal{Z}} \int \mathcal{D}[\bar{\psi}, \psi] \exp \left[ -\mathcal{S}_F(\psi, \bar{\psi}) - i \int d^4x (\partial_\mu J_\mu^a(x)) \omega^a(x) \right] \\ &\quad \times \left[ \mathcal{O}(x_1, x_2, \dots, x_n) + i \sum_{k=1}^n \omega^a(x_k) \mathcal{O}_1(x_1) \mathcal{O}_2(x_2) \dots \mathcal{R}_k^a \mathcal{O}_k(x_k) \dots \mathcal{O}_n(x_n) \right], \end{aligned} \quad (\text{A.11})$$

and we functionally expand it with respect to the parameter  $\delta\omega^b(y)$

$$\begin{aligned} \langle \mathcal{O}' \rangle &\simeq \frac{1}{\mathcal{Z}} \int \mathcal{D}[\bar{\psi}, \psi] e^{-\mathcal{S}_F(\psi, \bar{\psi})} \left( 1 - i \int d^4x (\partial_\mu J_\mu^a(x)) \frac{\delta\omega^a(x)}{\delta\omega^b(y)} \delta\omega^b(y) \right) \\ &\quad \times \left[ \mathcal{O} + i \sum_{k=1}^n \frac{\delta\omega^a(x_k)}{\delta\omega^b(y)} \mathcal{O}_1(x_1) \mathcal{O}_2(x_2) \dots \mathcal{R}_k^a \mathcal{O}_k(x_k) \dots \mathcal{O}_n(x_n) \delta\omega^b(y) \right] \\ &\simeq \langle \mathcal{O} \rangle - i\delta\omega^b(y) \left\{ \langle \partial_\mu^y J_\mu^b(y) \mathcal{O} \rangle - \sum_k \delta^4(y - x_k) \langle \mathcal{O}_1 \mathcal{O}_2 \dots \mathcal{R}_k^b \mathcal{O}_k \dots \mathcal{O}_n \rangle \right\}. \end{aligned} \quad (\text{A.12})$$

<sup>1</sup>We exclude anomalous symmetries.

By taking into account that the expectation values on l.h.s. and r.h.s. are identical and that the parameter  $\delta\omega^b(y)$  can be arbitrary varied we obtain that the quantity in curly brackets must vanish. After renaming variables and indexes we get

$$\langle \partial_\mu^x J_\mu^a(x) \mathcal{O}(x_1, x_2, \dots, x_n) \rangle = \sum_{k=1}^n \delta^4(x - x_k) \langle \mathcal{O}_1(x_1) \mathcal{O}_2(x_2) \dots \mathcal{R}_k^a \mathcal{O}_k(x_k) \dots \mathcal{O}_n(x_n) \rangle, \quad (\text{A.13})$$

which we can write in a more compact form in the simple case of one local operator

$$\langle \delta S_x \mathcal{O}_y \rangle = \delta_{xy} \langle \delta \mathcal{O}_y \rangle. \quad (\text{A.14})$$

The WTI in its final form is

$$\partial_\mu^x \langle J_\mu^a(x) \mathcal{O}(x_1, x_2, \dots, x_n) \rangle = \sum_{k=1}^n \delta^4(x - x_k) \langle \mathcal{O}_1(x_1) \mathcal{O}_2(x_2) \dots \mathcal{R}_k^a \mathcal{O}_k(x_k) \dots \mathcal{O}_n(x_n) \rangle. \quad (\text{A.15})$$

## A.2 Singlet One-point-split current

Here we derivate the WTI in the case of a vector transformation  $\mathbf{U}_V(1)$ , in the formal theory and on the lattice with un-improved Wilson fermions in the Euclidean space.

### A.2.1 Formal derivation

By considering  $\mathcal{O}_y = \mathbf{1}$ , and recalling that  $\delta S_x / \delta \alpha = \partial_\mu J_\mu(x)$ ,  $\alpha$  being the parameter of the symmetry transformation, we have

$$\partial_\mu \langle J_\mu(x) \rangle = 0. \quad (\text{A.16})$$

The vector transformation  $\mathbf{U}(1)_V$  is given by

$$\begin{aligned} \delta_V \psi_f(x) &= i\alpha(x) Q_f \psi_f(x), \\ \delta_V \bar{\psi}_f(x) &= -i\alpha(x) \bar{\psi}_f(x) Q_f, \end{aligned} \quad (\text{A.17})$$

and the fermionic action is

$$S = \int d^4x \bar{\psi}_f(x) (\not{D} + m_f) \psi_f(x). \quad (\text{A.18})$$

The variation of the action reads

$$\begin{aligned} \delta_V S &= i \int d^4x \bar{\psi}_f(x) Q_f [\alpha(x) (\not{D} + m_f) - (\not{D} + m_f) \alpha(x)] \psi_f(x) \\ &= -i \int d^4x \bar{\psi}_f(x) Q_f \gamma_\mu \psi_f(x) (\partial_\mu \alpha(x)) \\ &\stackrel{\text{by p.}}{=} i \int d^4x \alpha(x) \partial_\mu (\bar{\psi}_f(x) Q_f \gamma_\mu \psi_f(x)) \equiv 0, \end{aligned} \quad (\text{A.19})$$

that gives  $\partial_\mu \langle V_\mu^f(x) \rangle = 0$  with the following definition

$$V_\mu^f(x) = \bar{\psi}_f(x) Q_f \gamma_\mu \psi_f(x), \quad (\text{A.20})$$

which is the electromagnetic current used in Eq. 5.3.19 with the identification  $V_\mu^f(x) = Q_f J_\mu^f(x)$ .

### A.2.2 Lattice derivation

The Dirac-Wilson action on the lattice is, with  $r = 1$ , is given in Eq. E.1 and its variation under infinitesimal vector transformations on the lattice is found to be

$$\begin{aligned}
\delta_V S_F &= \sum_{x,\mu} \frac{i}{2} Q_f \left\{ \bar{\psi}_f(x) [-\alpha(x)] (\gamma_\mu - 1) U_\mu(x) \psi_f(x + a\hat{\mu}) + \bar{\psi}_f(x) (\gamma_\mu - 1) U_\mu(x) \alpha(x + a\hat{\mu}) \psi_f(x + a\hat{\mu}) \right. \\
&\quad \left. - \bar{\psi}_f(x) [-\alpha(x)] (\gamma_\mu + 1) U_\mu^\dagger(x - a\hat{\mu}) \psi_f(x - a\hat{\mu}) - \bar{\psi}_f(x) (\gamma_\mu + 1) U_\mu^\dagger(x - a\hat{\mu}) \alpha(x - a\hat{\mu}) \psi_f(x - a\hat{\mu}) \right\} \\
&= \sum_\mu \frac{i}{2} Q_f \left\{ - \sum_x \alpha(x) \bar{\psi}_f(x) (\gamma_\mu - 1) U_\mu(x) \psi_f(x + a\hat{\mu}) \right. \\
&\quad + \sum_{x'=x+a\hat{\mu}} \alpha(x') \bar{\psi}_f(x' - a\hat{\mu}) (\gamma_\mu - 1) U_\mu(x' - a\hat{\mu}) \psi_f(x') \\
&\quad + \sum_x \alpha(x) \bar{\psi}_f(x) (\gamma_\mu + 1) U_\mu^\dagger(x - a\hat{\mu}) \psi_f(x - a\hat{\mu}) \\
&\quad \left. - \sum_{x'=x-a\hat{\mu}} \alpha(x') \bar{\psi}_f(x' + a\hat{\mu}) (\gamma_\mu + 1) U_\mu^\dagger(x') \psi_f(x') \right\} \\
&= \sum_{x,\mu} \frac{i}{2} Q_f \alpha(x) \left\{ - \bar{\psi}_f(x) (\gamma_\mu - 1) U_\mu(x) \psi_f(x + a\hat{\mu}) + \bar{\psi}_f(x - a\hat{\mu}) (\gamma_\mu - 1) U_\mu(x - a\hat{\mu}) \psi_f(x) \right. \\
&\quad \left. - \bar{\psi}_f(x) (\gamma_\mu + 1) U_\mu^\dagger(x - a\hat{\mu}) \psi_f(x - a\hat{\mu}) + \bar{\psi}_f(x + a\hat{\mu}) (\gamma_\mu + 1) U_\mu^\dagger(x) \psi_f(x) \right\}, \tag{A.21}
\end{aligned}$$

which can be rewritten as a total divergence

$$\begin{aligned}
\delta_V S_F &= - \sum_{x,\mu} \frac{i}{2} Q_f \alpha(x) \partial_\mu^- \left[ \bar{\psi}_f(x) (\gamma_\mu - 1) U_\mu(x) \psi_f(x + a\hat{\mu}) + \bar{\psi}_f(x + a\hat{\mu}) (\gamma_\mu + 1) U_\mu^\dagger(x) \psi_f(x) \right] \\
&= -i \sum_{x,\mu} Q_f \alpha(x) \partial_\mu^- V_\mu^f(x), \tag{A.22}
\end{aligned}$$

where  $V_\mu^f$  matches the definition of the singlet one-point-split current in Eq. 5.3.27 with  $r = 1$

### A.3 Bare PCAC relation on the lattice

We give here a derivation of the bare PCAC relation on the lattice. To this end we recall the interaction part of the Lagrangian in the case of  $\Psi$  flavor multiplet

$$\mathcal{L}_F^I = \frac{1}{2a} \sum_\mu \left[ \bar{\Psi}(x) U_\mu(x) (\gamma_\mu - r) \Psi(x + a\hat{\mu}) - \bar{\Psi}(x + a\hat{\mu}) U_\mu^\dagger(x) (\gamma_\mu + r) \Psi(x) \right]. \tag{A.23}$$

The variation of the Lagrangian under Eq. 1.2.13 axial transformations is found to be

$$\begin{aligned} \delta\mathcal{L}_F^I = \frac{1}{2a} \sum_{\mu} \left[ \bar{\Psi}(x) \left( i\omega_f(x) \frac{\sigma_f}{2} \gamma_5 \right) U_{\mu}(x) (\gamma_{\mu} - r) \Psi(x + a\hat{\mu}) \right. \\ + \bar{\Psi}(x) U_{\mu}(x) (\gamma_{\mu} - r) \left( i\omega_f(x + a\hat{\mu}) \frac{\sigma_f}{2} \gamma_5 \right) \Psi(x + a\hat{\mu}) \\ - \bar{\Psi}(x + a\hat{\mu}) \left( i\omega_f(x + a\hat{\mu}) \frac{\sigma_f}{2} \gamma_5 \right) U_{\mu}^{\dagger}(x) (\gamma_{\mu} + r) \Psi(x) \\ \left. - \bar{\Psi}(x + a\hat{\mu}) U_{\mu}^{\dagger}(x) (\gamma_{\mu} + r) \left( i\omega_f(x) \frac{\sigma_f}{2} \gamma_5 \right) \Psi(x) \right]. \end{aligned} \quad (\text{A.24})$$

By renaming the variables of the second and third term we obtain

$$\begin{aligned} \delta\mathcal{L}_L^I = \frac{1}{2a} \sum_{\mu} \left[ \bar{\Psi}(x) \left( i\omega_f(x) \frac{\sigma_f}{2} \gamma_5 \right) U_{\mu}(x) (\gamma_{\mu} - r) \Psi(x + a\hat{\mu}) \right. \\ + \bar{\Psi}(x - a\hat{\mu}) U_{\mu}(x - a\hat{\mu}) (\gamma_{\mu} - r) \left( i\omega_f(x) \frac{\sigma_f}{2} \gamma_5 \right) \Psi(x) \\ - \bar{\Psi}(x) \left( i\omega_f(x) \frac{\sigma_f}{2} \gamma_5 \right) U_{\mu}^{\dagger}(x - a\hat{\mu}) (\gamma_{\mu} + r) \Psi(x - a\hat{\mu}) \\ \left. - \bar{\Psi}(x + a\hat{\mu}) U_{\mu}^{\dagger}(x) (\gamma_{\mu} + r) \left( i\omega_f(x) \frac{\sigma_f}{2} \gamma_5 \right) \Psi(x) \right]. \end{aligned} \quad (\text{A.25})$$

Now we use the anticommutator relation  $\{\gamma_{\mu}, \gamma_5\} = 0$  and we find

$$\begin{aligned} \delta\mathcal{L}_F^I = \frac{i\omega_f(x)}{2a} \sum_{\mu} \left[ \bar{\Psi}(x) U_{\mu}(x) (-\gamma_{\mu} - r) \gamma_5 \frac{\sigma_f}{2} \Psi(x + a\hat{\mu}) + \bar{\Psi}(x - a\hat{\mu}) U_{\mu}(x - a\hat{\mu}) (\gamma_{\mu} - r) \gamma_5 \frac{\sigma_f}{2} \Psi(x) \right. \\ \left. - \bar{\Psi}(x + a\hat{\mu}) U_{\mu}^{\dagger}(x) (\gamma_{\mu} + r) \gamma_5 \frac{\sigma_f}{2} \Psi(x) - \bar{\Psi}(x) U_{\mu}^{\dagger}(x - a\hat{\mu}) (-\gamma_{\mu} + r) \gamma_5 \frac{\sigma_f}{2} \Psi(x - a\hat{\mu}) \right] \\ \equiv i\omega_f(x) \left[ \partial_{\mu}^{-} A_{\mu}^f - \chi_A^f \right], \end{aligned} \quad (\text{A.26})$$

where we have defined the variation of the Wilson term as  $\chi_A^f$ , which cannot be cast in form of a total divergence, and the axial current in the following way

$$A_{\mu}^f = -\frac{1}{2} \left[ \bar{\Psi}(x + a\hat{\mu}) U_{\mu}^{\dagger}(x) \gamma_{\mu} \gamma_5 \frac{\sigma_f}{2} \Psi(x) + \bar{\Psi}(x) U_{\mu}(x) \gamma_{\mu} \gamma_5 \frac{\sigma_f}{2} \Psi(x + a\hat{\mu}) \right]. \quad (\text{A.27})$$

The variation is found to be

$$\frac{1}{i} \frac{\delta\mathcal{L}_F}{\delta\omega_f(x)} \Big|_{\omega_f(x)=0} = \partial_{\mu}^{-} A_{\mu}^f(x) - \chi_A^f - \bar{\Psi}(x) \gamma_5 \left\{ \frac{\sigma_f}{2}, M_0 \right\} \Psi(x). \quad (\text{A.28})$$

We arrived at the PCAC relation on the lattice between bare quantities,  $M_0 = m_0 \mathbf{1}$ ,

$$\partial_{\mu}^{-} \langle A_{\mu}^f(x) \mathcal{O}(y) \rangle = 2m_0 \langle P^f(x) \mathcal{O}(y) \rangle + \langle \chi_A^f(x) \mathcal{O}(y) \rangle. \quad (\text{A.29})$$

## Appendix B

# Reweighting factors and reweighted observables

### B.1 Tree-level reweighting factors

In the following we give the Dirac-Wilson spectrum in the case of PBCs and TBCs and the analytic evaluation of the tree-level reweighting factors. The lattice spacing is fixed to one.

#### B.1.1 Dirac-Wilson operator and eigenvalues

We replace the standard links using Eq. 3.1.7. In the free case ( $U = \mathbf{1}$ ), the forward and backward derivatives become

$$\begin{aligned}\nabla_{\mu}^{+}(\theta)\psi(x) &= [\mathcal{U}_{\mu}(x)\psi(x + \hat{\mu}) - \psi(x)] = \left[ e^{i\theta_{\mu}/L_{\mu}}\psi(x + \hat{\mu}) - \psi(x) \right], \\ \nabla_{\mu}^{-}(\theta)\psi(x) &= [\psi(x) - \mathcal{U}_{\mu}^{\dagger}(x - \hat{\mu})\psi(x - \hat{\mu})] = \left[ \psi(x) - e^{-i\theta_{\mu}/L_{\mu}}\psi(x - \hat{\mu}) \right].\end{aligned}\quad (\text{B.1.1})$$

The Dirac-Wilson action in momentum space reads

$$\begin{aligned}S_W(\theta) = \sum_{k \in \bar{\Lambda}} \tilde{\psi}(k) \left\{ \left[ (m+4) - \sum_{\mu=0}^3 \cos(k_{\mu} + \theta_{\mu}/L_{\mu}) \right] \mathbf{1}_{4 \times 4} \right. \\ \left. + i \left[ \sum_{\mu=0}^3 \gamma_{\mu} \sin(k_{\mu} + \theta_{\mu}/L) \right] \right\} \tilde{\psi}(k).\end{aligned}\quad (\text{B.1.2})$$

We recall that the  $k$ 's are now in the first Brillouin zone.

The Dirac-Wilson eigenvalues, at fixed momentum for each color degrees of freedom, are

$$\begin{aligned}\lambda_{1,2} &= (m+4) - \sum_{\mu=0}^3 \cos(k_{\mu} + \theta_{\mu}/L_{\mu}) + i \left( \sum_{\mu=0}^3 \sin^2(k_{\mu} + \theta_{\mu}/L_{\mu}) \right)^{1/2}, \\ \lambda_{3,4} &= (m+4) - \sum_{\mu=0}^3 \cos(k_{\mu} + \theta_{\mu}/L_{\mu}) - i \left( \sum_{\mu=0}^3 \sin^2(k_{\mu} + \theta_{\mu}/L_{\mu}) \right)^{1/2}.\end{aligned}\quad (\text{B.1.3})$$

In Fig. B.1 we show the effect of  $\theta_{\mu} = (0, \underline{\theta})$  on the Dirac-Wilson spectrum.



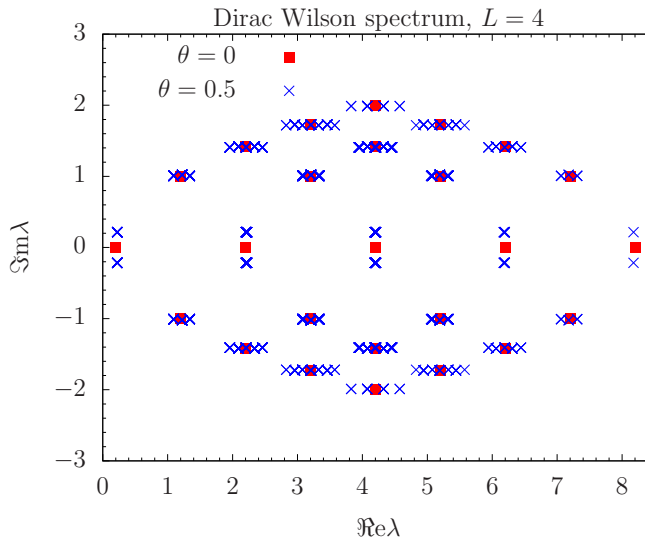


Figure B.1: *Dirac-Wilson spectrum for different values of  $\theta$  in  $V = 4^4$  volume and mass  $m_0 = 0.2$ .*

### B.1.2 Reweighting factors: tree-level analytic evaluation

From the knowledge of the eigenvalues Eq. B.1.3 we write down the tree-level reweighting factor Eq. 3.2.10

$$W_\theta = \prod_{k \in \tilde{\Lambda}} \left\{ \frac{\left[ (m+4) - \sum_\mu \cos(k_\mu + \theta_\mu/L_\mu) \right]^2 + \sum_\mu \sin^2(k_\mu + \theta_\mu/L_\mu)}{\left[ (m+4) - \sum_\mu \cos(k_\mu) \right]^2 + \sum_\mu \sin^2(k_\mu)} \right\}^{2N_c}, \quad (\text{B.1.4})$$

recalling that  $\theta_0 = 0$ .

**Small  $\theta$  expansion** We perform a perturbative expansion around  $\theta_\mu = 0$ . The exponential of the action becomes

$$\exp(-S_\theta) \simeq \exp(-S + \theta_\mu J_\mu) \simeq \exp(-S_\theta) (1 + \theta_\mu J_\mu), \quad (\text{B.1.5})$$

with a suitable current  $J_\mu$ . The vacuum expectation value of an operator  $\mathcal{O}$  becomes  $\langle \mathcal{O} \rangle_\theta \simeq \langle \mathcal{O} \rangle + \theta_\mu \langle \mathcal{O} J_\mu \rangle$ . We know that  $\langle \mathcal{O} J_\mu \rangle \equiv 0$  vanishes because of Lorentz invariance, so we conclude that any expectation value must start with a correction<sup>1</sup> of order  $\theta^2$

$$\langle \mathcal{O} \rangle_\theta \simeq \langle \mathcal{O} \rangle + \mathcal{O}(\theta^2). \quad (\text{B.1.6})$$

**Large  $m$  expansion** We analyze the behavior of the tree-level reweighting factor in Eq. B.1.4 for  $m \rightarrow \infty$ .

<sup>1</sup>Similar argument is made for the expansion of the observable in  $\theta$ , if it depends on the twisting angle.

We start by looking at the numerator

$$\begin{aligned} & \left[ (m+4) - \sum_{\mu=0}^3 \cos(k_\mu + \theta_\mu/L_\mu) \right]^2 + \sum_{\mu=0}^3 \sin^2(k_\mu + \theta_\mu/L_\mu) \\ & \simeq (m+4)^2 - 2m \sum_{\mu=1}^4 \cos(k_\mu + \theta_\mu/L_\mu) \simeq m^2 + 2m \left( 4 - \sum_{\mu=0}^3 \cos(k_\mu + \theta_\mu/L_\mu) \right). \end{aligned} \quad (\text{B.1.7})$$

We build the ratio and we obtain

$$\begin{aligned} & \frac{m^2 + 2m \left( 4 - \sum_{\mu=0}^3 \cos(k_\mu + \theta_\mu/L_\mu) \right)}{m^2 + 2m \left( 4 - \sum_{\mu=0}^3 \cos k_\mu \right)} \simeq \frac{m^2 + 2m \left( 4 - \sum_{\mu=0}^3 \cos(k_\mu + \theta_\mu/L_\mu) \right)}{m^2 \left[ 1 + \frac{2}{m} \left( 4 - \sum_{\mu=0}^3 \cos k_\mu \right) \right]} \\ & \simeq \left[ 1 + \frac{2}{m} \left( 4 - \sum_{\mu=0}^3 \cos(k_\mu + \theta_\mu/L_\mu) \right) \right] \left[ 1 - \frac{2}{m} \left( 4 - \sum_{\mu=0}^3 \cos k_\mu \right) \right] \\ & \simeq 1 + \frac{2}{m} \sum_{\mu=0}^3 [\cos k_\mu - \cos(k_\mu + \theta_\mu/L_\mu)]. \end{aligned} \quad (\text{B.1.8})$$

The reweighting factor become

$$\begin{aligned} W_\theta & \simeq \prod_{k \in \tilde{\Lambda}} \left\{ 1 + \frac{2}{m} \sum_{\mu=0}^3 [\cos k_\mu - \cos(k_\mu + \theta_\mu/L_\mu)] \right\}^{2N_c} \\ & \simeq \prod_{k \in \tilde{\Lambda}} \left\{ 1 + \frac{4N_c}{m} \sum_{\mu=0}^3 [\cos k_\mu - \cos(k_\mu + \theta_\mu/L_\mu)] \right\} \\ & \simeq 1 + \frac{4N_c}{m} \sum_{k \in \tilde{\Lambda}} \left\{ \sum_{\mu=0}^3 [\cos k_\mu - \cos(k_\mu + \theta_\mu/L_\mu)] \right\} \\ & \simeq 1 + \frac{4N_c}{m} \sum_{k \in \tilde{\Lambda}} \left\{ \sum_{j=1}^3 [\cos k_j - \cos(k_j + \theta/L_j)] \right\}. \end{aligned} \quad (\text{B.1.9})$$

Here the integral over the interval  $(-\pi, \pi)$  of the function in the curly brackets is vanishing, which implies that the correction in  $1/m$  starts to the second order,

$$W_\theta = 1 + \mathcal{O}(m^{-2}). \quad (\text{B.1.10})$$

## B.2 Observables with TBCs

Here we give the relevant formulae for the observables, i.e. the plaquette and the pion dispersion relation, studied in the reweighting project in Chap. 3.

### B.2.1 Plaquette

The most simple observable that we can think to reweight is the *plaquette* because it has no dependence on the field  $B = \theta/L$ .

The plaquette on the lattice is defined as the shortest loop path and is the product of links

$$P[U] = \text{Tr} \left\{ \prod_{(x,\mu) \in \text{loop}} U_\mu \right\}. \quad (\text{B.2.11})$$

In the case of constant  $\mathbf{U}(1)$  interaction (Eq. 3.1.7) the plaquette becomes

$$P[\mathcal{U}] = \text{Tr} \left\{ \prod_{(x,\mu) \in \text{loop}} \mathcal{U}_\mu \right\} = \text{Tr} \left\{ \prod_{(x,\mu) \in \text{loop}} e^{iB_\mu} U_\mu \right\} = \text{Tr} \left\{ \prod_{(x,\mu) \in \text{loop}} U_\mu \right\} = P[U], \quad (\text{B.2.12})$$

because we always find two different modified links pointing in opposition direction and therefore the constant  $B$ -term disappear.

The reweighted plaquette expectation value is then

$$\langle P[\mathcal{U}] \rangle_\theta = \langle P[U] \rangle_\theta = \frac{\langle P[U] W_\theta \rangle_0}{\langle W_\theta \rangle_0}. \quad (\text{B.2.13})$$

## B.2.2 Valence twisting and pion dispersion relation

We are interested in expectation values of meson interpolators when two flavors  $f_1, f_2$  are involved. The most general form for such interpolators is

$$\mathcal{O}_M(x) = \bar{\psi}^{(f_1)}(x) \Gamma \psi^{(f_2)}(x), \quad \bar{\mathcal{O}}_M(y) = \bar{\psi}^{(f_2)}(y) \Gamma \psi^{(f_1)}(y),$$

where  $\Gamma$  is an element of the Clifford algebra, i.e. combination of the  $\gamma$  matrices. The operator  $\bar{\mathcal{O}}$  creates a meson, with the right quantum numbers, from the vacuum and  $\mathcal{O}$  annihilates that state. We need to compute the Grassmann integrals in order to calculate the fermionic expectation value  $\langle \dots \rangle_F$ . We choose the two flavors to be  $f_1 = u, f_2 = d$ , in order to have an *iso-triplet* operator<sup>2</sup>. The fermionic expectation values can be computed by employing Wick contractions as follows

$$\begin{aligned} \langle \mathcal{O}(x) \bar{\mathcal{O}}(y) \rangle_F &= \langle (\bar{d} \Gamma u)(x) (\bar{u} \Gamma d)(y) \rangle_F \\ &= \Gamma_{\alpha_1 \beta_1} \Gamma_{\alpha_2 \beta_2} \langle (\bar{d}_{\alpha_1, c_1} u_{\beta_1, c_1})(x) (\bar{u}_{\alpha_2, c_2} d_{\beta_2, c_2})(y) \rangle_F \\ &= -\Gamma_{\alpha_1 \beta_1} \Gamma_{\alpha_2 \beta_2} \langle u_{\beta_1, c_1}(x) \bar{u}_{\alpha_2, c_2}(y) \rangle_u \langle d_{\beta_2, c_2}(y) \bar{d}_{\alpha_1, c_1}(x) \rangle_d \\ &= -\Gamma_{\alpha_1 \beta_1} \Gamma_{\alpha_2 \beta_2} D_u^{-1}(y, x)_{\beta_1, \alpha_2; c_1, c_2} D_d^{-1}(y, x)_{\beta_2, \alpha_1; c_2, c_1} \\ &= -\text{Tr} [\Gamma D_u^{-1}(x, y) \Gamma D_d^{-1}(y, x)], \end{aligned} \quad (\text{B.2.14})$$

where in the second line we explicitly showed Dirac indexes with Greek letters and color indexes with Latin ones; in third line we used the factorization property of the fermionic expectation value with respect to flavor<sup>3</sup>  $\langle \dots \rangle_F = \langle \dots \rangle_u \langle \dots \rangle_d$  and we interchanged the fermion spinors according to their Grassmann nature. In Fig. B.2 we draw in a diagrammatic way the result of the above Wick contractions in the case of  $\mathcal{O} = \bar{d} \gamma_5 u$  at zero momentum, which correspond to a charged pion  $\pi^\pm$ . In order to extract the *dispersion relation* from the correlator we project the interpolators to

<sup>2</sup>To avoid the contribution of disconnected diagrams that suffer from the signal-to-noise problem.

<sup>3</sup>The action and the partition function are separable in the flavor space, i.e.  $S_W = \sum_f \bar{\psi}_f D_W \psi_f = S_u + S_d$ ,  $\mathcal{Z}_F = \mathcal{Z}_u \mathcal{Z}_d$ . That implies that the fermionic expectation value can be written as  $\langle \dots \rangle_F = \mathcal{Z}_F^{-1} \int \mathcal{D}[u, \bar{u}] \mathcal{D}[d, \bar{d}] e^{-S_F}(\dots) = \left[ \mathcal{Z}_u^{-1} \int \mathcal{D}[u, \bar{u}] e^{-S_u}(\dots)_u \right] \left[ \mathcal{Z}_d^{-1} \int \mathcal{D}[d, \bar{d}] e^{-S_d}(\dots)_d \right] = \langle \dots \rangle_u \langle \dots \rangle_d$ .

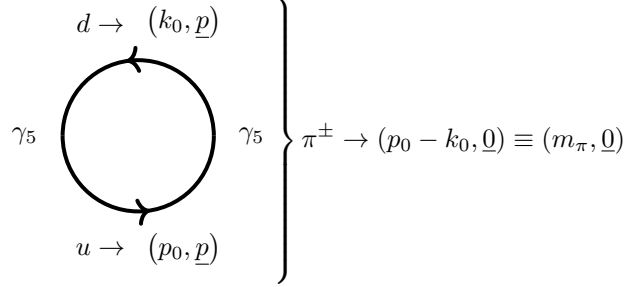


Figure B.2: Diagrammatic expression of the Eq. B.2.14. We show on the diagram the momentum flow.

a definite momentum, say  $p$ . The correlator has the following behaviour for large time separations ( $x_0 \gg 1$ )

$$\begin{aligned} \langle \tilde{\mathcal{O}}(x_0, \underline{p}) \bar{\mathcal{O}}(0) \rangle &= \frac{1}{\sqrt{|V|}} \sum_{x \in V_3} e^{-i\underline{x} \cdot \underline{p}} \langle \mathcal{O}(x) \bar{\mathcal{O}}(0) \rangle \\ &= \sum_k \langle 0 | \mathcal{O} | k \rangle \langle k | \mathcal{O}^\dagger | 0 \rangle e^{-x_0 E_k} \underset{x_0 \gg 1}{=} A e^{-x_0 E(\underline{p})}, \end{aligned} \quad (\text{B.2.15})$$

where  $E(\underline{0}) = m_\pi$ .

The free dispersion relation on the lattice is obtained from the free boson lattice propagator in momentum space (inverse of the Klein-Gordon operator on the lattice), and restoring the lattice spacing  $a$  we get

$$\cosh(aE) = \cosh(am_\pi) + \sum_{k=1}^3 [1 - \cos(ap_k)] \xrightarrow{ap \rightarrow 0} E^2 = m_\pi^2 + |\underline{p}|^2. \quad (\text{B.2.16})$$

In the presence of a constant  $\text{U}(1)$  interaction in the spatial direction we perform the substitution  $\underline{p} \rightarrow \underline{p} + \underline{B}$ . That corresponds to a twisting in the valence only. In Fig. B.3 we show the change on the momentum flow in the diagram in the zero momentum pion case. The dispersion

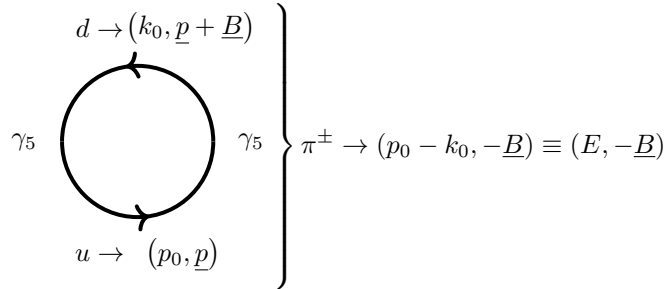


Figure B.3: Diagrammatic expression of the Eq. B.2.14 in the presence of the constant  $\text{U}(1)$  interaction. The state correspond to a charged pion with momentum  $\underline{B}$ .

relation in this case is

$$\cosh(aE) = \cosh(am_\pi) + \sum_{k=1}^3 [1 - \cos(ap_k + aB_k)] \xrightarrow{ap \rightarrow 0} E^2 = m_\pi^2 + |\underline{p} + \underline{B}|^2. \quad (\text{B.2.17})$$

It is clear that the charged pion momentum on the lattice becomes

$$\underline{p}_\pi = \underline{p} + \underline{B} = \frac{2\pi\underline{n} + \underline{\theta}}{aL}. \quad (\text{B.2.18})$$

# Appendix C

## HMC simulations

### C.1 Acceptance in HMC simulations

We follow Ref. (Gupta *et al.*, 1990) to work out the acceptance probability.

The acceptance is found from the Creutz equality, which comes from the area preserving requirement,

$$\langle e^{-\Delta H} \rangle = 1, \quad (\text{C.1.1})$$

where  $\Delta H = H_f - H_i$ , and by expanding it into cumulants we get

$$\langle \Delta H \rangle = \frac{1}{2} \text{Var}(\Delta H) + \text{higher cumulants}. \quad (\text{C.1.2})$$

When the volume is large enough, i.e. compared with the relevant correlation length, the cumulants will grow linearly while their dependence on the step size is different in  $\delta\tau$ . In order to have a finite  $\langle \Delta H \rangle$  then  $\delta\tau$  should be varied to keep the variance fixed,  $\text{Var}(\Delta H) = \text{const}$ .

The distribution for the acceptance will be a convolution of a Gaussian with mean and width related by  $\langle \Delta H \rangle = \text{Var}(\Delta H)/2 \equiv \sigma_0^2/2$  and an Metropolis test

$$\begin{aligned} P_{\text{acc}}(\Delta H) &= \frac{1}{\sqrt{2\pi}\sigma_0} \int_{-\infty}^{\infty} \min(1, e^{-x}) \exp\left[-\frac{(x - \langle \Delta H \rangle)^2}{2\sigma_0^2}\right] dx \\ &= \frac{1}{\sqrt{2\pi}\sigma_0} \left\{ \int_{-\infty}^0 \exp\left[-\frac{(x - \langle \Delta H \rangle)^2}{2\sigma_0^2}\right] dx + \int_0^{\infty} \exp\left[-\frac{(x - \langle \Delta H \rangle)^2}{2\sigma_0^2} - x\right] dx \right\}. \end{aligned} \quad (\text{C.1.3})$$

By changing the coordinates in the first integral to  $z = \frac{x - \langle \Delta H \rangle}{\sqrt{2}\sigma_0}$  we get

$$\begin{aligned} \text{first integral} &= 2\langle \Delta H \rangle^{1/2} \int_{-\infty}^{-\frac{\sqrt{\langle \Delta H \rangle}}{2}} e^{-z^2} dz = 2\langle \Delta H \rangle^{1/2} \int_{\frac{\sqrt{\langle \Delta H \rangle}}{2}}^{\infty} e^{-z^2} dz \\ &= \sqrt{\pi} \langle \Delta H \rangle^{1/2} \text{erfc}\left(\frac{\sqrt{\langle \Delta H \rangle}}{2}\right), \end{aligned} \quad (\text{C.1.4})$$

where we used the symmetry of the Gaussian integral in the first step.

For the second integral we first recognize the square and use the relation between the variance and

the mean

$$\frac{(x - \langle \Delta H \rangle)^2}{2\sigma_0^2} + x = \frac{(x + \langle \Delta H \rangle)^2}{4\langle \Delta H \rangle}, \quad (\text{C.1.5})$$

and then change the variable to  $z = \frac{x + \langle \Delta H \rangle}{2\sqrt{\langle \Delta H \rangle}}$ , obtaining

$$\text{second integral} = 2\langle \Delta H \rangle^{1/2} \int_{\frac{\sqrt{\langle \Delta H \rangle}}{2}}^{\infty} e^{-z^2} dz = \sqrt{\pi} \langle \Delta H \rangle^{1/2} \text{erfc} \left( \frac{\sqrt{\langle \Delta H \rangle}}{2} \right). \quad (\text{C.1.6})$$

By putting all together, with the right pre-factors, we get the formula

$$P_{\text{acc}}(\Delta H) = \text{erfc} \left( \frac{\sqrt{\langle \Delta H \rangle}}{2} \right). \quad (\text{C.1.7})$$

We use C.1.2 to trade  $\langle \Delta H \rangle$  with  $\text{Var}(\Delta H)$  because the latter is a better behaved quantity<sup>1</sup>

$$P_{\text{acc}}(\text{Var}(\Delta H)) = \text{erfc} \left( \sqrt{\frac{\text{Var}(\Delta H)}{8}} \right). \quad (\text{C.1.8})$$

## C.2 Multiple time-scale Omelyan shadow Hamiltonian

Following Ref. (Clark *et al.*, 2008) we give the expression for the shadow Hamiltonian in the case of multi-time scale.

Let the Hamiltonian be

$$H = T + \sum_i S_i, \quad (\text{C.2.9})$$

with  $i$  index running to as many multi-time scales are present.

Let be  $\exp Z = \exp A \exp B$ , then the Baker-Campbell-Hausdorff formula is given by

$$\begin{aligned} Z = & (A + B) + [A, B] + \frac{1}{12} ([A, [A, B]] + [B, [B, A]]) \\ & - \frac{1}{24} [B, [A, [A, B]]] - \frac{1}{720} ([B, [B, [B, [B, A]]]] + [A, [A, [A, [A, B]]]]) + \dots \end{aligned} \quad (\text{C.2.10})$$

From the above formula we can evaluate the following expression

$$\ln(\exp(X) \exp(Y) \exp(X)) = (2X + Y) + \frac{1}{6} ([[X, Y], X] + [[X, Y], Y]) + \dots \quad (\text{C.2.11})$$

We use the work done in Ref. (Reinsch, 2000) in MATHEMATICA to calculate BCH and consequently the shadow Hamiltonian.

---

<sup>1</sup>In the mean  $\langle \Delta H \rangle$  we can have negative and positive contributions and that may lead to large uncertainties.

### One level Leap-frog integrator

The Leap-frog integrator is given by the following evolution operator

$$\left[ \exp\left(\frac{\delta\tau}{2}\hat{S}\right) \exp(\delta\tau\hat{T}) \exp\left(\frac{\delta\tau}{2}\hat{S}\right) \right]^n, \quad (\text{C.2.12})$$

with  $\delta\tau = 1/n$ , and by employing the BCH formula in Eq. C.2.11 we get

$$\left( \exp\left[\hat{H}\delta\tau + \left(\frac{1}{12}[[\hat{S}, \hat{T}], \hat{T}] + \frac{1}{24}[[\hat{S}, \hat{T}], \hat{S}]\right)\delta\tau^3\right] \right)^n. \quad (\text{C.2.13})$$

By applying the BCH formula again we get

$$\tilde{H} = H + \left(\frac{1}{12}[[\hat{S}, \hat{T}], \hat{T}] + \frac{1}{24}[[\hat{S}, \hat{T}], \hat{S}]\right)\delta\tau^2. \quad (\text{C.2.14})$$

### One-level Omelyan integrator

The one-level Omelyan integrator is given by

$$\left[ \exp(\alpha\delta\tau\hat{S}_1) \exp\left(\frac{\delta\tau}{2}\hat{T}\right) \exp(\delta\tau(1-2\alpha)\hat{S}_1) \exp\left(\frac{\delta\tau}{2}\hat{T}\right) \exp(\alpha\delta\tau\hat{S}_1) \right]^n. \quad (\text{C.2.15})$$

The shadow Hamiltonian is found to be

$$\tilde{H} = H + \left[\frac{6\alpha^2 - 6\alpha + 1}{12}[[\hat{T}, \hat{S}_1], \hat{S}_1] + \frac{6\alpha - 1}{24}[[\hat{S}_1, \hat{T}], \hat{T}]\right]\delta\tau^2. \quad (\text{C.2.16})$$

### Two-level Omelyan integrator

The two-level Omelyan integrator is obtained by operating the following formal substitution to the one-level Omelyan integrator

$$\exp\left(\frac{\delta\tau}{2}\hat{T}\right) \longrightarrow \left[ \exp\left(\alpha\frac{\delta\tau}{2m}\hat{S}_2\right) \exp\left(\frac{\delta\tau}{4m}\hat{T}\right) \exp\left(\frac{\delta\tau}{2m}(1-2\alpha)\hat{S}_2\right) \exp\left(\frac{\delta\tau}{4m}\hat{T}\right) \exp\left(\alpha\frac{\delta\tau}{2m}\hat{S}_2\right) \right]^m. \quad (\text{C.2.17})$$

The shadow Hamiltonian is found to be

$$\begin{aligned} \tilde{H} = & H - \delta\tau^2 \frac{6\alpha^2 - 6\alpha + 1}{12} \left[ [[\hat{S}_1, \hat{T}], \hat{S}_1] + \frac{1}{2m^2} [[\hat{S}_2, \hat{T}], \hat{S}_2] \right] \\ & + \delta\tau^2 \frac{6\alpha - 1}{24} \left[ [[\hat{S}_1, \hat{T}], \hat{T}] + \frac{1}{2m^2} [[\hat{S}_2, \hat{T}], \hat{T}] + \frac{1}{2m^2} [[\hat{S}_2, \hat{T}], \hat{S}_1] \right]. \end{aligned} \quad (\text{C.2.18})$$

### Multi-level Omelyan integrator

By playing the same game we can recognize a structure in the shadows Hamiltonian, which will be given by

$$\begin{aligned} \tilde{H} = & H + \tau^2 \sum_{i=1} \left[ \frac{6\alpha^2 - 6\alpha + 1}{3} \left( \frac{[\hat{S}_i, [\hat{S}_i, \hat{T}]]}{\prod_{j=1}^i (2n_j)^2} \right) \right. \\ & \left. + \frac{6\alpha - 1}{6} \left( \frac{[\hat{T}, [\hat{T}, \hat{S}_i]] - \sum_{j<i} [\hat{S}_j, \{\hat{S}_i, \hat{T}\}]]}{\prod_{j=1}^i (2n_j)^2} \right) \right], \end{aligned} \quad (\text{C.2.19})$$

where  $\tau = \delta\tau \times n_0$  and  $n_0, n_1, \dots, n_i$  are the  $i$  number of integration steps per level.



### C.3 Forces in HMC

The forces in HMC are derived as in Ref. (Del Debbio *et al.*, 2010). In the following we omit the sum over space-time, color and spin. The Hamiltonian in the HMC evolution is given by  $H = T + S_G + S_F$ ,

- Gaussian weight for the momenta  $\pi$ ,

$$T = \frac{\pi^2}{2}, \quad (\text{C.3.20})$$

where  $\pi \in \mathfrak{su}(N_c)$ ,  $\pi_\mu(x) = i\pi_\mu^a(x)T_f^a$ , where  $T_f^a$  are the hermitian generators in the fundamental representation.

- Wilson plaquette gauge action

$$S_G = \beta \sum_{\mu < \nu} \left( 1 - \frac{1}{N_c} \Re \text{Tr} P_{\mu\nu} \right), \quad (\text{C.3.21})$$

where  $\beta = 2N_c/g^2$ , and  $P_{\mu\nu}$  the plaquette in the  $(\mu, \nu)$  plane

$$P_{\mu\nu} = U_\mu(x)U_\nu(x + \hat{\mu})U_\mu^\dagger(x + \nu)U_\nu^\dagger(x). \quad (\text{C.3.22})$$

- Fermionic action

$$S_F = \phi^\dagger (Q^2)^{-1} \phi, \quad (\text{C.3.23})$$

where  $\phi$  is a pseudofermion,  $Q = \gamma_5 D_m$  is the  $\gamma_5$  Dirac-Wilson operator,  $D_W$  that is given by the following equation

$$D_W \psi(x) = 8\psi(x) - \frac{1}{2} \sum_{\mu} [(1 - \gamma_\mu)U_\mu^R(x)\psi(x + \hat{\mu}) + (1 + \gamma_\mu)U_\mu^{R,\dagger}(x - \hat{\mu})\psi(x - \hat{\mu})] \quad (\text{C.3.24})$$

$$D_m \psi(x) = (D_W + m_0)\psi(x). \quad (\text{C.3.25})$$

The  $U_\mu^R$  are the link variables in the representation  $R$ .

A generic element  $x$  in the algebra  $\mathfrak{su}(N_c)$  is written as  $x = ix^a T_f^a$ , and its norm is given by  $\|x\|^2 = \text{Tr}(x^\dagger x) = T_f \sum_{i,j} |x_{ij}|^2$ .  $T_f$  is the normalization of the generators in the fundamental representation, for other representation we write  $T_R$ .

#### Equation of motion

The equation of motion for the links is found by taking the derivative with respect to  $\tau$  (the Markov time) of  $\mathbf{1} = U_\mu(\tau)U_\mu^\dagger(\tau)$

$$\dot{U}_\mu(\tau)U_\mu^\dagger(\tau) + U_\mu(\tau)\dot{U}_\mu^\dagger(\tau) = 0. \quad (\text{C.3.26})$$

The equation is fulfilled by taking

$$\dot{U}_\mu(x) = \pi_\mu(x)U_\mu(x). \quad (\text{C.3.27})$$

The equation of motion for the momenta can be obtained by requiring that the Hamiltonian  $H$  is a conserved quantity

$$\dot{H} = 0 = \dot{T} + \dot{S}_G + \dot{S}_F. \quad (\text{C.3.28})$$

For the first two derivatives we have

$$\dot{T} = T_f \sum_{x,\mu,a} \pi_\mu^a(x) \dot{\pi}_\mu^a(x), \quad (\text{C.3.29})$$

$$\begin{aligned} \dot{S}_G &= -\frac{\beta}{N_c} \sum_{x,\mu} \Re\text{Tr} \left[ \dot{U}_\mu(x) V_\mu^\dagger(x) \right] \\ &= -\frac{\beta}{N_c} \sum_{x,\mu} \Re\text{Tr} \left[ \pi_\mu(x) U_\mu(x) V_\mu^\dagger(x) \right] \\ &= -\frac{\beta}{N_c} \sum_{x,\mu,a} \pi_\mu^a(x) \Re\text{Tr} \left[ iT_f^a U_\mu(x) V_\mu^\dagger(x) \right], \end{aligned} \quad (\text{C.3.30})$$

where  $V_\mu(x)$  is sum of the staples around the link  $U_\mu(x)$ .

For the fermionic force we write

$$\dot{S}_F = -\phi^\dagger (Q^2)^{-1} (\dot{Q}^2) (Q^2)^{-1} \phi, \quad (\text{C.3.31})$$

and we define  $\eta = (Q^2)^{-1} \phi$  and  $\xi = Q\eta$ .

By using the hermiticity of  $Q^2$  we rewrite the derivative as

$$\dot{S}_F = -2\xi^\dagger \dot{Q} \eta. \quad (\text{C.3.32})$$

Inserting the explicit form of  $Q = \gamma_5 D_W$  we get

$$\begin{aligned} \dot{S}_F &= \Re \sum_{x,\mu} \xi^\dagger(x) \dot{U}_\mu^R(x) \gamma_5 (1 - \gamma_\mu) \eta(x + \hat{\mu}) \\ &\quad + \eta^\dagger(x) \dot{U}_\mu^{R,\dagger}(x) \gamma_5 (1 - \gamma_\mu) \xi(x + \hat{\mu}). \end{aligned} \quad (\text{C.3.33})$$

By collecting the results we get the equation of motion for the momenta

$$\dot{\pi}_\mu^a(x) = \dot{\pi}_\mu^{a,G}(x) + \dot{\pi}_\mu^{a,F}(x), \quad (\text{C.3.34})$$

$$\dot{\pi}_\mu^{a,G}(x) = \frac{\beta}{N_c} \frac{1}{T_f} \Re\text{Tr} \left[ iT_f^a U_\mu(x) V_\mu^\dagger(x) \right] \equiv F_G^{a\mu}(x), \quad (\text{C.3.35})$$

$$\dot{\pi}_\mu^{a,F}(x) = -\frac{1}{T_f} \Re\text{Tr} \left\{ iT_R^a U_\mu^R(x) \gamma_5 (1 - \gamma_\mu) \left[ \eta(x + \hat{\mu}) \otimes \xi^\dagger(x) + \xi(x + \hat{\mu}) \otimes \eta^\dagger(x) \right] \right\} \equiv F_F^{a\mu}(x). \quad (\text{C.3.36})$$

Where we denoted as  $F$  the associated driving forces to the different part of the action.

### C.3.1 Mass preconditioning forces

The mass preconditioning is given in Eq. 4.2.23. The  $Q_{\text{HMC}}$  part follows exactly as before but with a shift in the mass given by  $m_0 + \mu$ . We derive here the force associated to the Hasenbusch term. We write the associated action as, with  $\phi_2$  different set of pseudofermions,

$$S_{\text{Hase}} = \phi_2^\dagger Q^{-1} (D_m^\dagger + \mu) (D_m + \mu) Q^{-1} \phi_2. \quad (\text{C.3.37})$$

The operator can be rewritten as follows

$$\begin{aligned} Q^{-1} (D_m^\dagger + \mu) (D_m + \mu) Q^{-1} &= D_m^{-1} \gamma_5 (\gamma_5 D_m \gamma_5 + \mu) (D_m + \mu) D_m^{-1} \gamma_5 \\ &= (\gamma_5 + \mu D_m^{-1} \gamma_5) (\gamma_5 + \mu D_m^{-1} \gamma_5) \\ &= (\gamma_5 + \mu Q^{-1}) (\gamma_5 + \mu Q^{-1}), \end{aligned} \quad (\text{C.3.38})$$

and the action becomes

$$S_{\text{Hase}} = \phi_2^\dagger (\gamma_5 + \mu Q^{-1}) (\gamma_5 + \mu Q^{-1}) \phi_2. \quad (\text{C.3.39})$$

Now we take the derivative with respect to the Markov time

$$\begin{aligned} \dot{S}_{\text{Hase}} &= \phi_2^\dagger \left[ \mu (\dot{Q}^{-1}) (\gamma_5 + \mu Q^{-1}) + \mu (\gamma_5 + \mu Q^{-1}) (\dot{Q}^{-1}) \right] \phi_2 \\ &= -\mu \phi_2^\dagger \left[ Q^{-1} \dot{Q} Q^{-1} (\gamma_5 + \mu Q^{-1}) + (\gamma_5 + \mu Q^{-1}) Q^{-1} \dot{Q} Q^{-1} \right] \phi_2. \end{aligned} \quad (\text{C.3.40})$$

Note that the above equation has the standard form of a fermionic force in the HMC algorithm provided that

$$\begin{aligned} X &\equiv Q^{-1} \phi_2, \\ Y &\equiv Q^{-1} (\gamma_5 + \mu Q^{-1}) \phi_2, \end{aligned} \quad (\text{C.3.41})$$

in particular, see Eq. C.3.32,

$$\dot{S}_{\text{Hase}} = -2\mu X^\dagger \dot{Q} Y. \quad (\text{C.3.42})$$

The forces given by the different pieces of the action are

$$F_G^{a\mu}(x) = \frac{\beta}{N_c} \frac{1}{T_f} \Re \text{Tr} [i T_f^a U_\mu(x) V_\mu^\dagger(x)], \quad (\text{C.3.43})$$

$$F_{\text{HMC}}^{a\mu}(x) = -\frac{1}{T_f} \Re \text{Tr} \{ i T_R^a U_\mu^R(x) \gamma_5 (1 - \gamma_\mu) [\eta(x + \hat{\mu}) \otimes \xi^\dagger(x) + \xi(x + \hat{\mu}) \otimes \eta^\dagger(x)] \}, \quad (\text{C.3.44})$$

$$F_{\text{Hase}}^{a\mu}(x) = -\frac{\mu}{T_f} \Re \text{Tr} \{ i T_R^a U_\mu^R(x) \gamma_5 (1 - \gamma_\mu) [Y(x + \hat{\mu}) \otimes X^\dagger(x) + X(x + \hat{\mu}) \otimes Y^\dagger(x)] \}, \quad (\text{C.3.45})$$

where

$$\xi \equiv Q^{-1} \phi_1, \quad (\text{C.3.46})$$

$$\eta \equiv (Q^2)^{-1} \phi_1, \quad (\text{C.3.47})$$

$$X \equiv Q^{-1} \phi_2, \quad (\text{C.3.48})$$

$$Y \equiv Q^{-1} (\gamma_5 + \mu Q^{-1}) \phi_2, \quad (\text{C.3.49})$$

and we recall that  $Q$  in this case is the mass shifted  $\gamma_5$  Dirac-Wilson operator

$$Q = \gamma_5 (D_m + \mu) = \gamma_5 (D_W + m_0 + \mu). \quad (\text{C.3.50})$$

## C.4 Number of configurations and parameters in the optimization study

Here we collect the number of configurations analyzed in the force study in Chap. 4. Simulations correspond to a  $\mathbf{SU}(2)$  gauge group with a doublet of un-improved Wilson fermions in the fundamental representation and Wilson plaquette gauge action in a  $V = 32^4$  volume. The value  $m_c$  of the bare mass parameter yielding massless fermions is estimated to be  $-0.77(2)$  at  $\beta = 2.2$  (Lewis *et al.*, 2012, Hietanen *et al.*, 2014, Arthur *et al.*, 2016). The integrator choice is the Omelyan with  $\alpha = 1/6$ . The inversions of the  $\gamma_5$ -hermitian Dirac-Wilson operator are performed using a version of the Quasi-Minimal Residual (QMR). The algorithm is not absolutely convergent and in the case of no convergence our implementation switch to the BiCGstab algorithm. For the evolution of the gauge field we use the Minimal Residual Extrapolation (MRE) algorithm to build an initial guess for the inverter based on the past solutions (Brower *et al.*, 1997). In particular 5 past solutions were stored throughout the HMC simulation. The force precision was set to  $10^{-14}$  and the  $\Delta H$  measurement precision for the accept-reject step to  $10^{-14}$ , which is enough to ensure reversibility of the algorithm. The level parameters are  $n$  for the Hasenbusch,  $m$  HMC and  $k$  Gauge as described in Sect. 4.2.

$$m_0 = -0.72$$

$$n = 15, \quad m = 8, \quad k = 10.$$

$\mu$	$N_{\text{cnf}}$
0.05	109
0.1	98
0.15	128
0.2	153
0.25	128
0.3	136
0.35	144
0.4	155
0.45	112
0.5	115

$\mu$	$N_{\text{cnf}}$
0.6	124
0.7	130
0.75	133
0.8	69
0.9	137
1	1193
1.5	80
2	1487
2.5	88
3	92

$$m_0 = -0.735$$

$$n = 5, \quad m = 4, \quad k = 10.$$

$\mu$	$N_{\text{cnf}}$
0.05	133
0.1	189
0.15	202

$\mu$	$N_{\text{cnf}}$
0.2	202
0.25	202
0.3	202
0.35	202

$$m_0 = -0.75$$

$$n = 15, \quad m = 8, \quad k = 10.$$

$\mu$	$N_{\text{cnf}}$
0.05	57
0.1	79
0.15	119
0.2	147
0.25	152

$\mu$	$N_{\text{cnf}}$
0.3	178
0.35	178
0.4	196
0.45	186
0.5	201
0.6	193

## Appendix D

# Quantum electrodynamics on the lattice: supplementary material

### D.1 Fourier transform

We set the notation for the Fourier transform on the lattice. The reciprocal lattice  $\tilde{\Lambda}$ , with periodic boundary conditions for a functions  $f(n + \hat{\mu}L_\mu) = f(n) \forall \mu$ , is given by

$$\tilde{\Lambda} = \left\{ p = (p_0, p_1, p_2, p_3) : p_\mu = \frac{2\pi}{aL_\mu} k_\mu, \text{ with } k_\mu \in \left( -\frac{L_\mu}{2}, \frac{L_\mu}{2} \right] \subset \mathbb{Z} \right\}.$$

The delta functions are defined as

$$\begin{aligned} \delta(x - x') &= \frac{1}{V} \sum_{p \in \tilde{\Lambda}} \exp(ip \cdot (x - x')), \\ \delta(p - p') &= \frac{1}{V} \sum_{n \in \Lambda} \exp(i(p - p') \cdot x). \end{aligned} \tag{D.1.1}$$

The Fourier transform and the inverse are defined as

$$\begin{aligned} \tilde{f}(p) &= \frac{1}{\sqrt{V}} \sum_{n \in \Lambda} \exp(-ip \cdot x) f(x), \\ f(x) &= \frac{1}{\sqrt{V}} \sum_{p \in \tilde{\Lambda}} \exp(ip \cdot x) \tilde{f}(p). \end{aligned} \tag{D.1.2}$$

#### D.1.1 Reality condition

Let us consider the Fourier transform of a real quantity such as the electromagnetic field,  $A_\mu(x + a\hat{\mu}/2)$ . This will add some conditions on the Fourier coefficients  $\tilde{A}_\mu(p)$  (Blum *et al.*, 2007).

The Fourier transform of the gauge field is

$$A_\mu(x + a\hat{\mu}/2) = \frac{1}{\sqrt{V}} \sum_{p \in \tilde{\Lambda}} e^{ip \cdot (x + a\hat{\mu}/2)} \tilde{A}_\mu(p), \tag{D.1.3}$$

and the reality condition means that the imaginary part of the Fourier transform has to vanish, i.e.

$$\frac{1}{\sqrt{V}} \sum_{p \in \tilde{\Lambda}} \left\{ \sin(p \cdot x + ap_\mu/2) \Re \tilde{A}_\mu(p) + \cos(p \cdot x + ap_\mu/2) \Im \tilde{A}_\mu(p) \right\} = 0. \quad (\text{D.1.4})$$

We introduce the reflection operator in the first Brillouin zone

$$R(p)_\mu = \begin{cases} -p_\mu & \text{if } p_\mu \neq \pi \\ \pi & \text{if } p_\mu = \pi \end{cases}. \quad (\text{D.1.5})$$

We can now write the reality condition into three different ones:

1.  $p_\mu = 0$ , the zero mode is real,  $\Im \tilde{A}_\mu(0) = 0$ .
2.  $p_\mu \neq 0, \pi$ , there is a pairwise cancellation between one mode and the reflected-conjugate one, i.e.

$$\tilde{A}_\mu(p) = \tilde{A}_\mu^*(R(p)) \iff \begin{cases} \Re \tilde{A}_\mu(p) & = \Re \tilde{A}_\mu(R(p)) \\ \Im \tilde{A}_\mu(p) & = -\Im \tilde{A}_\mu(R(p)) \end{cases}.$$

3.  $p_\mu = \pi$ ,  $p_\nu = 0, \pi$  for  $\nu \neq \mu$ , there is no partner for these kind of modes, which means no pairwise cancellation and  $\Im \tilde{A}_\mu(p) = 0$ . While the real part is left unfixed since the sine in Eq. D.1.4 is vanishing.

We can incorporate these conditions in one, which reads

$$e^{iR(p)_\mu/2} \tilde{A}_\mu(R(p)) = \left( e^{ip_\mu/2} \tilde{A}_\mu(p) \right)^*. \quad (\text{D.1.6})$$

## D.2 Generation in Feynman gauge

We recall that the action in Feynman gauge in coordinate space is

$$S = -\frac{1}{2} \sum_{n \in \Lambda} \sum_{\mu, \nu} A_\nu(x + a\hat{\nu}/2) \partial_\mu^- \partial_\mu^+ A_\nu(x + a\hat{\nu}/2). \quad (\text{D.2.7})$$

To find the action in the momentum space we Fourier transform by inserting Eq. D.1.3

$$S = -\frac{1}{2V} \sum_{n \in \Lambda} \sum_{\mu, \nu} \sum_{p, p' \in \tilde{\Lambda}} e^{ip \cdot (x + a\hat{\nu}/2)} \partial_\mu^- \partial_\mu^+ e^{ip' \cdot (x + a\hat{\nu}/2)} \tilde{A}(p) \tilde{A}(p'). \quad (\text{D.2.8})$$

The Laplacian of the exponential is found to be

$$\begin{aligned} \partial_\mu^+ e^{ip' \cdot x} &= \frac{e^{ip' \cdot x}}{a} \left( e^{ip'_\mu} - 1 \right), \\ \partial_\mu^- \partial_\mu^+ e^{ip' \cdot x} &= \frac{e^{ip' \cdot x}}{a^2} \left( 1 - e^{-ip'_\mu} \right) \left( e^{ip'_\mu} - 1 \right) = [2i \sin(p'_\mu/2)]^2 \equiv -\hat{p}'_\mu{}^2, \\ \sum_\mu \partial_\mu^- \partial_\mu^+ e^{ip' \cdot x} &= -\sum_\mu \hat{p}'_\mu{}^2 \equiv -\hat{p}'^2, \end{aligned} \quad (\text{D.2.9})$$

and the action becomes

$$S = \frac{1}{2V} \sum_{n \in \Lambda} \sum_{\nu} \sum_{p, p' \in \tilde{\Lambda}} e^{i(p+p') \cdot (x+a\hat{\nu}/2)} \hat{p}' \tilde{A}(p) \tilde{A}(p'). \quad (\text{D.2.10})$$

We recognize the the delta function, Eq. D.1.1, hence we are left with

$$S = \frac{1}{2V} \sum_{\nu} \sum_{p, p' \in \tilde{\Lambda}} V \delta(p+p') e^{iap_{\nu}/2} e^{-iap'_{\nu}/2} \hat{p}'^2 \tilde{A}(p) \tilde{A}(p'). \quad (\text{D.2.11})$$

The delta function in the first Brillouin zone is equivalent to the reflection operation given in Eq. D.1.5

$$S = \frac{1}{2} \sum_{p \in \tilde{\Lambda}} \hat{p}^2 \sum_{\nu} e^{iap_{\nu}/2} \tilde{A}(p) e^{-iaR(p)_{\nu}/2} \tilde{A}(R(p)), \quad (\text{D.2.12})$$

and by using the reality condition, in Eq. D.1.6 we obtain the result

$$S = \sum_{p \in \tilde{\Lambda}} \frac{\hat{p}^2}{2} \sum_{\nu} |\tilde{A}(p)|^2. \quad (\text{D.2.13})$$

## D.3 Extended Coulomb gauge

The Coulomb gauge is defined by the constraint (see Faddeev-Popov approach in Sect. 2.3.1),

$$G(A) = \sum_j \partial_j A_j, \quad (\text{D.3.14})$$

and we shall take  $\alpha = 1$ . On the lattice the condition is translated

$$\sum_j \partial_j^- A_j(x + a\hat{j}/2) = 0, \quad \tilde{A}_0(p_0 \neq 0, \underline{p} = \underline{0}) = 0, \quad (\text{D.3.15})$$

with  $j$  spatial index. The second condition is a consequence of the non-completeness of the Coulomb gauge in finite volume, hence the name “extended”, see Sect. 2.4 for details.

### D.3.1 Extended Coulomb via Feynman gauge

We can generate first the Fourier component of the field in Feynman gauge and then switch to Coulomb by employing a gauge transformation

$$A_{\mu}(x + a\hat{\mu}/2) = A_{\mu}^C(x + a\hat{\mu}/2) + \partial_{\mu}^+ \alpha(x), \quad (\text{D.3.16})$$

where  $A_{\mu}$  is the field generated in Feynman gauge,  $A_{\mu}^C$  is the field we would like to satisfy the Coulomb gauge condition and  $\alpha$  is the gauge transformation that does the job, see Ref. (Borsanyi and others, 2015). By imposing the Coulomb gauge condition one can relate  $\alpha$  and  $A_{\mu}$ ,

$$\sum_j \partial_j^- A_j(x + a\hat{j}/2) = \sum_j \cancel{\partial_j^- A_j^C(x + a\hat{j}/2)} + \sum_j \partial_j^- \partial_j^+ \alpha(x). \quad (\text{D.3.17})$$



We Fourier transform the above relation

$$\begin{aligned} \text{l.h.s. : } \sum_j \partial_j^- A_j(x + a\hat{j}/2) &= \sum_{p \in \tilde{\Lambda}} e^{ip \cdot x} \sum_j \frac{1 - e^{-iap_j}}{a} e^{iap_j/2} \tilde{A}_j(p) \\ &= \sum_{p \in \tilde{\Lambda}} e^{ip \cdot x} \sum_j 2i \sin(ap_j/2) \tilde{A}_j(p), \end{aligned} \quad (\text{D.3.18})$$

$$\text{r.h.s. : } \sum_j \partial_j^- \partial_j^+ \alpha(x) = \sum_{p \in \tilde{\Lambda}} e^{ip \cdot x} \tilde{\alpha}(p) \sum_j \frac{(1 - e^{-iap_j})(e^{iap_j} - 1)}{a^2} = - \sum_{p \in \tilde{\Lambda}} e^{ip \cdot x} |\underline{\hat{p}}|^2 \tilde{\alpha}(p). \quad (\text{D.3.19})$$

In momentum space the condition reads

$$\tilde{\alpha}(p) = - \frac{i}{|\underline{\hat{p}}|^2} \sum_j \hat{p}_j \tilde{A}_j(p). \quad (\text{D.3.20})$$

The gauge transformation in Eq. D.3.16 in momentum space gives a relation between all the Fourier coefficients of the fields generated in different gauges, in particular

$$\tilde{A}_\mu^C(p) = \tilde{A}_\mu(p) - i\hat{p}_\mu \tilde{\alpha}(p), \quad (\text{D.3.21})$$

and by plugging in the result found for  $\alpha$  in Eq. D.3.20 we have

$$\begin{aligned} \tilde{A}_\mu^C(p) &\equiv P_{\mu\nu}^C \tilde{A}_\nu(p) = \tilde{A}_\mu(p) - \frac{\hat{p}_\mu}{|\underline{\hat{p}}|^2} \sum_j \hat{p}_j \tilde{A}_j(p) \\ &= \tilde{A}_\mu(p) - \frac{\hat{p}_\mu}{|\underline{\hat{p}}|^2} (0, \underline{\hat{p}})_\nu \tilde{A}_\nu(p) = \left( \delta_{\mu\nu} - \frac{\hat{p}_\mu (0, \underline{\hat{p}})_\nu}{|\underline{\hat{p}}|^2} \right) \tilde{A}_\nu(p). \end{aligned} \quad (\text{D.3.22})$$

Now the question is: what to do with the  $|\underline{\hat{p}}|^2 = 0$  modes?

Those are left unchanged with respect to the Feynman gauge because whatever value will not affect the Coulomb gauge. To match the extended Coulomb gauge we impose the other constraint on the following components

$$\tilde{A}_0(p_0 \neq 0, \underline{p} = \underline{0}) = 0. \quad (\text{D.3.23})$$

### D.3.2 Generation in the extended Coulomb gauge

The generation in the extended Coulomb gauge is carried out by following the appendix in Ref. (Blum *et al.*, 2007).

A component  $\tilde{A}_j(p)$  with  $\underline{p} \neq \underline{0}$  and  $p_j \neq 0$  is found from the other two spatial components through the Coulomb condition in momentum space (also called *transversality condition*)

$$\tilde{A}_j(p) = - \frac{1}{\hat{p}_j} \sum_{k \neq j} \hat{p}_k \tilde{A}_k(p). \quad (\text{D.3.24})$$

Let summarize what are the constraints on the modes.

- $\underline{p} \neq \underline{0}$  and  $p_3 \neq 0$ .

The weight we use to generate the components is

$$\frac{h_p}{2} \hat{p}^2 \left( |\tilde{A}_1(p)|^2 + |\tilde{A}_2(p)|^2 \right), \quad (\text{D.3.25})$$

where  $h_p$  takes into account the doubling in the action due to the contribution from the complex conjugate partner and it is defined as

$$h_p = \begin{cases} 2 & \text{when } R(p) \neq p \\ 1 & \text{otherwise} \end{cases}. \quad (\text{D.3.26})$$

Where the reflection operator in Eq. D.1.5 is applied to each component of the vector  $p$ . The zero component is draw from following distribution

$$\frac{h_p}{2} |\underline{\hat{p}}|^2 |\tilde{A}_0(p)|^2. \quad (\text{D.3.27})$$

- $\underline{p} \neq \underline{0}$  and  $(\hat{p}_1)^2 + (\hat{p}_2)^2 \neq 0$ .

In this case we change basis in order to diagonalize the operator. Let us call the new basis  $(\tilde{A}_-(p), \tilde{A}_+(p))$ , and the weight is given by

$$\frac{h_p}{2} \hat{p}^2 \left( m_- |\tilde{A}_-(p)|^2 + m_+ |\tilde{A}_+(p)|^2 \right), \quad (\text{D.3.28})$$

where the  $m_{\mp}$  are the following eigenvalues

$$\begin{aligned} m_- &= \hat{p}^2, \\ m_+ &= \hat{p}^2 \left( 1 + \frac{(\hat{p}_1)^2 + (\hat{p}_2)^2}{(\hat{p}_3)^2} \right). \end{aligned} \quad (\text{D.3.29})$$

Once we have generated the components in this basis we need to rotate back to the original

$$\begin{pmatrix} \tilde{A}_1(p) \\ \tilde{A}_2(p) \end{pmatrix} = \begin{pmatrix} r_2 & r_1 \\ -r_1 & r_2 \end{pmatrix} \begin{pmatrix} \tilde{A}_-(p) \\ \tilde{A}_+(p) \end{pmatrix}, \quad (\text{D.3.30})$$

where the  $r_i$  are given by

$$r_j = \frac{\hat{p}_j}{\sqrt{(\hat{p}_1)^2 + (\hat{p}_2)^2}} \quad \text{for } j = 1, 2. \quad (\text{D.3.31})$$

As in the previous case the zero component is draw from the distribution

$$\frac{h_p}{2} |\underline{\hat{p}}|^2 |\tilde{A}_0(p)|^2. \quad (\text{D.3.32})$$

- $\underline{p} = \underline{0}$ ,  $p_0 \neq 0$ .

The three spatial components are found independently according to the weight

$$\frac{h_p}{2} (\hat{p}_0)^2 \sum_j |\tilde{A}_j(p)|^2. \quad (\text{D.3.33})$$

The zero component is vanishing, i.e.  $\tilde{A}_0(p_0, \underline{0}) = 0$ .

## D.4 Zero mode fixing equation of motion

The zero mode fixing in Eq. 2.4.29 in momentum space corresponds to the following condition in coordinates space

$$\tilde{A}_\mu(p=0) = c_\mu \iff \int d^4x A_\mu(x) = c_\mu, \quad (\text{D.4.34})$$

with  $c_\mu \in \mathbb{R}$  constant, for each value of  $\mu$  is a non-local condition.

We want to impose the constraint on the zero mode in the partition function, and this reads

$$\int \mathcal{D}[A_\mu] \exp[-S(A)] \prod_{\mu=0}^3 \delta\left(\int d^4y A_\mu(y) - c_\mu\right). \quad (\text{D.4.35})$$

We rewrite the delta function as the limit of a gaussian

$$\delta(f) = \lim_{\alpha \rightarrow 0} \exp\left(-\frac{f^2}{2\alpha}\right), \quad (\text{D.4.36})$$

then the action becomes an effective one written as

$$\begin{aligned} S_{\text{eff}} &= S(A) + \frac{1}{2\alpha} \sum_{\mu=0}^3 \left(\int d^4y A_\mu(y) - c_\mu\right)^2 \\ &= \int d^4x (F_{\mu\nu}F_{\mu\nu} + j_\mu A_\mu) + \frac{1}{2\alpha} \sum_{\mu=0}^3 \left(\int d^4y A_\mu(y) - c_\mu\right)^2. \end{aligned} \quad (\text{D.4.37})$$

The Euler-Lagrange equations, which we recall to be

$$\frac{\delta S}{\delta A_\mu(x)} = \partial_\nu \frac{\delta S}{\delta (\partial_\nu A_\mu(x))}, \quad (\text{D.4.38})$$

gives the usual known terms for the local part, and for the new non-local part we get

$$\begin{aligned} \frac{\delta}{\delta A_\mu(x)} \left[ \frac{1}{2\alpha} \sum_{\nu=0}^3 \left(\int d^4y A_\nu(y) - c_\nu\right)^2 \right] &= \frac{1}{2\alpha} \sum_{\nu} 2 \left(\int d^4y A_\nu(y) - c_\nu\right) \int d^4z \delta(z-x) \delta_{\mu\nu} \\ &= \frac{1}{\alpha} \left(\int d^4y A_\mu(y) - c_\mu\right) \equiv b_\mu = \text{constant}. \end{aligned} \quad (\text{D.4.39})$$

Finally Euler-Lagrange equations are

$$\sum_{\nu} \partial_\nu F_{\nu\mu}(x) = j_\mu(x) + b_\mu. \quad (\text{D.4.40})$$

## D.5 Generation of quenched QED<sub>M</sub> configurations

In this section we give the recipe to generate massive QED configurations in Feynman and Coulomb gauge. The only difference with Subsect. 2.5.1 is the mass term, this reads

$$\frac{m_\gamma^2}{2} \sum_{x,\mu} A_\mu^2(x + a\hat{\mu}/2). \quad (\text{D.5.41})$$

In momentum space it becomes

$$\begin{aligned}
\frac{m_\gamma^2}{2} \sum_{x,\mu} A_\mu^2(x + a\hat{\mu}/2) &= \frac{m_\gamma^2}{2} \sum_{x,\mu} \frac{1}{V} \sum_{p,p'} e^{i(p+p') \cdot (x+a\hat{\mu}/2)} \tilde{A}_\mu(p) \tilde{A}_\mu(p') \\
&= \frac{m_\gamma^2}{2} \sum_{\mu,p,p'} \delta(p+p') e^{i(p+p')_\mu/2} \tilde{A}_\mu(p) \tilde{A}_\mu(p') \\
&= \frac{m_\gamma^2}{2} \sum_{\mu,p} \tilde{A}_\mu(p) e^{ip_\mu/2} e^{iR(p)_\mu/2} \tilde{A}_\mu(p),
\end{aligned} \tag{D.5.42}$$

where the reflection operator in the first Brillouin zone is given by Eq. D.1.5. We can identify  $e^{iR(p)_\mu/2} \tilde{A}_\mu(p') = \left( e^{ip_\mu/2} \tilde{A}_\mu(p) \right)^*$  (reality condition of the field  $A_\mu$ ) and obtain

$$\frac{m_\gamma^2}{2} \sum_{x,\mu} A_\mu^2(x + a\hat{\mu}/2) = \frac{m_\gamma^2}{2} \sum_{p,\mu} |\tilde{A}_\mu(p)|^2. \tag{D.5.43}$$

The Proca action in momentum space is

$$S = \frac{1}{2} \sum_{p \in \tilde{\Lambda}} \left[ \sum_{\nu < \mu} |\hat{p}_\mu \tilde{A}_\nu(p) - \hat{p}_\nu \tilde{A}_\mu(p)|^2 + \sum_{\mu} m_\gamma^2 |\tilde{A}_\mu(p)|^2 \right]. \tag{D.5.44}$$

### D.5.1 Feynman gauge

Now we need to include the gauge fixing term in Feynman gauge that cancels out the off diagonal part in  $\mu, \nu$  of the field-strength and gives

$$\begin{aligned}
S = \sum_{x \in \Lambda} \left[ \frac{1}{4} \sum_{\mu,\nu} (\partial_\mu^+ A_\nu(x + a\hat{\nu}/2) - \partial_\nu^+ A_\mu(x + a\hat{\mu}/2))^2 \right. \\
\left. + \frac{m_\gamma^2}{2} \sum_{\mu} A_\mu^2(x + a\hat{\mu}/2) + \frac{1}{2} \left( \sum_{\mu} \partial_\mu A_\mu(x + a\hat{\mu}/2) \right)^2 \right],
\end{aligned} \tag{D.5.45}$$

which in Fourier space reads

$$S = \frac{1}{2} \sum_{p \in \tilde{\Lambda}} (\hat{p}^2 + m_\gamma^2) \sum_{\mu} |\tilde{A}_\mu(p)|^2. \tag{D.5.46}$$

### D.5.2 Coulomb gauge

We might also consider the Coulomb gauge implemented exactly configuration by configuration. The generation in Coulomb gauge is done by inserting a mass term.

In momentum space we can solve the Coulomb gauge fixing constraint with respect the third component, this lead to the following identification

$$\tilde{A}_3 = -\frac{1}{\hat{p}_3} \left( \hat{p}_1 \tilde{A}_1 + \hat{p}_2 \tilde{A}_2 \right), \tag{D.5.47}$$

as long as  $\hat{p}_3 \neq 0$ . By inserting it in the mass term we get

$$\sum_{\mu} m_{\gamma}^2 |\tilde{A}_{\mu}(p)|^2 = m_{\gamma}^2 |\tilde{A}_0(p)|^2 + m_{\gamma}^2 \left[ 1 + \left( \frac{\hat{p}_1}{\hat{p}_3} \right)^2 \right] |\tilde{A}_1(p)|^2 + m_{\gamma}^2 \left[ 1 + \left( \frac{\hat{p}_2}{\hat{p}_3} \right)^2 \right] |\tilde{A}_2(p)|^2. \quad (\text{D.5.48})$$

The weight (action) to use to generate the Fourier component is

$$\sum_{p_3 \neq 0} \frac{1}{2} \left\{ (\hat{p}^2 + m_{\gamma}^2) |\tilde{A}_0(p)|^2 + \hat{p}^2 \sum_{k=1}^2 |\tilde{A}_k(p)|^2 + m_{\gamma}^2 \sum_{k=1}^2 \left[ 1 + \left( \frac{\hat{p}_k}{\hat{p}_3} \right)^2 \right] |\tilde{A}_k(p)|^2 + \frac{m_{\gamma}^2 + \hat{p}^2}{\hat{p}_3^2} \sum_{j,k=1}^2 \hat{p}_j \hat{p}_k \Re \left( \tilde{A}_j(p) \tilde{A}_k(p) \right) \right\}. \quad (\text{D.5.49})$$

Let us consider the different momenta and the corresponding weights.

- $\underline{p} \neq 0$  and  $p_3 \neq 0$  ( $\hat{p}_1 = 0 = \hat{p}_2$ ).  
The action is given by

$$\frac{h_p}{2} (\hat{p}^2 + m_{\gamma}^2) \left( |\tilde{A}_1(p)|^2 + |\tilde{A}_2(p)|^2 \right) \quad (\text{D.5.50})$$

where  $h_p$  takes into account the doubling in the action due to the contribution from the complex conjugate partner and it is defined as in Eq. D.3.26, while the third component is fixed through the Coulomb condition Eq. D.5.47.

The zero component is draw from the following distribution

$$\frac{h_p}{2} (\hat{p}^2 + m_{\gamma}^2) |\tilde{A}_0(p)|^2. \quad (\text{D.5.51})$$

- $\underline{p} \neq 0$  and  $p_3 \neq 0$  ( $\hat{p}_1^2 + \hat{p}_2^2 \neq 0$ ).  
In matrix form the action is given by

$$\begin{pmatrix} \tilde{A}_1^* & \tilde{A}_2^* \end{pmatrix} \left[ (\hat{p}^2 + m_{\gamma}^2) \begin{pmatrix} 1 + \left( \frac{\hat{p}_1}{\hat{p}_3} \right)^2 & \frac{\hat{p}_1 \hat{p}_2}{\hat{p}_3^2} \\ \frac{\hat{p}_1 \hat{p}_2}{\hat{p}_3^2} & 1 + \left( \frac{\hat{p}_2}{\hat{p}_3} \right)^2 \end{pmatrix} \right] \begin{pmatrix} \tilde{A}_1 \\ \tilde{A}_2 \end{pmatrix}, \quad (\text{D.5.52})$$

and by diagonalizing it we get the following eigenvalues

$$\begin{aligned} m_- &\equiv \hat{p}^2 + m_{\gamma}^2 \xrightarrow{m_{\gamma} \rightarrow 0} \hat{p}^2, \\ m_+ &\equiv \hat{p}^2 \frac{\hat{p}^2 + m_{\gamma}^2}{\hat{p}_3^2} \xrightarrow{m_{\gamma} \rightarrow 0} \hat{p}^2 \left( 1 + \frac{\hat{p}_1^2 + \hat{p}_2^2}{\hat{p}_3^2} \right), \end{aligned} \quad (\text{D.5.53})$$

that in the massless case become the ones in Eq. D.3.29.

The weight in the new basis is

$$\frac{h_p}{2} (\hat{p}^2 + m_{\gamma}^2) \left( m_- |\tilde{A}_-(p)|^2 + m_+ |\tilde{A}_+(p)|^2 \right). \quad (\text{D.5.54})$$

Once we have generated the components in this basis we need to rotate back to the original components and this is done through

$$\begin{pmatrix} \tilde{A}_1 \\ \tilde{A}_2 \end{pmatrix} = \begin{pmatrix} r_2 & r_1 \\ -r_1 & r_2 \end{pmatrix} \begin{pmatrix} \tilde{A}_- \\ \tilde{A}_+ \end{pmatrix}, \quad (\text{D.5.55})$$

where the  $r_j$  are given by

$$r_j = \frac{\hat{p}_j}{\sqrt{\hat{p}_1^2 + \hat{p}_2^2}} \quad \text{for } j = 1, 2. \quad (\text{D.5.56})$$

The zero component as the following weight

$$\frac{h_p}{2} (\underline{\hat{p}}^2 + m_\gamma^2) |\tilde{A}_0(p)|^2. \quad (\text{D.5.57})$$

- $p = 0$  and  $p_0 \neq 0$ .

The zero component weight is found to be

$$\frac{h_p}{2} m_\gamma^2 |\tilde{A}_0(p)|^2, \quad (\text{D.5.58})$$

while the three spatial components are generated independently according to

$$\frac{h_p}{2} (m_\gamma^2 + \hat{p}_0^2) |\tilde{A}_j(p)|^2. \quad (\text{D.5.59})$$

- $p = 0$  and  $p_0 = 0$ .

The zero mode is regularized by the mass term. The four components are integrated independently with the weight

$$\frac{h_p}{2} m_\gamma^2 |\tilde{A}_\mu(p)|^2. \quad (\text{D.5.60})$$

## D.6 Wilson loop in quenched approximation

In the quenched approximation the expectation value of the Wilson loop is given by (Rothe, 1992)

$$\langle W_C[A] \rangle = \frac{\int \mathcal{D}[A] \exp \left[ -\frac{1}{2} \int d^4x A_\mu \Omega_{\mu\nu} A_\nu + ieQ \oint dx_\mu A_\mu \right]}{\int \mathcal{D}[A] \exp \left[ \frac{1}{2} \int d^4x A_\mu \Omega_{\mu\nu} A_\nu \right]}. \quad (\text{D.6.61})$$

In the case of QED in Feynman gauge we know that  $\Omega_{\mu\nu} = -\delta_{\mu\nu} \square$ , while in the massive case we simply have  $\Omega_{\mu\nu} = \delta_{\mu\nu} (-\square + m_\gamma^2)$ .

By completing the square we can compute the Gaussian integral and we find

$$\langle W_C[A] \rangle = \exp \left[ -\frac{e^2 Q^2}{2} \oint dz_\mu \oint dz'_\mu \delta_{\mu\nu} G(z - z') \right], \quad (\text{D.6.62})$$

where  $G(x)$  is the Green's function associated to the discretized version of  $-\square$  (in QED) or  $-\square + m_\gamma^2$  in the massive theory for a scalar particle. Since the integral is proportional to  $\delta_{\mu\nu}$  the integral receives contribution only when  $z$  and  $z'$  are parallel to each other. We rewrite the expectation value manifestly on the lattice

$$\langle W_C[A] \rangle = \binom{4}{2} \sum_{\mu \neq \nu} \exp \left[ -\frac{e^2 Q^2}{2} \sum_{z \in R_{\mu\nu}, z' \in R_{\mu\nu}} G(z - z') \right], \quad (\text{D.6.63})$$

where now  $R_{\mu\nu}$  is a rectangle of size  $I \times J$  in the plane  $(\mu, \nu)$ . We introduce the function

$$C_\mu(I, x) = \sum_{i_1, i_2=0}^{I-1} G[x + a(i_1 - i_2)\hat{\mu}], \quad (\text{D.6.64})$$

and by operating the substitution  $\tau = i_1 - i_2$  and  $\sigma = i_1 + i_2$  we get

$$C_\mu(I, xn) = IG(x) + 2 \sum_{\tau=1}^{I-1} (I - \tau) G(x + a\tau\hat{\mu}). \quad (\text{D.6.65})$$

We can now rewrite the Wilson loop in the plane  $(\mu, \nu)$  expectation value in its final form

$$\langle W_{\mu\nu}[A](I, J) \rangle = \exp \{ -2e^2 Q^2 [C_\mu(I, 0) - C_\nu(I, J\hat{\nu})] \}. \quad (\text{D.6.66})$$

For Lorentz invariance we can average over  $\mu, \nu$  and write directly  $w(I, I)$ .

$I$	QED	Massive QED	
		$m_\gamma = 0.05$	$m_\gamma = 5$
1	0.500000000(1)	0.499806547(1)	0.118374259(1)
2	1.369311535(1)	1.368461017(1)	0.251479961(1)
3	2.305193057(1)	2.303260044(1)	0.381563158(1)
4	3.261483854(1)	3.258072049(1)	0.511425684(1)
5	4.228829967(1)	4.223555011(1)	0.641276934(1)
6	5.203604529(1)	5.196090337(1)	0.771127679(1)
7	6.183728249(1)	6.173606728(1)	0.900978402(1)
8	7.167859805(1)	7.154771070(1)	1.030829125(1)
9	8.155091868(1)	8.138684452(1)	1.160679847(1)
10	9.144788116(1)	9.124719122(1)	1.290530569(1)
11	10.136487567(1)	10.112422767(1)	1.420381292(1)
12	11.129846532(1)	11.101460414(1)	1.550232014(1)
13	12.124602305(1)	12.091578088(1)	1.680082737(1)
14	13.120549740(1)	13.082579344(1)	1.809933459(1)
15	14.117525653(1)	14.074309644(1)	1.939784182(1)
16	15.115398147(1)	15.066645656(1)	2.069634904(1)

Table D.1: Table showing the values of  $-\frac{2}{q^2} \ln(w(I, I))$  related to the Wilson loops in the infinite lattice in QED and massive QED (Feynman gauge), meant to save PhDs from struggling too much.

## D.7 Coordinate space method

The coordinate space method permits us to write the propagator in coordinate space by using a recursion relation. The only requirement is the knowledge of the Green's function in the corners of the unit hypercube. In the following we present the methods for the massless and massive propagator, useful for the computation of the Wilson loops.

### D.7.1 Luscher-Weisz

We consider an infinite lattice. The Green's function for a massless particle satisfies

$$\sum_{\mu} \partial_{\mu}^{-} \partial_{\mu}^{+} G(x) = \delta(x). \quad (\text{D.7.67})$$

We know that in the continuum limit ( $x \rightarrow \infty$ )  $G(x)$  converges to  $(4\pi^2 x^2)^{-1}$ , the Green's function of the continuum laplacian in  $\mathbb{R}^4$ . We would like to express the propagator through its values close to the origin. The key observation made by Vohwinkel is that

$$(\partial_\mu^- + \partial_\mu^+) G(x) = x_\mu H(x), \quad (\text{D.7.68})$$

with the following identifications

$$\begin{aligned} H(x) &= \int_{-\frac{\pi}{a}}^{\frac{\pi}{a}} \frac{d^4 p}{(2\pi)^4} e^{ip \cdot x} \ln(\hat{p}^2), \\ G(x) &= \int_{-\frac{\pi}{a}}^{\frac{\pi}{a}} \frac{d^4 p}{(2\pi)^4} \frac{e^{ip \cdot x}}{\hat{p}^2}. \end{aligned} \quad (\text{D.7.69})$$

### Proof of the formula

To prove the relation we calculate the l.h.s. of Eq. D.7.68

$$\begin{aligned} \partial_\mu^+ G(x) &= G(x + a\hat{\mu}) - G(x) = \int_{-\frac{\pi}{a}}^{\frac{\pi}{a}} \frac{d^4 p}{(2\pi)^4} \frac{1}{\hat{p}^2} \partial_\mu^+ e^{ip \cdot x} = \int_{-\frac{\pi}{a}}^{\frac{\pi}{a}} \frac{d^4 p}{(2\pi)^4} \frac{1}{\hat{p}^2} \frac{e^{ip \cdot x}}{a} (e^{ia p_\mu} - 1), \\ \partial_\mu^- G(x) &= G(x) - G(x - a\hat{\mu}) = \int_{-\frac{\pi}{a}}^{\frac{\pi}{a}} \frac{d^4 p}{(2\pi)^4} \frac{1}{\hat{p}^2} \partial_\mu^- e^{ip \cdot x} = \int_{-\frac{\pi}{a}}^{\frac{\pi}{a}} \frac{d^4 p}{(2\pi)^4} \frac{1}{\hat{p}^2} \frac{e^{ip \cdot x}}{a} (1 - e^{-ia p_\mu}), \\ (\partial_\mu^- + \partial_\mu^+) G(x) &= \int_{-\frac{\pi}{a}}^{\frac{\pi}{a}} \frac{d^4 p}{(2\pi)^4} \frac{e^{ip \cdot x}}{\hat{p}^2} i \left[ \frac{2}{a} \sin(ap_\mu) \right]. \end{aligned} \quad (\text{D.7.70})$$

We now integrate by parts the r.h.s. of Eq. D.7.68

$$\begin{aligned} x_\mu H(x) &= \int_{-\frac{\pi}{a}}^{\frac{\pi}{a}} \frac{d^4 p}{(2\pi)^4} x_\mu e^{ip \cdot x} \ln(\hat{p}^2) = \int_{-\frac{\pi}{a}}^{\frac{\pi}{a}} \frac{d^4 p}{(2\pi)^4} \left( -i \frac{d}{dp_\mu} e^{ip \cdot x} \right) \ln(\hat{p}^2) \\ &= -i \int_{-\frac{\pi}{a}}^{\frac{\pi}{a}} \frac{d^4 p}{(2\pi)^4} \frac{d}{dp_\mu} [e^{ip \cdot x} \ln(\hat{p}^2)] + i \int_{-\frac{\pi}{a}}^{\frac{\pi}{a}} \frac{d^4 p}{(2\pi)^4} e^{ip \cdot x} \left( \frac{d}{dp_\mu} \ln(\hat{p}^2) \right). \end{aligned} \quad (\text{D.7.71})$$

The first term vanishes since

$$\begin{aligned} \int_{-\frac{\pi}{a}}^{\frac{\pi}{a}} \frac{d^4 p}{(2\pi)^4} \frac{d}{dp_\mu} [e^{ip \cdot x} \ln(\hat{p}^2)] &= \left( \int_{-\frac{\pi}{a}}^{\frac{\pi}{a}} \prod_{\nu \neq \mu} \frac{dp_\nu}{(2\pi^3)} e^{ip_\nu x_\nu} \right) \left\{ \int_{-\frac{\pi}{a}}^{\frac{\pi}{a}} \frac{dp_\mu}{2\pi} \frac{d}{dp_\mu} [e^{ip_\mu x_\mu} \ln(\hat{p}^2)] \right\} \\ &= \left( \int_{-\frac{\pi}{a}}^{\frac{\pi}{a}} \prod_{\nu \neq \mu} \frac{dp_\nu}{(2\pi^4)} e^{ip_\nu x_\nu} \right) [e^{ip_\mu x_\mu} \ln(\hat{p}^2)]_{-\pi/a}^{\pi/a} = 0. \end{aligned} \quad (\text{D.7.72})$$

The result is

$$x_\mu H(x) = \int_{-\frac{\pi}{a}}^{\frac{\pi}{a}} \frac{d^4 p}{(2\pi)^4} \frac{e^{ip \cdot x}}{\hat{p}^2} 2i\hat{p}_\mu \cos\left(\frac{ap_\mu}{2}\right) = \int_{-\frac{\pi}{a}}^{\frac{\pi}{a}} \frac{d^4 p}{(2\pi)^4} \frac{e^{ip \cdot x}}{\hat{p}^2} i \left[ \frac{2}{a} \sin(ap_\mu) \right], \quad (\text{D.7.73})$$

which prove the equation Eq. D.7.68.



### Recursion formula

We can eliminate  $H(x)$  in Eq. D.7.68 by using Eq. D.7.67. We start by notice that

$$\sum_{\mu=0}^3 \partial_{\mu}^{-} \partial_{\mu}^{+} = \frac{1}{2} \sum_{\mu=0}^3 (\partial_{\mu}^{+} - \partial_{\mu}^{-}), \quad (\text{D.7.74})$$

and by taking Eq. D.7.67 we have

$$\sum_{\mu=0}^3 \partial_{\mu}^{-} \partial_{\mu}^{+} G(x) = 0 = \frac{1}{2} \sum_{\mu=0}^3 (\partial_{\mu}^{+} - \partial_{\mu}^{-}) G(x) \implies \sum_{\mu=0}^3 \partial_{\mu}^{+} G(x) = \sum_{\mu=0}^3 \partial_{\mu}^{-} G(x). \quad (\text{D.7.75})$$

Now we sum over  $\mu$  of Eq. D.7.68, and define  $\rho = \sum_{\mu} x_{\mu}$ ,

$$\left. \begin{aligned} \sum_{\mu} (\partial_{\mu}^{-} + \partial_{\mu}^{+}) G(x) &= 2 \sum_{\mu=0}^3 \partial_{\mu}^{-} G(x) \\ \sum_{\mu} x_{\mu} H(x) &= \rho H(x) \end{aligned} \right\} H(x) = \frac{2}{\rho} \sum_{\mu=0}^3 \partial_{\mu}^{-} G(x). \quad (\text{D.7.76})$$

In this way we have eliminated the function  $H(x)$  and we can rewrite Eq. D.7.68 as

$$(\partial_{\mu}^{-} + \partial_{\mu}^{+}) G(x) = \frac{2x_{\mu}}{\rho} \sum_{\mu=0}^3 \partial_{\mu}^{-} G(x). \quad (\text{D.7.77})$$

We can now relate the value of the propagator at a point  $x + a\hat{\mu}$  to the neighbor points

$$G(x + a\hat{\mu}) = G(x - a\hat{\mu}) + \frac{2x_{\mu}}{\rho} \sum_{\mu=0}^3 [G(x) - G(x - a\hat{\nu})], \quad (\text{D.7.78})$$

for  $\rho \neq 0$ . The propagator is independent of the sign and the order of the coordinates  $(x_0, x_1, x_2, x_3)$ , from its asymptotic expansion (Luscher and Weisz, 1995). We can restrict the attention to the points  $x = an$  with  $n_3 \geq n_2 \geq n_1 \geq n_0$  and the recursion relation allows us to express  $G(x)$  as a combination of the propagators at the corners of the unit hypercube.

Then the 5 initial values are further restricted when we take into account the following relations:

$$\begin{aligned} G(0, 0, 0, 0) - G(0, 0, 0, 1) &= \frac{1}{8a^2}, \\ G(0, 0, 0, 0) - 3G(0, 0, 1, 1) - 2G(0, 1, 1, 1) &= \frac{1}{a^2\pi^2}, \\ G(0, 0, 0, 0) - 6G(0, 0, 1, 1) - 8G(0, 1, 1, 1) - 3G(1, 1, 1, 1) &= 0. \end{aligned} \quad (\text{D.7.79})$$

In the end the only initial values we have to put are

$$\begin{aligned} a^2 G(0, 0, 0, 0) &= 0.154933390231060214084837208107\dots \\ a^2 G(0, 0, 1, 1) &= 0.012714703770934215428228758391\dots \end{aligned} \quad (\text{D.7.80})$$

The best values of the constants related to  $G(0, 0, 0, 0)$  and  $G(0, 0, 1, 1)$  are given in (Capitani, 2003).

### D.7.2 Borasoy-Krebs

The generalization in the case of a massive propagator is done in Ref. (Borasoy and Krebs, 2005). The Green's function satisfies the equation

$$\left(m_\gamma^2 + \sum_\mu \partial_\mu^- \partial_\mu^+\right) G(x) = \delta(x), \quad (\text{D.7.81})$$

and it still satisfies the Eq. D.7.68 with modified functions

$$\begin{aligned} H(x) &= \int_{-\frac{\pi}{a}}^{\frac{\pi}{a}} \frac{d^4 p}{(2\pi)^4} e^{ip \cdot x} \ln(\hat{p}^2 + m_\gamma^2), \\ G(x) &= \int_{-\frac{\pi}{a}}^{\frac{\pi}{a}} \frac{d^4 p}{(2\pi)^4} \frac{e^{ip \cdot x}}{\hat{p}^2 + m_\gamma^2}. \end{aligned} \quad (\text{D.7.82})$$

By following the same lines of arguments in the case of the Luscher-Weisz method we get that the recursion formula in the case of a massive propagator is given by

$$G(x + a\hat{\mu}) = G(x - a\hat{\mu}) + \frac{2x_\mu}{\rho} \sum_{\mu=0}^3 \left[ \left(1 + \frac{m_\gamma^2}{8}\right) G(x) - G(x - a\hat{\nu}) \right]. \quad (\text{D.7.83})$$

Now the 5 initial seeds are given by the modified Bessel functions  $I_n$ ,

$$G(x_0, x_1, x_2, x_3) = \frac{1}{2} \int_0^\infty d\lambda \exp[-m_\gamma^2 \lambda / 2 - 4\lambda] I_{x_0}(\lambda) I_{x_1}(\lambda) I_{x_2}(\lambda) I_{x_3}(\lambda). \quad (\text{D.7.84})$$

The seeds used in this work are generated using MATHEMATICA. Special thanks are given to Langæble, who helped me in writing a code free of raund-off errors.

## Appendix E

# Electromagnetic critical mass shift in lattice perturbation theory

In this appendix we calculate from first principle the critical mass shift induced by electromagnetic effects, to this purpose we use lattice perturbation theory. The different diagrams are calculated, this was done in order to be able to introduce a mass term for the photon, even though it is not presented here the modification is straightforward.

### E.1 Feynman rules of the Wilson theory

The Dirac-Wilson action on the lattice is, with  $r = 1$ ,

$$\begin{aligned}
 S_L &= \sum_{n \in \Lambda} \bar{\psi}_f(n) \left\{ \gamma_\mu \frac{\nabla_\mu^+ + \nabla_\mu^-}{2} - \frac{\nabla_\mu^+ \nabla_\mu^-}{2} + m_0^f \right\} \psi_f(n) \\
 &= \sum_{n \in \Lambda} \left\{ \bar{\psi}_f(n) \left( m_0^f + 4 \right) \psi_f(n) + \frac{1}{2} \sum_{\mu} \left[ \bar{\psi}_f(n) (\gamma_\mu - 1) U_\mu(n) \psi_f(n + \hat{\mu}) \right. \right. \\
 &\quad \left. \left. - \bar{\psi}_f(n) (\gamma_\mu + 1) U_\mu^\dagger(n - \hat{\mu}) \psi_f(n - \hat{\mu}) \right] \right\}. \tag{E.1}
 \end{aligned}$$

#### E.1.1 Photon propagator

$$\mu \text{---} \overset{\gamma}{\text{~~~~~}} \text{---} \nu \equiv \frac{1}{\hat{k}^2} \left[ \delta_{\mu\nu} + (1 - \alpha) \frac{\hat{k}_\mu \hat{k}_\nu}{\hat{k}^2} \right] \stackrel{\alpha \equiv 1}{\equiv} \frac{\delta_{\mu\nu}}{\hat{k}^2}. \tag{E.2}$$

#### E.1.2 Fermion propagator

$$\text{---} \overset{p}{\text{---}} \text{---} \equiv \frac{m + \frac{r}{2} \hat{p}^2 - i \hat{\vec{p}}}{\left( m + \frac{r}{2} \hat{p}^2 \right)^2 + \vec{p}^2}, \tag{E.3}$$

where we defined  $\bar{p}_\mu = \sin(p_\mu)$ .

### E.1.3 Vertexes

We want to expand the interaction part of the Dirac-Wilson action in the weak coupling  $e$  regime. We start by expanding the gauge link in  $e$  and we drop the index  $f$

$$U_\mu(n) = e^{ieQA_\mu(n+\hat{\mu}/2)} \simeq 1 + ieQA_\mu(n+\hat{\mu}/2) + \frac{(ieQ)^2}{2} A_\mu(n+\hat{\mu}/2)A_\mu(n+\hat{\mu}/2) + O(e^3). \quad (\text{E.4})$$

The interaction part is given by

$$\begin{aligned} S_L^{\text{int}} = \frac{1}{2} \sum_{n,\mu} \left\{ \bar{\psi}(n)(\gamma_\mu - 1) \left[ ieQA_\mu(n+\hat{\mu}/2) - \frac{e^2Q^2}{2} A_\mu(n+\hat{\mu}/2)A_\mu(n+\hat{\mu}/2) \right] \psi(n+\hat{\mu}) \right. \\ \left. - \bar{\psi}(n)(\gamma_\mu + 1) \left[ -ieQA_\mu(n-\hat{\mu}/2) - \frac{e^2Q^2}{2} A_\mu(n-\hat{\mu}/2)A_\mu(n-\hat{\mu}/2) \right] \psi(n-\hat{\mu}) \right\}. \end{aligned} \quad (\text{E.5})$$

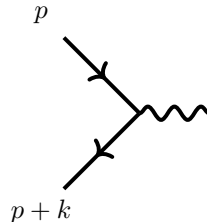
By Fourier transforming we read the Feynman rules directly from the action by recalling that the expansion at the action level is given by  $e^S \simeq 1 - S$  and we have to take an overall minus sign in the vertexes. The photon momentum is always flowing inside the vertex.

#### Terms in $e$

$$\begin{aligned} S_L^{\text{int},e} &= \frac{ieQ}{2} \sum_{n,\mu} \bar{\psi}(n) [(\gamma_\mu - 1)A_\mu(n+\hat{\mu}/2)\psi(n+\hat{\mu}) + (\gamma_\mu + 1)A_\mu(n-\hat{\mu}/2)\psi(n-\hat{\mu})] \\ &= \frac{ieQ}{2} \frac{1}{V^{3/2}} \sum_{n,\mu} \sum_{\bar{p},p,k} \tilde{\psi}(\bar{p}) \tilde{A}_\mu(k) e^{-i\bar{p}\cdot n} e^{ik\cdot n} e^{ip\cdot n} [(\gamma_\mu - 1)e^{ik_\mu/2} e^{ip_\mu} \\ &\quad + (\gamma_\mu + 1)e^{-ik_\mu/2} e^{-ip_\mu}] \tilde{\psi}(p), \end{aligned} \quad (\text{E.6})$$

and recalling that  $\delta(p-p') = \frac{1}{V} \sum_n e^{i(p-p')\cdot n}$ ,

$$\begin{aligned} S_L^{\text{int},e} &= \frac{ieQ}{2} \frac{1}{\sqrt{V}} \sum_\mu \sum_{\bar{p},p,k} \delta(k+p-\bar{p}) \tilde{\psi}(\bar{p}) \tilde{A}_\mu(k) \left[ \gamma_\mu 2 \cos\left(p_\mu + \frac{k_\mu}{2}\right) - 2i \sin\left(p_\mu + \frac{k_\mu}{2}\right) \right] \tilde{\psi}(p) \\ &= ieQ \frac{1}{\sqrt{V}} \sum_\mu \sum_{p,k} \tilde{\psi}(p+k) \tilde{A}_\mu(k) \left[ \gamma_\mu \cos\left(p_\mu + \frac{k_\mu}{2}\right) - i \sin\left(p_\mu + \frac{k_\mu}{2}\right) \right] \tilde{\psi}(p). \end{aligned} \quad (\text{E.7})$$

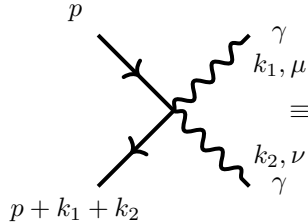


$$\gamma \equiv (V_1)_\mu(p, k) = -i \frac{eQ}{\sqrt{V}} \left[ \gamma_\mu \cos\left(p_\mu + \frac{k_\mu}{2}\right) - i \sin\left(p_\mu + \frac{k_\mu}{2}\right) \right]. \quad (\text{E.8})$$

**Terms in  $e^2$** 

This is going to be an irrelevant vertex, meaning that in the continuum there is no counterpart

$$\begin{aligned}
S_L^{\text{int}, e^2} &= -\frac{e^2 Q^2}{4} \sum_{n, \mu} \bar{\psi}(n) [(\gamma_\mu - 1) A_\mu(n + \hat{\mu}/2) A_\mu(n + \hat{\mu}/2) \psi(n + \hat{\mu}) \\
&\quad - (\gamma_\mu + 1) A_\mu(n - \hat{\mu}/2) A_\mu(n - \hat{\mu}/2) \psi(n - \hat{\mu})] \\
&= -\frac{e^2 Q^2}{4} \frac{1}{V^2} \sum_{n, \mu} \sum_{\bar{p}, p, k_1, k_2} \tilde{\bar{\psi}}(\bar{p}) \tilde{A}_\mu(k_1) \tilde{A}_\mu(k_2) e^{-i\bar{p}\cdot n} e^{ik_1\cdot n} e^{ik_2\cdot n} e^{ip\cdot n} [(\gamma_\mu - 1) e^{i(k_{1,\mu} + k_{2,\mu})/2} e^{ip_\mu} \\
&\quad - (\gamma_\mu + 1) e^{-i(k_{1,\mu} + k_{2,\mu})/2} e^{-ip_\mu}] \tilde{\psi}(p) \\
&= -\frac{e^2 Q^2}{4} \frac{1}{V} \sum_{\mu} \sum_{\bar{p}, p, k_1, k_2} \delta(p + k_1 + k_2 - \bar{p}) \tilde{\bar{\psi}}(\bar{p}) \tilde{A}_\mu(k_1) \tilde{A}_\mu(k_2) \left[ \gamma_\mu 2i \sin\left(p_\mu + \frac{k_{1,\mu} + k_{2,\mu}}{2}\right) \right. \\
&\quad \left. - 2 \cos\left(p_\mu + \frac{k_{1,\mu} + k_{2,\mu}}{2}\right) \right] \tilde{\psi}(p) \\
&= -\frac{e^2 Q^2}{2} \frac{1}{V} \sum_{\mu} \sum_{p, k_1, k_2} \tilde{\bar{\psi}}(p + k_1 + k_2) \tilde{A}_\mu(k_1) \tilde{A}_\mu(k_2) \left[ \gamma_\mu i \sin\left(p_\mu + \frac{k_{1,\mu} + k_{2,\mu}}{2}\right) \right. \\
&\quad \left. - \cos\left(p_\mu + \frac{k_{1,\mu} + k_{2,\mu}}{2}\right) \right] \tilde{\psi}(p). \tag{E.9}
\end{aligned}$$



$$\begin{aligned}
&\equiv (V_2)_{\mu, \nu}(p, k_1, k_2) = \frac{e^2 Q^2}{2V} \delta_{\mu\nu} \left[ \gamma_\mu i \sin\left(p_\mu + \frac{k_{1,\mu} + k_{2,\mu}}{2}\right) \right. \\
&\quad \left. - r \cos\left(p_\mu + \frac{k_{1,\mu} + k_{2,\mu}}{2}\right) \right]. \tag{E.10}
\end{aligned}$$

**E.1.4 Clover term**

The clover term in the action is given by (dropping the flavor index  $f$ )

$$S_{\text{clover}} = -\frac{i}{4} r c_{sw} \sum_{n \in \Lambda} \sum_{\mu, \nu} \bar{\psi}(n) \sigma_{\mu\nu} \psi(n) \hat{F}_{\mu\nu}, \tag{E.11}$$

where  $\sigma_{\mu\nu} = \frac{1}{2} [\gamma_\mu, \gamma_\nu]$  and  $\hat{F}_{\mu\nu} = \frac{1}{8i} [Q_{\mu\nu}(n) - Q_{\nu\mu}(n)]$ , with the definition

$$\begin{aligned}
Q_{\mu\nu}(n) &= U_\mu(n) U_\nu(n + \hat{\mu}) U_\mu^\dagger(n + \hat{\nu}) U_\nu^\dagger(n) + U_\nu(n) U_\mu^\dagger(n - \hat{\mu} + \hat{\nu}) U_\nu^\dagger(n - \hat{\mu}) U_\mu(n - \hat{\mu}) \\
&\quad + U_\mu^\dagger(n - \hat{\mu}) U_\nu^\dagger(n - \hat{\mu} - \hat{\nu}) U_\mu(n - \hat{\mu} - \hat{\nu}) U_\nu(n - \hat{\nu}) \\
&\quad + U_\nu^\dagger(n - \hat{\nu}) U_\mu(n - \hat{\nu}) U_\nu(n + \hat{\mu} - \hat{\nu}) U_\mu^\dagger(n). \tag{E.12}
\end{aligned}$$

The multiplication of two link is simply the sum of the exponent since we are dealing with an abelian group, i.e.

$$U_\mu(n)U_\nu(n) = e^{ieQ[A_\mu(n+\hat{\mu}/2)+A_\nu(n+\hat{\nu}/2)]}. \quad (\text{E.13})$$

By expanding Eq. E.12 linearly in  $e$ , we obtain for  $Q_{\mu\nu}$

$$\begin{aligned} Q_{\mu\nu}^e = ieQ & \left[ \cancel{A_\mu(n+\hat{\mu}/2)} + A_\nu(n+\hat{\mu}+\hat{\nu}/2) - A_\mu(n+\hat{\nu}+\hat{\mu}/2) - \cancel{A_\nu(n+\hat{\nu}/2)} \right. \\ & + \cancel{A_\nu(n+\hat{\nu}/2)} - A_\mu(n-\hat{\mu}/2+\hat{\nu}) - A_\nu(n-\hat{\mu}+\hat{\nu}/2) + \cancel{A_\mu(n-\hat{\mu}/2)} \\ & - \cancel{A_\mu(n-\hat{\mu}/2)} - A_\nu(n-\hat{\mu}-\hat{\nu}/2) + A_\mu(n-\hat{\mu}/2-\hat{\nu}) + \cancel{A_\nu(n-\hat{\nu}/2)} \\ & \left. - \cancel{A_\nu(n-\hat{\nu}/2)} + A_\mu(n+\hat{\mu}/2-\hat{\nu}) + A_\nu(n+\hat{\mu}-\hat{\nu}/2) - \cancel{A_\mu(n+\hat{\mu}/2)} \right]. \quad (\text{E.14}) \end{aligned}$$

By direct inspection in QED we have that  $Q_{\mu\nu}^e = -Q_{\nu\mu}^e$ , i.e. the  $Q^{(e)}$  is antisymmetric and it is contracted, in the action, with  $\sigma_{\mu\nu}$  (which is also antisymmetric). The result is that even powers in  $e$  vanish because the second order in  $e$  is given by the square of the first order, that is symmetric,  $Q_{\mu\nu}^{e^2} = (Q_{\mu\nu}^e)^2 = Q_{\nu\mu}^{e^2}$ , contracted with an antisymmetric tensor. The first order in  $e$  of  $\widehat{F}$  is then given by

$$\begin{aligned} \widehat{F}_{\mu\nu}^{(e)} = \frac{1}{8i} 2Q_{\mu\nu}^{(e)} = \frac{1}{4i} (ieQ) & \left[ A_\nu(n+\hat{\mu}+\hat{\nu}/2) - A_\mu(n+\hat{\nu}+\hat{\mu}/2) - A_\mu(n-\hat{\mu}/2+\hat{\nu}) - A_\nu(n-\hat{\mu}+\hat{\nu}/2) \right. \\ & \left. - A_\nu(n-\hat{\mu}-\hat{\nu}/2) + A_\mu(n-\hat{\mu}/2-\hat{\nu}) + A_\mu(n+\hat{\mu}/2-\hat{\nu}) + A_\nu(n+\hat{\mu}-\hat{\nu}/2) \right]. \quad (\text{E.15}) \end{aligned}$$

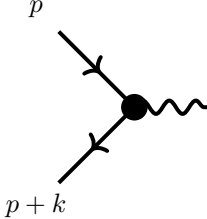
Since we want to calculate the extra vertexes coming from the clover term we take clover action at the first order in  $e$  and we perform the Fourier transform

$$\begin{aligned} S_{\text{clover}}^e &= -\frac{i}{4} \frac{rc_{sw}}{V^{3/2}} \frac{eQ}{4} \sum_{n,\mu\nu} \sum_{\bar{p},p,k} \widetilde{\psi}(\bar{p}) \sigma_{\mu\nu} \widetilde{\psi}(p) e^{i(p+k-\bar{p})\cdot n} \\ & \times \left[ e^{ik_\mu} e^{ik_\nu/2} \widetilde{A}_\nu(k) - e^{ik_\mu/2} e^{ik_\nu} \widetilde{A}_\mu(k) - e^{-ik_\mu/2} e^{ik_\nu} \widetilde{A}_\mu(k) - e^{ik_\nu/2} e^{-ik_\mu} \widetilde{A}_\nu(k) \right. \\ & \left. - e^{-ik_\nu/2} e^{-ik_\mu} \widetilde{A}_\nu(k) - e^{-ik_\mu/2} e^{-ik_\nu} \widetilde{A}_\mu(k) + e^{ik_\mu/2} e^{-ik_\nu} \widetilde{A}_\mu(k) + e^{-ik_\nu/2} e^{ik_\mu} \widetilde{A}_\nu(k) \right] \\ &= -\frac{ir}{16} \frac{eQ}{\sqrt{V}} c_{sw} \sum_{\mu\nu} \sum_{p,k} \widetilde{\psi}(p+k) \sigma_{\mu\nu} \widetilde{\psi}(p) \left\{ \widetilde{A}_\nu(k) 2i \sin k_\mu \left[ e^{ik_\nu/2} + e^{-ik_\nu/2} \right] \right. \\ & \left. + \widetilde{A}_\mu(k) 2 \cos \left( \frac{k_\mu}{2} \right) \left[ e^{-ik_\nu} - e^{ik_\nu} \right] \right\} \\ &= -\frac{i^2 r}{16} \frac{eQ}{\sqrt{V}} c_{sw} 4 \sum_{\mu\nu} \sum_{p,k} \widetilde{\psi}(p+k) \sigma_{\mu\nu} \widetilde{\psi}(p) \left\{ \widetilde{A}_\nu(k) \sin k_\mu \cos \left( \frac{k_\nu}{2} \right) - \widetilde{A}_\mu(k) \sin k_\nu \cos \left( \frac{k_\mu}{2} \right) \right\}. \quad (\text{E.16}) \end{aligned}$$

By renaming the first term  $\mu \leftrightarrow \nu$  and using that  $\sigma_{\mu\nu}$  is antisymmetric we get

$$S_{\text{clover}}^e = -\frac{r}{2} \frac{eQ}{\sqrt{V}} c_{sw} \sum_{\mu\nu} \sum_{p,k} \widetilde{\psi}(p+k) \sigma_{\mu\nu} \widetilde{\psi}(p) \widetilde{A}_\mu(k) \sin k_\nu \cos \left( \frac{k_\mu}{2} \right), \quad (\text{E.17})$$

from which we read the associated vertex

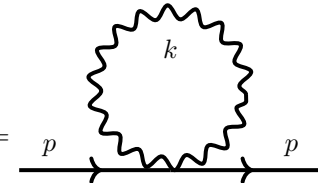


$$\gamma \equiv (V_c)_\mu(p, k) = \frac{r e Q c_{sw}}{2\sqrt{V}} \sum_\nu \sigma_{\mu\nu} \sin k_\nu \cos\left(\frac{k_\mu}{2}\right). \quad (\text{E.18})$$

## E.2 Electromagnetic fermion self-energy

We want to compute the 1-loop contribution to the quark self-energy, the Feynman diagrams contributing are the following ones.

### Tadpole in Feynman gauge



$$\begin{aligned} I_T^{\text{Feyn}} &= \left. \begin{array}{c} p \\ \text{---} \text{---} \text{---} \text{---} p \\ \text{---} \text{---} \text{---} \text{---} \\ \text{---} \text{---} \text{---} \text{---} \end{array} \right|_{p=0, m=0} = \sum_k \sum_{\mu, \nu} (V_2)_{\mu\nu}(0, -k, k) G_{\mu\nu}(k) \\ &= \sum_k \sum_{\mu, \nu} \delta_{\mu\nu} (-r) \frac{e^2 Q^2}{2V} \frac{\delta_{\mu\nu}}{\hat{k}^2} = -\frac{e^2 Q^2}{V} \frac{r}{2} \sum_k \frac{4}{\hat{k}^2}. \end{aligned} \quad (\text{E.19})$$

### Tadpole in Coulomb gauge

In order to calculate the tadpole diagram in Coulomb gauge it is sufficient to use the following gauge transformation

$$\tilde{A}_\mu^{\text{C}}(p) = \sum_\nu \left[ \delta_{\mu\nu} - \frac{\hat{p}_\mu \cdot (0, \hat{p})_\nu}{|\hat{p}|^2} \right] \tilde{A}_\nu(p), \quad (\text{E.20})$$

where  $\tilde{A}$  is the field generated in Feynman gauge and  $\tilde{A}^{\text{C}}$  the field in Coulomb gauge.

For the tadpole it is sufficient to calculate the propagator in Coulomb gauge

$$\begin{aligned} \langle \tilde{A}_\mu^{\text{C}} \tilde{A}_\nu^{\text{C}} \rangle &= \sum_{\rho, \sigma} \left[ \delta_{\mu\rho} - \frac{\hat{p}_\mu \cdot (0, \hat{p})_\rho}{|\hat{p}|^2} \right] \left[ \delta_{\nu\sigma} - \frac{\hat{p}_\nu \cdot (0, \hat{p})_\sigma}{|\hat{p}|^2} \right] \langle \tilde{A}_\rho(p) \tilde{A}_\sigma(p) \rangle \\ &= \sum_{\rho, \sigma} \left[ \delta_{\mu\rho} \delta_{\nu\sigma} - \frac{\delta_{\nu\sigma} \hat{p}_\mu \cdot (0, \hat{p})_\rho + \delta_{\mu\rho} \hat{p}_\nu \cdot (0, \hat{p})_\sigma}{|\hat{p}|^2} + \frac{\hat{p}_\mu \cdot (0, \hat{p})_\rho \hat{p}_\nu \cdot (0, \hat{p})_\sigma}{(|\hat{p}|^2)^2} \right] \langle \tilde{A}_\rho(p) \tilde{A}_\sigma(p) \rangle \\ &= \langle \tilde{A}_\mu(p) \tilde{A}_\nu(p) \rangle - \sum_\rho \frac{\hat{p}_\mu \cdot (0, \hat{p})_\rho}{|\hat{p}|^2} \langle \tilde{A}_\rho(p) \tilde{A}_\nu(p) \rangle \\ &\quad - \sum_\sigma \frac{\hat{p}_\nu \cdot (0, \hat{p})_\sigma}{|\hat{p}|^2} \langle \tilde{A}_\mu(p) \tilde{A}_\sigma(p) \rangle + \sum_{\rho, \sigma} \frac{\hat{p}_\mu \cdot (0, \hat{p})_\rho \hat{p}_\nu \cdot (0, \hat{p})_\sigma}{(|\hat{p}|^2)^2} \langle \tilde{A}_\rho(p) \tilde{A}_\nu(p) \rangle \end{aligned}$$

$$\begin{aligned}
&= \frac{\delta_{\mu\nu}}{\hat{p}^2} - \sum_{\rho} \frac{\hat{p}_{\mu} \cdot (0, \hat{p})_{\rho}}{|\hat{p}|^2} \frac{\delta_{\rho\nu}}{\hat{p}^2} - \sum_{\sigma} \frac{\hat{p}_{\nu} \cdot (0, \hat{p})_{\sigma}}{|\hat{p}|^2} \frac{\delta_{\mu\sigma}}{\hat{p}^2} + \sum_{\rho, \sigma} \frac{\hat{p}_{\mu} \cdot (0, \hat{p})_{\rho} \hat{p}_{\nu} \cdot (0, \hat{p})_{\sigma}}{(|\hat{p}|^2)^2} \frac{\delta_{\rho\sigma}}{\hat{p}^2} \\
&= \frac{\delta_{\mu\nu}}{\hat{p}^2} - \frac{\hat{p}_{\mu} \cdot (0, \hat{p})_{\nu} + \hat{p}_{\nu} \cdot (0, \hat{p})_{\mu}}{\hat{p}^2 |\hat{p}|^2} + \sum_{\rho} \frac{\hat{p}_{\mu} \cdot (0, \hat{p})_{\rho} \hat{p}_{\nu} \cdot (0, \hat{p})_{\rho}}{\hat{p}^2 (|\hat{p}|^2)^2}.
\end{aligned} \tag{E.21}$$

Now we can insert the propagator in the tadpole and calculate the value of the integral in Coulomb gauge

$$\begin{aligned}
I_T^{\text{Coul}} &= -\frac{e^2 Q^2}{V} \frac{r}{2} \sum_k \sum_{\mu} \left[ \frac{1}{\hat{k}^2} - 2 \frac{\hat{k}_{\mu} \cdot (0, \hat{k})_{\mu}}{\hat{k}^2 |\hat{k}|^2} + \frac{\hat{k}_{\mu}^2 \sum_j \hat{k}_j^2}{\hat{k}^2 (|\hat{k}|^2)^2} \right] = -\frac{e^2 Q^2}{V} \frac{r}{2} \sum_k \left[ \frac{4}{\hat{k}^2} - 2 \frac{\sum_j \hat{k}_j^2}{\hat{k}^2 |\hat{k}|^2} + \frac{\hat{k}^2}{\hat{k}^2 |\hat{k}|^2} \right] \\
&= -\frac{e^2 Q^2}{V} \frac{r}{2} \sum_k \left[ \frac{4}{\hat{k}^2} - \frac{2}{\hat{k}^2} + \frac{1}{|\hat{k}|^2} \right] = -\frac{e^2 Q^2}{V} \frac{r}{2} \sum_k \left[ \frac{2}{\hat{k}^2} + \frac{1}{|\hat{k}|^2} \right].
\end{aligned} \tag{E.22}$$

The tadpole result in Coulomb gauge is the same quoted in Ref. (Duncan *et al.*, 1996).

### Sunset in Feynman gauge

$$\begin{aligned}
I_S^{\text{Feyn}} &= \left. \begin{array}{c} k \\ \text{---} \\ \mu \quad p-k \quad \nu \\ \text{---} \end{array} \right|_{p=0, m=0} = \sum_k \sum_{\mu, \nu} (V_1)_{\nu}(-k, 0) S(-k) (V_1)_{\mu}(0, -k) G_{\mu\nu}(k) \\
&= -\frac{e^2 Q^2}{V} \sum_k \sum_{\mu, \nu, \sigma} \frac{\delta_{\mu\nu}}{\hat{k}^2} \left[ \gamma_{\nu} \cos\left(\frac{k_{\nu}}{2}\right) + ir \sin\left(\frac{k_{\nu}}{2}\right) \right] \frac{\frac{r}{2} \hat{k}_{\sigma}^2 + i \gamma_{\sigma} \bar{k}_{\sigma}}{\frac{r^2}{4} (\hat{k}^2)^2 + \bar{k}^2} \\
&\quad \times \left[ \gamma_{\mu} \cos\left(\frac{k_{\mu}}{2}\right) + ir \sin\left(\frac{k_{\mu}}{2}\right) \right].
\end{aligned} \tag{E.23}$$

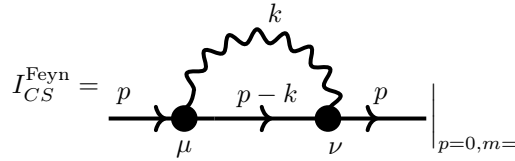
We retain only the even functions of  $k$  since the integration is done in a symmetric interval, this gives us

$$\begin{aligned}
I_S^{\text{Feyn}} &= -\frac{e^2 Q^2}{V} \sum_k \sum_{\mu, \sigma} \frac{1}{\hat{k}^2} \frac{1}{\frac{r^2}{4} (\hat{k}^2)^2 + \bar{k}^2} \left[ \gamma_{\mu}^2 \frac{r}{2} \hat{k}_{\sigma}^2 \cos^2\left(\frac{k_{\mu}}{2}\right) + \gamma_{\mu} \gamma_{\sigma} (i)^2 r \bar{k}_{\sigma} \sin\left(\frac{k_{\mu}}{2}\right) \cos\left(\frac{k_{\mu}}{2}\right) \right. \\
&\quad \left. + (ir)^2 \frac{r}{2} \sin^2\left(\frac{k_{\mu}}{2}\right) \hat{k}_{\sigma}^2 + \gamma_{\sigma} \gamma_{\mu} (i)^2 r \bar{k}_{\sigma} \sin\left(\frac{k_{\mu}}{2}\right) \cos\left(\frac{k_{\mu}}{2}\right) \right] \\
&= -\frac{e^2 Q^2}{V} \sum_k \sum_{\mu, \sigma} \frac{1}{\hat{k}^2} \frac{1}{\frac{r^2}{4} (\hat{k}^2)^2 + \bar{k}^2} \left[ \frac{r}{2} \hat{k}_{\sigma}^2 \left(1 - \sin^2\left(\frac{k_{\mu}}{2}\right)\right) - r \bar{k}_{\sigma} \frac{1}{2} \sin(k_{\mu}) \underbrace{\{\gamma_{\mu}, \gamma_{\sigma}\}}_{2\delta_{\mu\sigma}} \right. \\
&\quad \left. - \frac{r^3}{2} \sin^2\left(\frac{k_{\mu}}{2}\right) \hat{k}_{\sigma}^2 \right] \\
&= -\frac{e^2 Q^2}{V} \sum_k \sum_{\mu, \sigma} \frac{1}{\hat{k}^2} \frac{1}{\frac{r^2}{4} (\hat{k}^2)^2 + \bar{k}^2} \left[ \frac{r}{2} \hat{k}_{\sigma}^2 \left(1 - \frac{\hat{k}_{\mu}^2}{4}\right) - r \bar{k}_{\sigma} \bar{k}_{\mu} \delta_{\mu\sigma} - \frac{r^3}{2} \frac{\hat{k}_{\mu}^2}{4} \hat{k}_{\sigma}^2 \right]
\end{aligned}$$



$$\begin{aligned}
&= -\frac{e^2 Q^2}{V} \sum_k \frac{1}{\hat{k}^2} \frac{r}{\frac{r^2}{4} (\hat{k}^2)^2 + \bar{k}^2} \left[ \frac{\hat{k}^2}{2} \left( 1 - \frac{\hat{k}^2}{4} \right) - \bar{k}^2 - \frac{r^2}{2} \frac{(\hat{k}^2)^2}{4} \right] \\
&= -\frac{e^2 Q^2}{V} r \sum_k \frac{1}{\hat{k}^2} \frac{1}{\frac{r^2}{4} (\hat{k}^2)^2 + \bar{k}^2} \left[ 2\hat{k}^2 - \frac{(\hat{k}^2)^2}{8} - \bar{k}^2 - \frac{r^2}{8} (\hat{k}^2)^2 - \frac{\bar{k}^2}{2} + \frac{\bar{k}^2}{2} \right] \\
&= -\frac{e^2 Q^2}{V} \frac{r}{2} \sum_k \frac{1}{\hat{k}^2} \left[ \frac{\hat{k}^2 (4 - \hat{k}^2/4) - \bar{k}^2}{\frac{r^2}{4} (\hat{k}^2)^2 + \bar{k}^2} - 1 \right]. \tag{E.24}
\end{aligned}$$

### Clover sunset in Feynman gauge



$$\begin{aligned}
I_{CS}^{\text{Feyn}} &= \sum_k \sum_{\mu, \nu} (V_c)_\nu(-k, 0) S(-k) (V_c)_\mu(0, -k) G_{\mu\nu}(k) \\
&= \frac{r^2 c_{sw}^2 e^2 Q^2}{4V} \sum_k \sum_{\mu, \nu, \rho, \sigma, \gamma} \frac{\delta_{\mu\nu}}{\hat{k}^2} \left[ -\sigma_{\nu\rho} \sin k_\rho \cos \left( \frac{k_\nu}{2} \right) \right] \frac{\frac{r}{2} \hat{k}_\gamma^2 + i\gamma_\gamma \bar{k}_\gamma}{\frac{r^2}{4} (\hat{k}^2)^2 + \bar{k}^2} \sigma_{\mu\sigma} \sin k_\sigma \cos \left( \frac{k_\mu}{2} \right). \tag{E.25}
\end{aligned}$$

As usual we take only the even powers in  $k$  and we get

$$I_{CS}^{\text{Feyn}} = -\frac{r^3 c_{sw}^2 e^2 Q^2}{8V} \sum_{k, \mu, \rho, \sigma} \frac{\hat{k}^2}{\hat{k}^2} \frac{\sigma_{\mu\rho} \sigma_{\mu\sigma} \bar{k}_\sigma \bar{k}_\rho (1 - \hat{k}_\mu^2/4)}{\frac{r^2}{4} (\hat{k}^2)^2 + \bar{k}^2}. \tag{E.26}$$

We need to find what is the product of the two antisymmetric tensors

$$4\sigma_{\mu\rho} \sigma_{\mu\sigma} = [\gamma_\mu, \gamma_\rho][\gamma_\mu, \gamma_\sigma] = (\gamma_\mu \gamma_\rho - \gamma_\rho \gamma_\mu) (\gamma_\mu \gamma_\sigma - \gamma_\sigma \gamma_\mu) = 4\delta_{\rho\sigma} \delta_{\mu\sigma} - 2\gamma_\mu \gamma_\rho \gamma_\sigma \gamma_\mu - 2\gamma_\mu \gamma_\sigma \gamma_\rho \gamma_\mu. \tag{E.27}$$

The product  $\sigma_{\mu\rho} \sigma_{\mu\sigma}$  is contracted with  $\bar{k}_\sigma \bar{k}_\rho$  that is symmetric with respect to  $\sigma$  and  $\rho$ , this means we can retain only the symmetric part of the product with respect to  $\sigma$  and  $\rho$ , i.e.

$$\begin{aligned}
4\sigma_{\mu\rho} \sigma_{\mu\sigma} \bar{k}_\sigma \bar{k}_\rho &= 4\delta_{\rho\sigma} \delta_{\mu\sigma} \bar{k}_\sigma \bar{k}_\rho - 2\gamma_\mu \frac{1}{2} \{\gamma_\rho, \gamma_\sigma\} \gamma_\mu \bar{k}_\sigma \bar{k}_\rho - 2\frac{1}{2} \{\gamma_\rho, \gamma_\sigma\} \bar{k}_\sigma \bar{k}_\rho \\
&= 4\delta_{\rho\sigma} \delta_{\mu\sigma} \bar{k}_\sigma \bar{k}_\rho - 2\delta_{\rho\sigma} \bar{k}_\sigma \bar{k}_\rho - 2\delta_{\rho\sigma} \bar{k}_\sigma \bar{k}_\rho = 4\bar{k}_\sigma \bar{k}_\rho (\delta_{\rho\sigma} \delta_{\mu\sigma} - \delta_{\rho\sigma}). \tag{E.28}
\end{aligned}$$

The substituting back in the original integral we get

$$I_{CS}^{\text{Feyn}} = -\frac{r^3 c_{sw}^2 e^2 Q^2}{8V} \sum_{k, \mu, \rho, \sigma} \frac{1 - \hat{k}_\mu^2/4}{\frac{r^2}{4} (\hat{k}^2)^2 + \bar{k}^2} \bar{k}_\sigma \bar{k}_\rho (\delta_{\rho\sigma} \delta_{\mu\sigma} - \delta_{\rho\sigma}). \tag{E.29}$$

The first term in the parentheses gives

$$\begin{aligned}
\sum_{\mu, \rho, \sigma} \left( 1 - \hat{k}_\mu^2/4 \right) \bar{k}_\sigma \bar{k}_\rho \delta_{\rho\sigma} \delta_{\mu\sigma} &= \sum_{\mu, \sigma} \left( 1 - \hat{k}_\mu^2/4 \right) \bar{k}_\sigma^2 \delta_{\mu\sigma} = \sum_{\mu} \left( 1 - \hat{k}_\mu^2/4 \right) \bar{k}_\mu^2 \\
&= \bar{k}^2 - \frac{1}{4} \sum_{\mu} \hat{k}_\mu^2 \bar{k}_\mu^2 = \bar{k}^2 - \frac{1}{4} \hat{k}^4 + \frac{1}{16} \hat{k}^6, \tag{E.30}
\end{aligned}$$

where we used that  $\sin(x) = 2 \sin(x/2) \cos(x/2)$ . The second term in the parentheses gives

$$\sum_{\mu,\rho,\sigma} \left(1 - \hat{k}_\mu^2/4\right) \bar{k}_\sigma \bar{k}_\rho \delta_{\rho\sigma} = \sum_{\mu,\rho} \left(1 - \hat{k}_\mu^2/4\right) \bar{k}_\rho^2 = \left((4 - \hat{k}^2/4)\right) \bar{k}^2 = 4\bar{k}^2 - \frac{\bar{k}^2 \hat{k}^2}{4}. \quad (\text{E.31})$$

By subtracting the second term to the first one and putting everything together we get the final result

$$I_{CS}^{\text{Feyn}} = \frac{r^3 c_{sw}^2 e^2 Q^2}{8V} \sum_k \frac{3\bar{k}^2 + \hat{k}^4/4 - \hat{k}^6/16 - \hat{k}^2 \bar{k}^2/4}{\frac{r^2}{4} (\hat{k}^2)^2 + \bar{k}^2}. \quad (\text{E.32})$$

### Mixed sunset in Feynman gauge

The first diagram is given by

$$\begin{aligned} I_{M1}^{\text{Feyn}} &= p \left[ \text{Diagram: fermion line with a wavy photon loop} \right] \Big|_{p=0, m=0} = \sum_k \sum_{\mu, \nu} (V_1)_\nu(-k, 0) S(-k) (V_c)_\mu(0, -k) G_{\mu\nu}(k) \\ &= -i \left( \frac{eQ}{\sqrt{V}} \right)^2 \frac{r c_{sw}}{2} \sum_k \sum_{\mu, \nu, \sigma, \rho} \frac{\delta_{\mu\nu}}{\hat{k}^2} \left[ \gamma_\nu \cos\left(\frac{k_\nu}{2}\right) + ir \sin\left(\frac{k_\nu}{2}\right) \right] \frac{\frac{r}{2} \hat{k}_\rho^2 + i\gamma_\rho \bar{k}_\rho}{\frac{r^2}{4} (\hat{k}^2)^2 + \bar{k}^2} \\ &\quad \times \sigma_{\mu\sigma} (-\sin k_\sigma) \cos\left(\frac{k_\mu}{2}\right) \\ &\stackrel{(\text{even in } k)}{=} i \left( \frac{eQ}{\sqrt{V}} \right)^2 \frac{r c_{sw}}{2} \sum_k \sum_{\mu, \sigma, \rho} \frac{ir^2 \hat{k}_\rho^2 \hat{k}_\mu + i\gamma_\mu \gamma_\rho \bar{k}_\rho \cos\left(\frac{k_\mu}{2}\right)}{\hat{k}^2 \left( \frac{r^2}{4} (\hat{k}^2)^2 + \bar{k}^2 \right)} \sigma_{\mu\sigma} \bar{k}_\sigma \cos\left(\frac{k_\mu}{2}\right). \end{aligned} \quad (\text{E.33})$$

The second diagrams is

$$\begin{aligned} I_{M2}^{\text{Feyn}} &= p \left[ \text{Diagram: fermion line with a wavy photon loop} \right] \Big|_{p=0, m=0} = \sum_k \sum_{\mu, \nu} (V_c)_\nu(-k, 0) S(-k) (V_1)_\mu(0, -k) G_{\mu\nu}(k) \\ &= -i \left( \frac{eQ}{\sqrt{V}} \right)^2 \frac{r c_{sw}}{2} \sum_k \sum_{\mu, \nu, \sigma, \rho} \frac{\delta_{\mu\nu}}{\hat{k}^2} \sigma_{\nu\sigma} \sin k_\sigma \cos\left(\frac{k_\nu}{2}\right) \frac{\frac{r}{2} \hat{k}_\rho^2 + i\gamma_\rho \bar{k}_\rho}{\frac{r^2}{4} (\hat{k}^2)^2 + \bar{k}^2} \\ &\quad \times \left[ \gamma_\mu \cos\left(\frac{k_\mu}{2}\right) + ir \sin\left(\frac{k_\mu}{2}\right) \right] \\ &\stackrel{(\text{even in } k)}{=} -i \left( \frac{eQ}{\sqrt{V}} \right)^2 \frac{r c_{sw}}{2} \sum_k \sum_{\mu, \sigma, \rho} \sigma_{\mu\sigma} \bar{k}_\sigma \cos\left(\frac{k_\mu}{2}\right) \frac{ir^2 \hat{k}_\rho^2 \hat{k}_\mu + i\gamma_\rho \gamma_\mu \bar{k}_\rho \cos\left(\frac{k_\mu}{2}\right)}{\hat{k}^2 \left( \frac{r^2}{4} (\hat{k}^2)^2 + \bar{k}^2 \right)}. \end{aligned} \quad (\text{E.34})$$

By putting the two diagrams together the terms with  $\sigma_{\mu\sigma}$  cancel out because of its antisymmetric nature and we are left with

$$\begin{aligned} I_{M1}^{\text{Feyn}} + I_{M2}^{\text{Feyn}} &= \frac{e^2 Q^2}{V} \frac{rc_{sw}}{2} \sum_k \frac{1}{\hat{k}^2 \left( \frac{r^2}{4} (\hat{k}^2)^2 + \bar{k}^2 \right)} \sum_{\mu, \sigma, \rho} \bar{k}_\sigma \bar{k}_\rho \cos^2 \left( \frac{k_\mu}{2} \right) (\sigma_{\mu\sigma} \gamma_\rho \gamma_\mu - \gamma_\mu \gamma_\rho \sigma_{\mu\sigma}) \\ &= \frac{e^2 Q^2}{V} \frac{rc_{sw}}{2} \sum_{k, \mu, \sigma, \rho} \frac{\bar{k}_\sigma \bar{k}_\rho (1 - \hat{k}_\mu^2/4)}{\hat{k}^2 \left( \frac{r^2}{4} (\hat{k}^2)^2 + \bar{k}^2 \right)} (\sigma_{\mu\sigma} \gamma_\rho \gamma_\mu - \gamma_\mu \gamma_\rho \sigma_{\mu\sigma}). \end{aligned} \quad (\text{E.35})$$

The term with the antisymmetric tensor gives

$$(\sigma_{\mu\sigma} \gamma_\rho \gamma_\mu - \gamma_\mu \gamma_\rho \sigma_{\mu\sigma}) = \frac{1}{2} \delta_{\rho\sigma} - \frac{1}{2} \delta_{\sigma\mu} \delta_{\rho\mu}, \quad (\text{E.36})$$

and collecting everything we get

$$\begin{aligned} I_{M1}^{\text{Feyn}} + I_{M2}^{\text{Feyn}} &= \frac{e^2 Q^2}{V} \frac{rc_{sw}}{4} \sum_{k, \mu, \sigma, \rho} \frac{\bar{k}_\sigma \bar{k}_\rho (1 - \hat{k}_\mu^2/4)}{\hat{k}^2 \left( \frac{r^2}{4} (\hat{k}^2)^2 + \bar{k}^2 \right)} (\delta_{\rho\sigma} - \delta_{\sigma\mu} \delta_{\rho\mu}) \\ &= \frac{e^2 Q^2}{V} \frac{rc_{sw}}{4} \sum_k \frac{1}{\hat{k}^2 \left( \frac{r^2}{4} (\hat{k}^2)^2 + \bar{k}^2 \right)} \left( \sum_{\mu, \rho} \bar{k}_\rho^2 (1 - \hat{k}_\mu^2/4) - \sum_\mu \bar{k}_\mu^2 (1 - \hat{k}_\mu^2/4) \right) \\ &= \frac{e^2 Q^2}{V} \frac{rc_{sw}}{4} \sum_k \frac{3\bar{k}^2 + \hat{k}^4/4 - \hat{k}^6/16 - \hat{k}^2 \bar{k}^2/4}{\hat{k}^2 \left( \frac{r^2}{4} (\hat{k}^2)^2 + \bar{k}^2 \right)}. \end{aligned} \quad (\text{E.37})$$

## Self-energy resummation

We symbolically write the self-energy at 1-loop as

$$\Sigma^1(p; m, e^2) = \text{Sunset Diagram} = \text{Star Diagram} + \text{Leaf Diagram},$$

where for simplicity we assume the sunset diagram to be the sum of the ones with different vertexes insertion, without loss of generality.

By summing insertions of self-energy at 1-loop we get that the dressed propagator is given by

$$\begin{aligned}
\text{Dressed Propagator} &= \text{Bare Propagator} + \text{1-loop self-energy} + \text{2-loop self-energy} + \dots \\
&= \text{Bare Propagator} + \text{1-loop self-energy} + \text{2-loop self-energy} + \dots \\
&= \text{Bare Propagator} \left( 1 + \text{1-loop self-energy} + \text{2-loop self-energy} + \dots \right) \\
&= \text{Bare Propagator} \left( \sum_{k=0}^{\infty} \text{1-loop self-energy}^k \right) = \frac{\text{Bare Propagator}}{1 - \text{1-loop self-energy}} \\
&= \frac{1}{m + \frac{r}{2}\hat{p}^2 + i\hat{p} - \Sigma^1(p; m, e^2)},
\end{aligned}$$

where we noticed that the series of insertions of self-energy give rise to the geometric series. The  $\Sigma^1(p; m, e^2)$  is a function of the bare parameters. Now we add a mass counterterm to the Lagrangian  $\delta m \bar{\psi}\psi$  that gives the following additional vertex

$$\text{---} \times \text{---} \equiv \delta m. \quad (\text{E.38})$$

We interpret the renormalized mass as  $m_R = m + \delta m$  and replace in the self-energy calculations  $m$  with  $m_R$ :  $\Sigma^1(p; m, e^2) \rightarrow \Sigma^1(p; m_R, e^2)$ . The inverse propagator gets modified as

$$m_R + \frac{r}{2}\hat{p}^2 + i\hat{p} - (\Sigma^1(p; m_R, e^2) + \delta m). \quad (\text{E.39})$$

We require that the propagator has a pole when the renormalized mass and momentum vanishes, i.e.  $m_R = 0$  and  $p = 0$ . By imposing the condition we get the value of  $\delta m$

$$\begin{aligned}
m_R + \frac{r}{2}\hat{p}^2 + i\hat{p} - (\Sigma^1(p; m_R, e^2) + \delta m) \Big|_{m_R=0, p=0} &= -\Sigma^1(p=0; m_R=0, e^2) - \delta m = 0 \\
\Rightarrow \delta m = -\Sigma^1(p=0; m_R=0, e^2) &= - \left( \text{1-loop self-energy} + \text{2-loop self-energy} \right)_{m_R=0, p=0}.
\end{aligned} \quad (\text{E.40})$$

The critical mass  $m_c$  is the bare mass for which the renormalized mass is vanishing, i.e.  $m_c = -\delta m$ , and in terms of that we have the following relation

$$m_R = m - m_c = m - \Sigma^1(p=0; m_R=0, e^2) = m - (I_T + I_S + I_{CS} + I_{M1} + I_{M2}). \quad (\text{E.41})$$

### E.3 Tadpole improved lattice perturbation theory

We improve the perturbation theory result by summing a subclass of tadpole diagrams, which in the case of gluons (QCD) are called cactus diagrams (Constantinou *et al.*, 2006), to all order in perturbation theory. This procedure is an example of one-sided resummation, meaning that we will resum only tadpole insertions at the same locations. In principle this can ruin the partial cancellation between diagrams that are resummed and the one that are not, furthermore it may spoil the gauge invariance of the result.

In QED the gauge invariance is lost by resumming only tadpole diagrams. But the biggest effect is given by the tadpole diagrams hence the tadpole resummation is expected to capture most of the cutoff effects, see (Duncan *et al.*, 1996).

By expanding the interaction part of the action we get that the tadpole diagrams come as

$$\begin{aligned} \text{Impr} &= \text{Diagram} = \text{Diagram} + \text{Diagram} + \dots \\ &= - \sum_{n=1} \frac{(e^2 Q^2)^n}{(2n)! V^n} \left( \sum_k \sum_\mu G_{\mu\mu}(k) \right)^n (2n-1)!!, \end{aligned} \quad (\text{E.42})$$

where we wrote explicitly the integrals after contractions. There is an overall minus since the vertexes come all from the even powers of the interactions that gives  $(ieQ)^{2n}$  and each vertex comes with a factorial  $(2n)!$ , there is also a symmetry factor in the contractions of the photon legs that gives  $(2n-1)!!$ . We notice that the factor  $(2n)!/(2n-1)!! = (2n)!! = 2^n n!$  and from this we conclude that

$$\begin{aligned} \text{Impr} &= - \sum_{n=1} \frac{1}{n!} \left( \frac{e^2 Q^2}{V} \frac{1}{2} \sum_k \sum_\mu G_{\mu\mu}(k) \right)^n \\ &= - \sum_{n=1} \frac{1}{n!} [-\Sigma_T^1(p=0; m_R=0, e^2)]^n = 1 - e^{-\Sigma_T^1(0;0,e^2)}. \end{aligned} \quad (\text{E.43})$$

#### Electromagnetic critical mass shift

We imagine to have performed a simulation at a certain value of  $\beta = 6/g^2$  for QCD and we want to calculate in lattice perturbation theory the shift in the critical mass in the full theory. To do so we take the self-energy as the sum of the pure QCD part (from simulations), the pure QED part (from lattice perturbation theory) and the mixed terms in QCD and QED. In the mixed part there are diagrams in which we connect the pure QCD and the pure QED with a massless Dirac-Wilson propagator, and since we are considering zero momentum the only allowed momentum flowing in such propagator is vanishing. The limit of zero momentum of the D-W propagator is

$$\lim_{p \rightarrow 0} \frac{m + \frac{r}{2} \hat{p}^2 - i \hat{p}}{(m + \frac{r}{2} \hat{p}^2)^2 + \hat{p}^2} \Big|_{m=0} \stackrel{r=1}{=} \frac{1}{8} \quad (\text{E.44})$$

In this way we are including all the possible non-1PI diagrams built out of Q(C+E)D. Diagrammatically the self-energy is

$$\Sigma(p=0; m=0) = \text{shaded circle} \simeq \text{star loop} + \text{tadpole} + \text{sun loop} + \text{tadpole with fermion} + \text{sun loop with fermion} + \text{star loop with fermion} + \text{sun loop with fermion} + \text{tadpole with fermion} + \text{star loop with fermion} + \text{tadpole with fermion}.$$

The formula reads

$$\begin{aligned} \Sigma(p=0; m=0) &\simeq \Sigma_e(0;0) + \Sigma_g(0;0) + 2\Sigma_e(0;0) \lim_{k \rightarrow 0} S(k) \Sigma_g(0;0) \\ &= \Sigma_e(0;0) + \Sigma_g(0;0) + \frac{\Sigma_e(0;0) \Sigma_g(0;0)}{4}, \end{aligned} \quad (\text{E.45})$$

where we have a factor two in the last addendum because of the symmetry of the diagrams. Recalling that the critical mass (or the self-energy  $\Sigma$ ) is related to the critical  $\kappa$  (hopping parameter)

$$\kappa_c = \frac{1}{8r + 2\Sigma(0;0)}, \quad (\text{E.46})$$

we get that

$$\begin{aligned} \Delta m_c^{\text{Q(C+E)D}} &\simeq \Sigma(0;0) - \Sigma_g(0;0) = \frac{1}{2\kappa_c} - \frac{1}{2\kappa_c^{e=0}} = \Sigma_e(0;0) + \frac{1}{4} \Sigma_e(0;0) \Sigma_g(0;0) \\ &= \Sigma_e(0;0) + \frac{1}{4} \Sigma_e(0;0) \left( \frac{1}{2\kappa_c^{e=0}} - 4 \right) = \frac{\Sigma_e(0;0)}{8\kappa_c^{e=0}}. \end{aligned} \quad (\text{E.47})$$

We found the electromagnetic shift to the critical mass in the approximation where we sum only the self-energies from QCD and QED connected by a fermion line.

We can approximate the EM self-energy with 1-loop result and write

$$\Delta m_c^{\text{Q(C+E)D}} \simeq \frac{\Sigma_e^1(0;0)}{8\kappa_c^{e=0}}. \quad (\text{E.48})$$

We can also take as approximate EM self-energy the tadpole resummed one in Eq. E.43 we get that the shift is given by

$$\Delta m_c^{\text{Q(C+E)D}} \simeq \frac{\Sigma_e^{\text{T}}(0;0)}{8\kappa_c^{e=0}} = \frac{1}{8\kappa_c^{e=0}} \left( 1 - e^{-\Sigma_T^1(0;0,e^2)} \right) = \frac{1}{8\kappa_c^{e=0}} \left( 1 - e^{\delta m_{em}} \right). \quad (\text{E.49})$$

## Appendix F

# Explicit form of the HVP

Here we perform the Wick contractions for Eq. 5.3.29, and we set  $r = 1$ . As an example we work out only the following contribution, one out of four,

$$\frac{1}{4} \sum_{f,f'} [\bar{\psi}_f(n + \hat{\mu})(1 + \gamma_\mu)U_\mu^\dagger(n)\psi_f(n)] [\bar{\psi}_{f'}(\hat{\nu})(1 + \gamma_\nu)U_\nu^\dagger(0)\psi_{f'}(0)]. \quad (\text{F.1})$$

We write all the indexes out,  $f, f'$  are the flavor ones,  $\alpha, \beta, \gamma, \delta$  the Dirac ones and  $b, c, d$  the color ones, and we calculate the fermionic part of the expectation value ( $\langle \dots \rangle_{\text{F}} = \prod_f^{N_f} \langle \dots \rangle_{\text{f}}$ ) that factorizes with respect to flavor

$$\begin{aligned} I &= \frac{1}{4} \sum_{f,f'} \left\langle \bar{\psi}_f^{a,\alpha}(n + \hat{\mu})(1 + \gamma_\mu)_{\alpha\beta} (U_\mu^\dagger(n))_{ab} \psi_f^{b,\beta}(n) \bar{\psi}_{f'}^{c,\gamma}(\hat{\nu})(1 + \gamma_\nu)_{\gamma\delta} (U_\nu^\dagger(0))_{cd} \psi_{f'}^{d,\gamma}(0) \right\rangle_{\text{F}} \\ &= \sum_{f,f'} \frac{1}{4} (1 + \gamma_\mu)_{\alpha\beta} (U_\mu^\dagger(n))_{ab} (1 + \gamma_\nu)_{\gamma\delta} (U_\nu^\dagger(0))_{cd} \left\langle \bar{\psi}_f^{a,\alpha}(n + \hat{\mu}) \psi_f^{b,\beta}(n) \bar{\psi}_{f'}^{c,\gamma}(\hat{\nu}) \psi_{f'}^{d,\gamma}(0) \right\rangle_{\text{F}}. \end{aligned} \quad (\text{F.2})$$

We recall that Wick contractions give the propagator,

$$\langle \psi^{a,\alpha}(n) \bar{\psi}^{b,\beta}(m) \rangle = (D^{-1}(n, m))_{ab}^{\alpha\beta}, \quad (\text{F.3})$$

and can be used to obtain

$$\begin{aligned} I &= \frac{(-1)^2}{4} (1 + \gamma_\mu)_{\alpha\beta} (U_\mu^\dagger(n))_{ab} (1 + \gamma_\nu)_{\gamma\delta} (U_\nu^\dagger(0))_{cd} \left\{ \sum_{f \neq f'} \left\langle \psi_f^{b,\beta}(n) \bar{\psi}_f^{a,\alpha}(n + \hat{\mu}) \right\rangle_f \right. \\ &\quad \times \left. \left\langle \psi_{f'}^{d,\gamma}(0) \bar{\psi}_{f'}^{c,\gamma}(\hat{\nu}) \right\rangle_{f'} + \sum_f \left\langle \psi_f^{d,\gamma}(0) \bar{\psi}_f^{a,\alpha}(n + \hat{\mu}) \right\rangle_f \left\langle \psi_f^{b,\beta}(n) \bar{\psi}_f^{c,\gamma}(\hat{\nu}) \right\rangle_{f'} \right\} \\ &= \frac{1}{4} (1 + \gamma_\mu)_{\alpha\beta} (U_\mu^\dagger(n))_{ab} (1 + \gamma_\nu)_{\gamma\delta} (U_\nu^\dagger(0))_{cd} \left\{ \sum_{f \neq f'} (D_f^{-1}(n + \hat{\mu}, n))_{ab}^{\alpha\beta} (D_{f'}^{-1}(\hat{\nu}, 0))_{dc}^{\delta\gamma} \right. \\ &\quad \left. + \sum_f (D_f^{-1}(n + \hat{\mu}, 0))_{ab}^{\alpha\beta} (D_f^{-1}(\hat{\nu}, n))_{dc}^{\delta\gamma} \right\}. \end{aligned} \quad (\text{F.4})$$

In the first step we used the factorization of the fermionic expectation value with respect to flavor and we divided the case in which  $f = f'$  and  $f \neq f'$ , recalling that the fermionic variables are Grassmann variables and they anticommute. In the second step we performed the Wick contraction and displayed the propagator.

By collecting all the indexes together we get

$$\begin{aligned}
 I &= \frac{1}{4} \left( \underbrace{\sum_f \text{Tr} \left\{ D_f^{-1}(n + \hat{\mu}, n) U_\mu^\dagger(n) (1 + \gamma_\mu) \right\}}_{\text{disconnected piece}} \right) \left( \sum_{f'} \text{Tr} \left\{ D_{f'}^{-1}(\hat{\nu}, 0) U_\nu^\dagger(0) (1 + \gamma_\nu) \right\} \right) \\
 &+ \frac{1}{4} \underbrace{\sum_f \text{Tr} \left\{ (1 + \gamma_\nu) U_\nu^\dagger(0) D_f^{-1}(n + \hat{\mu}, 0) (1 + \gamma_\mu) U_\mu^\dagger(n) D_f^{-1}(\hat{\nu}, n) \right\}}_{\text{connected piece}}. \quad (\text{F.5})
 \end{aligned}$$

By using  $\gamma_5$ -hermiticity of the Dirac-Wilson operator ( $D^{-1} = \gamma_5 (D^\dagger)^{-1} \gamma_5$ ) we obtain

$$I_{\text{connected}} = \frac{1}{4} \sum_f \text{Tr} \left\{ (1 + \gamma_\nu) U_\nu^\dagger(0) \gamma_5 \left[ (D^\dagger)_f^{-1}(0, n + \hat{\mu}) \right] \gamma_5 (1 + \gamma_\mu) U_\mu^\dagger(n) D_f^{-1}(\hat{\nu}, n) \right\}. \quad (\text{F.6})$$

Analogously one can calculate the other pieces of the product and eventually obtain, for the connected part,

$$\begin{aligned}
 \Pi_{\mu\nu}^{\text{connected}}(n) &= \frac{1}{4} \sum_f \left( \text{Tr} \left\{ (1 + \gamma_\nu) U_\nu^\dagger(0) \gamma_5 \left[ (D^\dagger)_f^{-1}(0, n + \hat{\mu}) \right] \gamma_5 (1 + \gamma_\mu) U_\mu^\dagger(n) D_f^{-1}(\hat{\nu}, n) \right. \right. \\
 &\quad - (1 - \gamma_\nu) U_\nu(0) \gamma_5 \left[ (D^\dagger)_f^{-1}(\hat{\nu}, n + \hat{\mu}) \right] \gamma_5 (1 + \gamma_\mu) U_\mu^\dagger(n) D_f^{-1}(0, n) \\
 &\quad - (1 + \gamma_\nu) U_\nu^\dagger(0) \gamma_5 \left[ (D^\dagger)_f^{-1}(0, n) \right] \gamma_5 (1 - \gamma_\mu) U_\mu(n) D_f^{-1}(\hat{\nu}, n + \hat{\mu}) \\
 &\quad \left. \left. + (1 - \gamma_\nu) U_\nu(0) \gamma_5 \left[ (D^\dagger)_f^{-1}(\hat{\nu}, n) \right] \gamma_5 (1 - \gamma_\mu) U_\mu(n) D_f^{-1}(0, n + \hat{\mu}) \right\} \right). \quad (\text{F.7})
 \end{aligned}$$

The contraction for Eq. 5.3.30, the contact term, are done in the same way

$$\begin{aligned}
 \Pi_{\mu\nu}^{\text{ct}}(0) &= -\frac{\delta_{\mu\nu}}{2} \sum_f \left\langle \bar{\psi}_f(0) U_\mu(0) (1 - \gamma_\mu) \psi_f(\hat{\mu}) + \bar{\psi}_f(\hat{\mu}) U_\mu^\dagger(0) (\gamma_\mu + 1) \psi_f(0) \right\rangle_{\text{F}} \\
 &= -\frac{\delta_{\mu\nu}}{2} \sum_f \left\langle \bar{\psi}_f^{a,\alpha}(0) (U_\mu(0))_{ab} (1 - \gamma_\mu)_{\alpha\beta} \psi_f^{b,\beta}(\hat{\mu}) + \bar{\psi}_f^{a,\alpha}(\hat{\mu}) (U_\mu^\dagger(0))_{ab} (\gamma_\mu + 1)_{\alpha\beta} \psi_f^{b,\beta}(0) \right\rangle_f \\
 &= (-)^2 \frac{\delta_{\mu\nu}}{2} \sum_f \left[ (U_\mu(0))_{ab} (1 - \gamma_\mu)_{\alpha\beta} \left\langle \psi_f^{b,\beta}(\hat{\mu}) \bar{\psi}_f^{a,\alpha}(0) \right\rangle_f \right. \\
 &\quad \left. + (U_\mu^\dagger(0))_{ab} (\gamma_\mu + 1)_{\alpha\beta} \left\langle \psi_f^{b,\beta}(0) \bar{\psi}_f^{a,\alpha}(\hat{\mu}) \right\rangle_f \right]
 \end{aligned}$$



$$\begin{aligned}
&= \frac{\delta_{\mu\nu}}{2} \sum_f \left[ (U_\mu(0))_{ab} (1 - \gamma_\mu)_{\alpha\beta} \left( D_f^{-1}(0, \hat{\mu}) \right)_{ba}^{\beta\alpha} + (U_\mu^\dagger(0))_{ab} (\gamma_\mu + 1)_{\alpha\beta} \left( D_f^{-1}(\hat{\mu}, 0) \right)_{ba}^{\beta\alpha} \right] \\
&= \frac{\delta_{\mu\nu}}{2} \sum_f \left( \text{Tr} \left\{ (1 - \gamma_\mu) U_\mu(0) \left[ D_f^{-1}(0, \hat{\mu}) \right] + (1 + \gamma_\mu) U_\mu^\dagger(0) \left[ D_f^{-1}(\hat{\mu}, 0) \right] \right\} \right) \\
&= \frac{\delta_{\mu\nu}}{2} \sum_f \left( \text{Tr} \left\{ (1 - \gamma_\mu) U_\mu(0) \gamma_5 \left[ (D_f^\dagger)^{-1}(\hat{\mu}, 0) \right] \gamma_5 + (1 + \gamma_\mu) U_\mu^\dagger(0) \left[ D_f^{-1}(\hat{\mu}, 0) \right] \right\} \right), \quad (\text{F.8})
\end{aligned}$$

and by recalling that  $\{\gamma_5, \gamma_\mu\} = 0 \Rightarrow \gamma_5 \gamma_\mu \gamma_5 = -\gamma_\mu$  and  $\gamma_5^2 = \mathbf{1}$ , we find

$$\Pi_{\mu\nu}^{\text{ct}}(0) = \frac{\delta_{\mu\nu}}{2} \sum_f \left( \text{Tr} \left\{ (1 + \gamma_\mu) U_\mu(0) \left[ (D_f^\dagger)^{-1}(\hat{\mu}, 0) \right] + (1 + \gamma_\mu) U_\mu^\dagger(0) \left[ D_f^{-1}(\hat{\mu}, 0) \right] \right\} \right). \quad (\text{F.9})$$

By looking at Eq. F.7 and Eq. F.9 we see that to evaluate  $\Pi_{\mu\nu}$  we need to do five inversions on each gauge field configuration, which make the calculations quite expensive in computer time. The identification with the results in the appendix of (Gockeler *et al.*, 2004) is easily made.

# Bibliography

- [Amsler and others, 2008] Claude Amsler et al. Review of Particle Physics. *Phys. Lett.*, B667:1–1340, 2008.
- [Aoki and others, 2012] S. Aoki et al. 1+1+1 flavor QCD + QED simulation at the physical point. *Phys. Rev.*, D86:034507, 2012.
- [Arthur and Boyle, 2011] R. Arthur and P. A. Boyle. Step Scaling with off-shell renormalisation. *Phys. Rev.*, D83:114511, 2011.
- [Arthur *et al.*, 2016] Rudy Arthur, Vincent Drach, Martin Hansen, Ari Hietanen, Claudio Pica, and Francesco Sannino. SU(2) gauge theory with two fundamental flavors: A minimal template for model building. *Phys. Rev.*, D94(9):094507, 2016.
- [Aubin *et al.*, 2012] Christopher Aubin, Thomas Blum, Maarten Golterman, and Santiago Peris. Model-independent parametrization of the hadronic vacuum polarization and  $g-2$  for the muon on the lattice. *Phys. Rev.*, D86:054509, 2012.
- [Basak and others, 2014] Subhasish Basak et al. Finite-volume effects and the electromagnetic contributions to kaon and pion masses. *PoS, LATTICE2014*:116, 2014.
- [Bedaque, 2004] Paulo F. Bedaque. Aharonov-Bohm effect and nucleon nucleon phase shifts on the lattice. *Phys. Lett.*, B593:82–88, 2004.
- [Bernecker and Meyer, 2011] David Bernecker and Harvey B. Meyer. Vector Correlators in Lattice QCD: Methods and applications. *Eur. Phys. J.*, A47:148, 2011.
- [Bloch and Nordsieck, 1937] F. Bloch and A. Nordsieck. Note on the Radiation Field of the electron. *Phys. Rev.*, 52:54–59, 1937.
- [Blum and others, 2016] T. Blum et al. Lattice calculation of the leading strange quark-connected contribution to the muon  $g - 2$ . *JHEP*, 04:063, 2016. [Erratum: *JHEP*05,034(2017)].
- [Blum *et al.*, 2007] Thomas Blum, Takumi Doi, Masashi Hayakawa, Taku Izubuchi, and Norikazu Yamada. Determination of light quark masses from the electromagnetic splitting of pseudoscalar meson masses computed with two flavors of domain wall fermions. *Phys. Rev.*, D76:114508, 2007.
- [Blum *et al.*, 2010] T. Blum, R. Zhou, T. Doi, M. Hayakawa, T. Izubuchi, S. Uno, and N. Yamada. Electromagnetic mass splittings of the low lying hadrons and quark masses from 2+1 flavor lattice QCD+QED. *Phys. Rev.*, D82:094508, 2010.
- [Blum *et al.*, 2012] T. Blum, M. Hayakawa, and T. Izubuchi. Hadronic corrections to the muon anomalous magnetic moment from lattice QCD. *PoS, LATTICE2012*:022, 2012.

- [Blum, 2003] T. Blum. Lattice calculation of the lowest order hadronic contribution to the muon anomalous magnetic moment. *Phys. Rev. Lett.*, 91:052001, 2003.
- [Bochicchio *et al.*, 1985] Marco Bochicchio, Luciano Maiani, Guido Martinelli, Gian Carlo Rossi, and Massimo Testa. Chiral Symmetry on the Lattice with Wilson Fermions. *Nucl. Phys.*, B262:331, 1985.
- [Borasoy and Krebs, 2005] B. Borasoy and H. Krebs. Greens function of a free massive scalar field on the lattice. *Phys. Rev.*, D72:056003, 2005.
- [Borsanyi and others, 2015] Sz. Borsanyi *et al.* Ab initio calculation of the neutron-proton mass difference. *Science*, 347:1452–1455, 2015.
- [Boyle *et al.*, 2008] P. A. Boyle, A. Jüttner, C. Kelly, and R. D. Kenway. Use of stochastic sources for the lattice determination of light quark physics. *JHEP*, 08:086, 2008.
- [Boyle *et al.*, 2016] Peter Boyle, Vera Gülpers, James Harrison, Andreas Jüttner, Antonin Portelli, and Christopher Sachrajda. Electromagnetic Corrections to Meson Masses and the HVP. *PoS, LATTICE2016:172*, 2016.
- [Brandt *et al.*, 2013] Bastian B. Brandt, Andreas Jüttner, and Hartmut Wittig. The pion vector form factor from lattice QCD and NNLO chiral perturbation theory. *JHEP*, 11:034, 2013.
- [Brandt *et al.*, 2016] Bastian B Brandt, Gunnar Bali, Gergely Endrödi, and Benjamin Glässle. QCD spectroscopy and quark mass renormalisation in external magnetic fields with Wilson fermions. *PoS, LATTICE2015:265*, 2016.
- [Brower *et al.*, 1997] R. C. Brower, T. Ivanenko, A. R. Levi, and K. N. Orginos. Chronological inversion method for the Dirac matrix in hybrid Monte Carlo. *Nucl. Phys.*, B484:353–374, 1997.
- [Bussone and others, 2016] A. Bussone *et al.* Mass of the b quark and B -meson decay constants from  $N_f=2+1+1$  twisted-mass lattice QCD. *Phys. Rev.*, D93(11):114505, 2016.
- [Bussone *et al.*, 2016a] Andrea Bussone, Michele Della Morte, Vincent Drach, Martin Hansen, Ari Hietanen, Jarno Rantaharju, and Claudio Pica. A simple method to optimize HMC performance. *PoS, LATTICE2016:260*, 2016.
- [Bussone *et al.*, 2016b] Andrea Bussone, Michele Della Morte, Martin Hansen, and Claudio Pica. Reweighting twisted boundary conditions. *PoS, LATTICE2015:021*, 2016.
- [Bussone *et al.*, 2017] Andrea Bussone, Michele Della Morte, Martin Hansen, and Claudio Pica. On reweighting for twisted boundary conditions. *Comput. Phys. Commun.*, 2017.
- [Capitani *et al.*, 2015] S. Capitani, M. Della Morte, D. Djukanovic, G. von Hippel, J. Hua, B. Jäger, B. Knippschild, H. B. Meyer, T. D. Rae, and H. Wittig. Nucleon electromagnetic form factors in two-flavor QCD. *Phys. Rev.*, D92(5):054511, 2015.
- [Capitani, 2003] Stefano Capitani. Lattice perturbation theory. *Phys. Rept.*, 382:113–302, 2003.
- [Carloni Calame *et al.*, 2015] C. M. Carloni Calame, M. Passera, L. Trentadue, and G. Venanzoni. A new approach to evaluate the leading hadronic corrections to the muon  $g-2$ . *Phys. Lett.*, B746:325–329, 2015.

- [Chakraborty *et al.*, 2016] Bipasha Chakraborty, C. T. H. Davies, J. Koponen, G. P. Lepage, M. J. Peardon, and S. M. Ryan. Estimate of the hadronic vacuum polarization disconnected contribution to the anomalous magnetic moment of the muon from lattice QCD. *Phys. Rev.*, D93(7):074509, 2016.
- [Chetyrkin *et al.*, 1996] K. G. Chetyrkin, Johann H. Kuhn, and M. Steinhauser. Three loop polarization function and  $O(\alpha_s^2)$  corrections to the production of heavy quarks. *Nucl. Phys.*, B482:213–240, 1996.
- [Clark and Kennedy, 2007] M. A. Clark and A. D. Kennedy. Accelerating dynamical fermion computations using the rational hybrid Monte Carlo (RHMC) algorithm with multiple pseudofermion fields. *Phys. Rev. Lett.*, 98:051601, 2007.
- [Clark *et al.*, 2008] M. A. Clark, A. D. Kennedy, and P. J. Silva. Tuning HMC using Poisson brackets. *PoS, LATTICE2008:041*, 2008.
- [Clark *et al.*, 2010] M. A. Clark, Balint Joo, A. D. Kennedy, and P. J. Silva. Better HMC integrators for dynamical simulations. *PoS, LATTICE2010:323*, 2010.
- [Clark *et al.*, 2011] M. A. Clark, Balint Joo, A. D. Kennedy, and P. J. Silva. Improving dynamical lattice QCD simulations through integrator tuning using Poisson brackets and a force-gradient integrator. *Phys. Rev.*, D84:071502, 2011.
- [Constantinou *et al.*, 2006] M. Constantinou, H. Panagopoulos, and A. Skouroupathis. Improved perturbation theory for improved lattice actions. *Phys. Rev.*, D74:074503, 2006.
- [Creutz *et al.*, 1979] Michael Creutz, Laurence Jacobs, and Claudio Rebbi. Monte Carlo Study of Abelian Lattice Gauge Theories. *Phys. Rev.*, D20:1915, 1979. [,182(1979)].
- [Curci, 1986] Giuseppe Curci. Infrared Finiteness of Normalization Constants of Currents in Lattice Gauge Theories. *Phys. Lett.*, B167:425–428, 1986.
- [Cè *et al.*, 2017] Marco Cè, Leonardo Giusti, and Stefan Schaefer. A local factorization of the fermion determinant in lattice QCD. *Phys. Rev.*, D95(3):034503, 2017.
- [Davoudi and Savage, 2014] Zohreh Davoudi and Martin J. Savage. Finite-Volume Electromagnetic Corrections to the Masses of Mesons, Baryons and Nuclei. *Phys. Rev.*, D90(5):054503, 2014.
- [de Divitiis *et al.*, 2004] G. M. de Divitiis, R. Petronzio, and N. Tantalo. On the discretization of physical momenta in lattice QCD. *Phys. Lett.*, B595:408–413, 2004.
- [de Divitiis *et al.*, 2013] G. M. de Divitiis, R. Frezzotti, V. Lubicz, G. Martinelli, R. Petronzio, G. C. Rossi, F. Sanfilippo, S. Simula, and N. Tantalo. Leading isospin breaking effects on the lattice. *Phys. Rev.*, D87(11):114505, 2013.
- [DeGrand and Rossi, 1990] Thomas A. DeGrand and Pietro Rossi. Conditioning Techniques for Dynamical Fermions. *Comput. Phys. Commun.*, 60:211–214, 1990.
- [Del Debbio *et al.*, 2010] Luigi Del Debbio, Agostino Patella, and Claudio Pica. Higher representations on the lattice: Numerical simulations. SU(2) with adjoint fermions. *Phys. Rev.*, D81:094503, 2010.

- [Della Morte and Giusti, 2011] Michele Della Morte and Leonardo Giusti. A novel approach for computing glueball masses and matrix elements in Yang-Mills theories on the lattice. *JHEP*, 05:056, 2011.
- [Della Morte *et al.*, 2012] Michele Della Morte, Benjamin Jager, Andreas Juttner, and Hartmut Wittig. Towards a precise lattice determination of the leading hadronic contribution to  $(g - 2)_\mu$ . *JHEP*, 03:055, 2012.
- [Della Morte *et al.*, 2014] Michele Della Morte, Samantha Dooling, Jochen Heitger, Dirk Hesse, and Hubert Simma. Matching of heavy-light flavour currents between HQET at order  $1/m$  and QCD: I. Strategy and tree-level study. *JHEP*, 05:060, 2014.
- [Della Morte *et al.*, 2017] M. Della Morte, A. Francis, V. Gülpers, G. Herdoíza, G. von Hippel, H. Horch, B. Jäger, H. B. Meyer, A. Nyffeler, and H. Wittig. The hadronic vacuum polarization contribution to the muon  $g - 2$  from lattice QCD. 2017.
- [Di Chiara *et al.*, 2017] Stefano Di Chiara, Andrew Fowlie, Sean Fraser, Carlo Marzo, Luca Marzola, Martti Raidal, and Christian Spethmann. Minimal flavor-changing  $Z'$  models and muon  $g - 2$  after the  $R_{K^*}$  measurement. 2017.
- [Duane *et al.*, 1987] S. Duane, A. D. Kennedy, B. J. Pendleton, and D. Roweth. Hybrid Monte Carlo. *Phys. Lett.*, B195:216–222, 1987.
- [Duncan *et al.*, 1996] A. Duncan, E. Eichten, and H. Thacker. Electromagnetic splittings and light quark masses in lattice QCD. *Phys. Rev. Lett.*, 76:3894–3897, 1996.
- [Durr and Della Morte, 2004] S. Durr and M. Della Morte. Exploring two nonperturbative definitions of  $c(A)$ . *Nucl. Phys. Proc. Suppl.*, 129:417–419, 2004. [417(2003)].
- [Endres *et al.*, 2016] Michael G. Endres, Andrea Shindler, Brian C. Tiburzi, and Andre Walker-Loud. Massive photons: an infrared regularization scheme for lattice QCD+QED. *Phys. Rev. Lett.*, 117(7):072002, 2016.
- [Faddeev and Popov, 1967] L. D. Faddeev and V. N. Popov. Feynman Diagrams for the Yang-Mills Field. *Phys. Lett.*, 25B:29–30, 1967.
- [Finkenrath *et al.*, 2012] Jacob Finkenrath, Francesco Knechtli, and Bjorn Leder. Application of Domain Decomposition to the Evaluation of Fermion Determinant Ratios. *PoS, LATTICE2012*:190, 2012.
- [Finkenrath *et al.*, 2013] Jacob Finkenrath, Francesco Knechtli, and Björn Leder. One flavor mass reweighting in lattice QCD. *Nucl. Phys.*, B877:441–456, 2013. [Erratum: Nucl. Phys.B880,574(2014)].
- [Flynn *et al.*, 2007] J. M. Flynn, A. Juttner, C. T. Sachrajda, P. A. Boyle, and J. M. Zanotti. Hadronic form factors in Lattice QCD at small and vanishing momentum transfer. *JHEP*, 05:016, 2007.
- [Frezzotti *et al.*, 2000] Roberto Frezzotti, Pietro Antonio Grassi, Stefan Sint, and Peter Weisz. A Local formulation of lattice QCD without unphysical fermion zero modes. *Nucl. Phys. Proc. Suppl.*, 83:941–946, 2000.
- [Fritzsch *et al.*, 2012] Patrick Fritzsch, Francesco Knechtli, Bjorn Leder, Marina Marinkovic, Stefan Schaefer, Rainer Sommer, and Francesco Virotta. The strange quark mass and Lambda parameter of two flavor QCD. *Nucl. Phys.*, B865:397–429, 2012.

- [Gattringer and Lang, 2010] Christof Gattringer and Christian B. Lang. Quantum chromodynamics on the lattice. *Lect. Notes Phys.*, 788:1–343, 2010.
- [Gockeler *et al.*, 2004] M. Gockeler, R. Horsley, W. Kurzinger, D. Pleiter, Paul E. L. Rakow, and G. Schierholz. Vacuum polarization and hadronic contribution to muon  $g-2$  from lattice QCD. *Nucl. Phys.*, B688:135–164, 2004.
- [Goldstone, 1961] J. Goldstone. Field Theories with Superconductor Solutions. *Nuovo Cim.*, 19:154–164, 1961.
- [Golterman *et al.*, 2014] Maarten Golterman, Kim Maltman, and Santiago Peris. New strategy for the lattice evaluation of the leading order hadronic contribution to  $(g - 2)_\mu$ . *Phys. Rev.*, D90(7):074508, 2014.
- [Gupta *et al.*, 1990] Sourendu Gupta, A. Irback, F. Karsch, and B. Petersson. The Acceptance Probability in the Hybrid Monte Carlo Method. *Phys. Lett.*, B242:437–443, 1990.
- [Hasenbusch and Jansen, 2003] M. Hasenbusch and K. Jansen. Speeding up lattice QCD simulations with clover improved Wilson fermions. *Nucl. Phys.*, B659:299–320, 2003.
- [Hasenbusch, 2001] Martin Hasenbusch. Speeding up the hybrid Monte Carlo algorithm for dynamical fermions. *Phys. Lett.*, B519:177–182, 2001.
- [Hayakawa and Uno, 2008] Masashi Hayakawa and Shunpei Uno. QED in finite volume and finite size scaling effect on electromagnetic properties of hadrons. *Prog. Theor. Phys.*, 120:413–441, 2008.
- [Hietanen *et al.*, 2014] Ari Hietanen, Randy Lewis, Claudio Pica, and Francesco Sannino. Fundamental Composite Higgs Dynamics on the Lattice: SU(2) with Two Flavors. *JHEP*, 07:116, 2014.
- [Iwasaki, 1985] Y. Iwasaki. Renormalization Group Analysis of Lattice Theories and Improved Lattice Action: Two-Dimensional Nonlinear O(N) Sigma Model. *Nucl. Phys.*, B258:141–156, 1985.
- [Jackson, 1998] John David Jackson. *Classical Electrodynamics*. Wiley, 1998.
- [Jegerlehner and Nyffeler, 2009] Fred Jegerlehner and Andreas Nyffeler. The Muon  $g-2$ . *Phys. Rept.*, 477:1–110, 2009.
- [Joo *et al.*, 2000] Balint Joo, Brian Pendleton, Anthony D. Kennedy, Alan C. Irving, James C. Sexton, Stephen M. Pickles, and Stephen P. Booth. Instability in the molecular dynamics step of hybrid Monte Carlo in dynamical Fermion lattice QCD simulations. *Phys. Rev.*, D62:114501, 2000.
- [Kaplan, 1992] David B. Kaplan. A Method for simulating chiral fermions on the lattice. *Phys. Lett.*, B288:342–347, 1992.
- [Kennedy and Clark, 2007] A. D. Kennedy and M. A. Clark. Speeding up HMC with better integrators. *PoS*, LAT2007:038, 2007.
- [Kennedy *et al.*, 2013] A. D. Kennedy, P. J. Silva, and M. A. Clark. Shadow Hamiltonians, Poisson Brackets, and Gauge Theories. *Phys. Rev.*, D87(3):034511, 2013.
- [Kennedy, 2006] A. D. Kennedy. Algorithms for dynamical fermions. 2006.

- [Kinoshita, 1962] T. Kinoshita. Mass singularities of Feynman amplitudes. *J. Math. Phys.*, 3:650–677, 1962.
- [Kogut and Susskind, 1975] John B. Kogut and Leonard Susskind. Hamiltonian Formulation of Wilson’s Lattice Gauge Theories. *Phys. Rev.*, D11:395–408, 1975.
- [Lee and Nauenberg, 1964] T. D. Lee and M. Nauenberg. Degenerate Systems and Mass Singularities. *Phys. Rev.*, 133:B1549–B1562, 1964. [,25(1964)].
- [Lewis *et al.*, 2012] Randy Lewis, Claudio Pica, and Francesco Sannino. Light Asymmetric Dark Matter on the Lattice: SU(2) Technicolor with Two Fundamental Flavors. *Phys. Rev.*, D85:014504, 2012.
- [Lippert, 1997] Thomas Lippert. The Hybrid Monte Carlo algorithm for quantum chromodynamics. 1997. [Lect. Notes Phys.508,122(1998)].
- [Lucini *et al.*, 2016] Biagio Lucini, Agostino Patella, Alberto Ramos, and Nazario Tantalo. Charged hadrons in local finite-volume QED+QCD with C\* boundary conditions. *JHEP*, 02:076, 2016.
- [Luscher and Schaefer, 2011] Martin Luscher and Stefan Schaefer. Lattice QCD without topology barriers. *JHEP*, 07:036, 2011.
- [Luscher and Weisz, 1985] M. Luscher and P. Weisz. On-Shell Improved Lattice Gauge Theories. *Commun. Math. Phys.*, 97:59, 1985. [Erratum: *Commun. Math. Phys.*98,433(1985)].
- [Luscher and Weisz, 1995] Martin Luscher and Peter Weisz. Coordinate space methods for the evaluation of Feynman diagrams in lattice field theories. *Nucl. Phys.*, B445:429–450, 1995.
- [Luscher and Weisz, 2001] Martin Luscher and Peter Weisz. Locality and exponential error reduction in numerical lattice gauge theory. *JHEP*, 09:010, 2001.
- [Luscher *et al.*, 1997] Martin Luscher, Stefan Sint, Rainer Sommer, Peter Weisz, and Ulli Wolff. Nonperturbative O(a) improvement of lattice QCD. *Nucl. Phys.*, B491:323–343, 1997.
- [Luscher, 1977] M. Luscher. Construction of a Selfadjoint, Strictly Positive Transfer Matrix for Euclidean Lattice Gauge Theories. *Commun. Math. Phys.*, 54:283, 1977.
- [Luscher, 1998] Martin Luscher. Exact chiral symmetry on the lattice and the Ginsparg-Wilson relation. *Phys. Lett.*, B428:342–345, 1998.
- [Luscher, 2005] Martin Luscher. Schwarz-preconditioned HMC algorithm for two-flavour lattice QCD. *Comput. Phys. Commun.*, 165:199–220, 2005.
- [Luscher, 2010] Martin Luscher. Computational Strategies in Lattice QCD. In *Modern perspectives in lattice QCD: Quantum field theory and high performance computing. Proceedings, International School, 93rd Session, Les Houches, France, August 3-28, 2009*, pages 331–399, 2010.
- [Mages *et al.*, 2017] Simon Mages, Balint C. Toth, Szabolcs Borsanyi, Zoltan Fodor, Sandor D. Katz, and Kalman K. Szabo. Lattice QCD on nonorientable manifolds. *Phys. Rev.*, D95:094512, 2017.
- [Mück, 2013] Wolfgang Mück. Counting Photons in Static Electric and Magnetic Fields. *Eur. Phys. J.*, C73(12):2679, 2013.

- [Omelyan *et al.*, 2003] I.P. Omelyan, I.M. Mryglod, and R. Folk. Symplectic analytically integrable decomposition algorithms: classification, derivation, and application to molecular dynamics, quantum and celestial mechanics simulations. *Computer Physics Communications*, 151(3):272 – 314, 2003.
- [Osterwalder and Schrader, 1973] Konrad Osterwalder and Robert Schrader. AXIOMS FOR EUCLIDEAN GREEN’S FUNCTIONS. *Commun. Math. Phys.*, 31:83–112, 1973.
- [Osterwalder and Schrader, 1975] Konrad Osterwalder and Robert Schrader. Axioms for Euclidean Green’s Functions. 2. *Commun. Math. Phys.*, 42:281, 1975.
- [Patella, 2017] Agostino Patella. QED Corrections to Hadronic Observables. *PoS, LATTICE2016:020*, 2017.
- [Portelli, 2013] Antonin Portelli. Review on the inclusion of isospin breaking effects in lattice calculations. *PoS, KAON13:023*, 2013.
- [Reinsch, 2000] M. W. Reinsch. A simple expression for the terms in the Baker-Campbell-Hausdorff series. *Journal of Mathematical Physics*, 41:2434–2442, April 2000.
- [Reisz, 1988] Thomas Reisz. A Power Counting Theorem for Feynman Integrals on the Lattice. *Commun. Math. Phys.*, 116:81, 1988.
- [Rothe, 1992] H. J. Rothe. Lattice gauge theories: An Introduction. *World Sci. Lect. Notes Phys.*, 43:1–381, 1992. [World Sci. Lect. Notes Phys.82,1(2012)].
- [Ruegg and Ruiz-Altaba, 2004] Henri Ruegg and Marti Ruiz-Altaba. The Stueckelberg field. *Int. J. Mod. Phys.*, A19:3265–3348, 2004.
- [Sachrajda and Villadoro, 2005] C. T. Sachrajda and G. Villadoro. Twisted boundary conditions in lattice simulations. *Phys. Lett.*, B609:73–85, 2005.
- [Schwinger, 1948] Julian S. Schwinger. On Quantum electrodynamics and the magnetic moment of the electron. *Phys. Rev.*, 73:416–417, 1948.
- [Sexton and Weingarten, 1992] J. C. Sexton and D. H. Weingarten. Hamiltonian evolution for the hybrid Monte Carlo algorithm. *Nucl. Phys.*, B380:665–677, 1992.
- [Sheikholeslami and Wohlert, 1985] B. Sheikholeslami and R. Wohlert. Improved Continuum Limit Lattice Action for QCD with Wilson Fermions. *Nucl. Phys.*, B259:572, 1985.
- [Sommer *et al.*, 2004] R. Sommer, S. Aoki, M. Della Morte, R. Hoffmann, T. Kaneko, F. Knechtli, J. Rolf, I. Wetzorke, and U. Wolff. Large cutoff effects of dynamical Wilson fermions. *Nucl. Phys. Proc. Suppl.*, 129:405–407, 2004. [,405(2003)].
- [Symanzik, 1983a] K. Symanzik. Continuum Limit and Improved Action in Lattice Theories. 1. Principles and  $\phi^4$  Theory. *Nucl. Phys.*, B226:187–204, 1983.
- [Symanzik, 1983b] K. Symanzik. Continuum Limit and Improved Action in Lattice Theories. 2.  $O(N)$  Nonlinear Sigma Model in Perturbation Theory. *Nucl. Phys.*, B226:205–227, 1983.
- [Takaishi and de Forcrand, 2006] Tetsuya Takaishi and Philippe de Forcrand. Testing and tuning new symplectic integrators for hybrid Monte Carlo algorithm in lattice QCD. *Phys. Rev.*, E73:036706, 2006.



- [Tantalo, 2014] Nazario Tantalo. Isospin Breaking Effects on the Lattice. *PoS*, LATTICE2013:007, 2014.
- [Testa, 1998] M. Testa. Some observations on broken symmetries. *JHEP*, 04:002, 1998.
- [Urbach *et al.*, 2006] C. Urbach, K. Jansen, A. Shindler, and U. Wenger. HMC algorithm with multiple time scale integration and mass preconditioning. *Comput. Phys. Commun.*, 174:87–98, 2006.
- [Weinberg, 1973] Steven Weinberg. New approach to the renormalization group. *Phys. Rev.*, D8:3497–3509, 1973.
- [Weyrauch and Scholz, 2009] M. Weyrauch and D. Scholz. Computing the Baker-Campbell-Hausdorff series and the Zassenhaus product. *Computer Physics Communications*, 180:1558–1565, September 2009.
- [Wilson, 1974] Kenneth G. Wilson. Confinement of Quarks. *Phys. Rev.*, D10:2445–2459, 1974. [45(1974)].
- [Yoshida, 1990] Haruo Yoshida. Construction of higher order symplectic integrators. *Phys. Lett.*, A150:262–268, 1990.
- [Yoshida, 1992] H. Yoshida. Symplectic Integrators for Hamiltonian Systems: Basic Theory. In S. Ferraz-Mello, editor, *Chaos, Resonance, and Collective Dynamical Phenomena in the Solar System*, volume 152 of *IAU Symposium*, page 407, 1992.
- [Zinn-Justin, 2002] Jean Zinn-Justin. Quantum field theory and critical phenomena. *Int. Ser. Monogr. Phys.*, 113:1–1054, 2002.